ACRP

Final Report – Activity Report

Program control:
Climate and Energy Fund

Program management:
Kommunalkredit Public Consulting GmbH (KPC)

1 Project Data

Short title	URBANIA	
Full title	Influence of the development of outlying districts and urban growth on the urban heat island of the city of Vienna in the context of climate change	
Project number	B567119	
Program/Program line	ACRP 8th Call for Proposals	
Applicant	Institute of Meteorology, Department of Water, Atmosphere and Environment, University of Natural Resources and Applied Life Sciences (BOKU_Met) Ao.Prof.Dr.Mag. Philipp Weihs	
Project partners	MA22	
Project start and duration	Project start: 01.06.2016	Duration: 30 months
Reporting period	from 1.06.2016 to 30.11.2018	

Synopsis: Within the scope of URBANIA the influence of the development of outlying districts and urban growth on the urban heat island of the city of Vienna was investigated. We were using a multiscale modelling approach based on the coupling of the mesoscale model WRF with the microscale model TEB. Additional simulations with the high resolution urban model SOLWEIG have been performed and the model extended to calculate the thermal comfort index UTCI very precisely. Based on urban development and climate change scenarios the influence of urban growth, urban planning in conjunction with climate change on the climate of the central districts of Vienna was simulated.

2 Technical /Scientific Description of the Project

2.1 Project abstract (max. 2 pages)

2.1.1 Brief description of the project (initial situation, targets, methodology – activities)

To estimate the near surface temperatures (heat island effect) and thermal comfort of the city of Vienna, the town energy balance (TEB) model (Masson 2000) which includes a building energy model (BEM) was used. TEB is aimed to simulate the energy fluxes (radiation balance, latent and sensible heat) into the atmosphere at the surface und thus especially suited for the aims of the present project. Atmospheric airflows and circulation within the urban canyons are also taken into account in the energy balance. TEB is a single layer urban canopy model, which proposes a physically based (bottom-up) approach, which enables to estimate the urban climate at city scale (~50 km) with a resolution of a neighbourhood (~100 m). The urban surface is represented by simplified urban canyons. The model is forced by atmospheric data that either stem from observations (offline mode) or an atmospheric model (coupled mode). For the study, the Weather Research and Forecasting (WRF) model is being used for coupling with TEB. For the validation and the correct initialization of the model input parameters, observational data from the Austrian weather service are being used and additional routine and campaign measurements are being performed in chosen districts of Vienna. The project is a cooperation of three independent working groups of BOKU_MET with the Environmental Protection Department MA22 – section Spatial Development and with Meteo-France (subcontractor). MA22 is the official urban planning agency of the city of Vienna which is in charge of the sustainable development of the city which also takes into account climate change mitigation measures. Within the scope of URBANIA, MA22 ensured the direct link to the policy makers of the city of Vienna.

2.1.2 Results and conclusions of the project

WRF and TEB have been setup and all input data prepared. Maps of e.g. sky view factor and building height are available for whole Vienna. Simulations with TEB offline, WRF and WRF-TEB have been performed. First tests of the WRF model show no instability for resolutions of approximately 110 m. The real structure and geometry of the urban canyon does not correspond to the generalised urban canyon assumed in the TEB simulations. Therefore, an additional model (SOLWEIG - Solar Long-Wave Environmental Irradiance Geometry) was used in our investigations, which considers the real complex urban geometry. The model was extended to be able to calculate the thermal comfort index UTCI (Universal Thermal Comfort Index) and a wind model included, to be able to make a more precise calculation of the UTCI.
Measurements for validation of air temperature were installed at the end of December 2016 in 8 different morphological zones in Vienna and maintained until October 2018. In addition, during the same measurement period, measurements of short and long wave radiation on horizontal and vertical planes were taken in a street canyon and maintained until October 2018. The comparison with TEB showed a good agreement for radiation fluxes and radiation balance within the street canyon. Simulations of air temperature using TEB offline, WRF and WRF-TEB were validated using the measurements done within the urban Vienna structure in addition to observations from ZAMG, and the INCA data set.
A sensitivity analysis with TEB and WRF-TEB was done to estimate the model skills and uncertainties. Special emphasis was put on the interaction between surface and the boundary layer.
Urban development scenarios were prepared as model input, simulated and analysed.
Climate episodes were selected, prepared and used as model input.

The results were discussed within a workshop with experts from the Vienna municipal department 22. A website has been setup, giving an overview on the topic, the methodology and the results: http://urbania.boku.ac.at/

Conclusions for Modellers:

- The coupling of WRF and TEB lead was successful, after some modification in the source code of WRF
- Improvements in calculation accuracy were obtained using the coupling.
- The results of the coupled runs are reasonable and the structure of the urban heat island within the city of Vienna is reproduced much more realistic.

Conclusions for Urban Planning:

- The increase in air temperature expected by climate change exceeds the increase caused by potential maximum urban sprawl and densification.

- The expected magnitude depends on the assumed scenarios and is up to 5°C until 2050.
- Insulation of building could lead to slight increase of air temperature and thermal stress during the day, but also to a reduction during the night. During the day it is the primary cause of increased thermal discomfort.
- The combination of albedo and insulation works together as an effective mitigation method which has the potential to reduce the air temperature during the night by 1°C.
- Irrigated green roofs might be an effective measure to increase human comfort during heat waves.

2.1.3 Outlook and summary

Results obtained within the scope of URBANIA have shown that the multiscale modelling approach is promising and may be used for future investigations related to urban climate modelling. Especially the resolving of the urban and urban hinterland interaction allows the quantification of the impact of densification of the building structure at the border of the cities. Though climate change shows the largest impact on the magnitude of the heat island, some measures such as providing more shaded areas, inclusion of vegetation may help to locally reduce the heat and to improve the thermal comfort.

2.2 Contents and results of the project (max. 20 pages)

This part of the report provides thorough information about the project targets defined by the applicant, as indicated in the project application, and the methods employed to achieve these targets.

2.2.1 Initial situation / motivation for the project

Urban settlements are generally known for their high fractions of impermeable surfaces, large heat capacity and low humidity compared to rural areas which results in the well-known phenomena of urban heat islands. The urbanized areas in and around Vienna are growing rapidly which can amplify the intensity and frequency of situations with heat stress. The distribution of the urban heat island is not uniform, because the urban environment is highly diverse regarding its morphology as building heights, building contiguity and configuration of open spaces and trees vary, which cause changes in the aerodynamic resistance for heat transfers and drag coefficients for momentum. Furthermore, cities are characterized by highly variable physical surface properties as albedo, emissivity, heat capacity and thermal conductivity. The distribution of the urban heat island in Vienna is influenced by these morphological and physical parameters as well as the distribution of unsealed soil and vegetation. These aspects influence the urban climate on micro- and mesoscale. The global climate change further increases the temperature baseline, so during summer, thermal comfort might decline dramatically. Using multi scale numerical modelling different spatial configurations of urban density and predominant material properties can be calculated to improve setups, which can provide maximum thermal comfort for the increasing Viennese population in a challenging climate.

2.2.2 Objectives of the project

The objectives of the project were:

- An adaptation and validation of a multi-scale climate model for the city of Vienna and the determination of the accuracy of multiscale modelling. Eventually, appropriate methods to improve the accuracy should be identified
- Determination of the influence of climate change on the climate of the districts of the city of Vienna
- An estimation of the influence of city growth and the development of outlying districts on climate of the districts of Vienna
- Identification of the best urban planning measures for the outer districts of Vienna for mitigation of climate change impact on the urban heat island in Vienna. Those include the appropriate inclusion of vegetation in the new districts, choice of the dimensions of building heights and street width and choice of the building materials concerning their heating storage characteristics and their reflection properties.

2.2.3 Activities performed within the framework of the project, including methods employed

The management of the project (WP1) consisted of regular meetings and communication between the project groups, the project partners and the scientific community. The interim results were presented on national and international conferences. A project homepage was set up. Interim and final reports were delivered to the KPC. One of the first steps of our investigations was the preparation of the model input data and the adaptation of the models (WP2). A methodology to prepare the static data of land cover information was developed. The methodology was discussed using literature review, data mining, statistical analysis and expert judgement. The models WRF and TEB were coupled. Meteorological fields for historical heat waves were prepared. A validation of the town and building energy model was then performed using continuous meteorological measurements and comparing model simulations (WP3) of TEB, SOLWEIG, WRF, WRF-SURFEX and WRF-TEB. After validation of the models, scenarios as to urban development scenarios and future climate change scenarios were defined (WP4).
Runs of the coupled WRF-TEB model were performed for three climate scenarios and two urban development scenarios (WP5). Air temperature, UTCI and PET were analysed. Conclusions were drawn from the results.

2.2.4 Description of the results and project milestones (also on work package basis)

WP1 Project management and dissemination:

M1.1: Kick-off meeting

The first meeting with the project partner MA22 took place before project start. The official kick-off meeting was held on July 15 2016 at the Institute of Meteorology. Altogether 10 project meetings took place. 4 meetings were held with officials of the department of the Vienna city administration, with division MA18 (city planning and urban development), with centre of excellence (Smart-City Vienna) dealing with higher order urban planning. Additional information was obtained from the Institute for environmental and urban management (SUM), the Federal Planning Institution for eastern Austria (PGO), the Environmental planning divisions of Lower Austria and Burgenland and with the divisions MA21 and MA19 from the city of Vienna.
A one week stay for a scientist of BOKU_Met at the subcontractor Meteo-France's headquarter in Toulouse was organised for discussion, training and teaching. One scientist of Meteo-France also came to Vienna to meet our team and observe the project progress. The main questions regarding the methodology were discussed in detail.
The project was presented at one national and two international conferences.

M1.2: Progress/interim reports as agreed with KPC and final reports

One interim report has been delivered. As agreed, hereby the final report is presented. Deliverable **M1.3** (International publication) includes one accepted publication (Oswald et al., 2019) and two or maybe three publications to be submitted (Trimmel et al., 2019; Nadeem et al., 2019).

WP2 Preparation of input data, adaptation of the models:

The Weather Research and Forecasting model (WRF) is a mesoscale numerical weather prediction system designed for both atmospheric research and operational forecasting applications. It is used for simulating meteorological parameters based on ground elevation and land cover type. As lateral boundary conditions 6 hourly ECMWF analysis data were used, the Topography is given by the SRTM1Arc:30m dataset.
In this particular case results close to ground level are of interest.
The Town Energy Balance scheme (TEB) uses meteorological data close to ground level to perform meteorological estimations taking into account the built environment. Therefore, those two models require different input data and parameters. Finally, the models were coupled in order to take into account the mutual interaction between urban space and the planetary boundary layer and the free atmosphere.
As WRF is run in four nests, all input data (elevation, land cover class (LCZ), meteorological) was prepared with four different resolutions 3 km, 1 km, 333 m and 111 m and within

reasonable domains (fig 2.1). The first model runs were done for all four resolutions. As the innermost domain (111 m) required significantly increased simulation time and it was found that there was no benefit for the projects aims from using a higher resolution, the innermost domain was excluded from any later simulations.

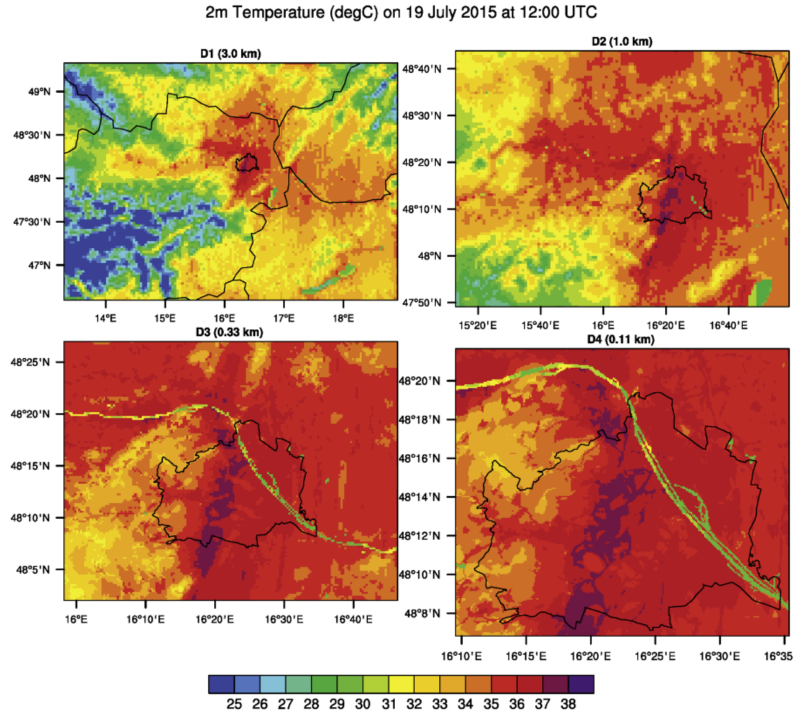

Figure 2.1 First test simulation of high resolution WRF, 4 nests with the resolutions 3 km, 1 km, 333 m and 111 m. The boundary of the city of Vienna is marked.

M 2.1: Vienna surface structure implemented in TEB

The surface structure and building parameters used for modelling were derived from several sources (see Annex: fig. A2.1). WRF uses slightly different input parameters as TEB. Therefore, some parameters required a conversion of units, others had to be calculated separately.

For Vienna high resolution vector (Flächenmehrzweckkarte, Baukörpermodell, Realnutzungskartierung) and raster geo-datasets (Digitales Oberflächenmodell) were processed to derive land use surface fractions and building morphology parameters following the methodology of Cordeau (2016).

A dataset of building age and typology was checked and extended using satellite visual and thermal bands. Then it was linked with information about building age and typology with typical physical building parameters obtained from different studies (Berger et al. 2012 and Amtmann M and Altmann-Mavaddat N (2014)) and the OIB (Österreichisches Institut für Bautechnik) (see Annex Table A2.1 – A2.4). The EPISCOPE categories were used to distinguish different building materials used in various periods.

The categories of building types were provided by the city of Vienna and were grouped to the categories used within the EPISCOPE project. The categories of land cover usage are dominated by apartment blocks (MGV), terraced houses (RH), industry (Industrie), office (Büro) and old city (Altstadt) (see Annex Table A2.5).
Further, a land cover classification was created using the WUDAPT methodology of Bechtel et al. (2015), which is based on machine learning algorithms depending on satellite imagery and expert knowledge (see Annex: fig. A2.2).
While the buildings heights have a standard deviation of 3.2 m, which is 15 % of the maximum average building height of one block, the built and unsealed surface fraction vary stronger with around 30 % standard deviation.
It was found that (1) the central and pre 1919 structure is clearly more uniform than the later building structure of Vienna regarding morphological as well as physical building parameters. Therefore, large uncertainties are possible at the urban rims where also the highest development is expected. (2) As Vienna is constantly transforming, the date of data collection has to be considered for all data sets (e.g. the satellite image date used for classification may not correspond to data of training zones). (3) Generally the spatial distribution detected by the WUDAPT method goes in line with CORINE land cover (EEA). The method was least robust in the recognizing different smooth surfaces (lakes, glasshouses, large concrete areas, uniform vegetation). Under-fit data lead to better, more general results, but missing unique land use areas. This can be improved by including more classes.
The data on urban land use and morphology are used for initialisation of the town energy balance scheme TEB, but are also useful for other urban canopy models or studies related to urban planning or modelling of the urban system.

M 2.2: Coupling of TEB and WRF ensured

The TEB has been previously implemented and tested as a parameterization for urban land into the 5th-generation Pennsylvania State University–National Center for Atmospheric Research Mesoscale Model (MM5) and COSMO-CLM (Consortium for Small Scale Modelling-Community Land Model) by Trusilova et al. (2008, 2009, 2013). The coupled TEB-MM5 was used for a study of the climate sensitivity to the urban warming in Europe at the spatial resolution of ~10 km and the coupled TEB-COSMO was evaluated over the area of Berlin at a spatial resolution of ~2.8 km.
The coupling of TEB and WRF was done based on the method similar to the method used for coupling of TEB and COSMO-CLM by Trusilova et al. 2013. Being coupled, WRF and TEB exchange intermediate results to consider the mutual interference between urban structure and the meteorological condition. Among others the following parameters are transferred from WRF to TEB: potential air temperature (lowest atmospheric level), mixing ratio, wind speed, direct and diffuse radiation; and from TEB to WRF: air temperature in 2 m

above ground, reflected short wave radiation, reflected and emitted long wave radiation, sensible heat flux, latent heat flux and (diagnostic) wind speed.

M 2.3: Meteorological fields for model evaluation prepared
Spatial evaluation of the model is based on the INCA (Integrated Nowcasting through Comprehensive Analysis) data set of ZAMG. The variables temperature, global radiation, relative humidity and wind speed with hourly temporal and 1x1 km spatial resolution were used.

M 2.4: Meteorological fields for historical heat waves prepared
The selection of the historical heat waves was based on the analyses of the observational data from the station Wien Hohe Warte, provided by the Austrian weather service ZAMG. Base for the selection was the five day average of the daily maximum temperature. This indicator was calculated for the last 30 years (1988 to 2017) and with Generalized Extreme Value Distribution (GEV; Fisher and Tippett, 1928) the return period of this fife day events was calculated. Due to the strong trend of more than 2 °C within the last three decades (see fig. 2.2), we had to de-trend the data before applying the GEV.
For final selection of the heat waves we decided to use a moderate heat wave with a return period of two years and an extreme heat wave with a return period of 15 years. The average maximum temperature for a two year event is actual 31.6 °C and a 15 year event 36.3 °C. The real periods closest to the calculated temperature, are the periods 9 to 13 July 2010 with 31.6 °C and the 11 to 15 August 2015 with 36.3 °C. They were selected for explicit modelling. .. Lateral boundary and initial conditions are based on the ECWMF analyses data set. These data have a similar spatial resolution (~10 km) as regional climate models. Gridded data: For the internal and lateral boundaries ECMWF analysis data for July 2010 and August 2015 (temporal resolution; 6 hours, horizontal resolution: 9 km) were used for air temperature, wind speed, air pressure, air humidity, soil moisture, ...).

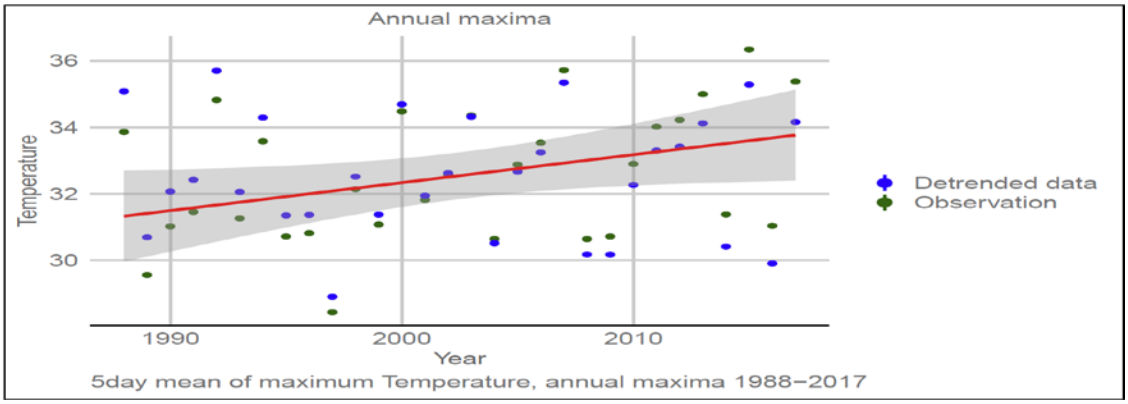

Figure 2.2 Annual maximum of the 5 day average of daily temperature maximum from 1988 to 2017 from Wien, Hohe Warte. Green dots are the original measurements and blue are the de-trended one. The red line indicate the linear trend of this indicator for this period.

Terrestrial data: for the topographical elevation the SRTM1Arc:30m data set was used. For the land cover information Corine data was reclassified to USGS classes.
It was planned to use the WUDAPT LCZ (Land cover zones) created in M2.1 to be used with WRF-TEB. Because the simulated nesting areas exceed the area for which the LCZ could be produced for, and also WRF was not able to include 7 classes, the Corine2012 data set was included in the research. Unlike the LCZs and the UrbanAtlas, Corine2012 is available for all nests simulated with WRF and there is an existing methodology for the usage of Corine in WRF. Corine is presently updated every 6 years. The next version, for 2018, became available only by the end of this project (https://land.copernicus.eu/pan-european/corine-land-cover/clc2018 last access: 2019.02.13) and therefore, was not used. Update cycles of 5 years are planned which makes it a very useful dataset.

WP3 Validation of the town and building energy model
M3.1: Overview of collected data and measurements
Measurement data was collected for two purposes: validation of the radiation flux inside an urban canyon and validation of the air temperature at several points distributed in Vienna.
The radiation flux was measured inside an exemplary street canyon at the University of Natural Resources and Life Sciences (BOKU) at Peter-Jordan-Strasse 82, Vienna. At three locations along a façade (top, middle and bottom) the incoming and outgoing long and short wave radiation was measured. In the middle point, the horizontal fluxes were measured as well. At three points distributed on the ground the incoming (horizontal) and reflected (vertical plane) short wave radiation was measured. At a measurement platform on the roof all other, necessary parameters for the validation of TEB (air temperature, humidity, pressure, wind speed and direction, direct and diffuse short wave radiation, long wave radiation) were obtained. The data was measured between August 2016 and October 2018.
For the distribution of air temperature and humidity in the city, eight additional measurement stations were installed, complementary to the air quality measurements at the sites of the Luftmessnetz (MA22) (fig. 3.1). An additional, ninth station was installed in Prater at Arenawiese to capture the effect of the recreational area Prater.
The difference in minimum and maximum temperature for selected stations is shown in fig. A3.1 und A3.2 in the Annex.

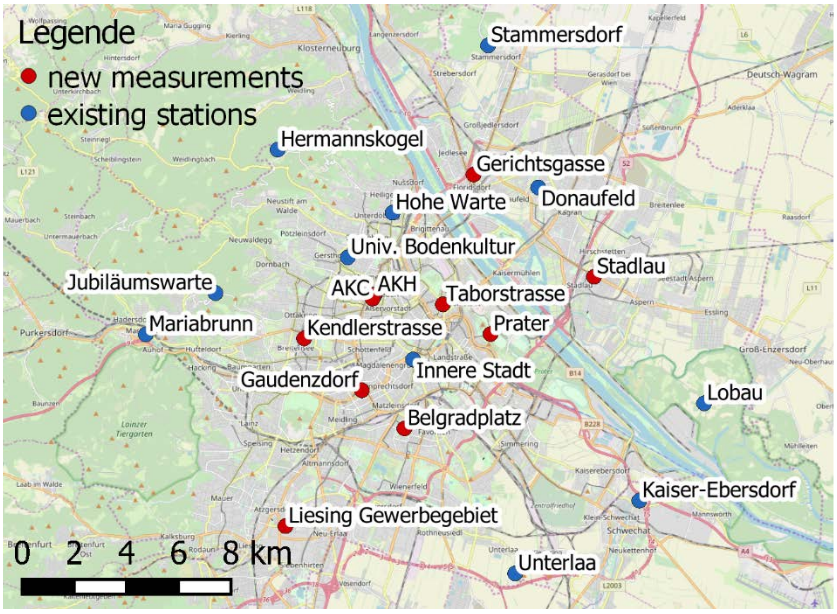

Figure 3.1 Position of existing and new measurement stations

M3.2: Simulations with model TEB accomplished

The parameters created in WP2 were averaged over the LCZ classifications. The canyon air temperature, sensible and latent heat flux as well as radiation balance were simulated using TEB (Masson, 2000) for the different LCZs that are predominant in Vienna (see Annex, fig. A3.3). The result allows to deduct the sensitivity of those variables to parameters used for the characterisation of the urban structure of Vienna. Also effects of expected changes (see MA 18 (2011, 2014a+b), PGO (2011), Amtmann M and Altmann-Mavaddat N (2014)) were calculated. It was found that using the Viennese data averaged over the LCZ produced by the WUDAPT-method leads to clearer differentiated zones in regard to energy fluxes than using existing classifications for Vienna such as the Realnutzungskartierung (MA18/21/41).

M3.3: Validation report showing the achieved accuracy and possible improvements of multiscale modelling approach

The obtained data (see Milestone M3.1) was used for validating different models. The net radiation simulated with TEB was compared to the data from inside the street canyon at BOKU in August 2016 (see Annex, fig. A3.4).

The results indicate a strong relationship between the measured radiation balance at roof level and the simulated radiation balance using TEB. The comparison in fig. 3.2 shows a squared Spearman's rank correlation coefficient of 0.94 and that TEB results are slightly underestimated. Further, the input values global and direct solar radiation, used for the TEB simulation, were compared with Secondary Standard measurements of ARAD site Wien Hohe Warte. The deviation concerning the interquartile range is below 3 %.

fig. 3.3 shows a comparison of a time series of the Universal Thermal Climate Index (UTCI) inside the street canyon at BOKU. The UTCI was simulated with TEB and with the model SOLWEIG (Lindberg et al., 2008) for two locations, one in the sun and one in the shadow. SOLWEIG is a radiation balance model which allows the simulation of complex and real urban geometries. The results from SOLWEIG in the sun fall back to the shadow-results due to shading by buildings.

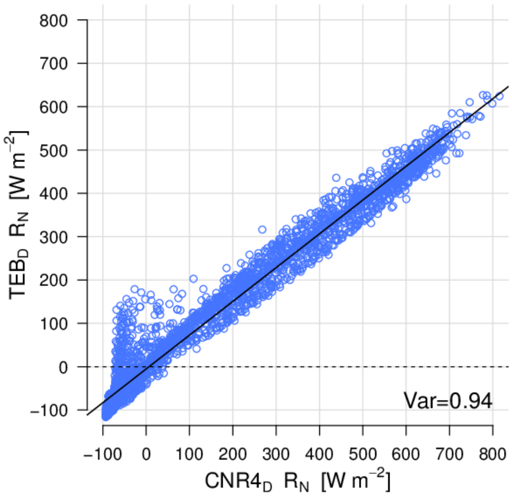

Figure 3.2 Correlation of simulated and measured net radiation.

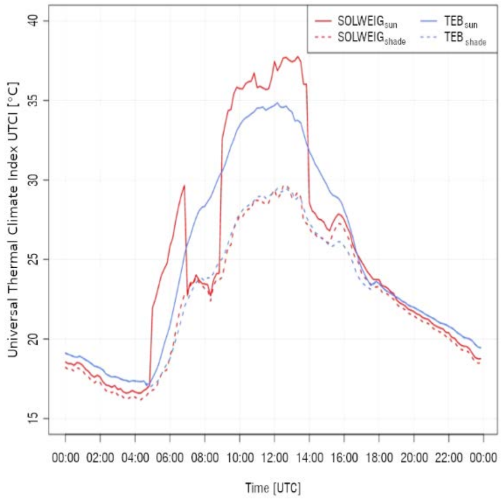

Figure 3.3 Comparison of Universal Thermal Climate Index simulated by TEB and SOLWEIG for sun (—) and shade (- - -).

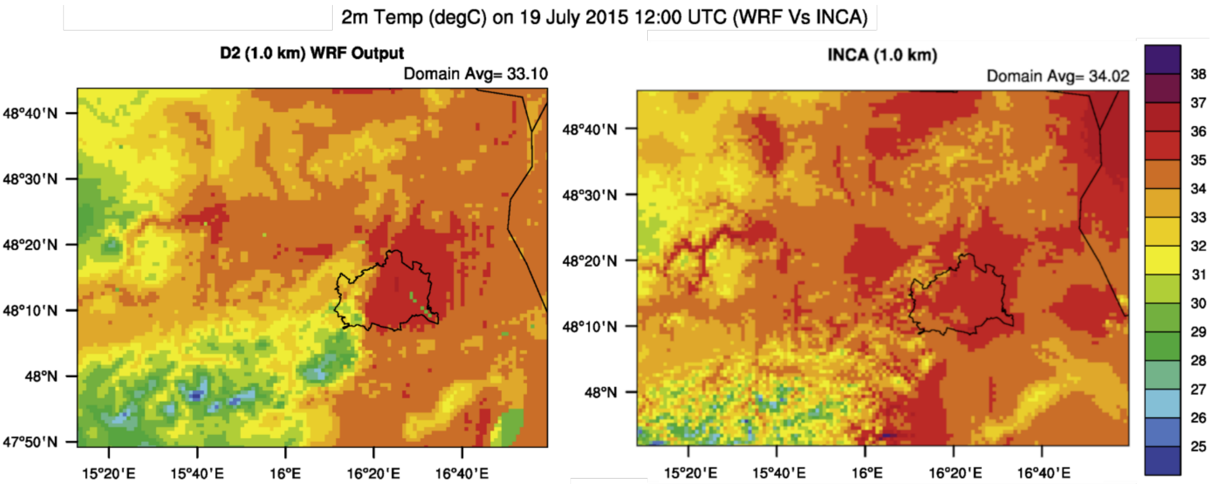

Figure 3.4 Spatial comparison of WRF and observations: The WRF model results for 2 m air temperature (left) show good agreement with the gridded INCA observation (right). Small scale features as the river Danube or lake Neusiedlersee are seen by the model while

invisible for the INCA dataset, as INCA do not use land use information for interpolation. The domain average differs less than 1 °C.

The WRF output for air temperature at 2 m is compared to grid interpolated observations from the INCA database (see fig. 3.4). Besides the differences due to the interpolation method, both show good agreement. The average air temperature from WRF over the complete domain is almost less than 1 °C lower than from the INCA database. Also comparisons of results from WRF, TEB forced by WRF and WRF coupled with TEB with observed data show good agreement (see Annex, fig. A3.5 a, b).
Further, it was found that the coupling of WRF with TEB gives slightly more accurate results than the regular WRF and the correlation with the observed data is better (fig. 3.5).

Within the scope of URBANIA small adjustments were performed (see former sections). Additional future improvements in the microscale would be:

- include building elevation maps in the coupled microscale model. This would help to better include micro scale effects due the ventilation and air exchange in larger scale urban climate simulations. One possible way would be the coupling of the SOLWEIG model with WRF.
- include irrigation in the models: in TEB no irrigation is assumed on green roofs. Evaporative cooling is however known to be one of the most important components.

Improvement of the determination of latent seems also to be needed in macro scale modelling: heat episode with no precipitation are usually correlated with arid soils. The soil parametrisations in WRF, however, do not allow enough differentiations of the soil characteristics during a heat episode, e.g. forests or irrigated fields seem to be too arid.

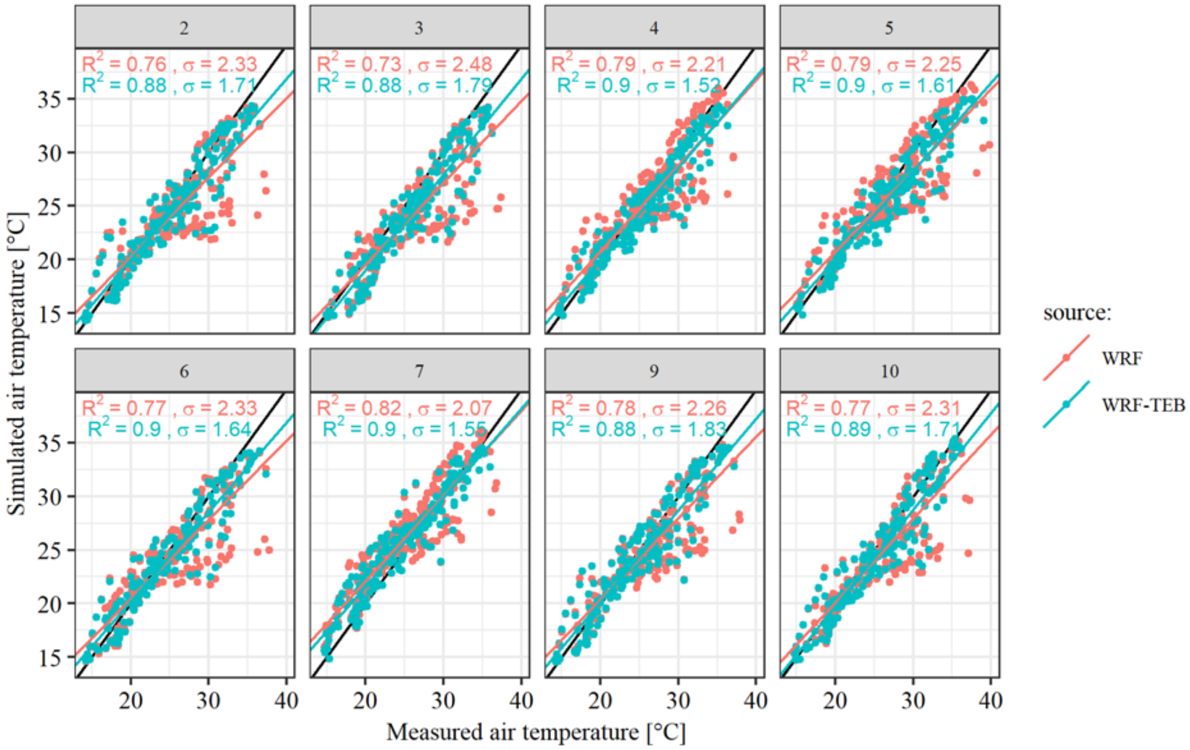

Figure 3.5 Comparison of simulations with WRF and the coupled WRF-TEB to observations at eight locations within Vienna within a clear-sky period between 28. July and 03.August 2017.

WP4 Creation of scenarios

M4.1: Urban development scenarios for the time frame 2030 and 2050

For the urban development scenarios governmental regulations and plans, as well as statistical data were taken as a source of information. Those provide limitations and information about known projects and directives on how settlements are intended to grow. Besides aerial growth and densification, building type, spatial distribution of the development and the change of the material properties to be used are taken into account.

However, actual changes within the buildings are difficult to estimate, as those depend on private decisions and financing. Outside Vienna most of the urban development is reconstruction of presently unused built areas into dense residential or commercial areas. In many municipalities there is currently no permission for building multi-storied buildings and dense urban development.

Basis for estimating urban growth were population development scenarios. According to Planungsgemeinschaft Ost (2011) the population is expected to grow by 400.000 until 2030 and by 800.000 until 2050. Further parameters were the distribution of building types (regarding their built height), the amount of workspace required per person (in contrast to living space) and the required floor area for living space, workspace and production lines per

person. That gave the amount of additional gross floor area due to either densification or development of additional urban areas. For details, see Table A2.5 in the Annex.
Three different growth scenarios were developed: “Reference”, “Sprawl” and “Optimized”. The “reference” corresponds to the current state. The other two scenarios include growth of urban area on the known development areas (see fig. 4.1, areas in green colour). Those provide additional 18 km^2 of gross floor area and are:

- Vienna Airport – third runway (sealed surface, barren and un-vegetated) (https://www.viennaairport.com/unternehmen/flughafen_wien_ag/3_piste/bauprojekt_3_piste last access: 18.6.2018)
- Strategic plan for the development area metro-line U2 – Donaustadt (MA 21, 2013)
- 13 development areas (STEP05), amongst mainly:
  - Floridsdorf – axis Brünnerstrasse, Siemens-Allissen, Donaufeld
  - Donaustadt/Aspern (Mühlgrund, Hausfeld, Apernstrasse, Seestadt)
  - Waterfront (Nordbahnhof, Nordwestbahnhof), Prater-Messe-Krieau-Stadion
  - Railway station Wien – Europa Mitte – Erdberger Mais (Arsenal, Aspanggründe)
  - Rothneusiedl, Liesing Mitte (In den Wiesen), Westgürtel

Scenario – Sprawl (SPR):
Besides the known areas, “Sprawl” considers additional growth. This additional area is distributed at the urban rims, taking into account protected areas (STEP 2005, Natura 2000, “Naturschutzgebiete” NÖ, Strategie Niederösterreich – Landesentwicklungskonzept (2004) / Regionale Raumordnungsprogramme, Landesentwicklungsplan Burgenland (LEP, 2011)) to cover the required gross floor area (see fig. 4.1, areas in red colour). The distribution of the urban growth is based on prognoses and scenarios published by the Planungsgemeinschaft Ost (2009, 2011) and integrates information from the “Leitbild Siedlungsentwicklung” of STEP 2025 and the prognoses of ÖROK and MA23. The new buildings’ types were derived from the current building types, taking into account the study “Siedlungsformen der Stadterweiterung” (MA18, 2011) and the current land use.

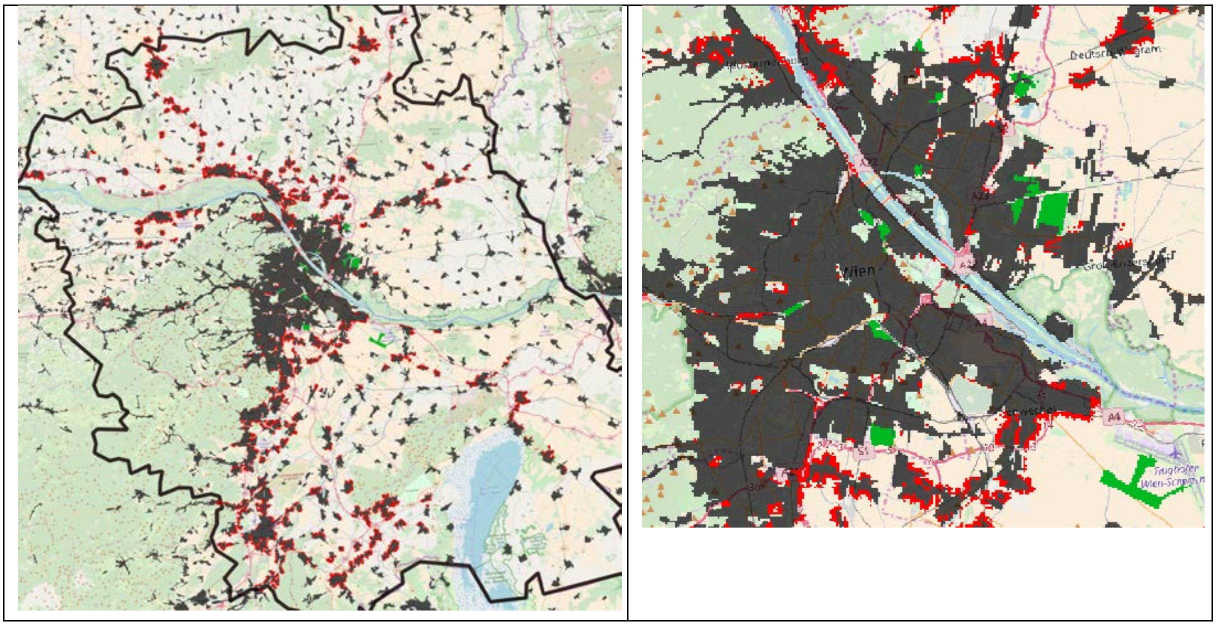

Figure 4.1 Spatial distribution of new urban areas within the region “Stadtregion+” (green: known development areas, red: urban expansion). Left: Whole area of “Stadtregion+”; right: zoomed into Vienna. In SPR both new urban areas are built (green + red areas), in OPT only the known development areas (green areas).

Scenario – Optimised (OPT):

The second scenario is “Optimised” and contains no growth of the urban area, except for the known development areas. In this case, the required growths in gross floor area is achieved by densification of the existing built areas. The densification is achieved by either adding floors to low- and mid-rise buildings or converting commercial and industrial buildings to multi-storeyed residential buildings. Further, idle floor area and attics shall be used.

Apart from the spatial changes the optimised scenario differs from the “sprawl”-scenario in three aspects that tend to mitigate the urban heat island, insolation, albedo and unsealing. The described measures are taken for all three urban categories (commercial, low-density and high-density residential buildings) to obtain maximum effects.

Insulation (ISO):

First in the OPT-scenario, the thermal conductivity of roofs and walls was decreased to 0.1 W/mK, for the windows to 0.9 W/mK (Amtmann M and Altmann-Mavaddat N (2014)) and the thermal conductivity of roads was decreased to 0.4 W/mK (https://www.engineeringtoolbox.com/thermal-conductivity-d_429.html, last access: 11.6.2018). This change in material properties slows down the process of storing heat and incoming energy in the urban structure. Thus, the ability to take up heat is reduced during the day. This causes lower temperatures during the night time, but higher air temperatures especially in the morning. This is also an important factor to facilitate night time natural ventilation.

Albedo (ALB):

The second measure in the OPT-scenario counteracts and complements this diurnal behaviour. The albedo of the walls and of the ground was increased to 0.3, which is low enough to avoid impairing visual and thermal comfort (Weihs et al. 2018). The albedo of roofs was increased to 0.68. This is technically possible and due to its location unlikely to impair the visual and thermal comfort.

The increase of the albedo increases the reflection of radiation back to the atmosphere and thus, reduces the energy absorbed by the urban structure. Therefore, the negative effects of a decreased thermal conductivity should be mitigated.

The albedo increase does not depend on the availability of water or on space demands. The effects of increased surface albedo were investigated in various studies (KELVIN Project, Morini et al. 2016, Taha et al.1997) and does not have known negative effects on the boundary layer height and pollutant concentrations.

Unsealing surfaces:

According to Umweltbundesamt (2017) the sealing of ground surface per person in Austria increased by 25 % between 2001 and 2012/2017. The degree of sealing in built up area in 2017 was at 43 % in Vienna, including traffic areas, road side areas and parking lots (Umweltbundesamt 2018). These areas could be further reduced, as only the actual roads need to be sealed to ensure transport (Communication with TU-Landscape). To estimate the effect of significant and feasible changes in sealing, a reduction of the sealed roof surfaces by 20 % for high residential and commercial buildings and a slightly smaller reduction by 15 % for low residential building was assumed. Those changes were included in the OPT-scenario.

Changes in Height/Width ratio – Densification (DEN):

In high density residential areas, no increase in building density is likely. The building density in low density residential areas was increased from 0.22 to 0.242. In commercial areas the density was increased from 0.16 to 0.242.

Additional changes in material properties for offline runs:

Green roofs (GRR) and Photovoltaic on roof (PVR)

Additional effective options for changes in the urban material properties, which could not be simulated with the coupled WRF-TEB are the installation of green roofs and photovoltaic panels. Although, there are various protection zones to ensure the ensemble view of the city, the focus of preservation applies mainly to the facades. Therefore, there is more freedom to alter the roofs. Photovoltaic installations on walls are only likely in unprotected areas, while photovoltaic on roofs and green roofs are possible in the whole city. For green roofs an extensive sedum cover was chosen. The photovoltaic roofs were calculated with an efficiency of 20 % and an albedo of 10 %.

Table 4.1: Description of the urban parameters used for the urban scenarios “reference”, “sprawl” and “optimised” in WRF-TEB

		„REF“	„SPR“	„OPT“
Urban area: total built area [km²] (area compared to REF [%])		929 (100)	1115 (120)	939 (101)
Portion of built area per type of building-area [%]	**Low density residential**	22	22	24.2
	High density residential	46	46	46
	Commercial	16	16	24.2
Thermal conductivity [W/mK]	**Roof**	1.7	1.7	0.1
	Wall	1.4	1.4	0.1
	Ground	0.9	0.9	0.4
	Windows			0.9
Albedo [-]	**Roof**	0.15	0.15	0.68
	Wall	0.2	0.2	0.3
	Ground	0.138	0.3	0.3

M4.2: Selection of typical heat waves for 2030 and 2050

With the method developed for the selection of the historical heat wave, we analysed the ensemble of bias corrected and localized climate change scenarios of ÖKS 15. In fig. 4.2 the 10-year average of the used indicator is shown for the whole 21st century. Table A4.1 (see Annex) gives the average temperature for this indicator for 2, 5, 10, 15, 20 and 30 year return period from the observations and the climate change signal for the ensemble median of the RCP 4.5 and RCP 8.5 runs for 2030 (2016-2045) and 2050 (2036 to 2065). Additionally the most extreme model per time frame is also given. As can be seen in fig. 4.2 the differences between RCP 4.5 and 8.5 mainly occur at the second half of the century. Till 2030 even the RCP 4.5 ensembles show a stronger increase in heat wave temperature as RCP 8.5.

For the concrete modelling of future heat waves we selected the historical event from 31 July to 4. August 2017 with a 5-day maximum temperature of 35.4 °C. This corresponds to a two year heat wave in 2050 based on the most extreme scenario out of the ÖKS 15 ensemble. To represent an extreme heat wave we selected the extreme scenario for the 15 year heat wave in 2050. This corresponds with an average 5-day maximum temperature of 41.2 °C.

For the explicit modelling we selected the most extreme models for the 2 year and 15 year event for the period 2050. This leaded to an average 5-day temperature maximum of 35.4 °C.

M4.3: Meteorological data for heat wave episodes for 2030 and 2050 prepared.
The lateral boundary conditions for this extreme heat wave were taken from a high-resolution regional climate scenario form Nadeem and Formayer, 2015. With this two cases we represent all possible developments for moderate and extreme heat waves till the middle of the 21st century. Periods with equivalent Index value (41.2 °C) are used as lateral and initial boundary conditions to run high resolution coupled WRF-TEB. Additionally to the 5-day period a spin-off period of two days was used.

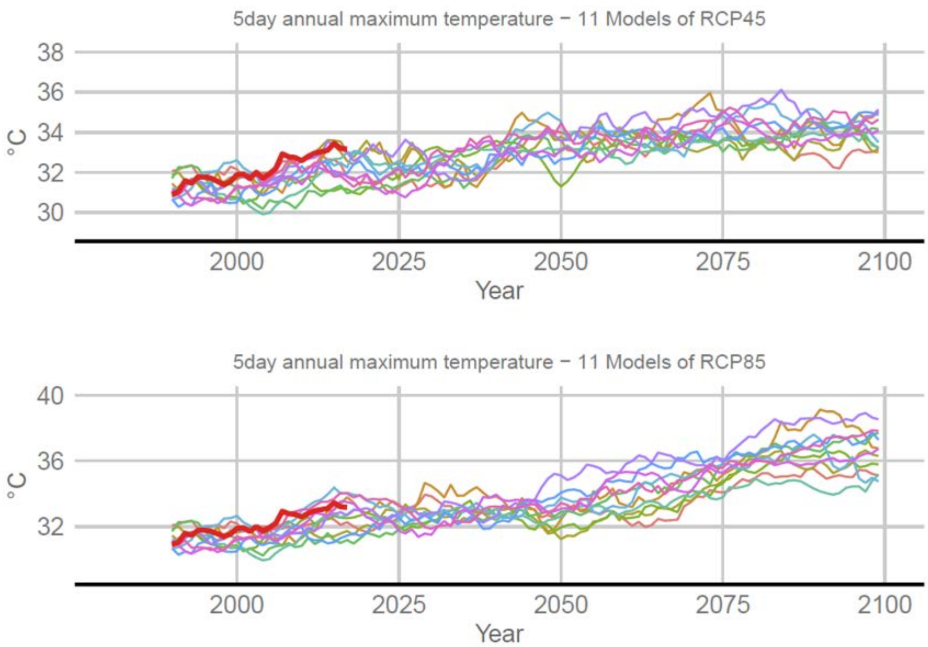

Figure 4.2 Development of the annual maximum of the average 5-day temperature maximum during the 21st century for RCP 4.5 (up) and RCP 8.5 (down) ÖKS15 ensemble for the grid cell nearest to Wien Hohe Warte. The thick red line indicates the real development of the last 30 years. Values are smooth using a 10-year running average.

WP5 Calculation of scenarios and analysis
M5.1: Model simulations performed
Selection of sub regions
For the analysis of the results, the focus was laid on 9 sub regions (see Annex, fig. A5.1). The main sub region covers the central districts (CE/IS). Together with the rural (RU) sub region information about the magnitude of the urban heat island can be quantified. The new development areas around Seestadt Aspern was chosen (SA) to trace the change caused by

the erection of this new urban area. North Rim (NO), South Industrial (SI), South east rim (SE), were chosen as areas with high industrial coverage, which is likely to be densified, but are in suburban areas in different cardinal directions and thus exposed to different wind regimes. South Expansion (SX) is chosen as another suburban area where not urban densification but urban sprawl is likely. Further, a sub region in the west-elevated low density residential (WE) was chosen as representative for the climatological situation in the areas influenced by Wienerwald and without change in the land use. Finally, an area in the Valley of Wien (VW) shall give information about changes in this climatologically distinct area.
The differences between the analyses regions are quite small concerning the daily maximum temperature. In fig. 5.1 it can be seen, that the median value of the daily maximum temperature in all analyses regions is close to 34 °C and the maximum difference between the regions is in the order of one degree. It is also interesting that the rural area (RU) and Seestadt Aspern (SA) are hotter than the centre of Vienna (CE). This can be explained, that within the city centre, the active layer is mainly at the roofs and thus the 2 m temperature is slightly reduced compared to the unshaded rural areas. Additionally, the soil moisture was quit low in 2015, due to less than normal precipitation from the middle of May till the heat wave. This leads to a reduced transpiration cooling. This is partly not in line with reality, as some of the arable land in the surrounding of Vienna is irrigated. The main impact of the urban area is seen during the night-time. Here the city centre (CE) is clearly the warmest region with values little below 25 °C whereas the rural area has values around 22 °C. During night time also the spatial variability of the temperature is higher within the regions (~ 5 degree) compared to daytime (~ 3 to 4 degree). This can be explained by better mixing due to higher wind speeds during daytime.

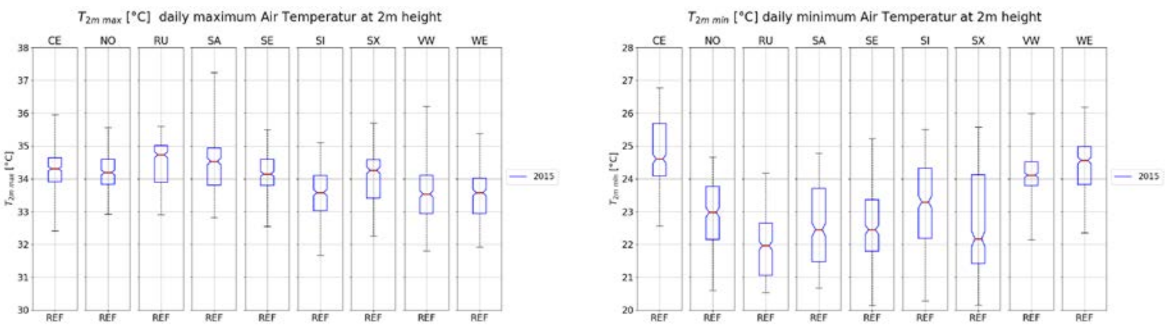

Figure 5.1 Average daily temperature maximum within the 9 analyses regions for the daily maximum temperature (left) and the daily minimum temperature (right) for the reference run 2015.

Climate and urban scenarios simulated by WRF-TEB

The results of the coupled model were stored every hour. This allows the analyses of the diurnal cycle during the heat wave period. Fig. 5.2 shows the diurnal cycle of the temperature during the heat wave 2015 for the three urban scenarios. The sprawl-run (red) is always warmer during night time as the reference run (black) and the optimized run (green) is roughly 1 degree cooler than the reference run. The higher thermal insulation (OPT) causes over the whole day a reduction of air temperature inside the canyon, which however reaches almost the temperature levels of REF and SPR scenario around noon. Nevertheless, it leads to a significant reduction of the temperature between afternoon and the early morning. The same effects may be see in the future heat episodes.

These low differences between the three urban scenarios during daytime can be seen in all subareas and also under extreme climate change conditions. Fig. 5.3 shows the ranges of the daily maximum temperature within the 9 regions for the three different urban scenarios and a 15 year heat wave for actual climate (blue) and extreme scenario for 2050 (red). The differences between the urban scenarios are in the order of a few tenth of a degree, where the optimized scenario is always the coolest. This stays constant also for future extreme heat waves.

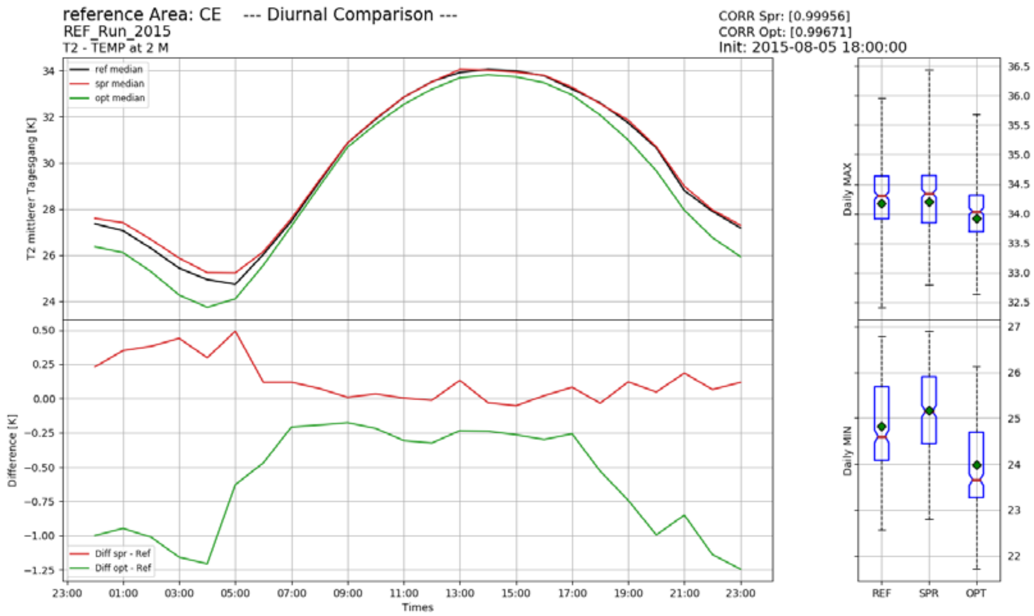

Figure 5.2 Average diurnal cycle of the temperature for the heat wave 2015 (upper left) and the corresponding boxplots for the daily maximum and minimum (right) and the three urban scenarios. The lower left shows the difference of optimized and sprawl scenario to the reference.

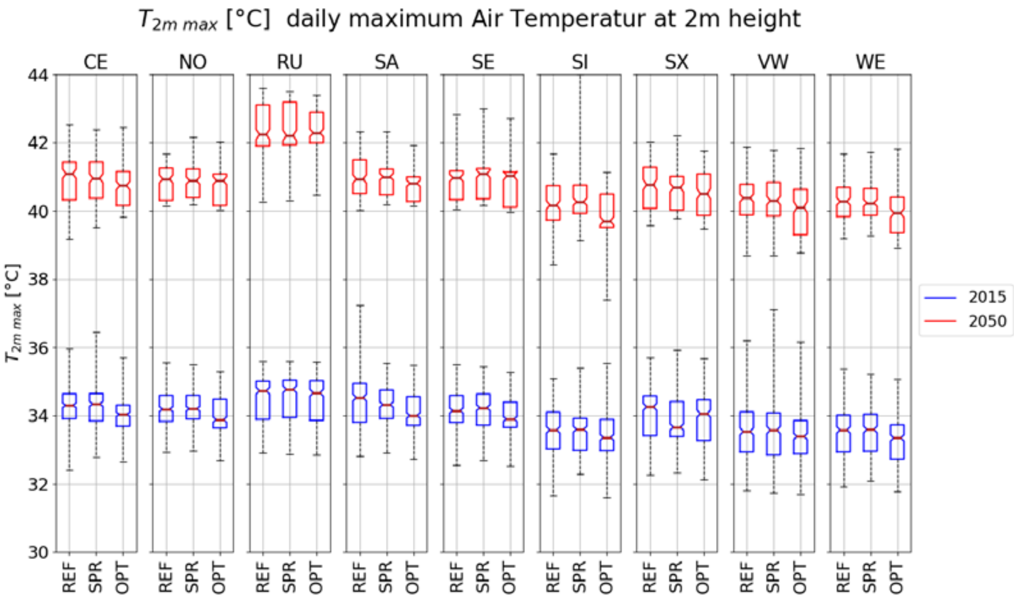

Figure 5.3 Box and Whiskery of the daily maximum temperature within the sub regions for the three different urban scenarios (REF, SPR, OPT) for the actual 15 year heat wave (blue) and in 2050 (red).

The difference between the two climate scenarios is quite extreme for the daily maximum temperature. In the actual 15 year heat wave the medians of the regions is in the order of 35 °C with maximum values of ~ 37 °C at the hottest places within the regions. In 2050 the medians are around 41 °C and at the rural area it is above 42 °C. At the hottest places even values above 43 °C are reached. The bigger difference between the rural and the city regions under climate conditions can be explained by the very try soils during this heat wave, where the transpiration cooling is more or less totally missing.

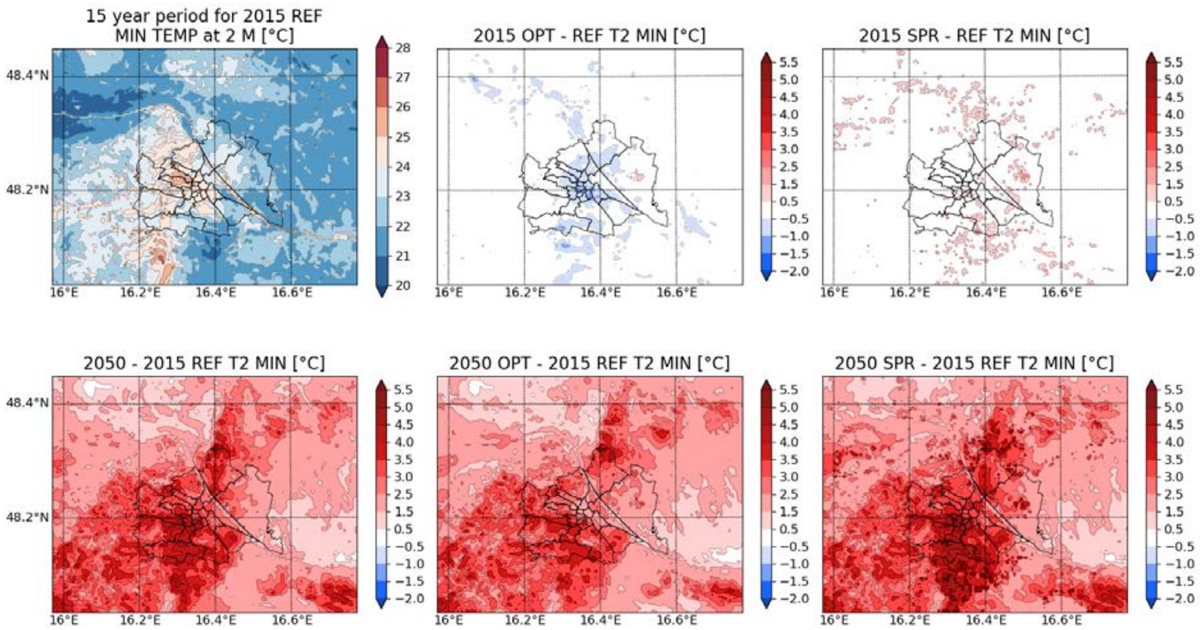

Figure 5.4 Average daily minimum temperature during the actual 15 y heat wave in Vienna (up, left) and the difference **between** the this reference to the other two urban scenarios (up) and the three urban scenarios with a 15 year heat wave in 2050.

During night time the differences between the urban scenarios are bigger as shown for the city centre in fig. 5.2. In fig. 5.4 the spatial distribution of the differences between the individual scenarios and the reference run of the actual 15 year heat wave is shown. During the actual heat wave the minimum temperatures reaches values above 25 degree within the city centre and at the border in the south and east the values are in the order of 21 °C. With the optimization of the buildings a cooling in the order of up to one degree can be reached within the city centre and large areas of the city are cooled by ~ 0.5 °C. A simple growing of the city would lead to a further warming between 0.5 to 1 °C mainly in areas where open land is converted into buildings.
The climate change scenario leads to temperature generally two degrees warmer than today, but within the city the warming in generally higher and reaches partly more than 4 degrees. With the optimized scenario this strong warming can only partly be compensated and still a warming of 3.5 °C can be seen in some regions. Without adaptation measures the warming in the city centre and in the south-west of Vienna exceeds even 5 °C.

Human thermal comfort:
Currently there are three accepted indices to assess human thermal comfort: PET, its successor mPET and UTCI. The important difference between UTCI and PET is the definition of the reference condition. PET uses a sitting person indoors with a fixed clothing, comparable to a man in a suit (Höppe, 1993). In contrast, UTCI uses a walking person, dressed according to the weather condition (Broede et al., 2012; Havenith et al., 2012).

mPET is an adaptation which uses an adaptable clothing model. Especially due to the difference in the clothing model PET is discussed to have deficiencies compared to advanced indices (Chen, 2018). This was confirmed by using Rayman (Matzarakis et al., 2007, 2010) to simulate and compare those indices at Taborstrasse/Glockengasse in Vienna. Therefore, only the UTCI was assessed using an implementation in TEB.
The UTCI was simulated using TEB offline and the meteorological condition being forced by the results using WRF-TEB. The simulation was done only for populated areas and distinguishes between a person walking in the shadow and in the sun. Results for a 15-year heatwave and the reference urban scenario are shown in fig. 5.5. In the shadow a person walking in the centre districts and at some spots in the north-east area would feel hot, but warm in the outer districts. However, in the sun this person would feel hot everywhere.
In general, it was found that a 15-year heat wave around 2050 would increase the discomfort by one category on the UTCI scale. The discomfort level in the shadow would be the same as today in the sun. In the sun this would be feeling “very hot”.

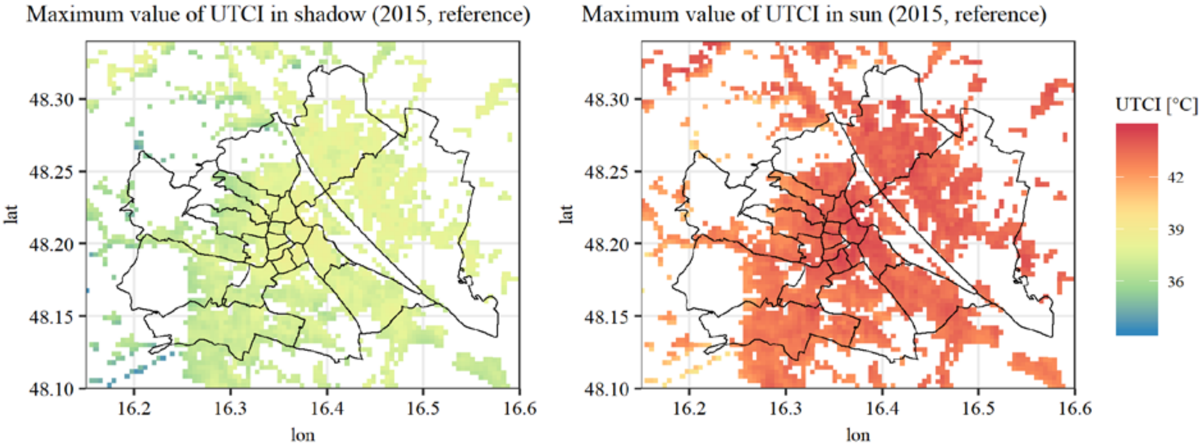

Figure 5.5 Map of the maximum UTCI in shadow (left) and in the sun (right) during a 15-year heat wave in 2015, based on the reference urban scenario.

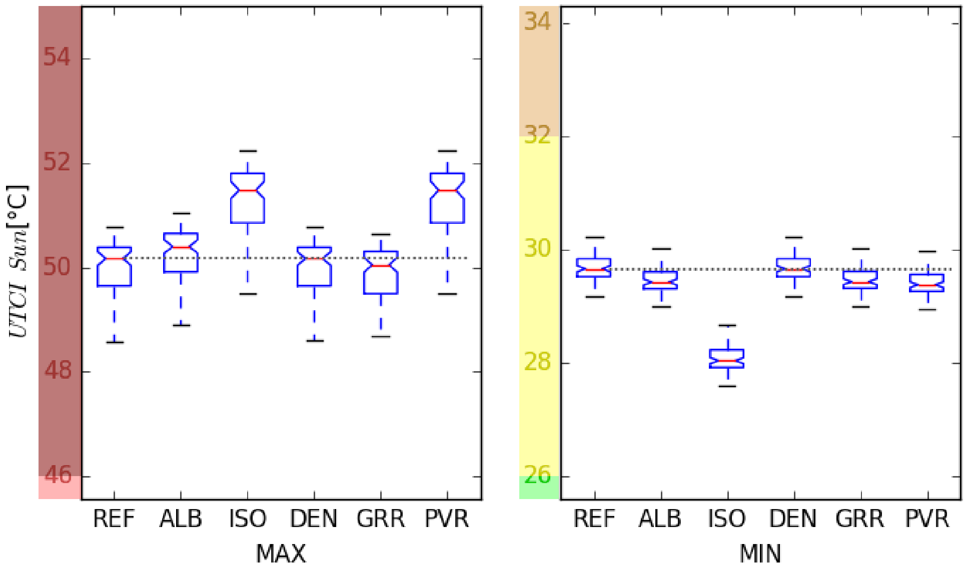

Figure 5.6 Effects of different urban planning measures on the human thermal comfort index UTCI for a person walking in the shadow during a 15-year heat wave around 2050. Effect of increased albedo (ALB), thermal insulation (ISO), building density (DEN), green roof without irrigation (GRR). Left: daily maximum, right, daily minimum.

Optimising the building materials for mitigating heat islands compared to the urban scenario "sprawl" shows a tendency for improved thermal comfort. However, the effect is very little with only about 0.5 °C on the UTCI scale. The effects of the urban building scenarios on the thermal comfort are shown in detail in fig. A5.2 and A5.3 in the appendix.
Fig. 5.6 shows the effect of the different optimisation measures used for the OPT scenario. Each of the changes (see Table 4.1) were applied independent. This showed that the main influence on the UTCI is caused by the albedo and the insulation of the building envelope.

M5.2: Final report
The final report is submitted.

M5.3: Final workshop with experts from the Vienna municipal department 22
The final workshop took place on the 26th of February 2019.at MA22. Representant of MA18, MA20, MA22 and "Klimaschutzdirektion" of city of Vienna were present. The results were presented and discussed. The outcome of the discussions will be implemented in the leaflet.

M5.4: Publication in international scientific journal
see: section 4.

M5.5: Preparation of a brochure for decision makers and for the general public

Based on the feedback from the last workshop with stakeholders of the city of Vienna (see M5.3) a brochure will be created within the next 3 months and will be downloadable on the project website ttps://urbania.boku.ac.at/

2.2.5 Description of difficulties, if any, encountered in the achievement of project targets

WP2: The data sets and studies available had different temporal categories. While the data set for Vienna on building age included many entries which only differentiated e.g. between *“Nachkriegszeit”* (1945 - 1976) and present (after 1976) from a building energy point of view (EPISCOPE Project), since the second world nearly every decade there was a change in used distinguished materials(see Annex Table A2.1 – A2.4). For the determination of dominant types, the categories of EPISCOPE were used.
Another problem posed the years appearance of the data sets. While certain data sets have no or a very long update cycle (10 years or longer), others are updated on a regular basis up to 4 times a year. It was tried to focus on as few datasets as possible to avoid errors of different data achievement dates.
The building age data set did not cover large parts of presumably newer building areas. At one point in the future several categories of the “*Realnutzungskartierung”* will be dominated by buildings of newer building age, which corresponds with changed thermal response, therefore an updated data set for future simulation is of even greater importance.
The coupling of the WRF and TEB model was much more effort as expected. Information gained from literature of coupling TEB with other limited area models, only partly could be used for the coupling with WRF.

WP3: It was not possible to install the instrumentation needed for the precise validation of the energy fluxes calculated by TEB and WRF at three sites in Vienna. We visited several sites and short-listed the bunker close to the Luftmessnetzstation Gerichtsgasse to measure the canyon energy fluxes at two levels. Through legal difficulties, we were not allowed to access the site, so we changed our concept and installed the full setup close to our Institute. To densify the air and humidity temperature information at street level within Vienna to validate simulations of temperature distribution of our models, we installed 8 additional simpler stations at different urban structure types in Vienna.

2.2.6 Description of project “highlights”

- Comparison of simulated radiation balance of TEB and measured radiation correlated with R^2=0.96
- Comparison of the high resolution model (0.5 m) SOLWEIG and TEB yielded very good results

- First WRF runs showed that the absolute air temperature values show good agreement to the gridded INCA Data set based on measurements (fig. 5.1).
- The analyses of the coupled WRF-TEB run show a very realistic representation of the UHI within Vienna. This increases the reliability of results from the different urban scenarios.
- The analyses of heat wave indicators from observations show a very strong trend within the last 3 decades. The 5 day average of the maximum temperature of the hottest heat wave of the year increased by 2 degree within this period.

2.2.7 Description and motivation of deviations from the original project application

Priority was given to the accuracy of the WRF-TEB simulations. We discovered a shift of land use due to a wrong projection of land use GIS information in the WRF grid. We had to repeat the WRF simulations. Instead of calculating explicit scenarios for the time frames around 2030 and 2050 we have been able to calculate the climate change signals for heat waves with different intensities (from 2 years up to 30 years return period) for the 2 emission scenarios and the two time frames. So for every emission scenario, heat wave intensity and any arbitrary time frame from now till 2050 the average 5 day temperature of the heat wave can be constructed using the actual respective temperature and the climate change signal. We explicitly calculated the actual heat wave with 2 and 15 years return period and heat waves with the same frequency in 2050 according to the most extreme trend within the ÖKS 15 ensemble. Thus we have the possible worst case till mid-century and 3 more moderate realizations which can be used as examples for different return periods/ time frame/ combinations that give the same change in heat wave temperature.
Since urban scenarios were of utmost importance and climate change until 2030 was less interesting than the 2050 period, we skipped - because of time shortage - the simulations for the 2030 period.

2.3 Conclusions to be drawn from project results (max. 5 pages)

– Which findings have been derived from the project by the project team?

The coupled WRF/TEB model is a useful tool to investigate the interaction between urban and urban hinterland interactions. The comparison with measurements showed a good agreement.
A weakness within the WRF model, is the representation of the agricultural area surrounding the city of Vienna. The used NOAH land use scheme do not allow irrigation or different crop rotation systems or access of plants to ground water. Thus the evapotranspiration is partly underestimated at these agricultural areas, which leads to higher maximum temperatures

The different urban scenarios have a clear impact on the thermal structure within the city of Vienna. These impacts are minimal during daytime and maximal during nigh time. The adaptation measures analysed in the scenarios can reduce the night time temperature in the order of one degree and more for the whole city centre, and in large parts of the city of Vienna the cooling reaches 0.5 °C (see fig. 6). This cooling potential of the measures stays constant in the climate change scenarios.

The observed trend in the average maximum temperature during 5 day heat waves is much higher than for the annual mean temperature for the same period and even for the summer temperature. This is also true for the climate change scenarios. The scenario analyses even shows, that the warming trend is higher for more extreme heat waves (see Table A4.1 in Annex).

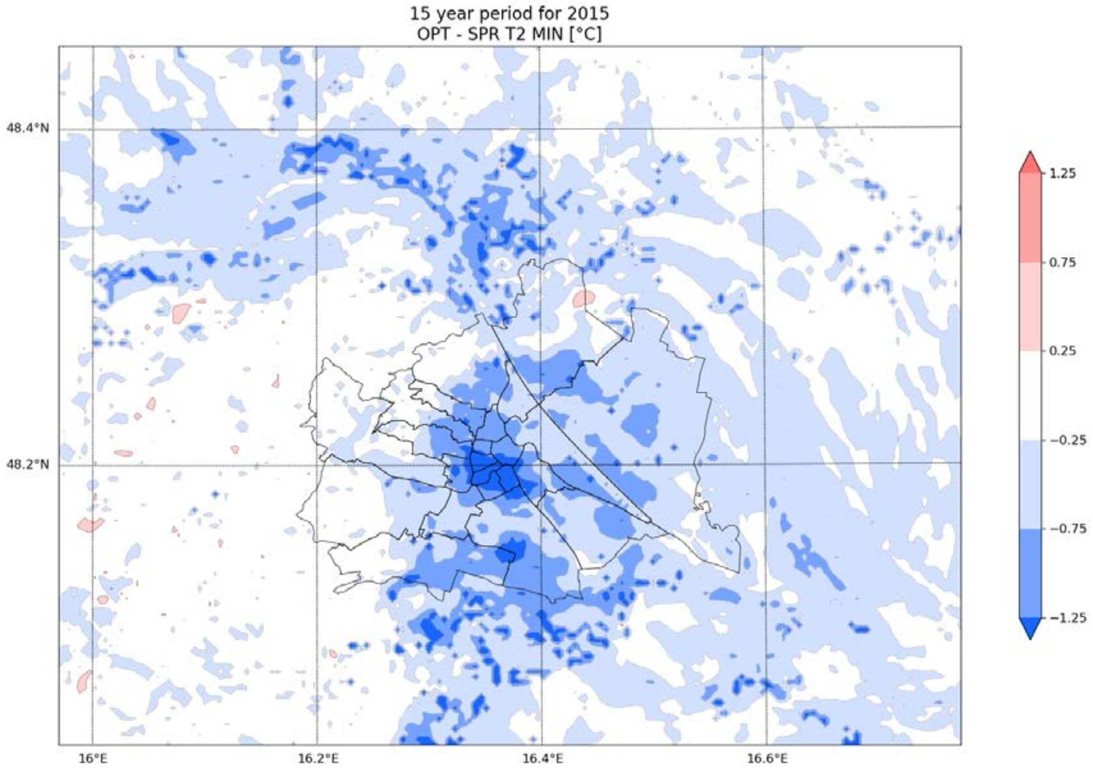

Figure 6 Difference in the average daily minimum temperature during the actual 15 y heat wave between the optimized and the sprawl scenario.

The temperature increase due to climate change is much larger than the influence of urban planning. Worst case climate change scenarios show an increase in air temperature of up to 5 °C until 2050.

Which further steps will be taken by the project team on the basis of the results obtained?

+ Implementing a more realistic representation of the agricultural areas around Vienna in the land use scheme of WRF

+ For soil humidity the yet experimental 1km SCATSAR-SWI data set, which combines Sentinel-1 and MetOp ASCAT (advanced scatterometer) data and is developed by the Department of Geodesy and Geoinformation of the TU Wien will be tested.

+ An automated update of geodata would be very helpful for future urban simulations to be able to rapidly take into account new building development.

+ Create a map of anthropogenic sensible and latent heat fluxes caused by traffic and industry and include them in model simulations. (Global map res ~1km existing?! David)

+ Prepare data sets derived from "Solardachpotentialkataster" and "Gründachpotentialkataster" to create realistic model input

+ Influence of HVAC systems.

- Effects of waste heat
- Impact on electricity demands in extreme heat periods

+ Impact of more effective green roofs with irrigation as well as irrigation of agricultural areas around Vienna on the urban climate during heat waves.

+ Investigate potential negative effects of mitigation measures on air chemistry, as no decrease of NOx emissions is expected (-> according to JP):

- Effect of changes in urban boundary height/lability due to higher surface temperatures on concentration of atmospheric pollutants.
- Effect of increased radiation caused by mitigation measure albedo increases on tropospheric ozone production (was investigated, but not for Vienna)

+ Within this project only a first overview of the vast possibilities is given. More detailed spatially varied scenarios / recommendations ought to be developed together with urban planners and simulated. Maybe in collaboration with the INKA network.

+ Possibilities for waste heat reduction and conversion as measures for heat island mitigation.

– Which other target groups can draw relevant and interesting conclusions from the project results and who can continue working on that basis?

Other modelling groups can draw conclusions from our experience coupling WRF.
The coupled version will be made available from the URBANIA homepage.
Urban planners and planning institutions can use the simulations and the meteorological fields created with WRF to perform even smaller scale simulations for smaller districts using more detailed building elevation maps.

For the greater area of Vienna maps of land cover zone, sky view factor, albedo, width to height ratio of the streets, physical properties of the buildings (emissivity factor, thermal conductivity, specific heat capacity), and ratio of sealed surfaces are available for the present situation and for future urban plan scenarios. Climate maps for previous heat episodes and previous time periods (2015 and 2017) as well as for future heat episodes as a function of urban planning scenarios are available.

2.4 Work and time schedule (max. 2 pages)

– Presentation of the final work and time schedule

	Month 1-4	Month 5-8	Month 9-12	Month 13-16	Month 17-20	Month 21-24	Month 25-30
WP1							
WP2							
WP3							
WP4							
WP5							

– Explanations of deviations, if any, from the original work and time schedule contained in the project application

The project was prolonged for 6 month to obtain longer measurement time series and more time for the model simulations.

2.5 Annex

All scientific publications resulting from the ACRP project have to be included in the annex. Furthermore, a list of planned, but not yet released publications has to be included (indicate, title, abstract, journal, date of submission, etc).

Any supplementary information, which is necessary to complete the final report but cannot be included in the main body of the report on account of its volume, is to be presented in the Annex.

This includes studies (possibly as a “final product” of the project itself), **test reports, publications, guidelines produced, training material, etc.**

The bibliography, the list of photographs/diagrams and the list of tables are to be included in the Annex, if relevant to the project.

REFERENCES:

Amtmann M and Altmann-Mavaddat N (2014) Eine Typology österreichischer Wohngebäude, Österreichische Energieargentur – Austrian Energy Agency, TABULA/EPISCOPE

Bechtel B, Alexander P, Böhner J, et al (2015) Mapping Local Climate Zones for a Worldwide Database of the Form and Function of Cities. ISPRS Int J Geo-Inf 4:199–219. doi: 10.3390/ijgi4010199

T. Berger, H. Formayer, R. Smutny, C. Neururer, R. Passawa (2012) Auswirkungen des Klimawandelsauf den thermischen Komfort in Bürogebäuden, Berichte aus Energie- und Umweltforschung

Bröde, P., Fiala, D., Błażejczyk, K. et al. (2012). Deriving the operational procedure for the Universal Thermal Climate Index (UTCI). Int J Biometeorol 56: 481. https://doi.org/10.1007/s00484-011-0454-1

Chen Y.C. and Matzarakis A (2018) Modified physiologically equivalent temperature – basics and application for western European climate. Theor. Appl. Climatol. 132, 1275 – 1289. https://doi.org/10.1007/s00704-017-2158-x

Cordeau, Erwan / Les îlots morphologiques urbains (IMU) / IAU îdF / 2016

Corine land cover data set 2012, https://land.copernicus.eu/pan-european/corine-land-cover , last access: 2018.05.23.

Dong, Y., Varquez, A. C. G., & Kanda, M. (2017). Global anthropogenic heat flux database with high spatial resolution. Atmospheric Environment, 150, 276–294. https://doi.org/10.1016/j.atmosenv.2016.11.040

Fallmann, J., Forkel, R., & Emeis, S. (2016). Secondary effects of urban heat island mitigation measures on air quality. Atmospheric Environment, 125, 199–211. https://doi.org/10.1016/j.atmosenv.2015.10.094

Fisher R., Tippett L. (1928), Limiting forms of the frequency distributions of the largest or smallest meber of a sample. Proc Camb Philos Soc 24: 180-190.

Flughafen Wien Schwechat – 3te Piste (as sealed surface // barren and unvegetated) (https://www.viennaairport.com/unternehmen/flughafen_wien_ag/3_piste/bauprojekt_3_piste last access: 18.6.2018)

Havenith G, Fiala D, Blazejczyk K, Richards M, Bröde P, Holmér I, Rintamäki H, Benshabat Y, Jendritzky G. The UTCI-clothing model. Int J Biometeorol 56-3: 461-470, 2012.

Höppe P.R. (1993) Heat balance modelling. Experientia 49(9): 741 – 746. https://doi.org/10.1007/BF01923542

LEP 2011, Landesentwicklungsgrogramm Burgenland LEP 2011 – Raumordnung Burgenland.

Lindberg, Fredrik, Björn Holmer, and Sofia Thorsson 2008: SOLWEIG 1.0 – Modelling Spatial Variations of 3D Radiant Fluxes and Mean Radiant Temperature in Complex Urban Settings. International Journal of Biometeorology 52(7): 697–713.

MA 18 (2005) STEP05 – Stadtentwicklungsplan 2005

MA 18 (2011) Siedlungsformen für die Stadterweiterung

MA 18 (2012) Smart City Wien - Vision 2050, Roadmap for 2020 and beyond, Action Plan for 2012-15

MA 18 (2014a) Smart City Wien - Rahmenstrategie

MA 18 (2014b) Stadtentwicklungsplan STEP 2025, www.step.wien.at

MA21 (2013) Strategieplan für das Zielgebiet U2 – Donaustadt

MA23 (2013) kleinräumige Bevölkerungsprognose für Wien

Masson V (2000) A physically-based scheme for the urban energy budget in atmospheric models. Bound-Layer Meteorol 94:357–397. doi: 10.1023/A:1002463829265

Matzarakis, A.; Rutz, F.; and Mayer, H., 2007: Modelling radiation fluxes in simple and complex environments - application of the RayMan model. International Journal of Biometeorology 51(4), 323–334. doi: 10.1007/s00484-006-0061-8.

Matzarakis, A.; Rutz, F.; and Mayer, H., 2010: Modelling radiation fluxes in simple and complex environments: basics of the RayMan model. International Journal of Biometeorology 54(2), 131–139. doi: 10.1007/s00484-009-0261-0.

Morini, E., Touchaei, A., Castellani, B., Rossi, F., & Cotana, F. (2016). The Impact of Albedo Increase to Mitigate the Urban Heat Island in Terni (Italy) Using the WRF Model. Sustainability, 8(10), 999. https://doi.org/10.3390/su8100999

Nadeem, I. and Formayer, H. (2015): Regionales Klimaszenario basierend auf dem GFDL-CM3 RCP 8.5 Lauf In: Climate Change Center Austria, Tagugsband 16. Klimatag Aktuelle Klimaforschung in Österreich

Loibl W., Giffinger, R., Sedlacek S., Kramar H., Schuh B.: „STAU-Wien“, Stadt-Umlandbeziehungen in der Region Wien: Siedlungsentwicklung, Interaktionen und Stofflüsse, Endbericht Teil A, Seibersdorf research Report, ARC---S-0181a, BV, 67pp., September 2008.

PGO (2009), Fassmann H, Görgl P, Helbich M, Atlas der wachsenden Stadtregion

PGO (2011) stadtregion +, Planungskooperation zur räumlichen Entwicklung der Stadtregion Wien Niederösterreich Burgenland.

PGO (2017), P. Görgl, J. Eder, E. Gruber, H. Fassmann, Monitoring der Siedlungsentwicklung in der Stadtregion+, Strategien zur räumlichen Entwicklung der Ostregion, ÖAW – Institut für Stadt- und Regionalforschung, Modul 5 Raumforschung und Raumkommunikation

Stewart ID, Oke TR (2012) Local climate zones for urban temperature studies. Bull Am Meteorol Soc 93:1879–1900.

Trusilova, K., M. Jung, G. Churkina, U. Karstens, M. Heimann, and M. Claussen, 2008: Urbanization impacts on the climate in Europe: Numerical experiments by the PSU–NCAR Mesoscale Model (MM5). J. Appl. Meteor. Climatol., 47, 1442–1455

Trusilova, K., M. Jung, and G. Churkina, 2009: On climate impacts of a potential expansion of urban land in Europe. J. Appl. Meteor. Climatol., 48, 1971–1980.

Trusilova, K., B. Früh, S. Brienen, A. Walter, V. Masson, G. Pigeon, and P. Becker, 2013: Implementation of an Urban Parameterization Scheme into the Regional Climate Model COSMO-CLM. J. Appl. Meteor. Climatol., 52, 2296–2311, https://doi.org/10.1175/JAMC-D-12-0209.1

Umweltbundesamt 2017, Bodenversiegelung, http://www.umweltbundesamt.at/umweltsituation/raumordnung/rp_flaecheninanspruchnahme/bodenversiegelung/ last access: 2018.07.17

Umweltbundesamt 2018, Flächeninanspruchnahmein Österreich 2017, http://www.umweltbundesamt.at/fileadmin/site/umweltthemen/raumplanung/Pdfs/Flaecheninanspr_2017.pdf, last access: 2018.07.17

Weihs, P., Zamini S., S. Krispel, S. Oswald, M. Peyerl, M. Revesz, A. Schneider, H. Trimmel: Optimierung reflektierender Materialien und Photovoltaik im Stadtraum bezüglich Strahlungsbilanz und Bioklimatik (PVOPTI-Ray), Berichte aus Energie- und Umweltforschung 18/2018 Nachhaltig wirtschaften, Bundesministerium für Verkehr, Innovation und Technologie, Wien, 2018.

Additional Figures and Tables:

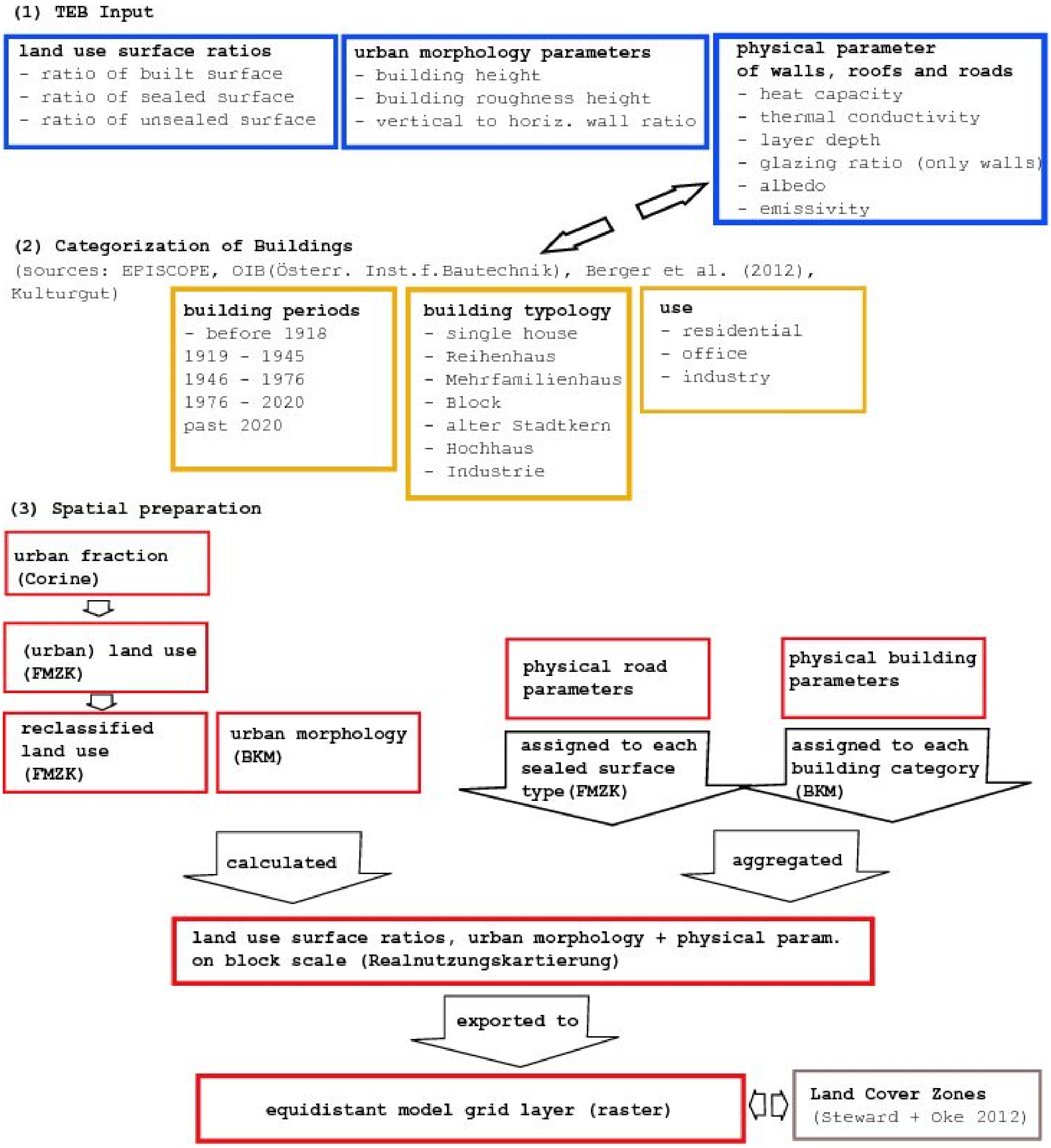

Figure A2.1 Schematic method of deriving the urban morphology, land use surface ratios and physical parameters for TEB

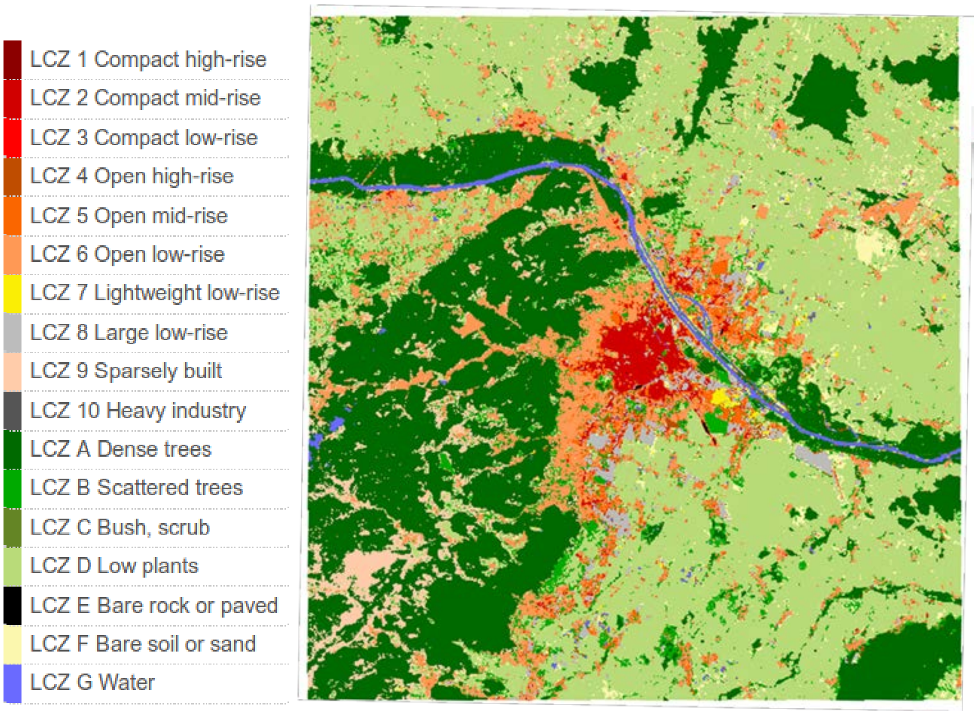

Figure A2.2 Land Cover Zones of Vienna derived using the methodology of WUDAPT

Tabelle A2.1: Materialcharacteristics of buildings – roof and ceiling

	Einfamilienhaus	Reihenhaus	Mehrfamilienhaus	Mehrgeschossige Wohnbauten
until 1919	**0.45 (Holzbalkendecke + D)**	**1.05 (Holzbalkendecke + D)**	**0.45 (Holzbalkendecke + D)**	**0.51 (Dippelbaumdecke, Beschüttung)**
1920 - 44	2.1 (Stahlbeton, Beschüttung, Estrich)	1.05 (Holzbalkendecke, Beschüttung)	0.9 Holzbalkendecke, Beschüttung, Hobeldielen	0.68 Holzbalkendecke, Dämmung
1945-1959	0.49 Holzbalkendecke, Beschüttung, Dämmung, Estrich	1.35 Holzbalkendecke, Dämmung	0.9 Ziegelholkörper, Estrich	0.9 Stahlbeton, Dämmung
1960 -1979	0.2 (Stahlbeton, Beschüttung, Estrich)	1.5 Stahlbeton, Beschüttung, Dämmung	0.94 Stahlbeton, Beschüttung, Dämmung	1.83 Stahlbeton, Beschüttung, Dämmung
1980-1989	0.25 (Betonhohlkörper, Dämmung, Estrich)	1.18 Stahlbeton, Dämmung, Estrich	0.26 Zangendecke, Glaswolle	0.4 Hohlkörper, Beschüttung, Estrich
1990-1999	0.15 Sparrendach +D	0.25 Stahlbeton, Dämmung, Estrich	0.32 Sparrendach +D	0.3 Stahlbeton, Dämmung, Estrich
2000- 2020	0.17 Flachdach als Umkehrdach	0.17 Flachdach als Kaltdach	0.17 Fertigteildecke+D	0.2 Sparrendach, Dämmung
Ab 2020:	0.1 Massivholz-Flachdach als Warmdach	0.08 Doppel-T-Träger-Flachdach	0.08 Sparrendach + D	0.1 Stahlbetondecke+ D

*D, WD = Wärmedämmung, VS = Verbundsystem

Tabelle A2.2: Materialcharacteristics in the building– U-valued [W/m2K] fassade

	Einfamilienhaus	Reihenhaus	Mehrfamilienhaus	Mehrgeschossige Wohnbauten
until 1919	1.9 (Vollziegel)	1.20 (Ziegelmauerwerk, Putz)	1.4 Ziegelmauerwerk, verputzt	1.1 Ziegelmauewerk, Putz
1920 - 44	0.8 (Vollziegel-Mauerwerk, Dämmung)	1.2 (Vollziegel-Mauerwerk, Dämmung)	1.4 Vollziegelmauerwerk	1.16 Vollziegel Mauerwerk
1945-1959	1.23 (Vollziegel)	1.35 Vollziegel	1.2 Hohlbockstein	0.9 Betonhohlstein + D
1960 -1979	0,90 Betonholblockstein + D	1.4 Hochlochziegel Mauerwerk	1.31 Betonhohlblockstein	0.36 Stahlbetonfertigteil + WD VS
1980-1989	1.24 Schlackenbeton+D	0.80 Hochlochziegel	0.5 Fertigteilbeton + D	0.67 Betonhohlblockstein + D
1990-1999	0.25, Holzriegelwand gedämmt, hinterlüftete Fassade	0.49 Lecahohlblockstein mit WD	0.56 Blähton Wandsteine, Putz	0.73 Betonhohlblockstein + D
2000- 2020	0.16, vorgefertigte Holzsystemwand	0.22 Ziegel, WD VS / Stahlbeton- Wand XPS	0.16 Blähton Wandsteine +D	0.27 vorgefertigte Holzsystemwand
Ab 2020:	0.08, Holzständerwand verputzt	0.12, Holz-Fertigteilwände	0.1 Brettstapel-Außenwand, hinterlüftet	0.1 Hochlochziegelwand +D

*D, WD = Wärmedämmung, VS = Verbundsystem

Table A2.3: Materialcharacteristics in the building – windows

	Einfamilienhaus	Reihenhaus	Mehrfamilienhaus	Mehrgeschossige Wohnbauten
until 1919	2.5 (Kastenfenster, Einfachverglasung)	2.2 (Kastenfenster, Einfachverglasung)	1.68 (Kastenfenster, Einfachverglasung)	3.1 Kastenfenster, Einfachverglasung
1920 - 44	1.55 (Kunststoff Isolierverglasung)	2.24 (Kastenfenster, Einfachverglasung)	1.55 Kastenfenster	2.3 Kastenfenster, Einfachverglasung
1945-1959	1.98 (Kunststoffverbund)	1.99 Holz Isolierverglasung	2.5 Holzverbundfenster	2.3 Holzverbundfenster
1960 -1979	2.54 (Kunsstoffverbund)	2.28 Holzverbundfenster	1.14 Holzfenster, Isolierverglasung	1.4 Holzfenster, Isolierverglasung
1980-1989	1.5 (Isolierverglasung Kunststoffrahmen)	2.1 Isolierverglasung Kunststoffrahmen	2.39 Kunststoffverbundfenster	1.95 Isolierverglasung
1990-1999	1.8 (Holzfenster Isolierverglasung)	1.38 Kunststoff Isolierverglasung	1.51 Kunststoff Isolierverglasung	1.66 Kunststoff Isolierverglasung
2000- 2020	1.4 (Kunsttoffenster Wärmeschutzverglasung)	1.2 Kunststoff Isolierverglasung	1.1 Kunststofffenster Wärmeschutzverglasung	0.4 Kunststoff Isolierverglasung
Ab 2020:	0.7 (Passivhausfenster)	0.7 (Passivhausfenster)	0.7 Kunststofffenster Wärmeschutzverglasung	0.15 Kunststofffenster Wärmeschutzverglasung

*D, WD = Wärmedämmung, VS = Verbundsystem

Table A2.4: Materialcharacteristics in the building –floors

	Einfamilienhaus	Reihenhaus	Mehrfamilienhaus	Mehrgeschossige Wohnbauten
until 1919		0.9, Kappendecke auf Stahlträger,Beschüttung, Holzfussboden	2.1 Stahlbeton	0.95 Ziegelgewölbe, Beschüttung
1920 - 44		0.9 Stahlbeton, Dämmung, Estrich	1.05 Stahlbeton, Beschüttung, Estrich	1.05 Stahbeton, Dämmlange, Estrich
1945-1959		1.95, Stahlbeton, Beschüttung, Dämmung, Estrich	1.05 Stahbeton, Dämmlange, Estrich	1.07 Stahlbeton, Beschüttung, Dämmung, Estrich
1960 -1979		1.5 Stahlbeton, Dämmung, Estrich	1.23 Stahlbeton, Beschüttung, Dämmung, Estrich	1.4 Stahlbeton, Beschüttung, Dämmung, Estrich
1980-1989		0.62 Stahlbeton, Trittschalldämmung, Estrich	0.63 Stahlbeton, Trittschalldämmung, Estrich	0.36 Hohlkörper, Beton, Dämmung
1990-1999	0.59, Stampfbeton, Dämmung, Estrich	0.4 Stampfbeton, Dämmung, 3,2Estrich	0.44 Stahlbeton, Dämmung, Estrich	0.39 Stahlbeton, Beschüttung, Dämmung, Estrich
2000- 2020	0.21, Fertigteildecke +WD	0.32 XPS, Stahlbeton, Schüttung, Trittschalldämmung	0.21 Fertigteildecke + WD	0.4 Stahlbeton, Dämmung, Estrich
Ab 2020:	0.1 , Fertigteildecke +WD	0.1 , Fertigteildecke +WD	0.1 Fertigteildecke + WD	0.15 Stahlbeton, Dämmung, Estrich

*D, WD = Wärmedämmung, VS = Verbundsystem

Table A2.5: List of dominant types

1 locker bebautes Wohn(misch)gebiet	**RH**	**vor 1919**
2 Gartenstadt	RH	1920 - 1944
3 dichtes Wohn(misch)gebiet	MGV	vor 1919
4 großvolumiger solitärer Wohn(misch)bau	RH	vor 1919
5 Büro- und Verwaltungsviertel	MGV	vor 1919
6 solitäre Handelsstrukturen	Büro	vor 1919
7 Geschäfts- Kern- u. Mischgebiete	MGV	vor 1919
8 Mischnutzung wenig dicht	MGV	vor 1919
9 Industrie prod. Gewerbe Großhandel inkl. Lager	Industrie	vor 1919
10 Kultur Freizeit Messe	Altstadt	vor 1919
11 Gesundheit und Einsatzorg.	Altstadt	vor 1919
12 Bildung	MGV	vor 1919
13 Sport und Bad (Indoor)	Industrie	vor 1919
14 Militärische Anlagen	MGV	vor 1919
15 Kläranlage Deponie	Industrie	vor 1919
16 Energieversorgung u. Rundfunkanlagen	Büro	vor 1919
17 Wasserversorgung	0	0
18 Transformationsfläche Baustelle Materialgew.	0	0
19 Straßenraum begrünt	0	0
20 Straßenraum unbegrünt	0	0
21 Parkplätze u. Parkhäuser	0	0
22 Bahnhöfe und Bahnanlagen	Industrie	vor 1919
23 Transport und Logistik inkl. Lager	Altstadt	vor 1919
24 Park Grünanlage	Altstadt	vor 1919
25 Sport und Bad (Outdoor) Camping	0	0
26 Friedhof	0	0
27 Acker	0	0
28 Weingarten	0	0
29 Gärtnerei Obstplantagen	0	0
30 Wald	0	0
31 Wiese	0	0
32 Gewässer inkl. Bachbett	0	0

Table A2.6: Urban parameters extracted for the LCZs

	LCZ NAME	PERCENTAGE OF LCZ OF TOTAL URBAN AREA WITHIN ROI	BUILT	SEALED FRAC. OF UNBUILT	HEIGHT	SVF	VERT/HOR AREA
2	Compact mid-rise	7.0%	0.4	0.16	14.6	0.48	2.5
4	Open high-rise	2.4%	0.74	0.52	20.6	0.65	0.9
5	Open mid-rise	9.4%	0.2	0.38	19.2	0.57	1.1
6	Open low-rise	44.7%	0.15	0.55	5.9	0.61	0.64
7	Lightweight low-rise	1.4%	0.37	0.65	3	0.62	0.3
8	Large low-rise	9.4%	0.37	0.21	7.3	0.62	0.73
9	Sparsely built	25.7%	0.03	0.65	3.7	0.62	0.3

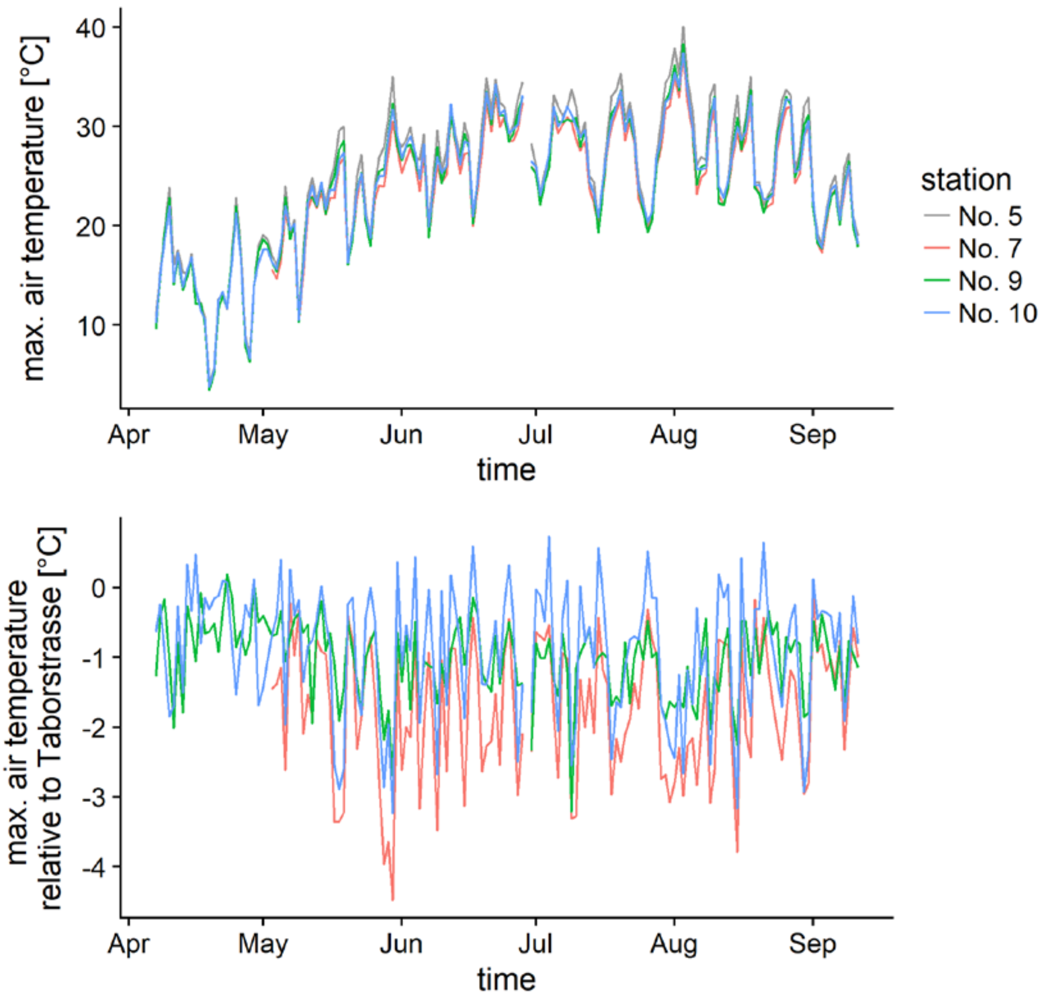

Figure A3.1 Difference in maximum temperature for stations 5 (Taborstraße), 7 (Arenawiese, Prater), 9 (Belgradplatz) and 10 (Gerichtsgasse)

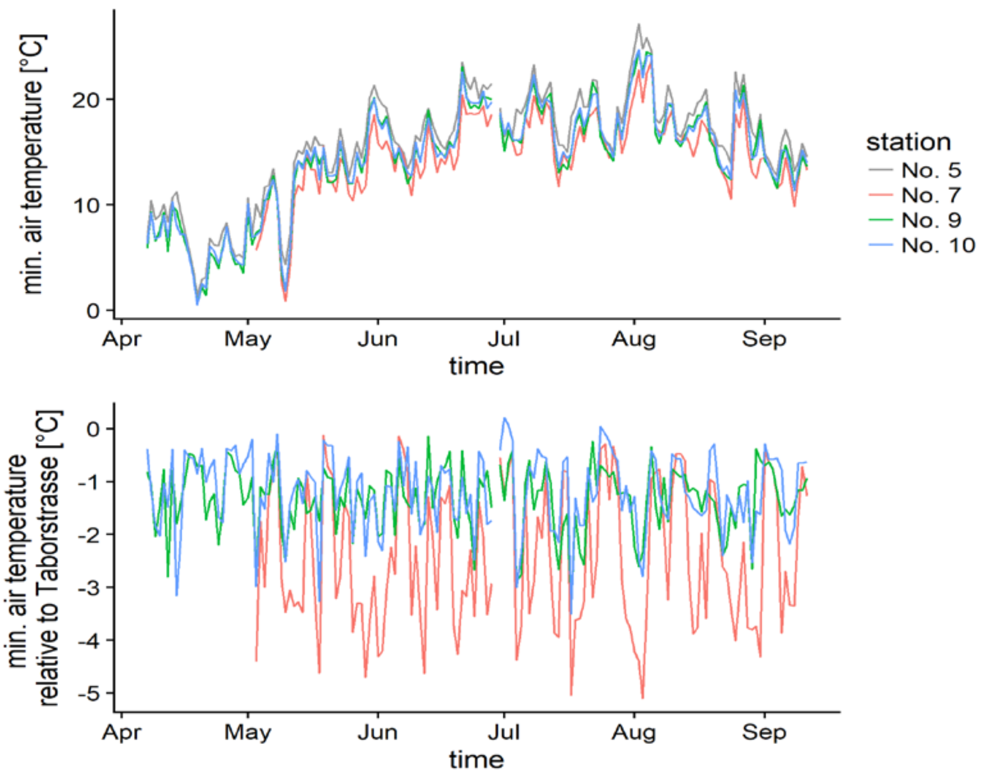

Figure A3.2 Difference in minimum temperature for station 5 (Taborstraße), 7 (Arenawiese, Prater), 9 (Belgradplatz) and 10 (Gerichtsgasse)

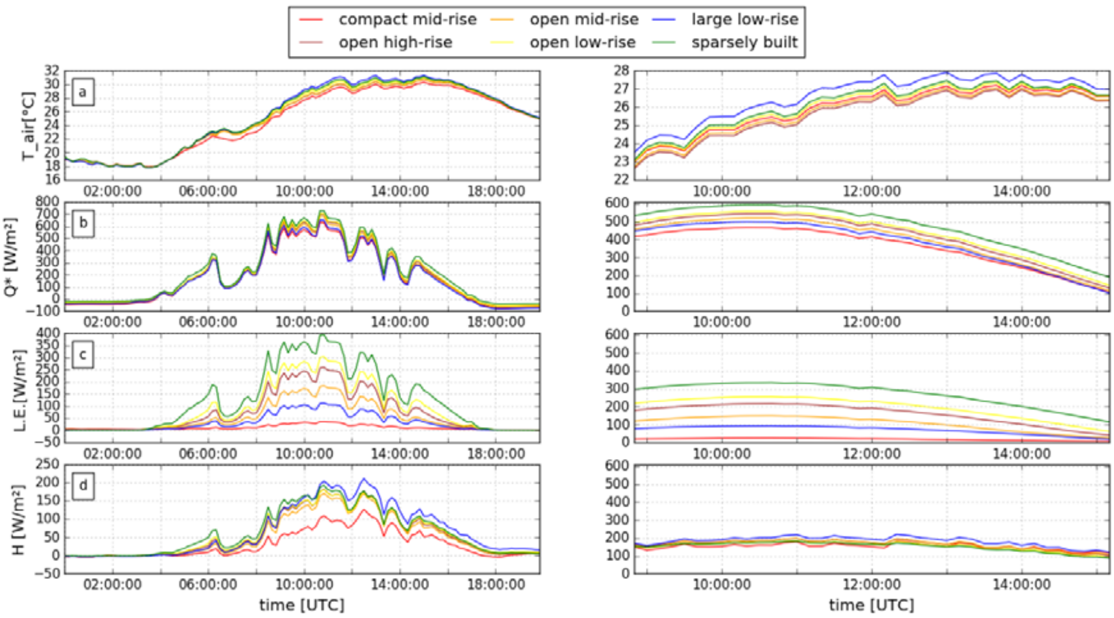

Figure A3.3 TEB simulation of (a) canyon temperature, (b) radiation balance, (c) latent and (d) sensible heat flux for the 24 August 2016 (diurnal range, left) and (around midday, right) for the average values of the dominant LCZ of Vienna: Compact mid-rise, open high-, mid- and low-rise, large low-rise and sparsely built.

Figure A3.4 Comparison of absolute net radiation measured by CNR4 and simulated by TEB (upper panel) and the difference between measurement and simulation (lower panel).

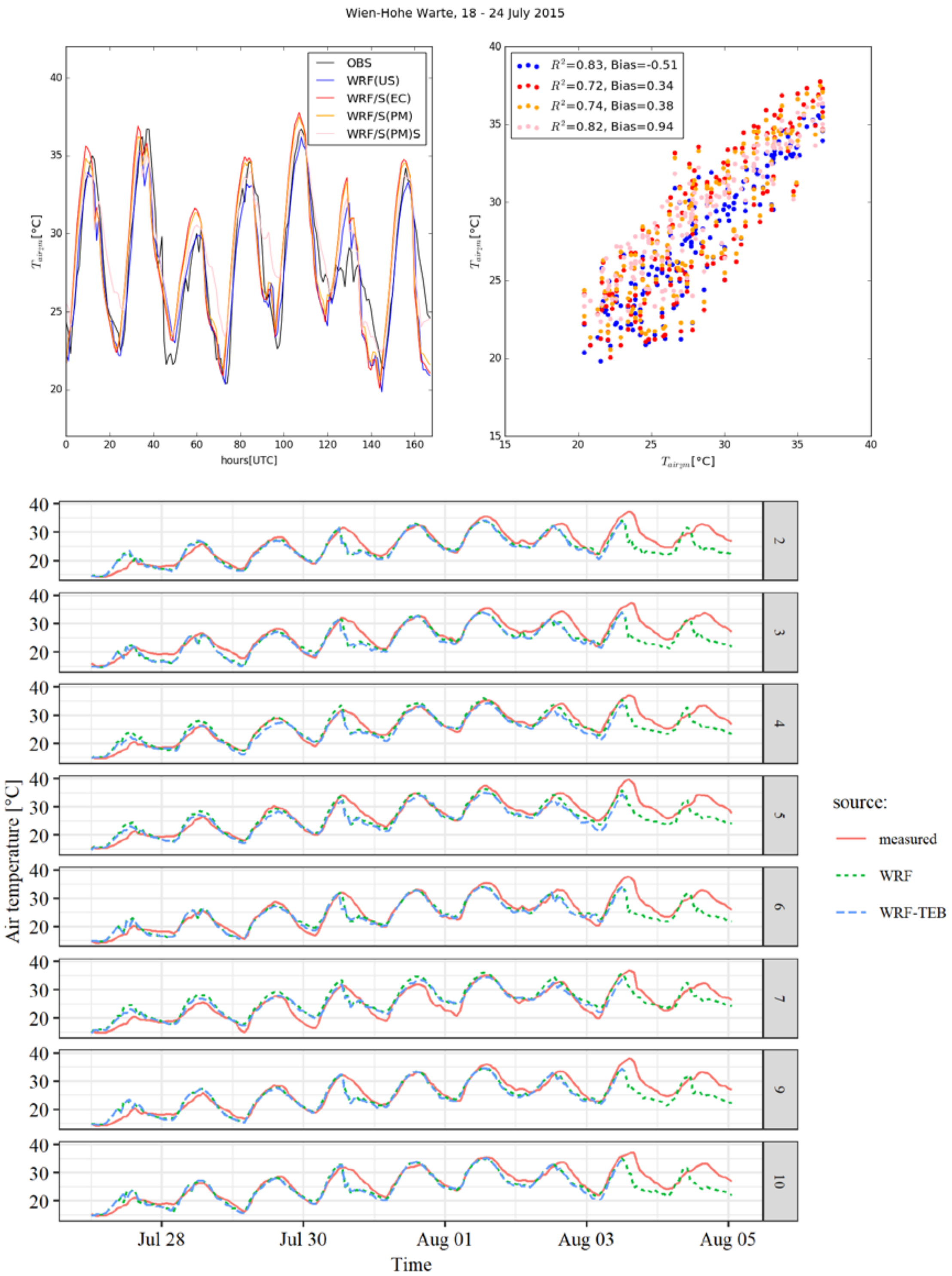

Figure A3.5 a) Temporal comparison of ZAMG observations at Wien Hohe Warte with WRF and TEB forced by WRF model results for the 18 - 24 July 2017, b) own measurements compared to WRF and WRF-TEB for 27 July – 5 August 2017. The locations are: 2 – Kendlerstraße, 3 – Hausgrudweg (Stadlau), 4 – Borschkegasse (AKH), 5 – Taborstraße, 6 – Liesing, 7 – Arenawiese (Prater), 9 – Belgradplatz, 10 – Gerichtsgasse.

Table A4.1: Average 5-day temperature maximum for heat waves and climate change signal for ensemble median of RCP 4.5 and 8.5 and the most extreme model per period.

Period	2 year	5 year	10 year	15 year	20 year	30 year
1988-2017 (obs)	31.6	35.41	36.25	36.30	36.91	37.23
2016-2045 (RCP4.5, median)	0.61	1.26	1.79	2.05	2.16	1.9
2016-2045 (RCP8.5, median)	0.7	0.86	1.24	1.33	1.37	1.37
2016-2045 (RCP8.5, extreme)	2.28	1.99	2.29	2.81	3.27	3.92
2036-2065 (RCP4.5, median)	1.53	1.84	1.84	2.09	2.25	2.31
2036-2065 (RCP8.5, median)	1.78	2.12	2.31	2.64	2.82	3
2036-2065 (RCP8.5, extreme)	5.05	6.03	6.55	6.77	6.93	7.11

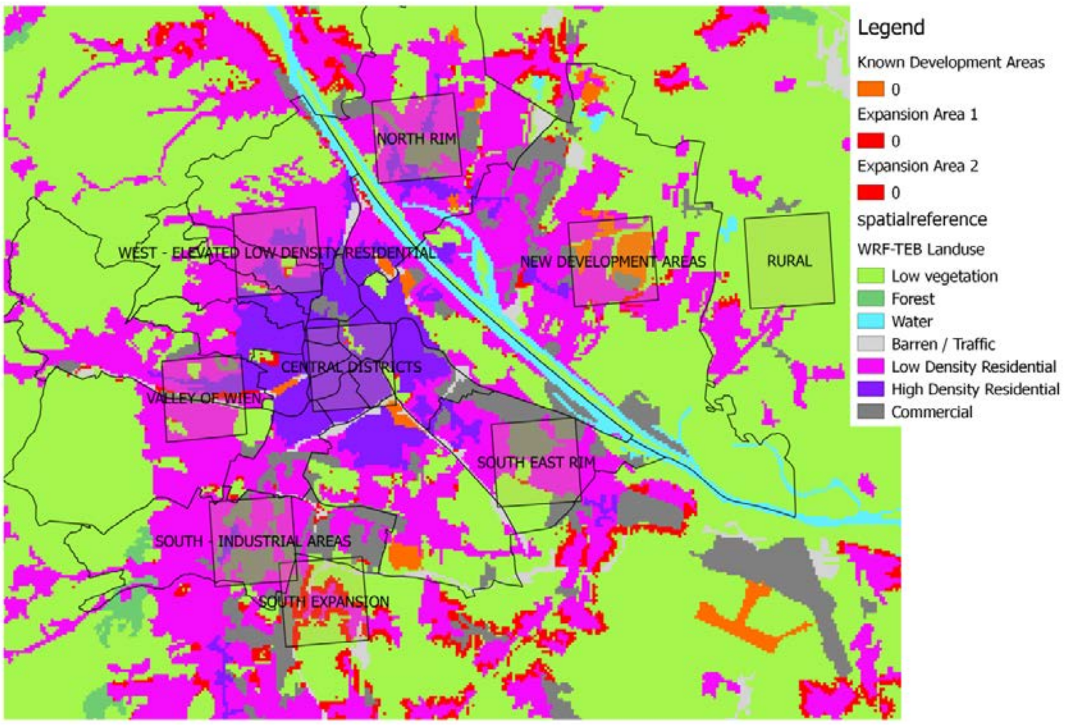

Figure A5.1 Selection of sub regions

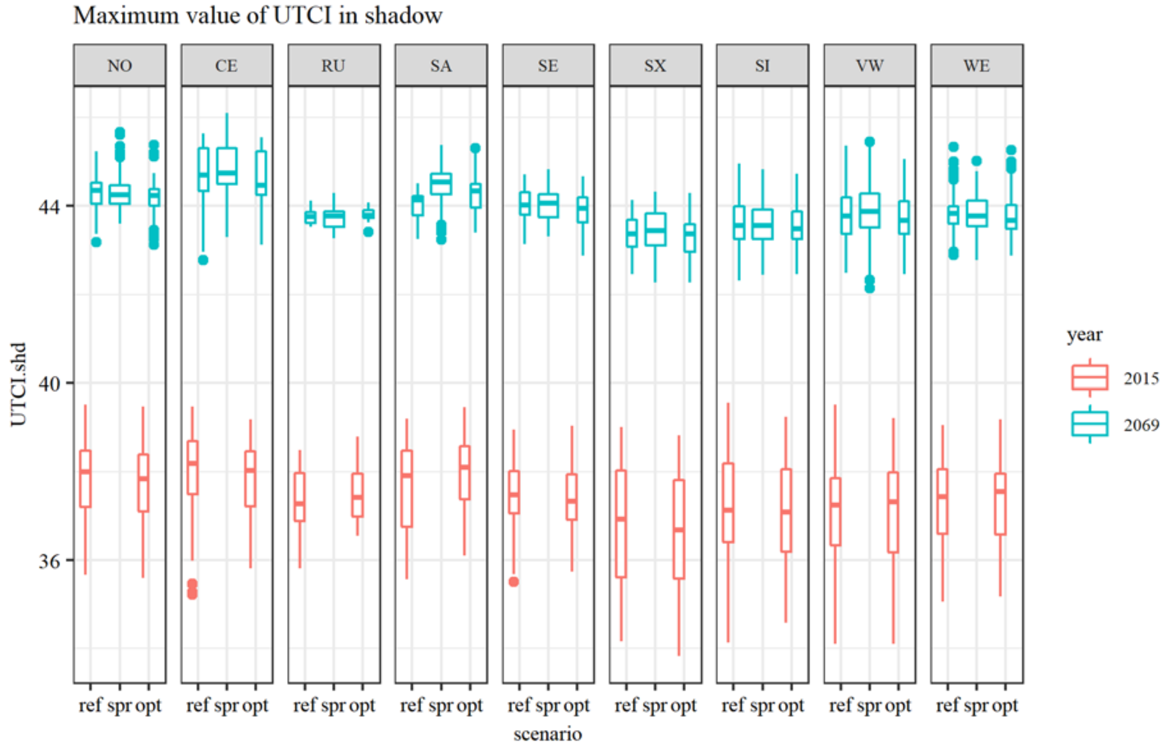

Figure A5.2 Daily maximum UTCI for the three urban scenarios "REF", "SPR" and "OPT for a person walking in the shadow. The results are shown for each of the nine selected subregions. Red: For a 15-year heat wave around 2015; Blue: for a 15-year heat wave around 2050.

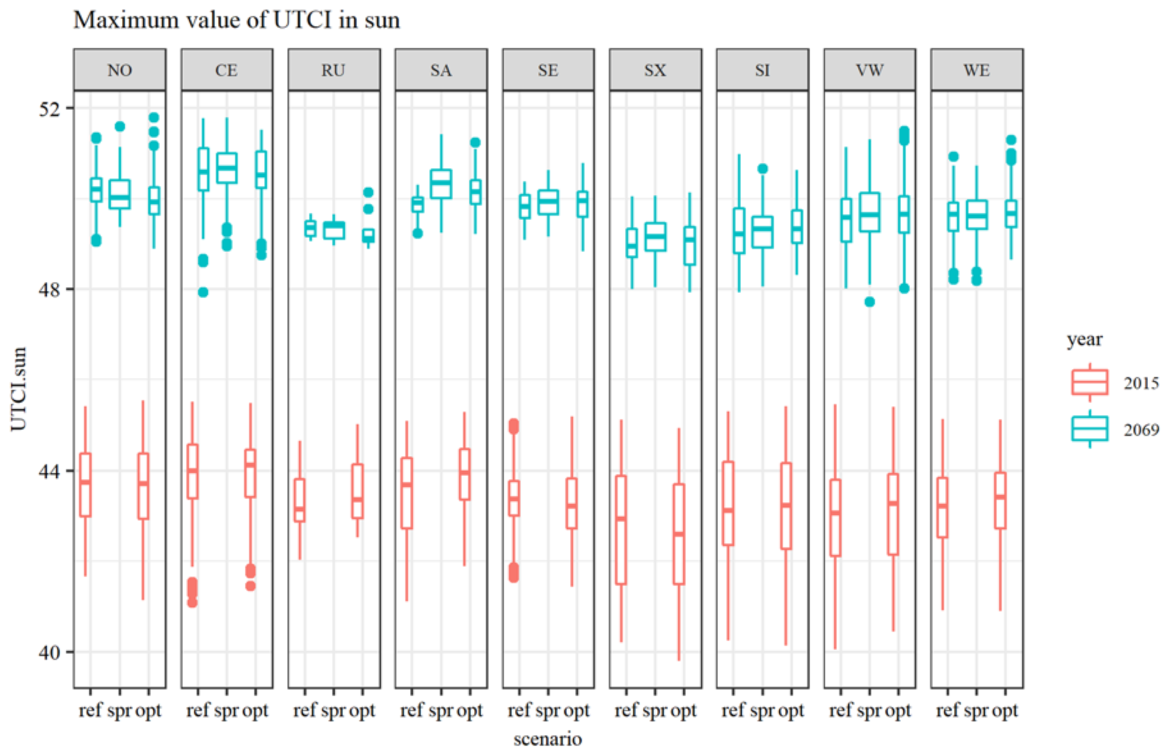

Figure A5.3 Daily maximum UTCI for the three urban scenarios “REF”, “SPR” and “OPT for a person walking in the sun. The results are shown for each of the nine selected subregions. Red: For a 15-year heat wave around 2015; Blue: for a 15-year heat wave around 2050.

3 Presentation of Costs

3.1 Table of costs for the entire project duration

The following table provides an aggregated overview of the costs incurred by the applicant and the project partners throughout the entire project duration, broken down by staff costs, capital expenditure, travel expenses, administrative and material expenses, and third-party costs. It must correspond to the cost accounting form (annexed to the support contract and/or available for downloading under www.publicconsulting.at).

All figures in EURO.
Please add further columns for additional partners or start a new table.

Cost category	**Eligible total costs according to contract**	**Cumulative costs during the project term** Total costs for the consortium*	**Applicant** Costs incurred during the project term from - to	**Partner 1** Costs incurred during the project term from - to	**Partner 2** Costs incurred during the project term from - to
Staff costs	219233	255856,51	255856,51	0	
Capital expenditure	12291	14542,33	14542,33	0	
Travel expenses	8750	9645,68	9645,68	0	
Administrative and material expenses	19875	10125,5	10125,5	0	
Third-party costs	35000	12000	12000	0	
Total	295149	302170	302170	0	

* Sum total of costs incurred / cost category of the applicant and all partners

3.2 Statement of costs for the entire project duration

The costs incurred in the outstanding reporting period and over the entire duration of the project must be stated for each partner and/or each set of activities according to the cost schedule specified in the contract and the underlying application.
Personal costs (255857,--) were used for paying salaries of 6 persons: Imran Nadeem and Maria Wind who worked on the WRF adaptations and simulations, Heidi Trimmel who worked on coupling of TEB with WRF, preparing ground input data and preparing the urban scenarios. Sandro Oswald worked on the validation of WRF and TEB (performing measurements) and on the model SOLWEIG. Michael Revesz worked on model simulations, data analysis, and final report.
Costs for capital expenditure (14542,--) include depreciation for ADV infrastructure (Rodlauer HP), for two SN-500 Kanal Netradiometer, for 1 Campell CR1000 Datalogger, and for one ultrasound radiometer.
Costs for travel (9646,--) include costs for ICUC conference, for two travels to Meteo-France Toulouse for training, travel to one WRF Workshop in Boulder Colorado, and costs for small travels in the greater area of Vienna to perform servicing of the stations.
Costs of material (10126,--) included all kind of material below 400 euros which was needed for the validation measurements.
A subcontract (12000,--) was given to Meteo France for TEB training.

3.3 Cost reclassification

– Presentation and motivation of cost reclassifications, if any (between partners and/or cost categories), during the duration of the project.

There has been a reclassification between MA22 and BOKU. In the proposal a subcontract to an external company which should have worked on the Presentation of data, and work with GIS was planned. It was however evident that it was easier and time saving for the partners to perform these task oneself.

Please note the following: for the purposes of final reporting, copies of invoices (e.g. for capital expenditure, travel expenses, etc.) as well as detailed information on staff costs must be annexed to the cost accounting form. The ACRP Program Management reserves the right to perform random checks of the invoices submitted within the framework of the examination of the reports.

4 Utilization (max. 5 pages)

– **Publication**: Please describe the publication and dissemination activities carried out during the project term (project workshops, publications and presentations at external events).

Dissemination of Project workshop:
10 workshops and meetings were held.

Website: http://urbania.boku.ac.at/

List of publications:

Reviewed publications

Oswald, SM; Revesz, M; Trimmel, H; Weihs, P; Zamini, S; Schneider, A; Peyerl, M; Krispel, S; Rieder, HE; Mursch-Radlgruber, E; Lindberg, F; .
(2018): Coupling of urban energy balance model with 3-D radiation model to derive human thermal (dis)comfort. Int J Biometeorol. 2018; (in press)

Trimmel H., H. Formayer, E. Mursch-Radlgruber, I. Nadeem, S. Oswald, P. Weihs, S. Faroux, A. Lemonsu, V. Masson, and R. Schoetter (2018): Evolution of the Viennese Urban Heat Island and Mitigation Strategies in the Context of Urban Growth, Compacting and Climate Change by optimizing the Urban Surface Energy Balance, ICUC-10, New York, 6-10 Aug 2018 – [Oral Presentation] accepted.

Trimmel, H. and Formayer, H. and Masson, V. and Mursch-Radlgruber, E. and Nadeem, I. and Oswald, S. and Schoetter, R. and Weihs,P. (2018): Entwicklung der Urbanen Wärmeinsel Wiens bis 2030/2050 bei Berücksichtigung der Erweiterung der Stadt Wien, Tagungsband, 19. Österreichischer Klimatag, 2018, 23-15.April, Salzburg. [Poster]

Trimmel H., Formayer H., Gützer Ch., Nadeem I., Oswald S., Weihs Ph., Faroux St., Lemonsu A., Masson V., and Schoetter R. (2018): Evolution of the Viennese Urban Heat Island caused by expected Reduction of Vegetation Fraction in favour of Built-Up Land until 2030/2050.[European Geophysical Union, Wien, 8.-13.4.2018] [Oral Presentation]
In: EGU General Assembly 2018 , Geophysical Research Abstracts Vol. 20, EGU2018-7927-3, 2018, © Author(s) 2018. CC Attribution 4.0 license

Weihs, P., Formayer, H., Mursch-Radlgruber, E., Trimmel H., Oswald, S., Nadeem, I., Preiss, J., Masson, V., 2017: Einfluß von Stadterweiterung auf die Wärmeinsel der Stadt Wien im Kontext des Klimwandels, [Vortrag] [Klimatag, Vienna, AUSTRIA, MAY 22 – 24, 2017]

Trimmel, H., P.Weihs, S. Oswald, V. Masson, R. Schoetter, 2017: Land use and urban morphology parameter for Vienna required for initialization of the urban canopy model TEB derived via the concept of "local climate zones". [Poster] [EGU - European Geoscience Union General Assembly, Vienna, AUSTRIA, APR 23-28, 2017]

Oswald, S., Trimmel, H., Revesz, M.,Nadeem I., Weihs, P. First characterization and comparison of TEB model simulations with in situ measurements regarding radiation balance in a single urban canyon at the BOKU site (Vienna) [Poster] [EGU - European Geoscience Union General Assembly, Vienna, AUSTRIA, APR 23-28, 2017]

- **Market**: Please outline the market outlook and the economic potential as perceived at the end of the reporting period.
- **Patents**: Please list the applications for patents filed during the reporting period on the basis of the project.
- **Doctoral dissertations**: If applicable, please list the names of the doctoral students involved in the project and indicate the status of their dissertations (doctoral dissertation started, in progress, terminated).

  Sandro Oswald (in progress)
  Heidelinde Trimmel (in progress)
  Michael Revesz (in progress)

5 Outlook (max. 1 page)

Please draft recommendations for follow-up research and development activities.

+ For soil humidity the yet experimental 1km SCATSAR-SWI data set, which combines Sentinel-1 and MetOp ASCAT (advanced scatterometer) data and is developed by the Department of Geodesy and Geoinformation of the TU Wien will be tested.

+ An automated update of geodata would be very helpful for future urban simulations to be able to rapidly take into account new building development.

+ Create a map of anthropogenic sensible and latent heat fluxes caused by traffic and industry and include them in model simulations. (Global map res ~1km existing?! David)

+ Prepare data sets derived from "Solardachpotentialkataster" and "Gründachpotentialkataster" to create realistic model input

+ Influence of HVAC systems.

- Effects of waste heat
- Impact on electricity demands in extreme heat periods

+ Impact of more effective green roofs with irrigation as well as irrigation of agricultural areas around Vienna on the urban climate during heat waves.

+ Investigate potential negative effects of mitigation measures on air chemistry, as no decrease of NOx emissions is expected (-> according to JP):

- Effect of changes in urban boundary height/lability due to higher surface temperatures on concentration of atmospheric pollutants.
- Effect of increased radiation caused by mitigation measure albedo increases on tropospheric ozone production (wurde untersucht, aber nicht für Wien)

+ Within this project only a first overview of the vast possibilities is given. More detailed spatially varied scenarios / recommendations ought to be developed together with urban planners and simulated. Maybe in collaboration with the INKA network.

+ Possibilities for waste heat reduction and conversion as measures for heat island mitigation.

+ Do more detailed simulations (100m and finer) including information of:

- Flächenwidmungsplan: Schutzzonen,Baulandwidmungen (MA21)

6 Signature

I herewith confirm that the report in its entirety has been accepted by the project partners.

Wien, 23/7/2019

Place, date

Signature of the applicant (coordinator)

Please note: the signature has to be scanned in and inserted into the document.

International Journal of Biometeorology
https://doi.org/10.1007/s00484-018-1642-z

ORIGINAL PAPER

Coupling of urban energy balance model with 3-D radiation model to derive human thermal (dis)comfort

Sandro M. Oswald[1] · Michael Revesz[2] · Heidelinde Trimmel[1] · Philipp Weihs[1] · Shokufeh Zamini[2] · Astrid Schneider[2] · Martin Peyerl[3] · Stefan Krispel[3] · Harald E. Rieder[4] · Erich Mursch-Radlgruber[1] · Fredrik Lindberg[5]

Received: 11 May 2018 / Revised: 24 September 2018 / Accepted: 28 October 2018

Abstract

While capabilities in urban climate modeling have substantially increased in recent decades, the interdependency of changes in environmental surface properties and human (dis)comfort have only recently received attention. The open-source solar long-wave environmental irradiance geometry (SOLWEIG) model is one of the state-of-the-art models frequently used for urban (micro-)climatic studies. Here, we present updated calculation schemes for SOLWEIG allowing the improved prediction of surface temperatures (wall and ground). We illustrate that parameterizations based on measurements of global radiation on a south-facing vertical plane obtain better results compared to those based on solar elevation. Due to the limited number of ground surface temperature parameterizations in SOLWEIG, we implement the two-layer force-restore method for calculating ground temperature for various soil conditions. To characterize changes in urban canyon air temperature (T_{can}), we couple the calculation method as used in the Town Energy Balance (TEB) model. Comparison of model results and observations (obtained during field campaigns) indicates a good agreement between modeled and measured T_{can}, with an explained variance of $R^2 = 0.99$. Finally, we implement an energy balance model for vertically mounted PV modules to contrast different urban surface properties. Specifically, we consider (i) an environment comprising dark asphalt and a glass facade and (ii) an environment comprising bright concrete and a PV facade. The model results show a substantially decreased T_{can} (by up to -1.65 °C) for the latter case, indicating the potential of partially reducing/mitigating urban heat island effects.

Keywords SOLWEIG · PV energy balance · Surface temperature parameterization · UTCI

Electronic supplementary material The online version of this article (https://doi.org/10.1007/s00484-018-1642-z) contains supplementary material, which is available to authorized users.

✉ Sandro M. Oswald
sandro.oswald@boku.ac.at

1 Institute of Meteorology, University of Natural Resources and Life Sciences (BOKU), Vienna, Austria

2 AIT Austrian Institute of Technology GmbH, Vienna, Austria

3 Smart Minerals GmbH, Vienna, Austria

4 Wegener Center for Climate and Global Change and IGAM/Institute of Physics, University of Graz, Graz, Austria

5 Department of Earth Sciences, University of Gothenburg, Gothenburg, Sweden

Introduction

Today about half of the world's population resides in urban areas. Future projections show pronounced urbanization rates and it is expected that by 2050, about two thirds of the world's population will be urban (UN 2014). Several studies report on increased thermal heat stress in urban microclimates, e.g., Grimmond et al. (2010). In order to adapt to climate change, some countries aim to reduce solar absorption in urban environments by maximizing the area of highly reflective surfaces through installation of the so-called white roofs. Also, at a time where sustainable energy production becomes more and more important, "solar cities" aim on maximizing "solar harvest", i.e., the solar yield from photovoltaic (PV) modules, by directing their roofs and

Published online: 05 December 2018

facades towards the sun to avoiding shadowing. Reflections from the ground and surrounding buildings cause an increase of the solar radiation directed to the PV module, thus increased PV yield (Kotak et al. 2015; Lindberg et al. 2015). The role of PV modules in a city or as a facade in an urban canyon was discussed in the work of Brito et al. (2017). This study has shown that for specific study areas, the non-baseload electricity demand can be satisfied by cost-effective PV investments on roofs and facades at today's market conditions for up to 10 months of the year. Further, winter mid-day electricity demand can only be achieved if the solar yield of PV facades is taken into account.

In terms of human thermal stress, this increase in reflection can cause more discomfort. Human (dis)comfort is commonly described by various bioclimatic indices. The Universal Thermal Climate Index (UTCI) (Fiala et al. 2001; Bröde et al. 2011; Blazejczyk et al. 2011) aggregates many of these in one standardized metric. The UTCI is based on complex multi-node thermophysiological models and allows to predict whole body thermal effects (e.g., hypothermia and hyperthermia; heat and cold discomfort) as well as localized effects (e.g., frostbite). Thereby, UTCI allows addressing all kinds of thermal stress and discomfort (e.g., extreme cold or warm) as well as conditions in which the human heat balance and the perceived outdoor temperature are affected by solar radiation. The accuracy of UTCI depends on a suite of input parameters; among these, especially a precise calculation of the mean radiant temperature T_{mrt} is of uttermost importance (Weihs et al. 2011).

To provide T_{mrt} with highest accuracy, we employ here an updated version (see below) of the open-source solar long-wave environmental irradiance geometry (SOLWEIG) model which is a part of the urban multi-scale environmental predictor (UMEP) (Lindberg et al. 2018). SOLWEIG is a state-of-the-art model which combines building and vegetation surface models and spatial variations of 3-D radiative fluxes in complex urban settings. SOLWEIG has been extensively evaluated in urban environments over the last decade (Lindberg et al. 2008; Lindberg and Grimmond 2011; Lindberg et al. 2016).

In its present configuration (Lindberg and Grimmond 2016), SOLWEIG uses only observed ambient air temperature, independent of its measurement height, to estimate the temperatures of surrounding surfaces (i.e., wall and ground temperature) via a simple parameterization scheme. Moreover, according to the authors' knowledge, to date, no evaluation and simulation tools are available for urban areas, which can estimate the effects of a broad rollout of photovoltaic facade and different ground surfaces in urban districts necessary to characterize the change of ambient air temperature and in general microclimate in urban street canyons.

This study aims on closing this gap by coupling SOLWEIG with parts of the Town Energy Balance (TEB) model (Masson 2000). Below, we detail the model setup as well as results from a recent field campaign for model evaluation. During this field campaign, measurements of short-wave radiation, wind speed, air, and surface temperatures were performed. The campaign took place between August 2016 and September 2017 on the campus of the University of Natural Resources and Life Sciences (BOKU) in Vienna.

The study focuses on (i) the simulation of canyon air temperature based on measured input parameters and its comparison to observed canyon air temperature in the study domain (see dashed yellow box in Figure S1 in the supplemental material); and (ii) evaluating the impact of potential changes in the surface structure parameters of wall and ground (i.e., albedo and energy balance of the PV module) on the canyon air temperature and human comfort.

Methods

Based on the standard meteorological input file of SOLWEIG, we developed a model structure which uses only the required and available variables (ambient air temperature T_a, wind speed U, relative humidity RH, barometric pressure p_a, and incoming short-wave global radiation G_h on a horizontal plane).

Instrumentations

For model development and evaluation, measurements which are routinely performed at the meteorological monitoring platform located at the rooftop of the Schwackhöfer-Haus (at approximately 26-m height above ground) have been used. Additional measurements have been performed within a street canyon nearby (southward-orientated at 3 m above ground). Figure 1a and b shows both platforms and the related measurements; Figure S1 in the supplemental material shows the measurement sites from the top (dark green ellipse = rooftop, green point = canyon). During the campaign, radiation measurements were performed with two types of pyranometer: on the rooftop with a MS-802 global radiation pyranometer (EKO Instruments) with a wavelength range of 285–3000 nm; in the urban canyon with a vertically mounted EMS 11 silicone diode sensor (EMS Brno) covering a wavelength range of 400–1100 nm. The ambient air temperature and relative humidity at the rooftop have been measured with a thermocouple type K combined with a humidity sensor (inside a radiation shield) in direct vicinity to the wind sensor (for speed and direction) on the rooftop (see Fig. 1a). Air temperature and wind speed measurements in the canyon were performed with a

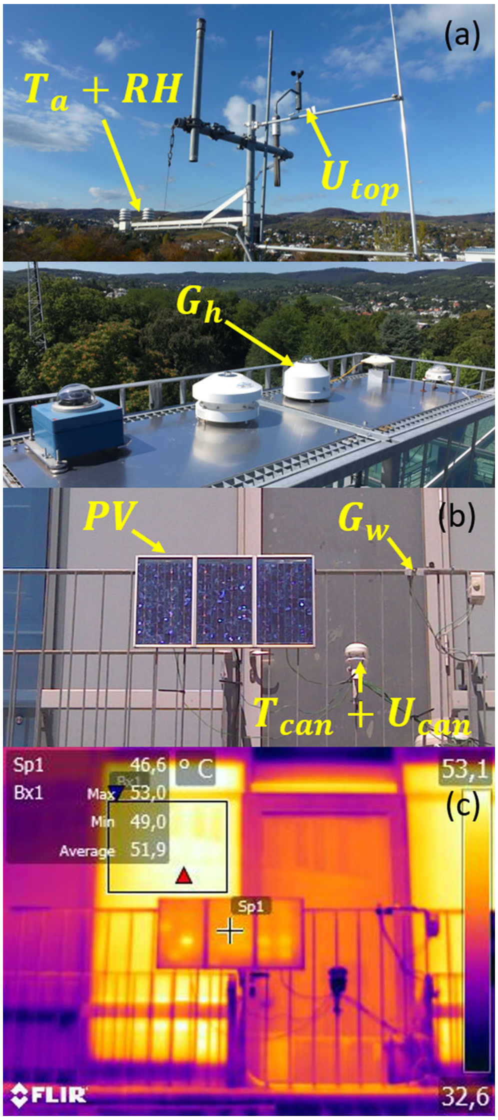

Fig. 1 Measurement setup used in this study. **a** The observational platform of the University of Natural Resources and Life Sciences (BOKU), located at the rooftop of the Schwackhöfer-Haus. **b** Additional instrumentation in the studied urban canyon. **c** Infrared picture of the setup shown in **b** taken on 19 June 2017 at 11:12 UTC. The acronyms in **a** and **b** indicate individual meteorological variables obtained; arrows point towards the corresponding instrument/sensor. These are ambient air temperature T_a and relative humidity RH; both measured with a thermocouple located 26 m above ground; wind speed U_{top} at the rooftop, measured with a Kroneis anemometer 27 m above ground; horizontal global radiation G_h, obtained with a MS-802 pyranometer (EKO Instruments); global radiation on a south-oriented vertical plane G_w in the urban canyon, obtained with an EMS 11 global radiation silicone diode sensor (EMS Brno); canyon air temperature T_{can} and canyon wind speed U_{can}, both obtained with a DS-2 sonic anemometer (METER Group, Inc). The three photovoltaic modules PV are of type SX10M (SOLAREX). In the upper left of panel **c**, surface temperatures of the PV modules (Sp1) and the building facade of the Schwackhöfer-Haus (Bx1) are given

DS-2 sonic anemometer (METER Group, Inc.) with a speed range of 0–30 m s^{-1} and an accuracy of 0.3 m s^{-1} (see Fig. 1b). The measurement outputs of the individual sensors in the urban canyon have been aggregated to 10-min averages to match the temporal resolution of the routine rooftop measurements.

The surface temperatures were additionally measured with an infrared camera of type FLIR E60bx (FLIR Systems), which has an accuracy of ± 2% between 0 and 650 °C (see Fig. 1c).

The potential electricity production inside the urban canyon was determined with three PV modules of type SX10m (SOLAREX). The surface temperature was measured with three thermocouples on the back side of the PV modules.

Parameterization of wall surface temperature

Bogren et al. (2000) proposes to estimate the surface temperatures T_s (horizontal or vertical) via a linear relationship between maximum solar elevation and the maximum difference between measured T_a and T_s under clear-sky conditions (Lindberg et al. 2008). Here, we propose a different approach, using global radiation measured on a south-oriented vertical plane G_w instead of solar elevation. G_w is calculated as

$$G_w = G_h \frac{sin(\alpha + \beta)}{sin(\alpha)} \tag{1}$$

where β is the tilt angle of the vertical plane measured from the horizontal and α is a function of the geographical latitude ϕ and the declination angle δ given by

$$\begin{aligned} \delta = {} & (180/\pi) \cdot (0.006918 - 0.399912 \cdot cos(B) \\ & + 0.070257 \cdot sin(B) - 0.006758 \cdot cos(2B) \\ & + 0.000907 \cdot sin(2B) - 0.002697 \cdot cos(3B) \\ & + 0.00148 \cdot sin(3B)), \end{aligned} \tag{2}$$

$$\alpha = 90 - \phi - \delta \tag{3}$$

where $B = (n-1)\frac{360}{365}$ with the nth day of the year (Spencer 1971; PVEducation 2017).

To obtain the wall surface temperature T_w, we apply the amplitude from the before mentioned linear relationship to a sinusoidal wave function with maximum temperature difference at 15:00 (local time) (Lindberg et al. 2016).

Parameterization of ground surface temperature

To calculate the ground temperature T_g, we apply the force-restore method following Blackadar (1976) with a two-layer approximation, i.e., with a parameterization of the sensible heat flux H_s (2nd term in Eq. 4) and the ground heat flux

H_g (3rd term in Eq. 4). The change in T_g per time step is given as:

$$\frac{\partial T_g}{\partial t} = \frac{F}{S\, z_g} - a_{FR}\left(T_g - T_{as}\right) - \Omega\left(T_g - T_m\right) \tag{4}$$

Here, F represents the net radiation balance at the ground surface (which can be directly calculated with SOLWEIG), S is the soil heat capacity given as a product of a materials density ρ and its specific heat capacity c, Ω is the angle velocity of the Earth, and a_{FR} which is a time-of-day dependent factor (3×10^{-4} s^{-1} for daytime, 1×10^{-4} s^{-1} for nighttime). T_m is the approximately constant temperature of the bottom slab. The depth of the thermal active layer z_g is calculated using time period τ and thermal conductivity λ (Stull 1988):

$$z_g = \sqrt{\frac{\tau\,\lambda}{4\,\pi\, S}} \tag{5}$$

It follows that the near-surface air temperature T_{as} has to be simulated based on measurements of T_a on the rooftop. To model such continuous time series of T_g at time step $(t+1)$, we apply the Euler method with a given T_g at time step (t) and the rate of change from Eq. 4 times a value i for the size of every step:

$$T_g(t+1) = T_g(t) + \frac{\partial T_g}{\partial t} \cdot i \tag{6}$$

Parameterization of urban canyon air temperature

As detailed above, we are interested in the air temperature near the ground surface T_{as}. For simplification, we set T_{as} as $\widehat{T}_{can}$ which is calculated in analogy to the TEB model.

$$\widehat{T}_{can} = \frac{\frac{T_g}{RES_g} + \frac{2\,h}{w}\frac{T_w}{RES_w} + \frac{T_a}{RES_{top}}}{\frac{1}{RES_g} + \frac{2\,h}{w}\frac{1}{RES_w} + \frac{1}{RES_{top}}} \tag{7}$$

Note we did not parameterize the anthropogenic sensible heat flux and snow cover terms given the general lack of traffic at the case study site and summer time conditions. Further required terms for estimating $\widehat{T}_{can}$ are $\frac{h}{w}$, the canyon aspect ratio (building height h to street width w) and RES, the aerodynamic resistance for the ground (RES_g), wall (RES_w), and rooftop (RES_{top}), respectively, given as:

$$RES_g = RES_w = \frac{c_p\,\rho_a}{\left(11.8 + 4.2\sqrt{U_{can}^2 + (u_* + w_*)^2}\right)} \tag{8}$$

$$RES_{top} = \left(U_{top}\, C_d\right)^{-1} \tag{9}$$

whereby U_{can} (parameterized as in the TEB model) and U_{top} (measured) are the wind speeds for canyon and rooftop, respectively. The characteristic scale of turbulent wind $u_* + w_*$ is calculated using T_a, U_{top}, and the drag coefficient C_d (computed with the roughness length $z0_{town} = \frac{h}{10}$ and $\widehat{T}_{can}$ of the previous time step) (Moigne 2012). For estimating the surface heat flux, we consider the rate of warming $\left(\frac{\partial T_a}{\partial t}\right)_r$ at the rooftop as representative for the whole convective boundary layer:

$$u_* + w_* = \sqrt{C_d}\, U_{top} + \left[\frac{g\,h^2}{T_a}\left(\frac{\partial T_a}{\partial t}\right)_r\right]^{1/3} \tag{10}$$

where g is the gravitational constant (Arya 2001).

Energy balance model for PV modules

Following the concept of the heat dynamics model for building-integrated photovoltaic (BIPV) systems of Lodi et al. (2012), we introduce a modified energy balance model for PV module(s) mounted in urban canyons. As model input, we use besides global radiation information (see above) the measured surface temperature on the back side of the PV module $T_{b_{PV}}$, and information from a 2-D sonic anemometer. At our study site, the thermal radiative heat transfer between the back side of the PV module and the gray glass facade of the Schwackhöfer-Haus (see Fig. 1b) behind can be calculated following:

$$Ql_b = \frac{A_{PV}\,\sigma}{\frac{1}{\varepsilon_{b_{PV}}} + \frac{1}{\varepsilon_w} - 1}\left(T_{b_{PV}}^4 - T_w^4\right) \tag{11}$$

where A_{PV} represents the area of the photovoltaic module with a value of 0.11 m^2. $\varepsilon_{b_{PV}}$ and ε_w are the emissivity for the back side of PV modules and the facade of the Schwackhöfer-Haus, respectively. T_{PV}, the front temperature of the PV module (which might be higher than $T_{b_{PV}}$), can be calculated following:

$$T_{PV} = T_{b_{PV}} + \frac{G_w}{1000\ \mathrm{W\,m^{-2}}}\,\Delta T \tag{12}$$

where ΔT is the temperature difference between the front and back sides of the PV module. ΔT is set to 1.9 °C at an irradiance level of 1000 W m^{-2} (King et al. 2004).

Now, the long-wave radiation exchange Ql_f between the sky, ground, the opposite building (Exner-Haus, see Figure S1 in the supplemental material), and the front side of the PV module is given as:

$$Ql_f = A_{PV}\,\sigma\left(\Psi_{sky}\,\varepsilon_c\,T_{sky}^4 + \Psi_g\,\varepsilon_c\,T_g^4 + \Psi_b\,\varepsilon_c\,T_b^4 - \varepsilon_{gl}\,T_{PV}^4\right) \tag{13}$$

The parameter Ψ is the view factor for surrounding surfaces. Figure S2 in the supplemental material shows a fisheye lens picture of the PV module perspective combined with three digitalized images for the sky, for the ground, and for buildings. The respective area percentage calculation yields a sky view factor of $\Psi_{sky} = 0.23$, ground view factor $\Psi_g = 0.43$, and a building's view factor of $\Psi_b = 0.35$. For the emissivity ε_c, we assume a combined value of 0.95. Due to the available information of dew point temperature T_{dew} on the rooftop, the sky temperature T_{sky} can be calculated using the method of Duffie and Beckman (2013). The temperature of the Exner-Haus T_b, which is shaded throughout the day, is set to T_a (Lindberg and Grimmond 2011).

To determine the convective heat transfer Qc between the front (Eq. 14) and back sides (Eq. 15) of the PV module and the surrounding air, we apply Newton's law of cooling following Palyvos (2008) and Sharples (1984):

$$Qc_f = A_{PV}\,(7.35 + 3.75 \cdot U_{can})\,(T_{can} - T_{PV}), \qquad (14)$$
$$Qc_b = A_{PV}\,(1.8 + 1.93 \cdot U_{can})\,(T_{can} - T_{b_{PV}}) \qquad (15)$$

The absorbed solar radiation is estimated through the transmittance-absorptance product $(\tau\alpha)_{PV} \cong 1.01\,\tau_{gl}\,\alpha_{PV}$ (Duffie and Beckman 2013) and the incidence angle modifier $\mathrm{IAM}(\theta_{aoi})$ (Barker and Norton 2003):

$$Q_s = A_{PV}\,1.01\,\tau_{gl}\,\alpha_{PV}\,G_w\,\mathrm{IAM}(\theta_{aoi}) \qquad (16)$$

The remaining term of the heat transfer process is transformed solar energy (i.e., electricity production of the PV module), which is given as a function of T_{PV}:

$$Q_e = A_{PV}\,G_w\,\mathrm{IAM}(\theta_{aoi})\,\eta_{ref}\left[1 - \beta_0\left(T_{PV} - T_{PV,ref}\right)\right] \qquad (17)$$

where η_{ref} is the reference PV module efficiency (determined by laboratory measurements), β_0 is a temperature coefficient (see Table 1), and $T_{PV,ref} = 25\ ^\circ\mathrm{C}$ is the reference temperature at 1000 W m^{-2} (manufacturer provided).

Continuous Time Stochastic Modeling for unknown parameters

Continuous Time Stochastic Modeling (CTSM) is widely used to estimate unknown parameters of non-linear systems (Jazwinski 1970; Nielsen et al. 2000). Following the scheme of a gray box model, which combines prior physical knowledge and information from measurements, one can use a set of stochastic differential equations (SDEs) of form

$$dX_t = f(X_t, U_t, t, \Theta)\,dt + W(X_t, U_t, \Theta)\,d\omega_t \qquad (18)$$

and a set of discrete time observation equations of form

$$y_k = M(X_k, U_k, t_k, \Theta) + e_k \qquad (19)$$

where t is the time, X_t is a vector of state variables, U_t is a vector of input variables, Θ is a vector of unknown parameters, and y_k is a vector of output variables. $f(\cdot)$, $W(\cdot)$, and $H(\cdot)$ are non-linear functions, ω_t is a Wiener process, and e_k is the Gaussian white noise with the covariance $\sum_t$. The CTSM package in R (Juhl 2016) applies a maximum likelihood estimation of a time series with joint probability density function

$$L(\Theta) = \left(\prod_{k=1}^{\mathrm{N}} p(y_k \mid \Upsilon_{k-1}, \Theta)\right) p(y_0 \mid \Theta) \qquad (20)$$

with $\Upsilon_{\mathrm{N}} = [y_0, y_1, ..., y_k, ..., y_{\mathrm{N}}]$ as a time series of N observations. CTSM-R computes the likelihood function and uses an optimization method to locate the most probable set of parameters (Juhl et al. 2016).

Given the relatively small area of the PV module used in this study (compared to, e.g., modules used in Jones and Underwood (2001) and Lodi et al. (2012)), we considered a single-state model to predict the average cell temperature. In our case, the unknown parameters are the absorptivity of the cells inside PV modules α_{PV} and the heat capacity C_{PV}. The non-linear system for the photovoltaic energy balance model to estimate these parameters is given as:

$$\begin{aligned} dT_{PV} &= C_{PV}^{-1}\,\left(Qc_f + Qc_b + Ql_f\right. \\ &\qquad \left. + Ql_b + Q_s - Q_e\right)\,dt + W\,d\omega_t, \\ T_{PV,m} &= T_{PV} + e_k \end{aligned} \qquad (21)$$

Once the unknown parameters are determined, the Euler method from Eq. 6 can be used to calculate the estimated PV module temperature $\widehat{T}_{PV}(i)$ based on knowledge of global radiation (on a vertical plane), wind speed, and ambient air temperature at the rooftop, the angle of incidence of the current step (i), and the back-side PV module temperature with the canyon air temperature from the previous time step $(i-1)$.

Results

Model evaluation for wall, ground, and air temperature

As shown in Lindberg et al. (2016), the surface temperature parameterization in SOLWEIG affects the mean radiant temperature. Thus, precise measurements of the temperature of surrounding surfaces are needed to accurately simulate the canyon air temperature.

To this aim, infrared measurements (with a FLIR E60bx) were taken of the facade behind the PV modules around the time of maximum solar elevation. Due to the possible settings in FLIR Tools (FLIR Systems 2016), the position where pictures were taken was 5 m in front looking normal to the wall of the Schwackhöfer-Haus and the emissivity was set to $\varepsilon_w = 0.95$.

Following Lindberg et al. (2016), we show in Fig. 2a the difference in wall surface temperature T_w and air (in our case canyon) temperature T_{can}, as a function of the maximum solar elevation. The regression coefficients found

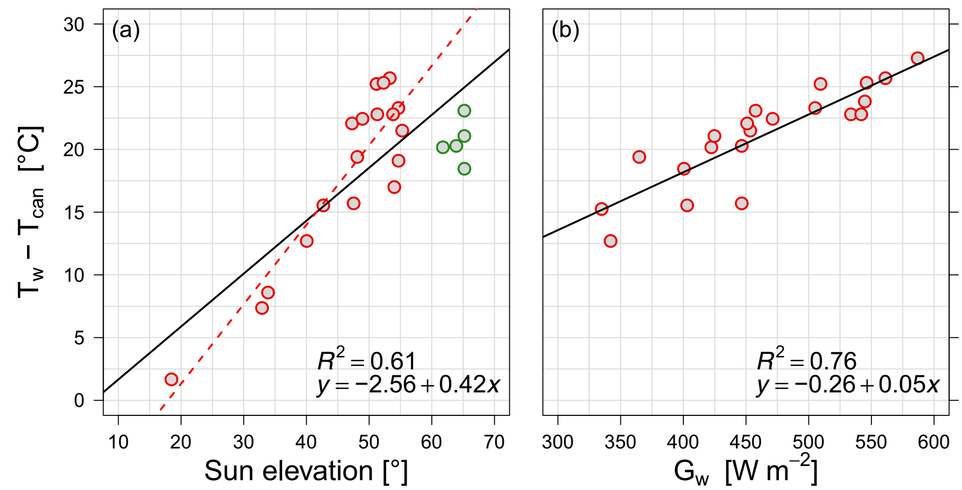

Fig. 2 Scatter plots of the difference in temperature between the wall surface temperature (T_w) and canyon air temperature (T_{can}) as a function of **a** the solar elevation and **b** global radiation on a south-facing vertical wall (G_w). The green points in panel **a** mark the outliers from the theoretical curve (dashed red line) describing higher surface temperature at higher solar elevation. The squared Pearson correlation coefficient (R^2) and the regression analysis with the coefficients are provided in each panel. Note the number of measurements in **a** and **b** are not the same as global radiation measurements have not been available on 2 days

in the present analysis are in close agreement with those originally described by Lindberg et al. (2016). Despite a general agreement, a few individual measurements (marked in green) deviate from the theoretical curve (dashed red line) describing higher surface temperature at higher solar elevation. However, the study of Lindberg et al. (2016) considered only temperatures at solar elevation below 56 ° due to the higher geographic latitude in Sweden compared to Vienna. Figure 2b shows a new method regarding the difference of T_w and T_{can} as a function of the observed values G_w. The explained variance of the temperature difference is strongly improved using G_w as predictor (compare $R^2 = 0.61$ in panel (a) with $R^2 = 0.76$ in panel (b)).

Calculating the ground temperature with the force-restore method, we apply the following quantities: the heat capacity of asphalt given as $S_{asphalt} = 920\ \mathrm{J\,kg^{-1}\,K^{-1}} \cdot 2120\ \mathrm{kg\,m^{-3}} = 1.95 \times 10^6\ \mathrm{J\,m^{-3}\,K^{-1}}$ and the thermal conductivity $\lambda_{asphalt} = 0.7\ \mathrm{W\,m^{-1}\,K^{-1}}$ (Lumitos 2017). T_m was set as an average of the daily mean of T_a and the annual average temperature in 2 m depth of 12 °C to account for seasonal ground temperature variations (possible maximum temperature was measured in 2-m depth of 18.6 °C) (ZAMG 2018). To obtain F in Eq. 4 with highest accuracy in SOLWEIG, measurements of the albedo of the Schwackhöfer-Haus (gray panels faced with glass in the upper part of Figure S3 in the supplemental material) yielded a value of 0.27.

The canyon aspect ratio was calculated taking the average height of both buildings and a street width of 17 m which yields a value of $\frac{\bar{h}}{w} = \frac{20.2\ \mathrm{m}}{17\ \mathrm{m}} \simeq 1.19$. As now all required parameters for the calculation of the canyon air temperature $\widehat{T_{can}}$ are available, we derive it following Eq. 7.

Figure 3 provides a time series of the measured and simulated air temperature inside and above the urban canyon. We show the estimates for $\widehat{T_{can}}$ for both the currently implemented SOLWEIG scheme (CS) and the here proposed calculation scheme (PS). While both, CS and PS agree quite well with the measurements of T_{can}, a closer comparison reveals structural differences among the two approaches. Estimates from CS agree closer with observations during morning hours (before 10:00 UTC), while estimates from PS are closer to the measured canyon air temperature around noon and during the afternoon/early evening (until about 19:00 UTC). A disadvantage of CS compared to PS is the circumstance that the ground temperature decreases immediately to T_a due to the shadow matrix. This is clearly visible in Figure S4 (supplemental material) where at around 14:00 UTC, $T_{asphalt}$ (CS) rapidly decreases due to shading of the canyon (by the bridge marked with yellow lines in Figure S1). The two outliers in CS between 18:00 and 20:00 UTC stem from the fractional cloud cover function as described in Lindberg et al. (2008). Due to application of the parameterization throughout the night, the simulated air temperatures are too low, especially at the end of the time series after a pronounced heat wave.

The statistical analysis of the modeled versus observed canyon air temperature for CS and PS is shown in Fig. 4a and b, respectively. While both parameterization schemes work generally well, PS shows an improved explained variance (squared Spearman's rank correlation coefficient) compared to CS. More importantly though, the root mean

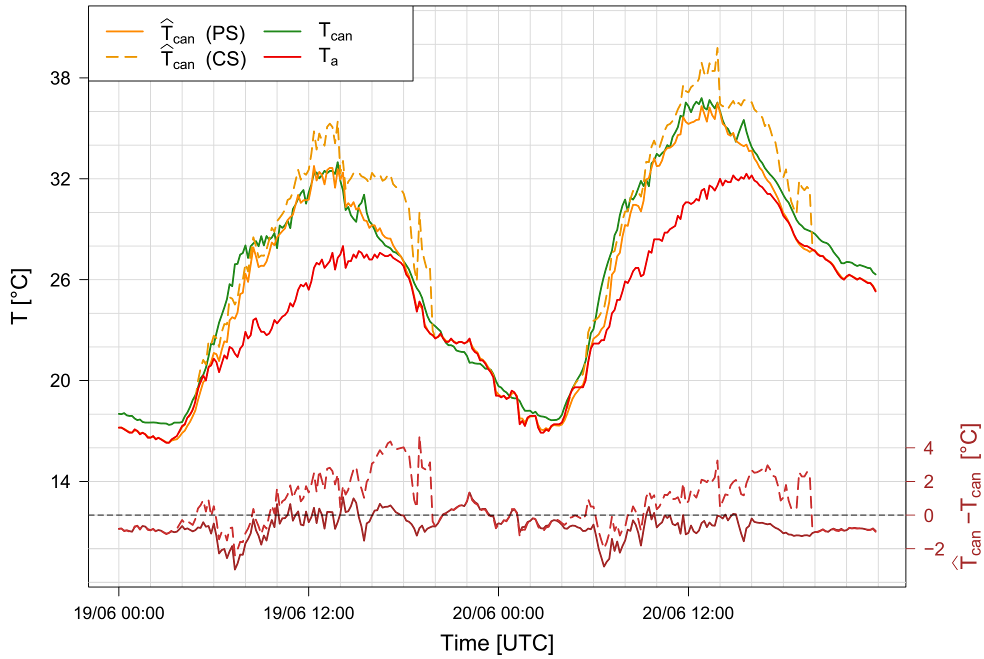

Fig. 3 Time series of the air temperature (T) measured at the rooftop (T_a, red) and inside the urban canyon (T_{can}, green), and simulated canyon air temperature with the currently implemented SOLWEIG scheme (CS) ($\widehat{T}_{can}$, orange, dashed line) and the proposed calculation scheme (PS) ($\widehat{T}_{can}$, orange, solid line). Time series of the difference between T_{can} and $\widehat{T}_{can}$, respectively, is shown in the lower part (brown dashed (CS) and solid (PS) lines)

square error (RMSE) for PS is reduced compared to CS. In summary, the here-presented calculation scheme (PS) performs better than the standard scheme (CS). Nevertheless, also PS shows slight underestimations in the heating phase of the urban canyon.

Parameter estimation and simulation for PV modules

As manufacturers commonly do not provide optical or thermal specifications of a PV module, this information was compiled through literature review (see Table 1). The initial value of C_{PV} for the CTSM system was estimated using a value given in Jones and Underwood (2001) with a total heat capacity of 2918 J K^{-1} and a total area of 0.51 m^2. Assuming the mounted PV modules are very similar to the ones in Jones and Underwood (2001), the heat capacity of each module is 2918 J K^{-1} $\cdot$ $\frac{0.11\,\mathrm{m}^2}{0.51\,\mathrm{m}^2}$ $\approx$ 650 J K^{-1} (scaled by total area). The final value of C_{PV} is given in Table 1. α_{PV} was also estimated by CTSM using an initial value of Moralejo-Vàzquez et al. (2015).

Lodi et al. (2012) suggests parameter estimation based on data from partly cloudy days, given that the modeled heat transfer processes are less correlated under cloudy than under clear-sky conditions. For the present study, parameter estimation is based on data taken on 18 June 2017 between

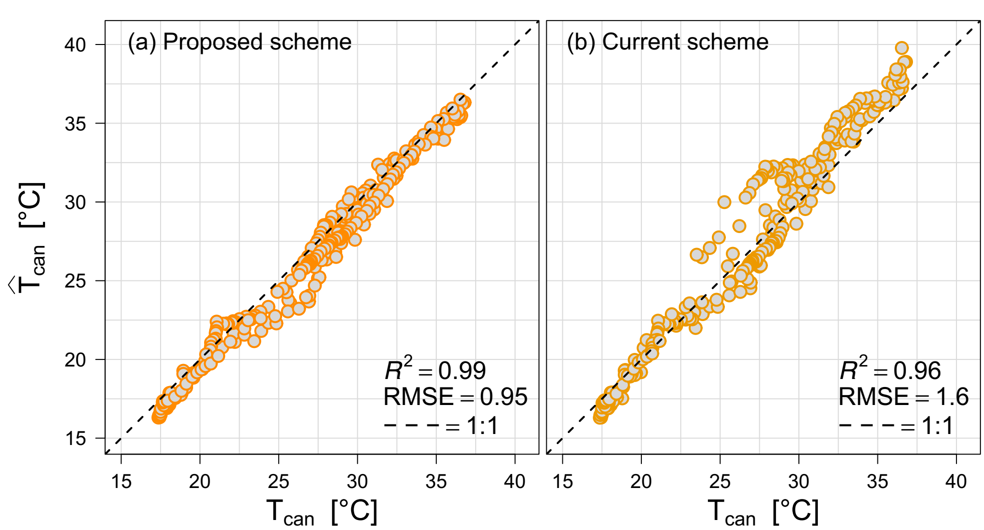

Fig. 4 Scatter plots of measured (T_{can}) and simulated ($\widehat{T}_{can}$) canyon air temperature for **a** the proposed calculation scheme and **b** the currently implemented SOLWEIG scheme. Each panel provides the squared Spearman's rank correlation coefficient (R^2) and the root mean square error (RMSE)

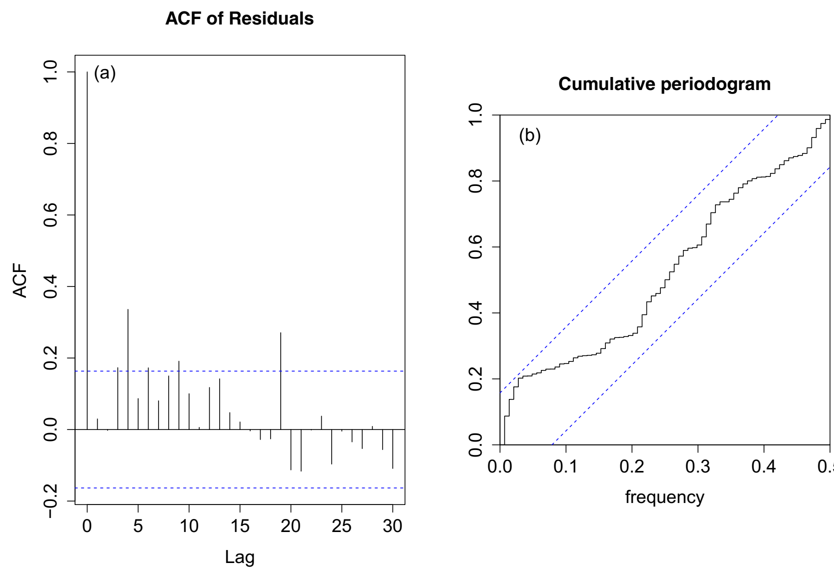

Fig. 5 **a** The auto-correlation function (ACF) and **b** the cumulated periodogram of the residuals for the continuous time stochastic model used for the mounted photovoltaic module. The blue dashed lines mark the 95% confidence limits for random noise

00:00 and 23:50 UTC with 10-min temporal resolution. Measurements include several input values for the CTSM system including G_w, U_{can}, T_a, T_{can}, T_{dew}, and $T_{b_{PV}}$. Ground temperature T_g in front of the PV module and wall temperature T_w behind the PV module have been simulated with the PS scheme in SOLWEIG. T_g was averaged over an area of $7 \cdot 7$ m^2 (see Figure S1 in the supplemental material, red square), seen as the distance from the PV module to parked cars. In Fig. 5, we show the white noise verification of the model considering the auto-correlation function (ACF, panel (a)) and the cumulative periodogram (panel (b)). Here, the blue dashed lines mark the confidence level of 95% under the hypothesis that the model residuals are white noise. The PS describes heat transfer in and around the PV module enough sufficiently. We note in passing that for characterizing a larger PV unit, the model would need to be expanded to a two-state model as used for example by Lodi et al. (2012).

Applying the estimated parameters (Table 1) in Eq. 21 combined with the Euler method, the PV module temperature is predicted. The output of the simulated $\widehat{T}_{b_{PV}}$ is compared with the measured $T_{b_{PV}}$ for 18 to 20 June 2017 in Fig. 6a. In panel (b), we show the difference between model prediction and observations. The model shows most satisfactory results on June 18, a day with partial cloud cover. In contrast, larger differences are found for 19 and 20 June 2017, which have been characterized by prevailing clear-sky conditions. Clear-sky days are more difficult to model due to overall higher temperatures and reflections of obstacles in the environment (see second sun in Figure S3 in the supplemental material). However, the statistical analysis of the CTSM-based system (provided in Fig. 7) shows good agreement throughout the time series, with an explained variance of $R^2 = 0.99$ and a RMSE = 1.2 °C (N = 432).

Simulations for various surface conditions

Urban planning strives to reduce the urban canyon air temperature and generally undesirable effects of the urban heat island. Therefore, the UTCI can describe human thermal comfort inside different surface structures and is thus an important planning quantity.

This study seeks to model the urban thermal environment at a study site in Vienna, Austria. We compare the influence of the current urban structure at the study site (dark asphalt on the ground combined with a glass facade) with those of a ground of bright concrete combined with a

Table 1 Technical specifications of the three PV modules used in this study

Type of solar cell		Poly-crystalline[1]
Total aperture area	0.11	m^2
Voltage at MPP[2]	16.80	V
Current at MPP[2]	0.59	A
Nominal power	10.00	W
PV module efficiency[3] η_{ref}	8.07	%
Temperature coefficient β_0	0.50	% K^{-1}
Absorptivity of cell α_{PV}	0.84	
Emissivity of glass[4] ε_{gl}	0.91	
Transmittance of glass[5] τ_{gl}	0.90	
Emissivity of back side[4] $\varepsilon_{b_{PV}}$	0.85	
Heat capacity C_{PV}	754.95	J K^{-1}

[1]p-Si
[2]Maximum Power Point
[3]Average of all three PV modules
[4](Armstrong and Hurley 2010)
[5](Herrando et al. 2014)

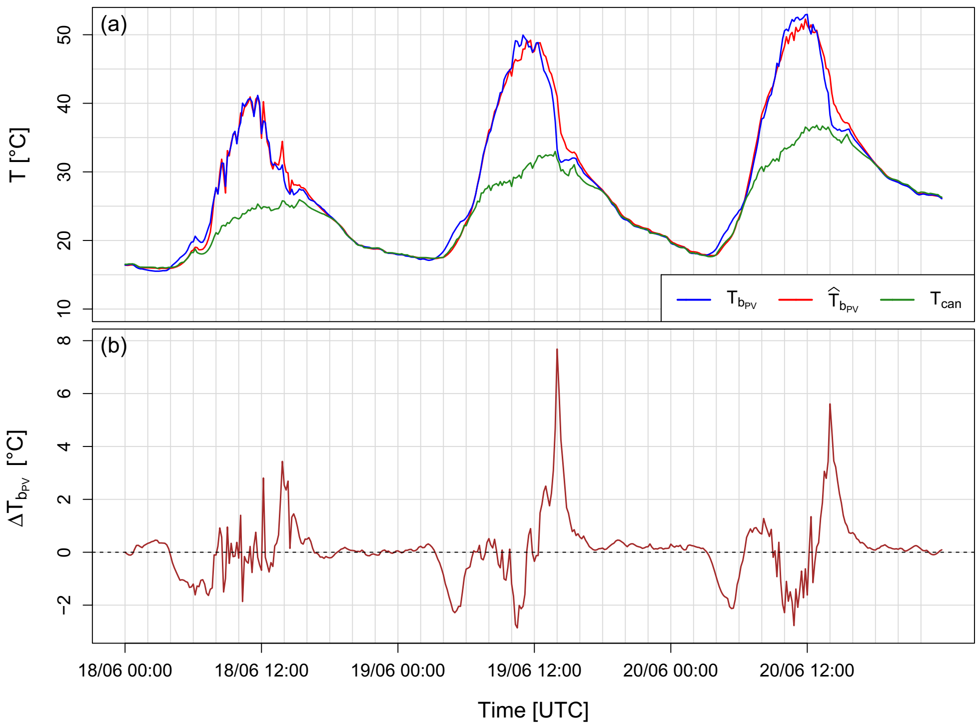

Fig. 6 Time series of **a** the temperature (T) measured inside the urban canyon (T_{can}, green) and at the back side of the PV module ($T_{b_{PV}}$, blue) and simulated at the back side of the PV module ($\widehat{T}_{b_{PV}}$, red) and **b** the difference ($\Delta T_{b_{PV}}$) between the measured and simulated back-side photovoltaic module temperature

photovoltaic facade. To this aim, we assume conditions where PV modules cover the whole southern wall of the building in the study domain, as the distance between the PV modules and the back-side wall is large enough to assume that the convective heat transfer is the same as used in the CTSM system. The largest uncertainty of this assumption is that we do not have knowledge about the surface temperature of the back-side wall which is an input variable for thermal radiative heat transfer. Therefore, we need to make assumptions for T_w. Here, we assume that it can be calculated with the same regression coefficients as given in Fig. 2b but considering addition of an average value of $\widehat{T}_{can}$, T_a, and daily average of T_a (considering that the daily average will not change its value, only the amplitude varies). Further, we make the assumption that the calculated U_{can} as in the TEB model can be taken as wind speed for calculating the UTCI.

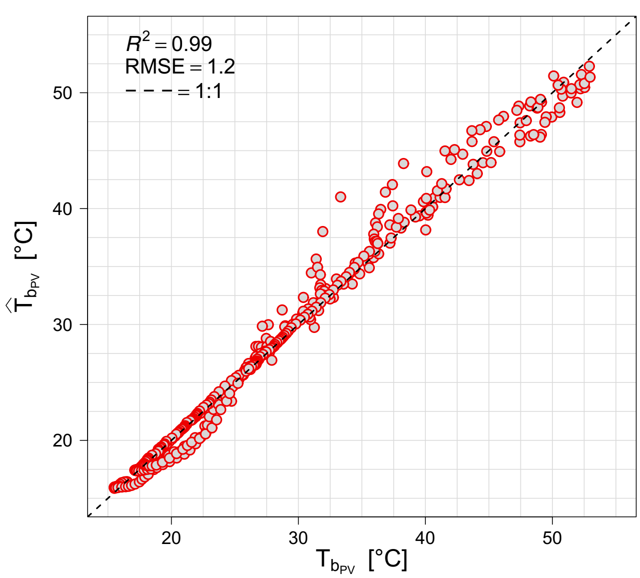

Fig. 7 Scatter plot of the measured temperature ($T_{b_{PV}}$) and simulated temperature ($\widehat{T}_{b_{PV}}$) of the PV module. The upper-left corner provides the squared Spearman's rank correlation coefficient (R^2) and the root mean square error (RMSE)

After defining the new modeling systems, a comparison of the canyon air temperature between different surface conditions can be done. For such calculations, the albedo κ of each surface has to be defined. The albedo value for asphalt $\kappa_g = 0.18$ was chosen based on Lindberg et al. (2016). The value for concrete $\kappa_g = 0.56$ was measured in the work of Krispel et al. (2017) and the value for the PV modules $\kappa_{PV} = 0.10$ was taken from Moralejo-Vàzquez et al. (2015).

Figure 8a, b, and c shows time series of $\widehat{T}_{can}$ and the UTCI for these different surface conditions including an additional simulation for UTCI with T_a. The related differences, $\Delta\widehat{T}_{can}$ and ΔUTCI, are shown in Fig. 8d, e, and f, respectively. Our results show that a bright ground surface and a slightly decreased wall temperature (see Figures S4 and S5 in the supplemental material) can substantially reduce air temperature (by up to -1.30 °C) and the UTCI (by up to -1.10 °C) in the sun between 7:00 and 14:00

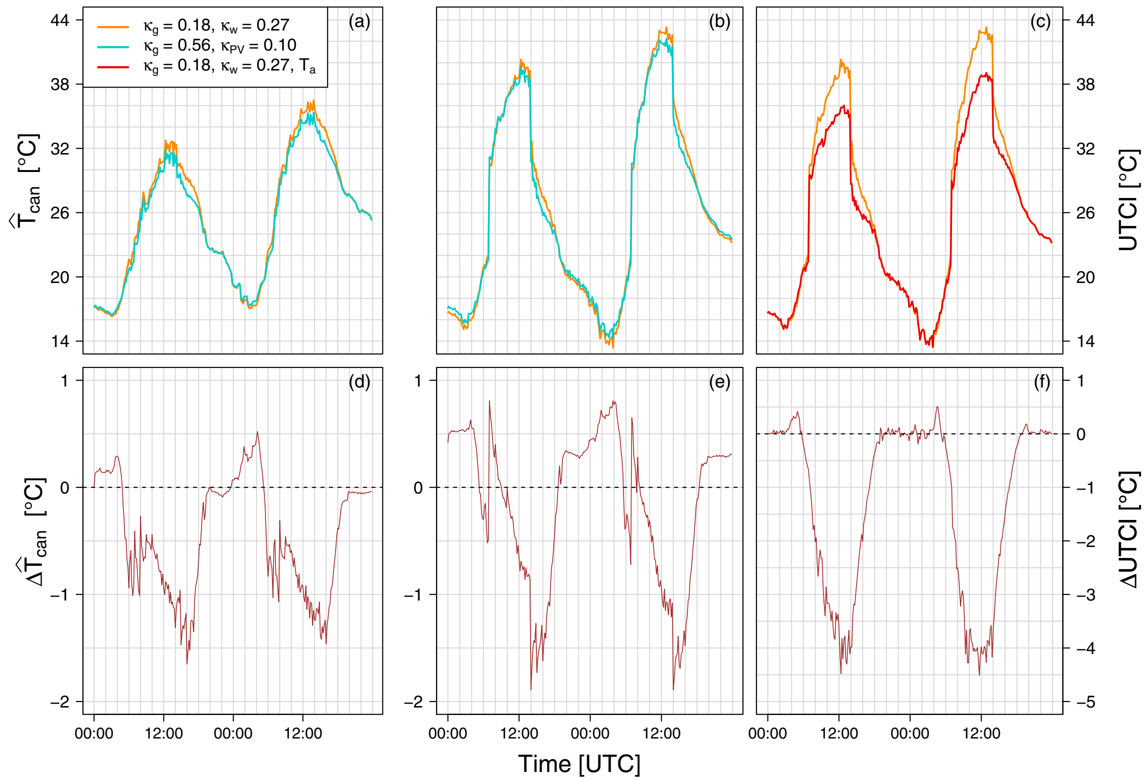

Fig. 8 Time series of **a** the modeled urban canyon air temperature ($\widehat{T}_{can}$), (**b**, **c**) the modeled Universal Thermal Climate Index (UTCI) with $\widehat{T}_{can}$ (orange and cyan), and the air temperature measured at the rooftop T_a (red) between 19 and 20 June 2017. The legend in panel **a** shows the reflectance (κ) for different surfaces ($\kappa_g = 0.18$ for asphalt, $\kappa_w = 0.27$ for glass facade, $\kappa_g = 0.56$ for concrete, and $\kappa_{PV} = 0.10$ for photovoltaic facade). Panels **d**, **e**, and **f** provide the difference between each surface condition regarding $\widehat{T}_{can}$ and UTCI, respectively

UTC. Even larger reductions are found in the shade between 14:00 and 16:00 UTC for both canyon air temperature (by up to − 1.65 °C) and UTCI (by up to − 1.85 °C). Further, Fig. 8f shows that an air temperature measured at a site which is not related to the actual surrounding surfaces results in a highly erroneous estimate of thermal (dis)comfort. In our case, ΔUTCI simulated with T_a shows a difference up to − 4.50 °C and misses the very strong occurring heat stress (defined as UTCI between 38 and 46 °C) on the first day of the simulation period (see Fig. 8c).

These results indicate that even small, local changes to the surface and thus albedo can have a measurable effect on air temperature and UTCI in an urban canyon. While this decrease between − 1 and − 2 °C seems to be noticeable but yet small, it shall not be underestimated in its effect on human comfort in a warmer future climate.

Discussion and conclusions

This study seeks to improve the simulation of air temperature in urban canyons. To this aim, field measurements have been performed in 2016 and 2017, to evaluate/update the wall and ground temperature parameterization and an energy balance model for photovoltaic (PV) modules within the solar and long-wave environmental irradiance geometry (SOLWEIG) model and couple it with parts of the Town Energy Balance (TEB) model.

For the parameterization of the wall surface temperature, we take infrared pictures of the Schwackhöfer-Haus at the University of Natural Resources and Life Sciences (BOKU), Vienna, with a FLIR E60bx to evaluate the accuracy of the current calculation scheme in SOLWEIG. Results show a clear overestimation of the surface temperature at solar elevation angles over 56 ° ($R^2 = 0.61$). We use global radiation measurements on a vertical plane instead to generate new regression coefficients ($R^2 = 0.76$).

We implement an updated calculation scheme for simulating ground temperature, which allows considering surface with user-specified albedo value and thermal conductivity properties. To develop this scheme, we used the force-restore method combining the radiation, sensible, and ground heat flux with the Euler method to estimate a time series of the ground temperature.

At the BOKU site, the ambient air temperature has been measured routine at the rooftop (26-m height above ground) but outputs show a difference up to 6 °C to the measured canyon air temperature (3 m height above ground). This huge difference is compensated with parts of the TEB model calculating the canyon air temperature.

We compare the performance of the currently implemented SOLWEIG scheme (CS) and the here-proposed calculation scheme (PS). The results of the canyon air temperature show a better performance of PS, particularly a substantial reduction in RMSE. While the PS shows generally satisfactory skill in predicting temperatures inside the studied urban canyon, we note that further updates are needed for the representation of open areas, street crossings, and different canyon orientations. Further, an implementation of the glazing ratio for buildings would also increase the overall quality of SOLWEIG.

Considering the importance of sustainable energy production and climate warming, we perform scenario calculations to investigate effects of potential changes to the wall surface inside an urban canyon. We do so by evaluating a heat transfer single-state model for a vertically mounted photovoltaic (PV) module.

A comparison between model results for current surface conditions (dark asphalt on the ground combined with a glass facade) and possible modification conditions (ground covered with bright concrete and a PV facade) was performed. The results indicate a robust decrease in canyon air temperature by up to − 1.65 °C for the modified canyon environment. To estimate human thermal comfort, we focus to calculate the Universal Thermal Climate index (UTCI). UTCI decreases by approx. − 1.00 °C in the sun and − 1.85 °C in the shade considering a change from present to modified conditions. We note in passing that future work should focus on effects of brighter surfaces for potentially increased human thermal stress.

We note in closing that additional field experiments for PV facades or building-integrated PV systems on large scales (e.g., a size of 60 · 20 m^2 like the south-facing wall of the Schwackhöfer-Haus) would strongly increase the quality of energy balance models, as the one presented here, and the possibility to mitigate, at least partially, urban heat island effects.

Acknowledgements The authors thank Meteo France and Valéry Masson for providing the Town Energy Balance model. The authors are grateful to Christian Gützer (University of Natural Resources and Life Sciences (BOKU), Vienna) for the technical support. This work received financial support from the University of Natural Resources and Life Sciences (BOKU) in Vienna.

Funding information This work was supported by the project "Optimizing reflecting materials and photovoltaics in urban areas regarding the radiation balance and bioclimatic" funded by the Austrian Research Promotion Agency (FFG) and the project "Influence of urban expansions on the urban heat island in Vienna" funded by the Klima- und Energiefonds.

Abbreviations a, time-of-day dependent factor (force-restore method) (1/s); A, area (m^2); B, day of the year dependent factor (declination angle) (−); c, specific heat capacity (J/); C, heat capacity (J/K); C_d, drag coefficient (−); CS, currently implemented SOLWEIG scheme; CTSM, continuous time stochastic model; e, Gaussian white noise (−); f, non-linear function; F, net radiation balance (W/m^2); g, gravitational constant (m/s^2); G, global radiation (W/m^2); h, building height (m); $\overline{h}$, average building height (m); H, heat flux (W/m^2); i, value for the size of every step (Euler method) (−); IAM, incidence angle modifier (−); M, non-linear function; n, day of the year (−); N, number of observations (−); p, pressure (hPa); PS, proposed calculation scheme; Q, heat transfer (W/m^2); Qc, convective heat transfer (W/m^2); Ql, long-wave heat transfer (W/m^2); RES, aerodynamic resistance (s/m); RH, relative humidity (%); S, soil heat capacity (J/m^3 K); t, time (s); T, measured temperature (°C); $\hat{T}$, modeled temperature (°C); $u_* + w_*$, turbulent wind (m/s); U, wind speed (m/s); w, street width (m); W, non-linear function; y, discrete time observation; z, depth of thermal layer (m); z_0, roughness length (m).

Greek symbols α, absorptivity (−); β, tilt angle of a vertical plane from the horizontal (°); β_0, temperature coefficient of photovoltaic module (%/K); δ, declination angle (°); ΔT, temperature difference (K); ε, emissivity (−); η, photovoltaic module efficiency (%); θ_{aoi}, angle of incidence (°); Θ, vector of unknown parameters; κ, reflectance (−); λ, thermal conductivity (W/(m K)); ρ, material density (kg/mÂş); σ, Stefan-Boltzmann constant (W/(m^2 K^4)); Σ, covariance; Υ, time series of N observations; ϕ, geographical latitude (°); Ψ, view factor (−); ω, Wiener processs; Ω, Earth's angle velocity (1/s).

Subscripts a, air; as, near-surface air; $asphalt$, index for asphalt properties; b, back side; b_{PV}, back side of photovoltaic module; c, combined value; can, urban canyon; dew, dew point; e, electricity; f, front side; g, ground; gl, glass; h, horizontal plane; m, approximately constant value; p, constant pressure; PV, photovoltaic module; r, rate; ref, reference; s, solar; sky, sky; top, rooftop; w, wall.

References

Armstrong S, Hurley WG (2010) A thermal model for photovoltaic panels under varying atmospheric conditions. Appl Therm Eng 30(11-12):1488–1495

Arya P (ed.) (2001) Introduction to micrometeorology, Academic Press

Barker G, Norton P (2003) Building america system performance test practices: part 1 – photovoltaic systems, technical report, Office of Scientific and Technical Information (OSTI)

Blackadar AmKa (1976) Modeling the nocturnal boundary layer, Reprints third symp. Atmospheric turbulence, diffusion and air quality, Raleigh, Am Meteorol Soc, pp 46–49

Blazejczyk K, Epstein Y, Jendritzky G, Staiger H, Tinz B (2011) Comparison of UTCI to selected thermal indices. Int J Biometeorol 56(3):515–535

Bogren J, Gustavsson T, Karlsson M, Postgard U (2000) The impact of screening on road surface temperature. Meteorlogical Applications 7(2):97–104

Brito MC, Freitas S, Guimarães S, Catita C, Redweik P (2017) The importance of facades for the solar PV potential of a mediterranean city using liDAR data. Renew Energy 111:85–94

Bröde P, Fiala D, Błażejczyk K, Holmér I, Jendritzky G, Kampmann B, Tinz B, Havenith G (2011) Deriving the operational procedure for the universal thermal climate index (utci). Int J Biometeorol 56(3):481–494

Duffie JA, Beckman WA (2013) Solar engineering of thermal processes. Wiley, New York

Fiala D, Lomas KJ, Stohrer M (2001) Computer prediction of human thermoregulatory and temperature responses to a wide range of environmental conditions. Int J Biometeorol 45(3):143–159

FLIR Systems Inc. (2016) http://www.flir.com

Grimmond CSB, Blackett M, Best MJ, Barlow J, Baik J-J, Belcher SE, Bohnenstengel SI, Calmet I, Chen F, Dandou A et al (2010) And The international urban energy balance models comparison project: first results from phase 1. J Appl Meteorol Climatol 49(6):1268–1292

Herrando M, Markides CN, Hellgardt K (2014) A UK-based assessment of hybrid PV and solar-thermal systems for domestic heating and power: system performance. Appl Energy 122:288–309

Jazwinski AH (1970) Stochastic processes and filtering theory, Elsevier, pp vii–viii

Jones AD, Underwood CP (2001) A thermal model for photovoltaic systems. Sol Energy 70(4):349–359

Juhl R (2016) Ctsmr: Ctsm for r. R package version 0.6.10

Juhl R, Moller J, Madsen H (2016) ctsmr - continuous time stochastic modeling in r, The R Journal

King DL, Boyson WE, Kratochvil JA (2004) Photovoltaic array performance model, http://energy.sandia.gov/download/21046/

Kotak Y, Gul MS, Muneer T, Ivanova SM (2015) Investigating the impact of ground albedo on the performance of pv systems

Krispel S, Peyerl M, Maier G, Weihs P (2017) Urban heat islands - reduktion von innerstädtischen wärmeinseln durch whitetopping. Bauphysik 39(1):33–40

Lindberg F, Grimmond CSB, Gabey A, Huang B, Kent CW, Sun T, Theeuwes NE, Järvi L, Ward HC, Capel-Timms I (2018) Urban multi-scale environmental predictor (umep): an integrated tool for city-based climate services. Environ Model Softw 99:70–87

Lindberg F, Grimmond CSB (2011) The influence of vegetation and building morphology on shadow patterns and mean radiant temperatures in urban areas: model development and evaluation. Theor Appl Climatol 105(3-4):311–323

Lindberg F, Grimmond CSB (2016) Solweig, http://urban-climate.net/umep/SOLWEIG

Lindberg F, Holmer B, Thorsson S (2008) SOLWEIG 1.0 – modelling spatial variations of 3d radiant fluxes and mean radiant temperature in complex urban settings. Int J Biometeorol 52(7):697–713

Lindberg F, Jonsson P, Honjo T, Wästberg D (2015) Solar energy on building envelopes - 3d modelling in a 2d environment. Sol Energy 115:369–378

Lindberg F, Onomura S, Grimmond CSB (2016) Influence of ground surface characteristics on the mean radiant temperature in urban areas. Int J Biometeorol 60(9):1439–1452

Lodi C, Bacher P, Cipriano J, Madsen H (2012) Modelling the heat dynamics of a monitored test reference environment for building integrated photovoltaic systems using stochastic differential equations. Energy and Buildings 50:273–281

Lumitos GmbH (2017) http://www.chemie.de/

Masson V (2000) A Physically-based scheme for the urban energy budget in atmospheric models. Bound-Layer Meteorol 94(3):357–397

Moigne PL (2012) Surfex scientific documentation

Moralejo-Vàzquez FJ, Martín-chivelet N, Olivieri L, Caamaño-martín E (2015) Luminous and solar characterization of PV modules for building integration. Energy and Buildings 103:326–337

Nielsen JN, Madsen H, Young PC (2000) Parameter estimation in stochastic differential equations: an overview. Annu Rev Control 24:83–94

Palyvos JA (2008) A survey of wind convection coefficient correlations for building envelope energy systems' modeling. Appl Therm Eng 28(8-9):801–808

PVEducation (2017) http://pvcdrom.pveducation.org/SUNLIGHT/MODTILT.HTM

Sharples S (1984) Full-scale measurements of convective energy losses from exterior building surfaces. Build Environ 19(1):31–39

Spencer JW (1971) http://www.mail-archive.com/sundial@uni-koeln.de/msg01050.html

Stull RB (ed.) (1988) An introduction to boundary layer meteorology, Springer Netherlands

UN (2014) World urbanization prospects, United Nations. visited on https://esa.un.org/unpd/wup/Publications/Files/WUP2014-Highlights.pdf

Weihs P, Staiger H, Tinz B, Batchvarova E, Rieder H, Vuilleumier L, Maturilli M, Jendritzky G (2011) The uncertainty of UTCI due to uncertainties in the determination of radiation fluxes derived from measured and observed meteorological data. Int J Biometeorol 56(3):537–555

ZAMG HoheWarte (2018) Meteorological measurements, data set from 1981 to 2017, Central Institution for Meteorology and Geodynamics

URBANIA

Einfluß von Stadterweiterung auf die Wärmeinsel der Stadt Wien im Kontext des Klimawandels

1.Juni 2016 – 31.Mai 2018
ACRP 8th call: KR14AC7K11944

Inst. für Meteorologie, Dep. Wasser, Atmosphäre, Umwelt, BOKU Wien:
BOKU-Rad: Philipp Weihs, Heidelinde Trimmel, Sandro Oswald
BOKU-Klim: Herbert Formayer, Imran Nadeem
BOKU-Biomet: Erich Mursch-Radlgruber, Christian Gützer

MA22: Jürgen Preiss, Christian Härtel

Météo-France: Valéry Masson

Wärmeinseleffekt von Wien beträgt im Schnitt 1,6°C (Schwab und Steinicke, 2003) und kann an einem typischen Wärmeinseltag (Wintertag mit geringer Windgeschwindigkeit 4 bis 5°C erreichen (Baumann, 2000)

Urbane Wärmeinsel wird hauptsächlich durch Absorption der Strahlung durch die versiegelten und bebauten Flächen (durch größere Oberfläche) und durch einen kleineren Vegetationsanteil verursacht

Wien erwartet einen Zuzug von ca. 200000 Menschen bis zum Jahr 2030. Deswegen müssen Wohnflächen geschaffen werden (Quelle: Statistik Austria) .

OBERFLÄCHENTEMPERATUR VON WIEN

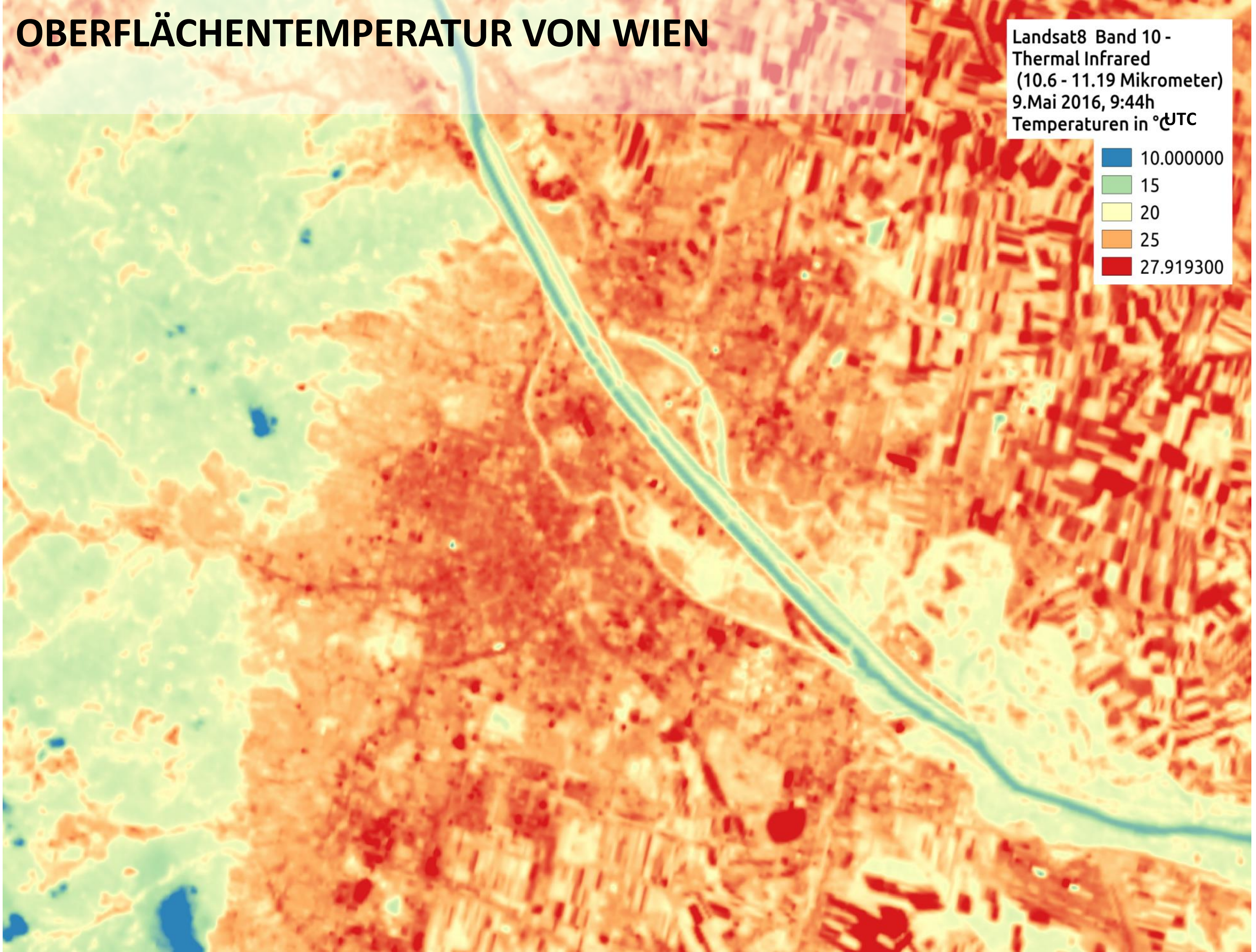

METHODIK

- Kopplung von Mesoskaligem Modell Weather research and Forecasting (WRF) Modell mit mikroskaligem Modell Town Energy Balance (TEB) Modell

- Adaptierung, Überprüfung und Validierung der Modelle

- Simulation von Klima und Stadtentwicklungszenarien

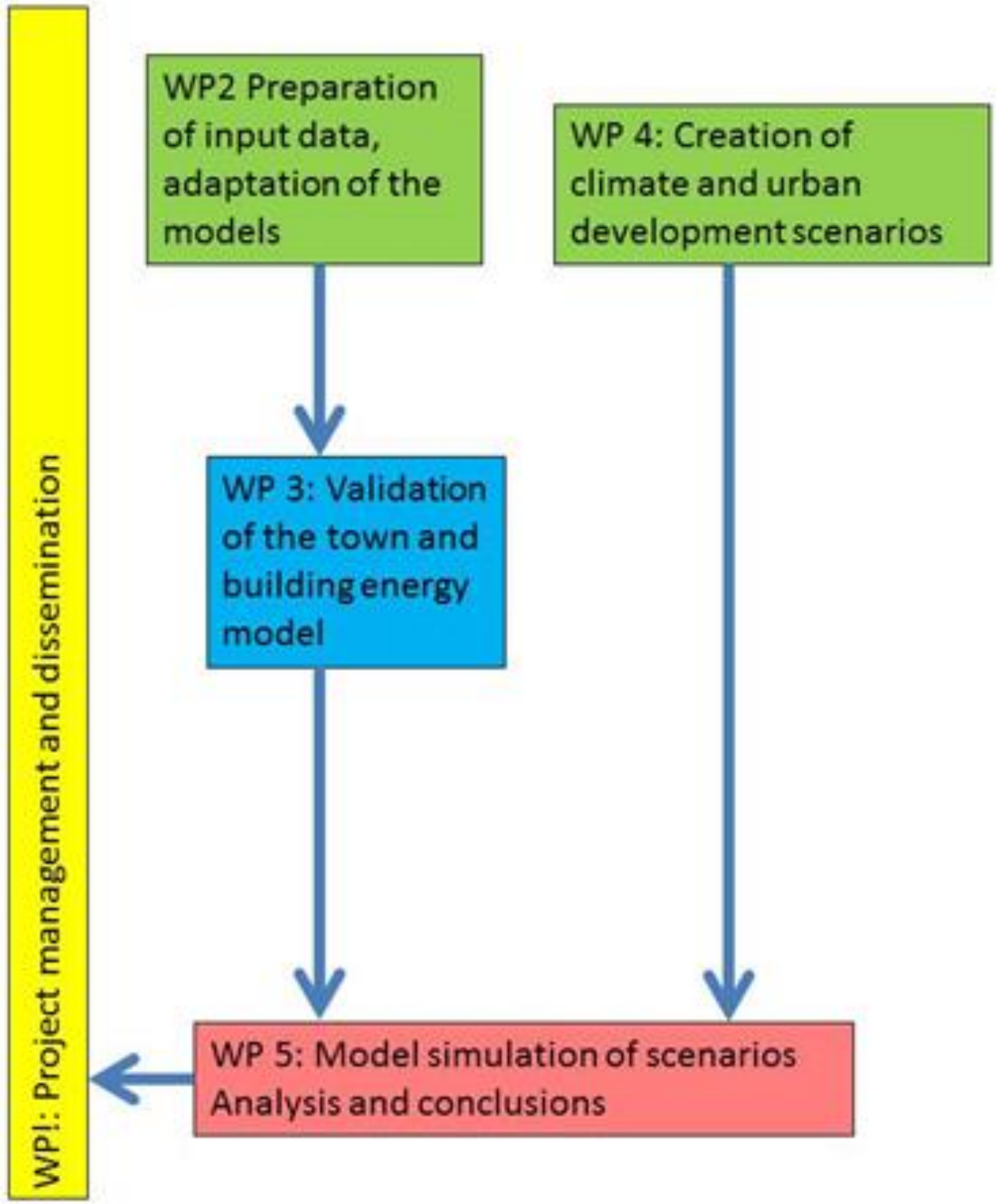
WP2 Preparation of input data, adaptation of the models
WP 4: Creation of climate and urban development scenarios
WP 3: Validation of the town and building energy model
WP 5: Model simulation of scenarios Analysis and conclusions
WPI: Project management and dissemination

Town Energy Balance Modell

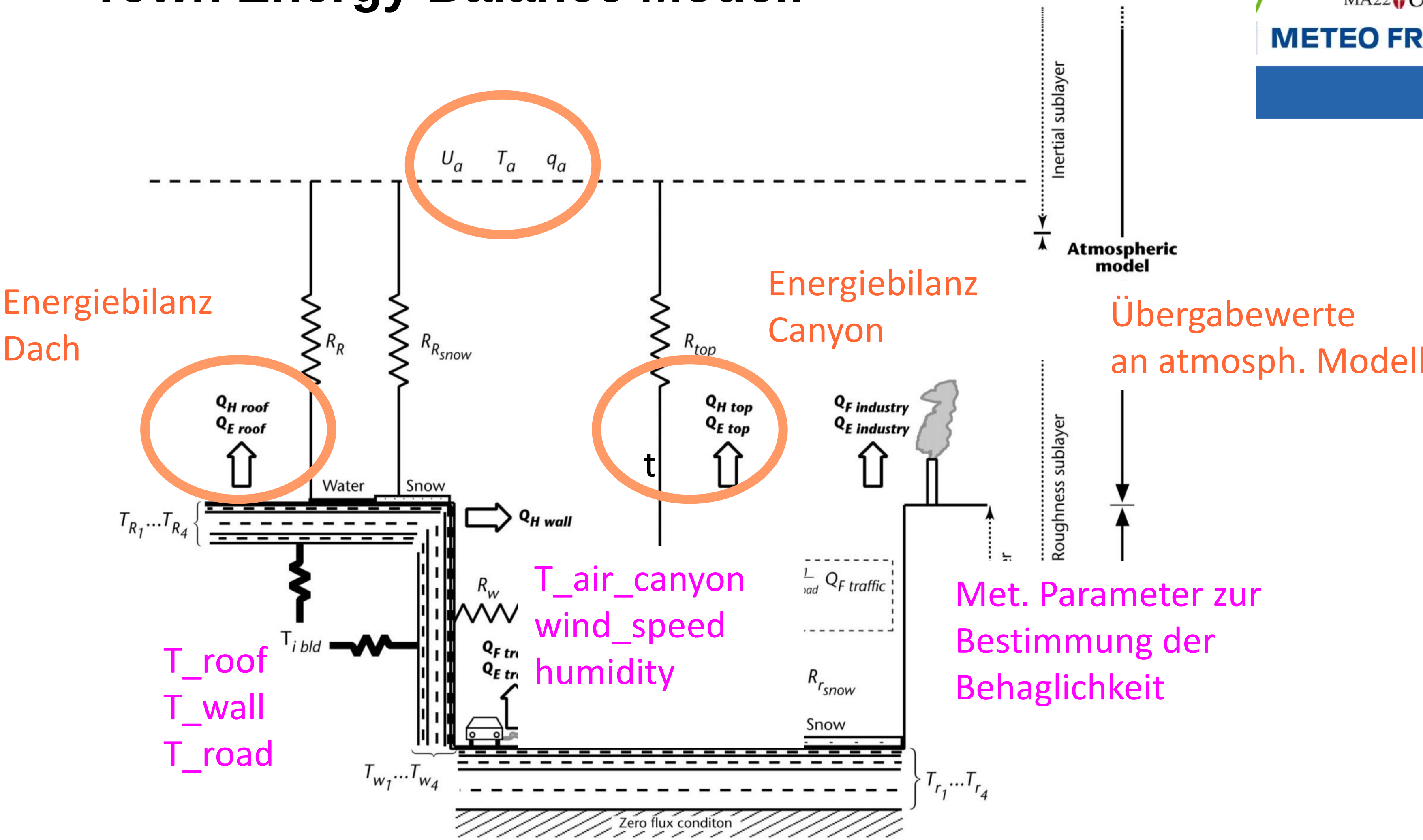

FIG. 2. Schematic representation of the surfaces (roof, wall, road indicated by subscript R, w, and r, respectively), prognostic temperatures (T), and aerodynamic resistances (R) used in TEB and the output fluxes. Resistances shown with thick lines have been altered from the original scheme (Masson 2000). Thus, $Q_{HTEB} = f_{\text{roof}} Q_{H\text{roof}} + f_{\text{road}} Q_{H\text{top}} + Q_{F\text{industry}}$ and $Q_{ETEB} = f_{\text{roof}} Q_{E\text{roof}} + f_{\text{road}} Q_{E\text{top}} + Q_{E\text{industry}}$.

Source: Masson V et al. 2002, adaptiert

Town Energy Balance Modell

Bei der Kopplung zu übergebende Größen zw. TEB und WRF: (Auswahl)

WRF zu TEB: u.a. potentielle Lufttemperatur (niedrigste atm. Schicht), Mischungsverhältnis,Wind, diffuse und direkte kurzwellige Strahlung

TEB zu WRF
 u.a. 2 Meter Lufttemperatur, Kurzwellige nach oben, Langellige nach oben, fühlbare Wärme, latente Wärme, (diagnostischer) Wind

WRF Modeling System Flow Chart

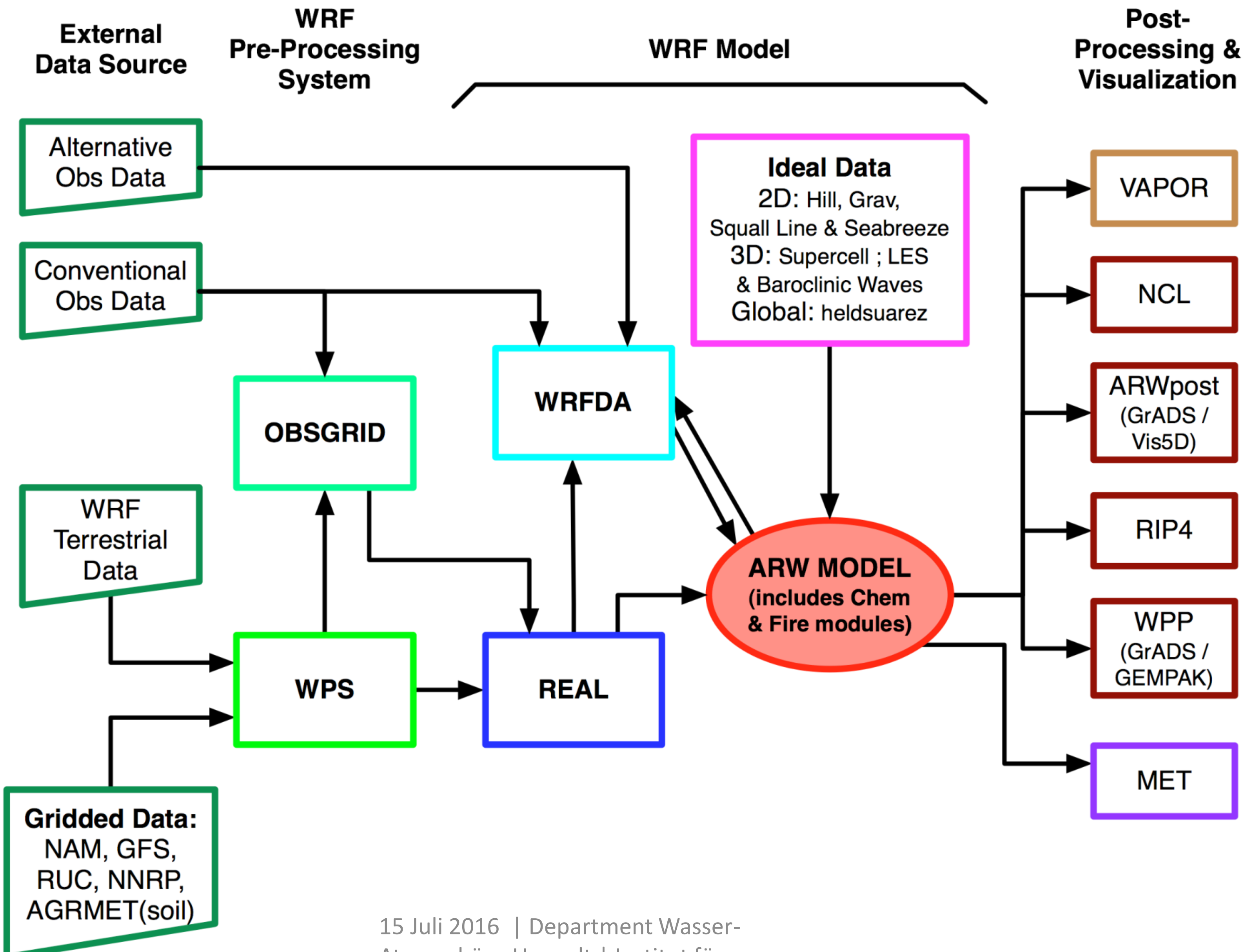

WRF Modeling System Flow Chart

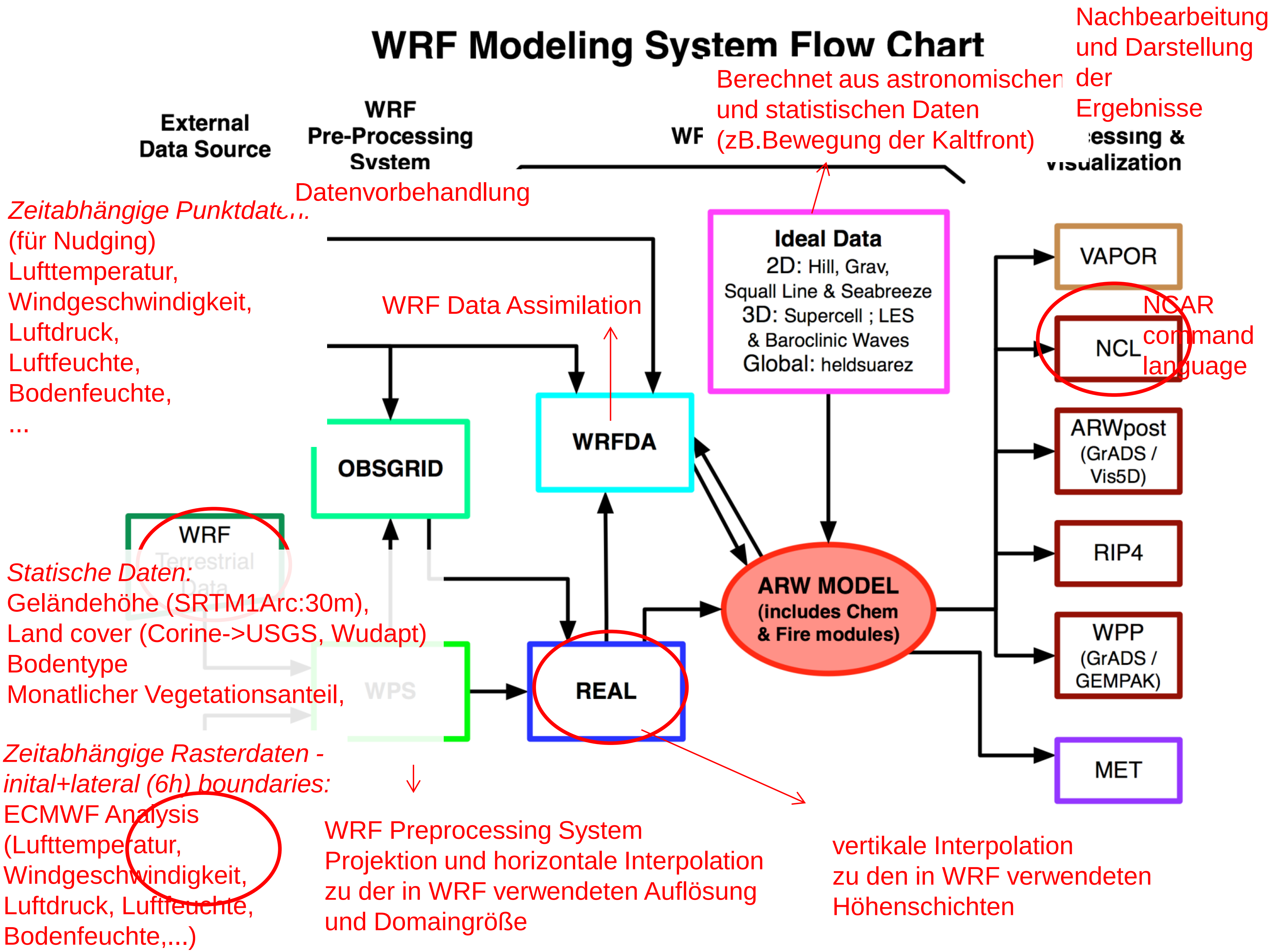

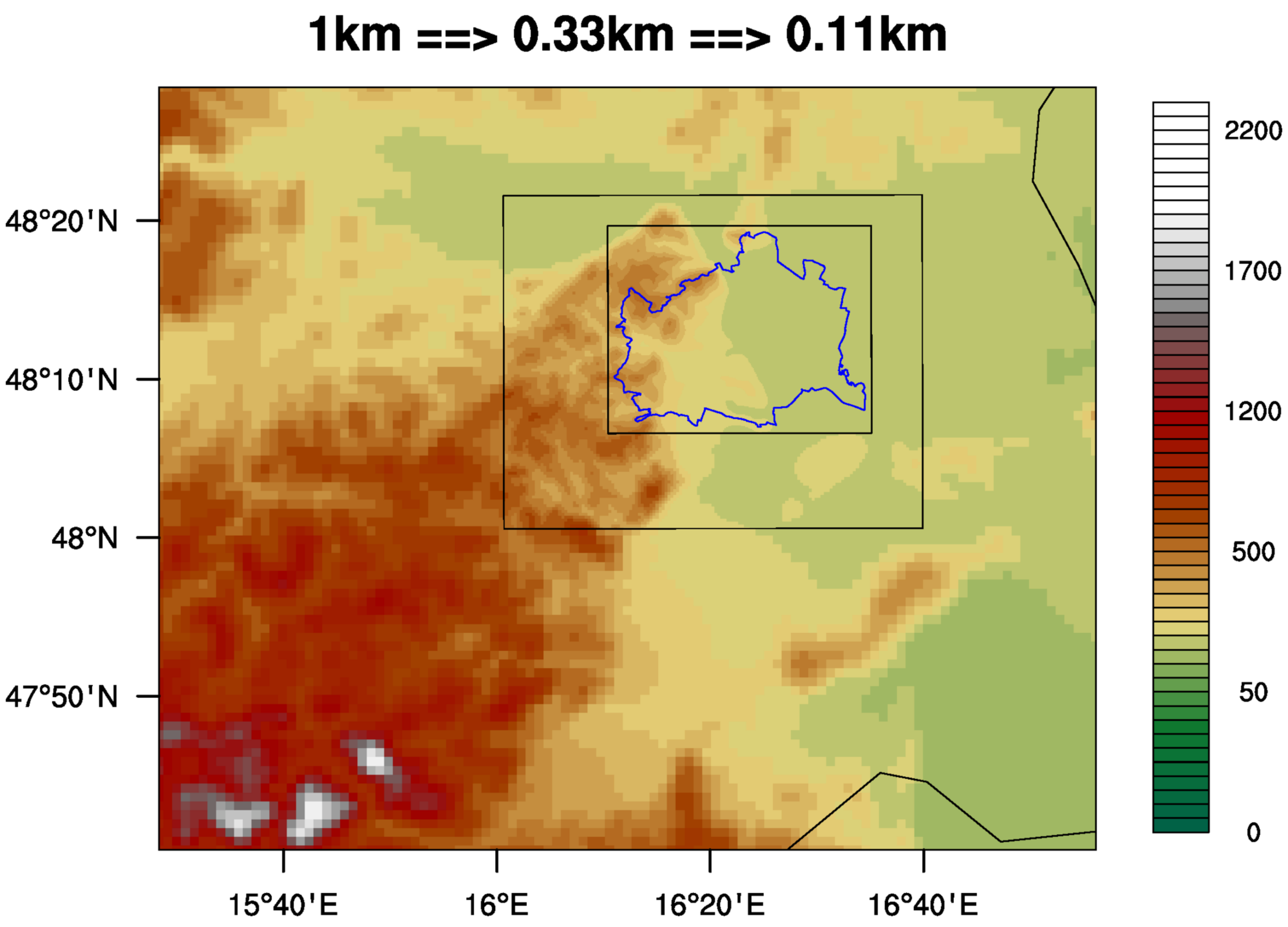
1km ==> 0.33km ==> 0.11km
48°20'N
48°10'N
48°N
47°50'N
15°40'E
16°E
16°20'E
16°40'E
2200
1700
1200
500
50
0

The Modelling system

THE SOLWEIG MODEL (Solar and LongWave Environmental Irradiance Geometry)

(Lindberg et al. 2008 and Lindberg & Grimmond 2011)

- Simulates spatial variations of 3D radiation fluxes and T_{mrt} in complex urban settings
- T_{mrt} derived by modelling shortwave and longwave radiation fluxes
- Sky view factor and shadow patterns are a central elements when estimating the fluxes

Mean radiant temperature (T_{mrt}) = A sum of all shortwave and longwave radiation fluxes to which the human body is exposed.

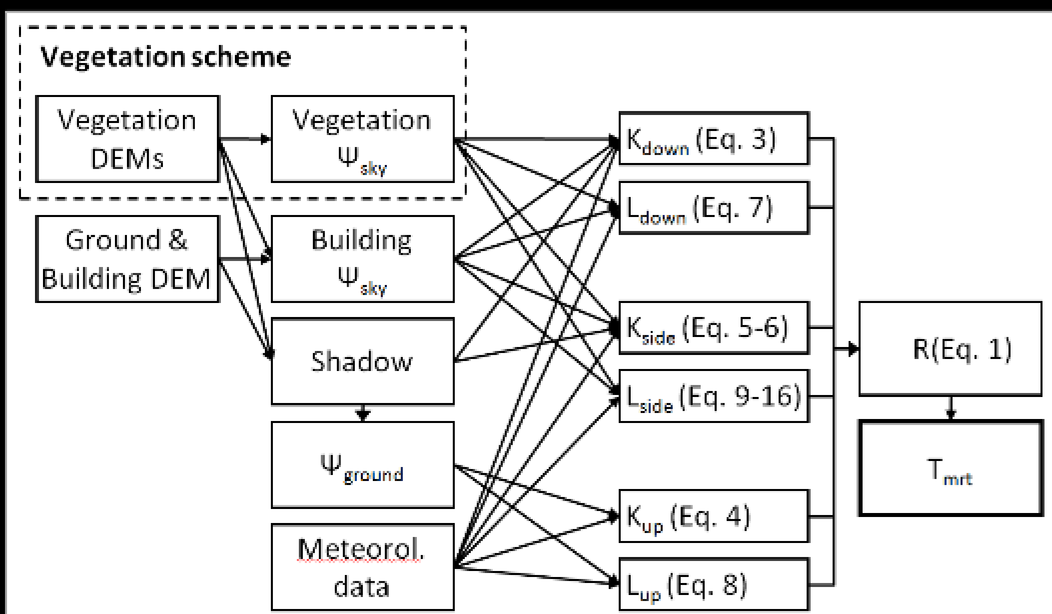

Digital Surface Model, Göteborg (Sweden)

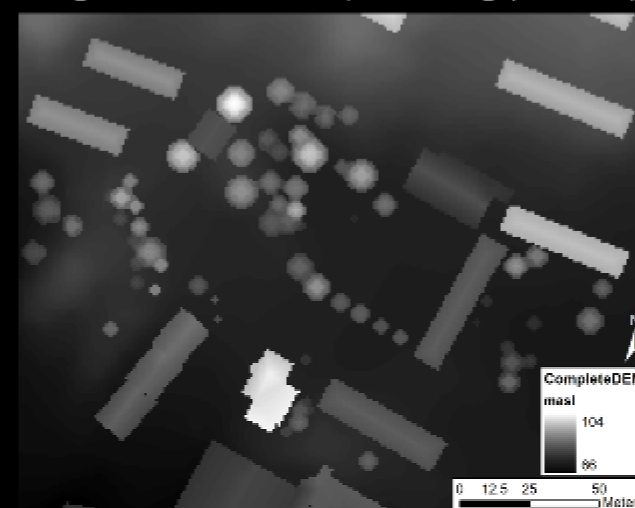

Arbeitspaket 2:

Vorbereitung der Modellinputdaten

Adaptierung der Modelle

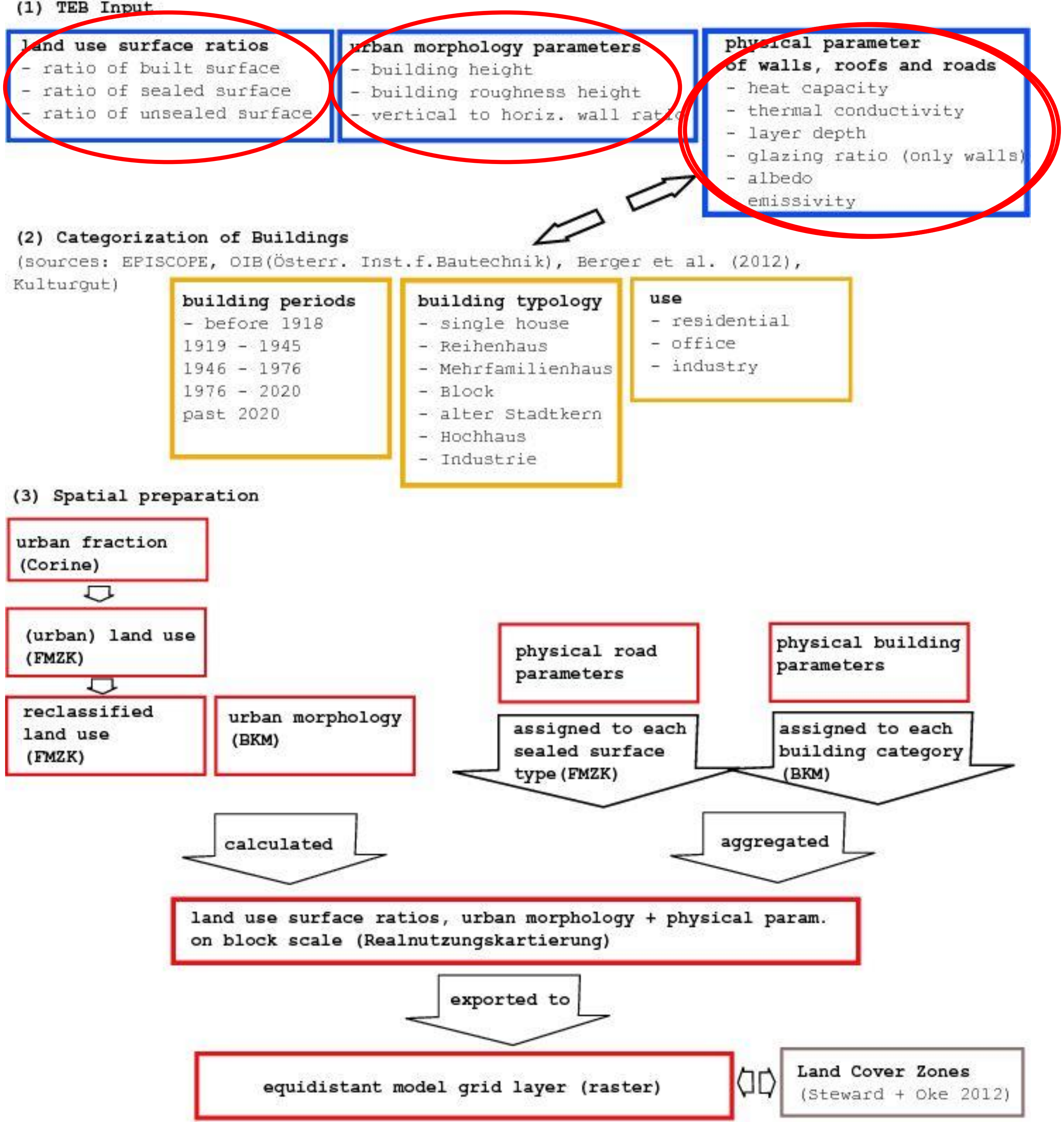
(1) TEB Input
land use surface ratios
- ratio of built surface
- ratio of sealed surface
- ratio of unsealed surface
urban morphology parameters
- building height
- building roughness height
- vertical to horiz. wall ratio
physical parameter
of walls, roofs and roads
- heat capacity
- thermal conductivity
- layer depth
- glazing ratio (only walls)
- albedo
emissivity
(2) Categorization of Buildings
(sources: EPISCOPE, OIB(Österr. Inst.f.Bautechnik), Berger et al. (2012), Kulturgut)
building periods
- before 1918
1919 - 1945
1946 - 1976
1976 - 2020
past 2020
building typology
- single house
- Reihenhaus
- Mehrfamilienhaus
- Block
- alter Stadtkern
- Hochhaus
- Industrie
use
- residential
- office
- industry
(3) Spatial preparation
urban fraction (Corine)
(urban) land use (FMZK)
reclassified land use (FMZK)
urban morphology (BKM)
physical road parameters
physical building parameters
assigned to each sealed surface type (FMZK)
assigned to each building category (BKM)
calculated
aggregated
land use surface ratios, urban morphology + physical param. on block scale (Realnutzungskartierung)
exported to
equidistant model grid layer (raster)
Land Cover Zones (Steward + Oke 2012)

Anteil unversiegelter Fläche

Anteil bebauter Fläche

Sky view Factor (SVF)

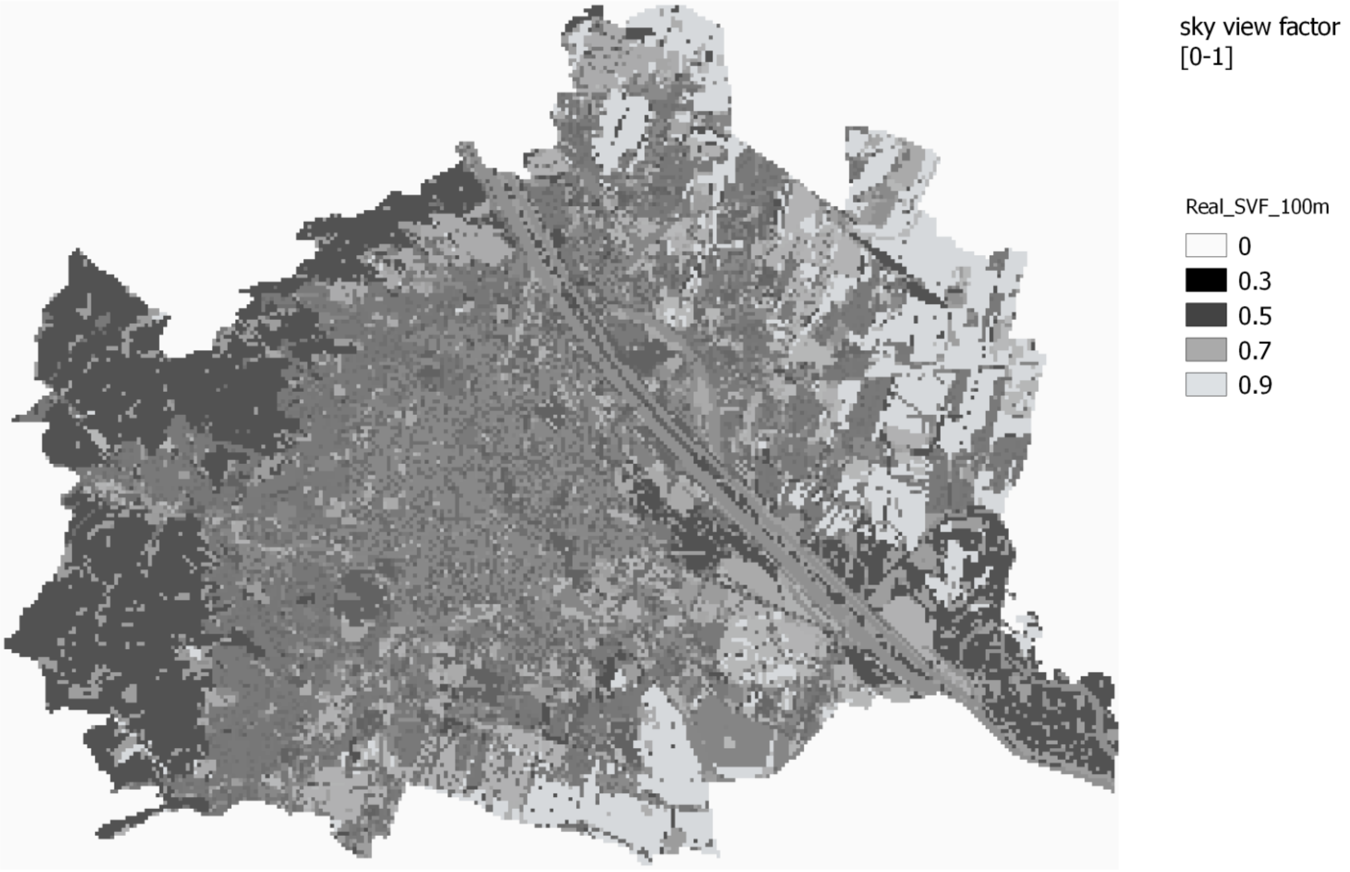

Arbeitspaket 3:

Validierung der Modelle

Überprüfung von Modellen in zwei Schritten

1. Überprüfung der von TEB berechneten Strahlungsflüssen in einem Strassencanyon

a) mit Hilfe von Messungen.
(Strassencanyon oft nicht regelmäßig wie von TEB vorgegeben)

b) Vergleich der Strahlungsflüsse mit anderem Modell (SOLWEIG od. Envi-Met)

2. Validierung der berechneten Temperaturverteilungen

a) Satellitendaten

b) Bodenstationen

- Bestehende kontinuierliche Stationen

- Ergänzende kontinuierliche Stationen

- ergänzende Messungen im Zuge von Messkampagnen

- TEB wurde bereits für viele Städte validiert (Mexiko City, Oklahoma City, Marseille, Toulouse, Vancouver, Paris, Nantes, Lodz, Montréal, …)
- Noch nie für Wien verwendet

BOKU - Messstandort

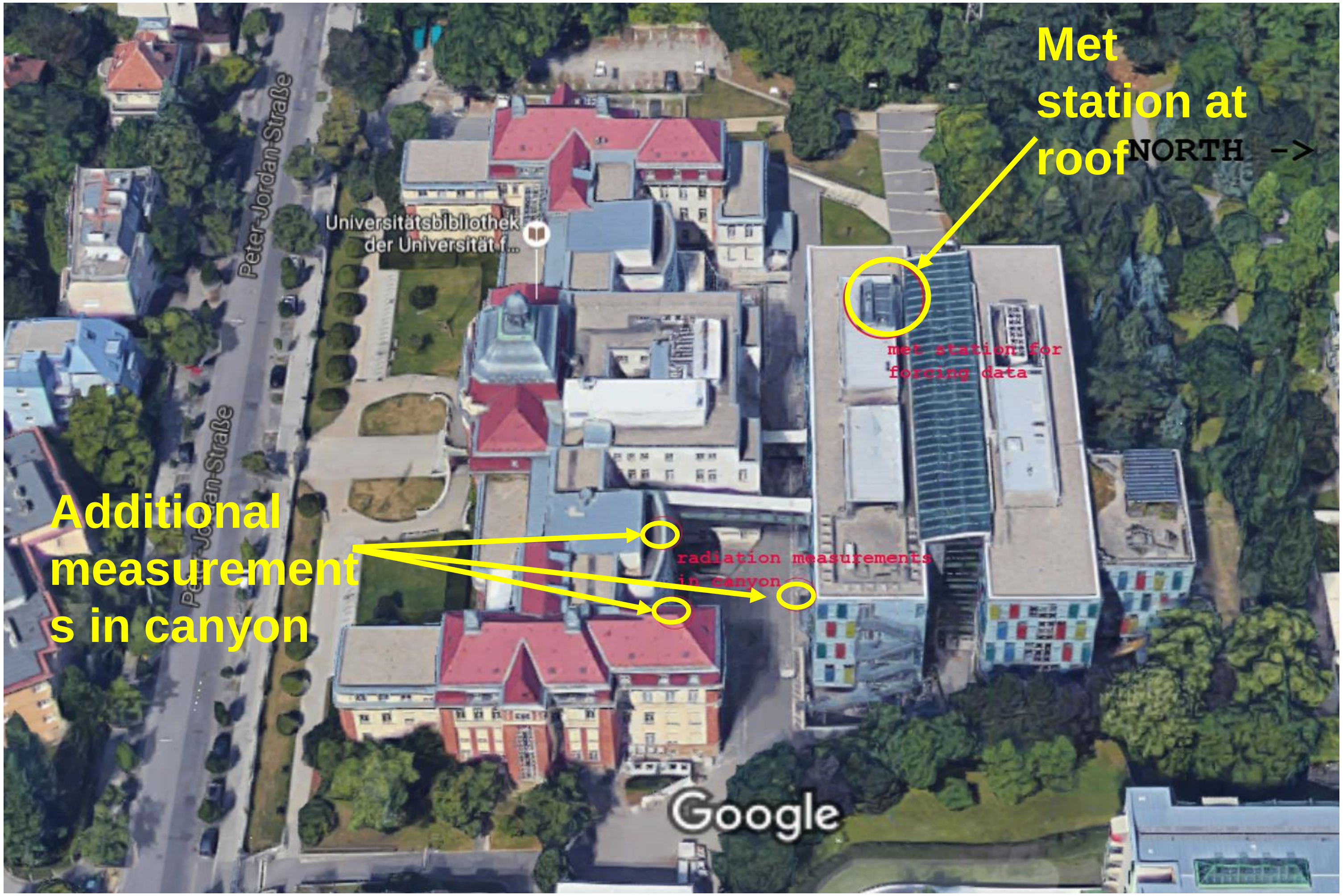

3.1. Überprüfung der von TEB berechneten Strahlungsflüssen in einem Strassencanyon

Forcing data - Dach

Air temperature, humidity, pressure,
wind speed and direction at the BOKU weather station

Fotos: S.Oswald

Canyon Messungen 1

Detailed additional measurements:

- Long-wave and short wave radiation balance
- At the top, in the middle (vertical and horizontal) and bottom of canyon

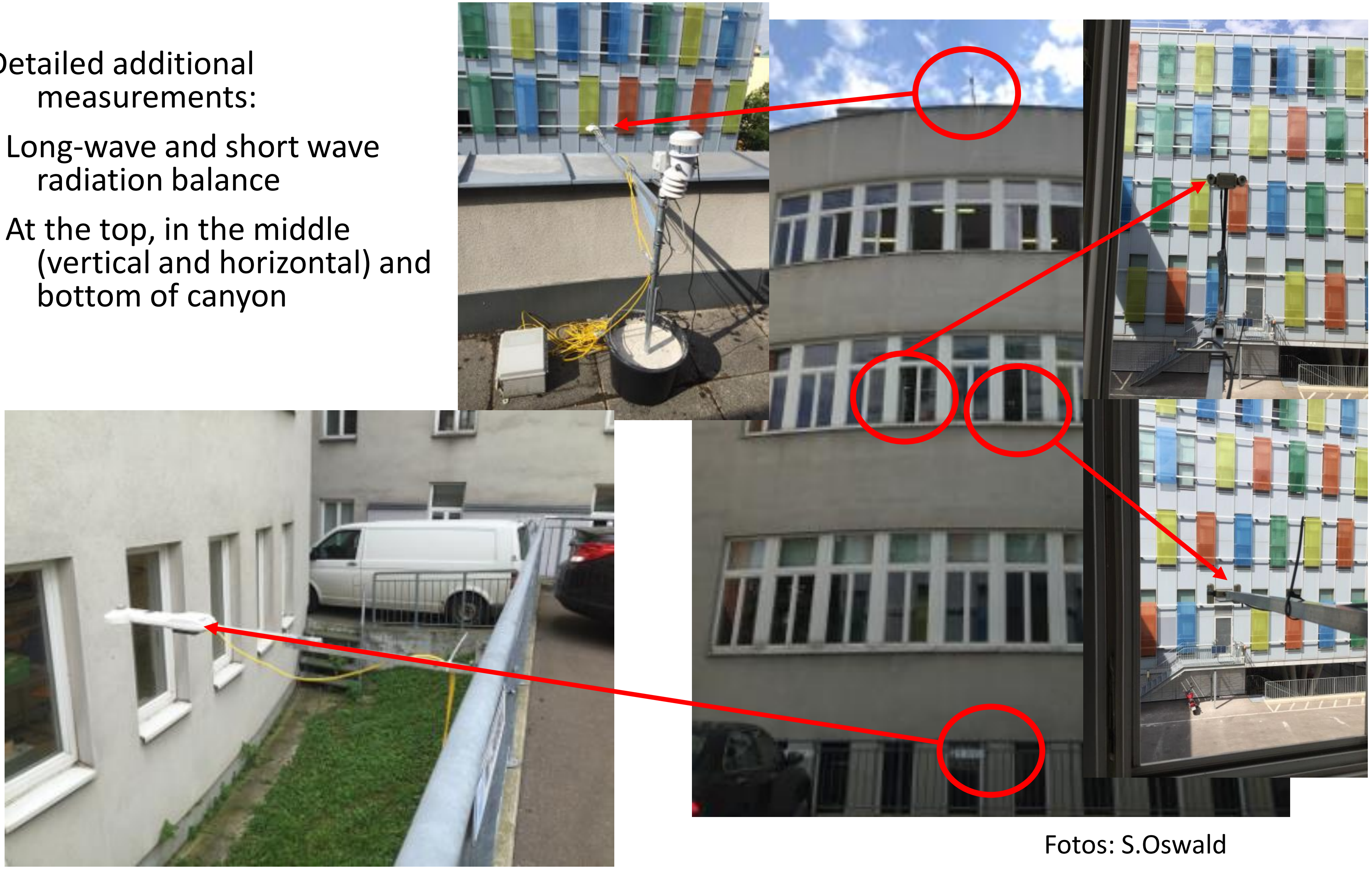

Fotos: S.Oswald

Canyon Messungen 2

- Incoming / reflected short wave radiation in canyon
- Three points, in six directions

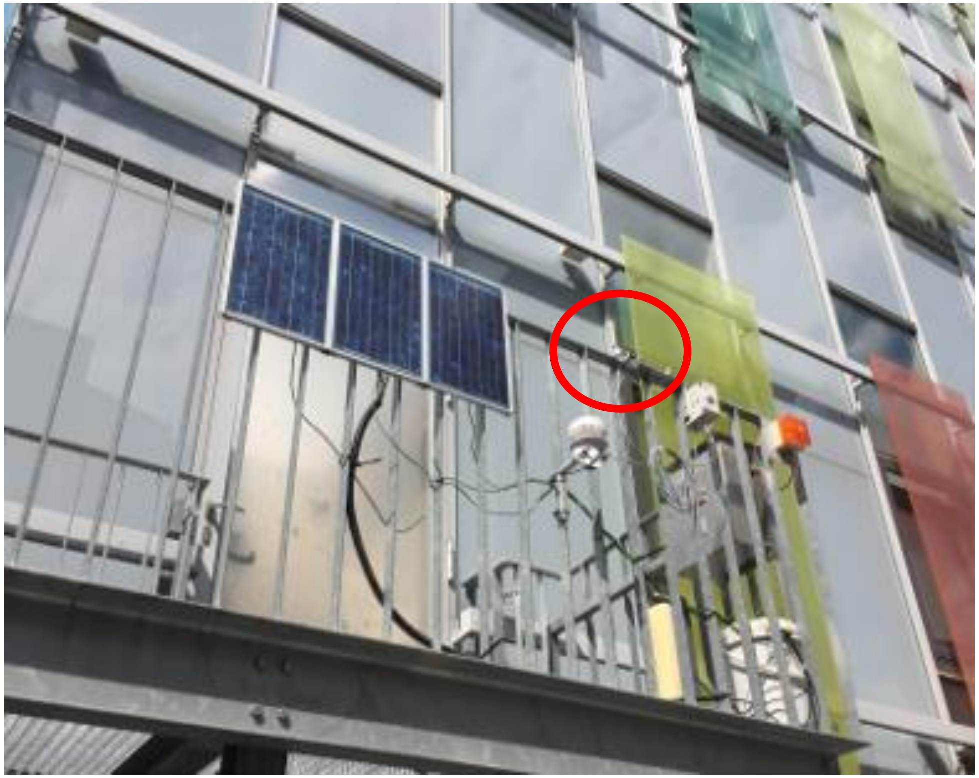

3.1. Überprüfung der von TEB berechneten Strahlungsflüssen in einem Strassencanyon

Kurzwellige Globalstrahlung Messterrasse

Kurzwellige Globalstrahlung Zwischenniveau

Kurzwellige Globalstrahlung Strassenschlucht

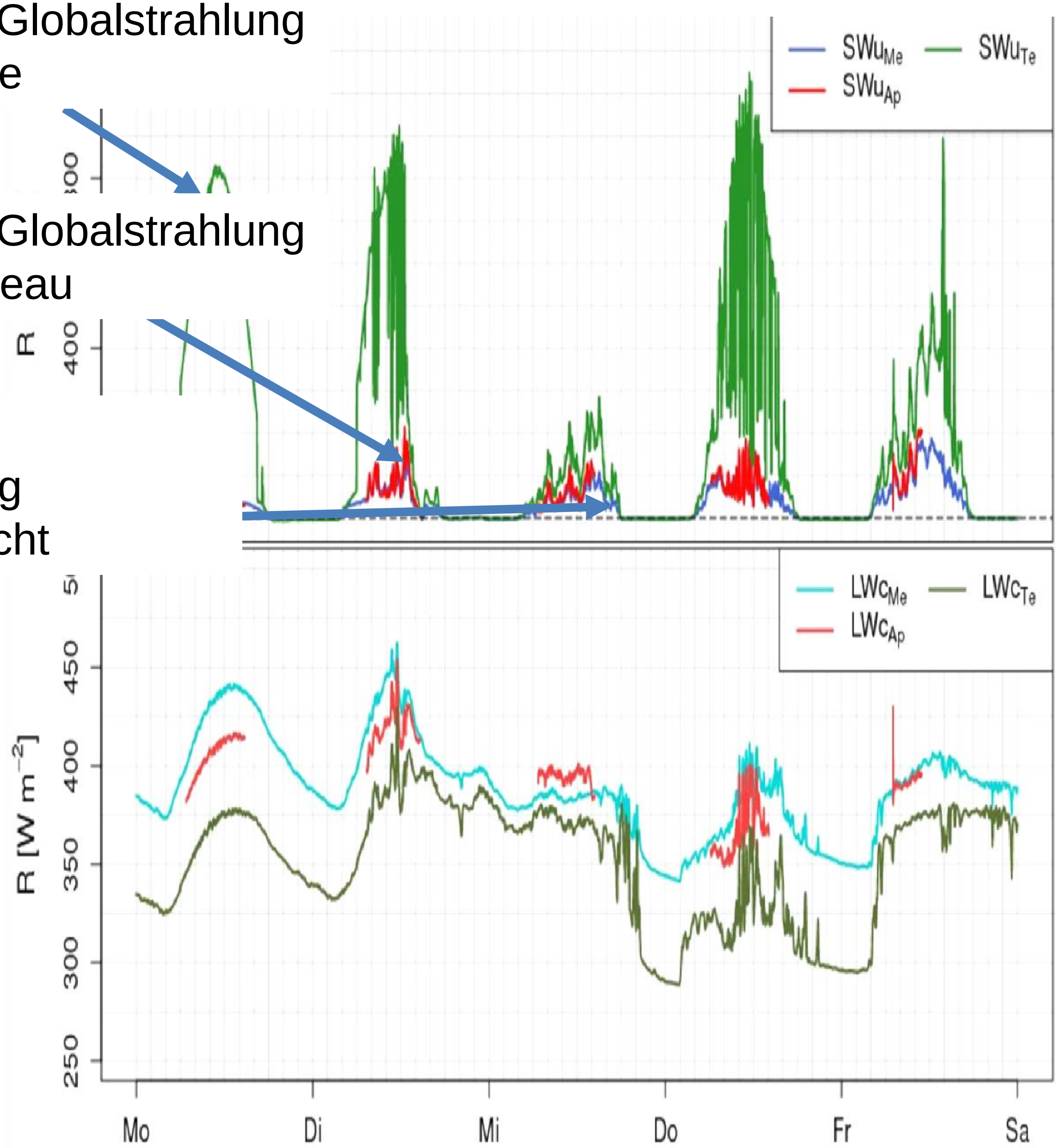

3.1. Überprüfung der von TEB berechneten Strahlungsflüssen in einem Strassencanyon

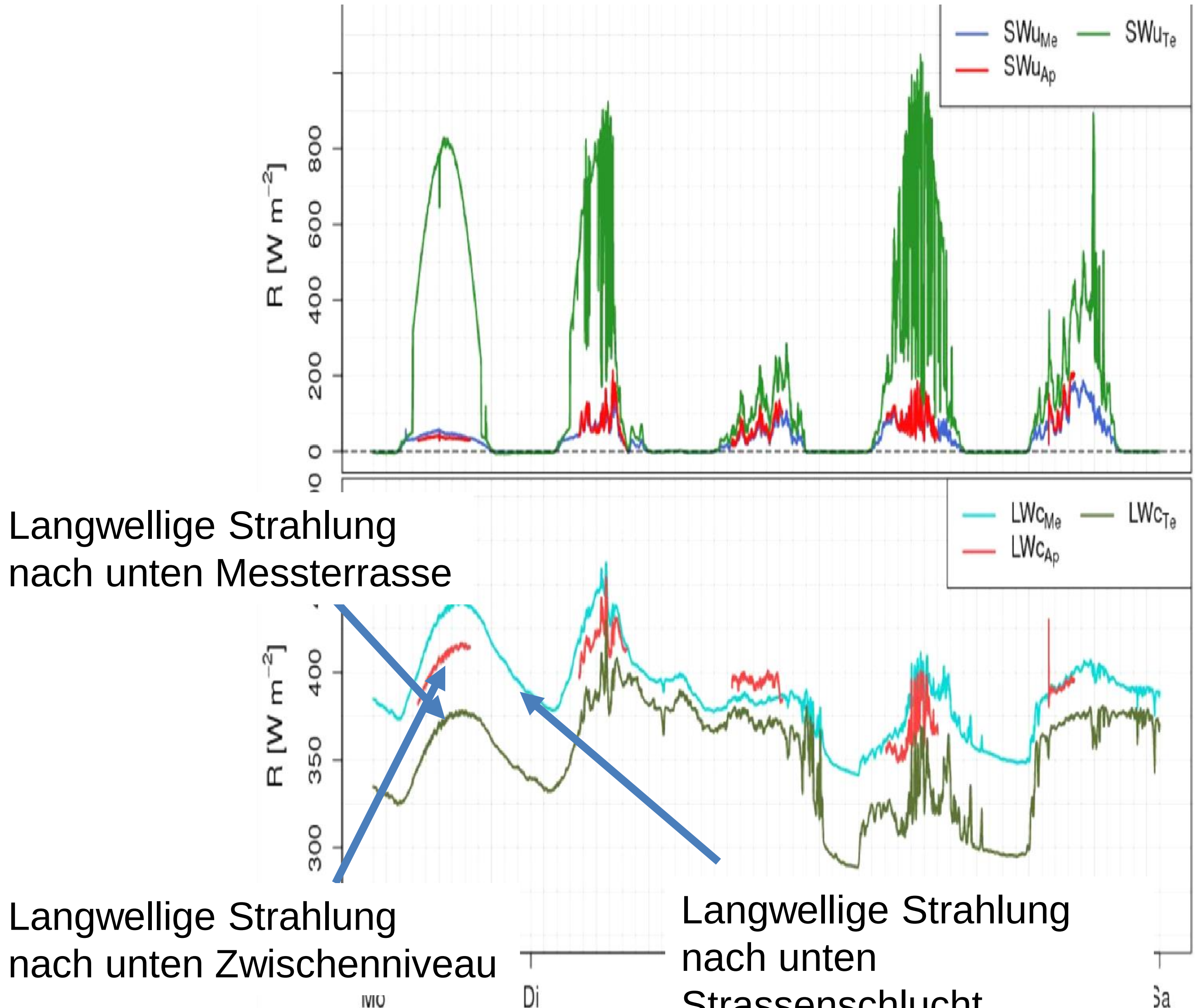

1. Ergebnisse – Vergleich TEB mit

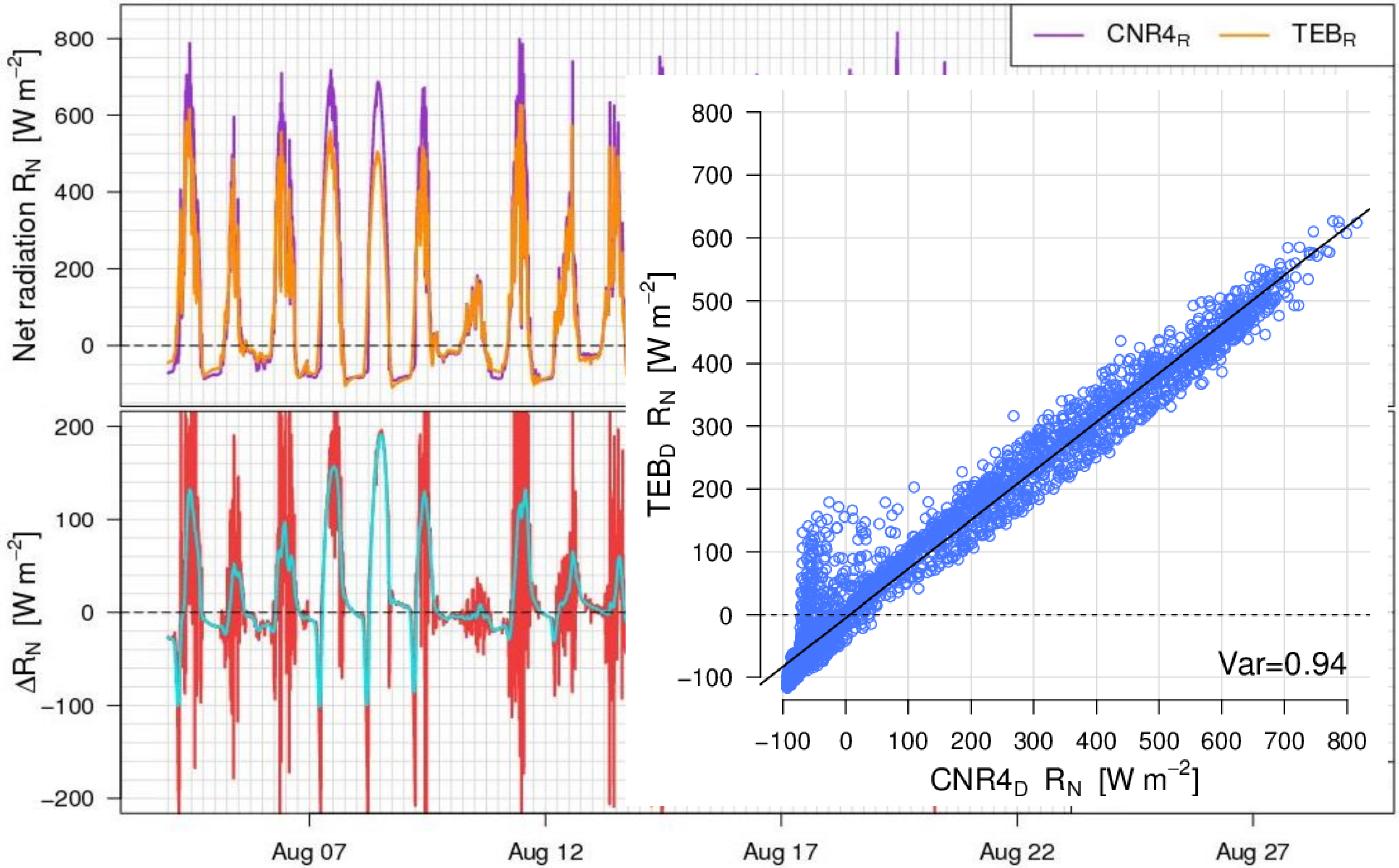

3.1. Überprüfung der von TEB berechneten Strahlungsflüssen in einem Strassencanyon

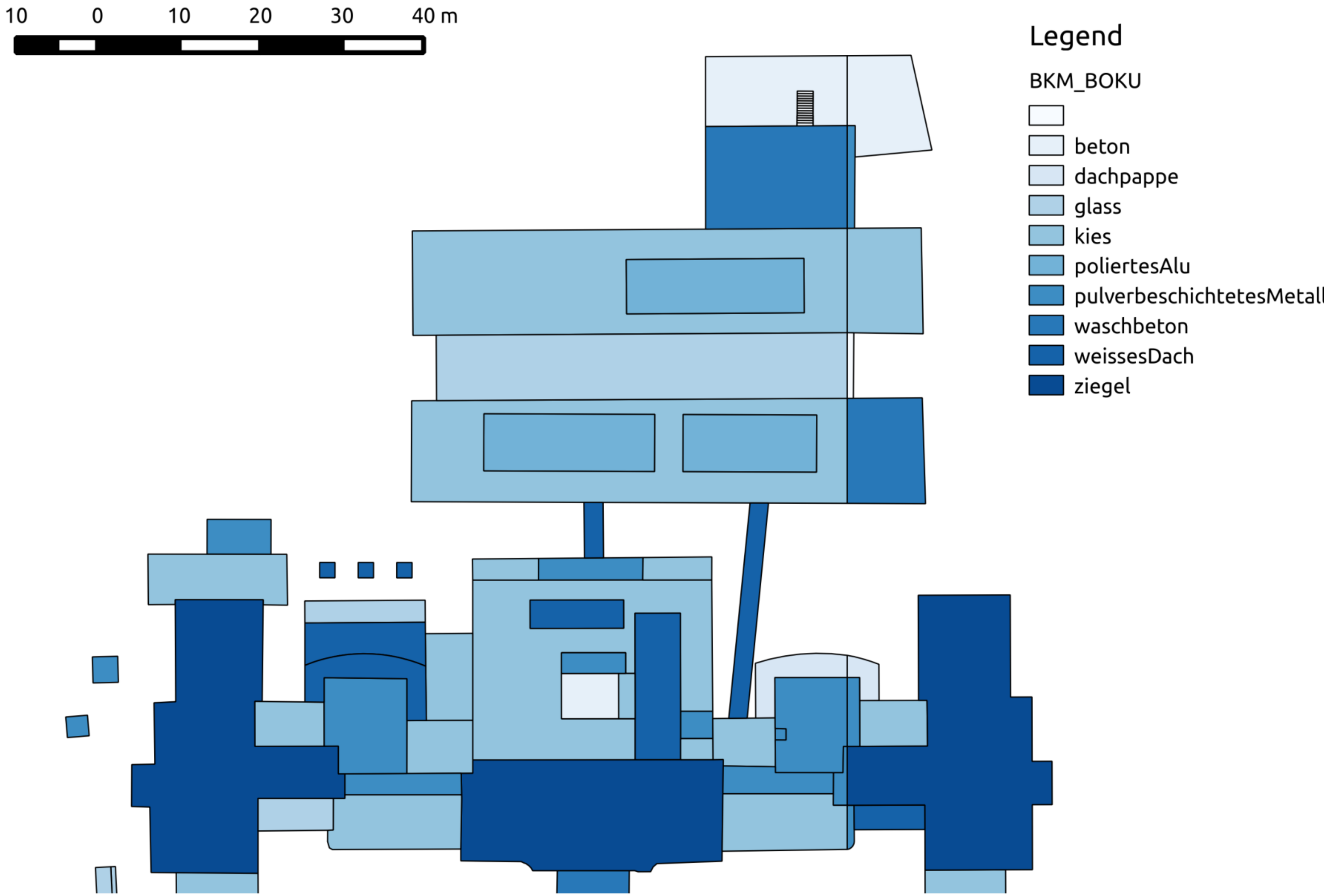

Mit SOLWEIG simulierte mittlere Strahlungstemperatur Strassenschlucht zwischen Schwackhöferhaus und Exnerhaus

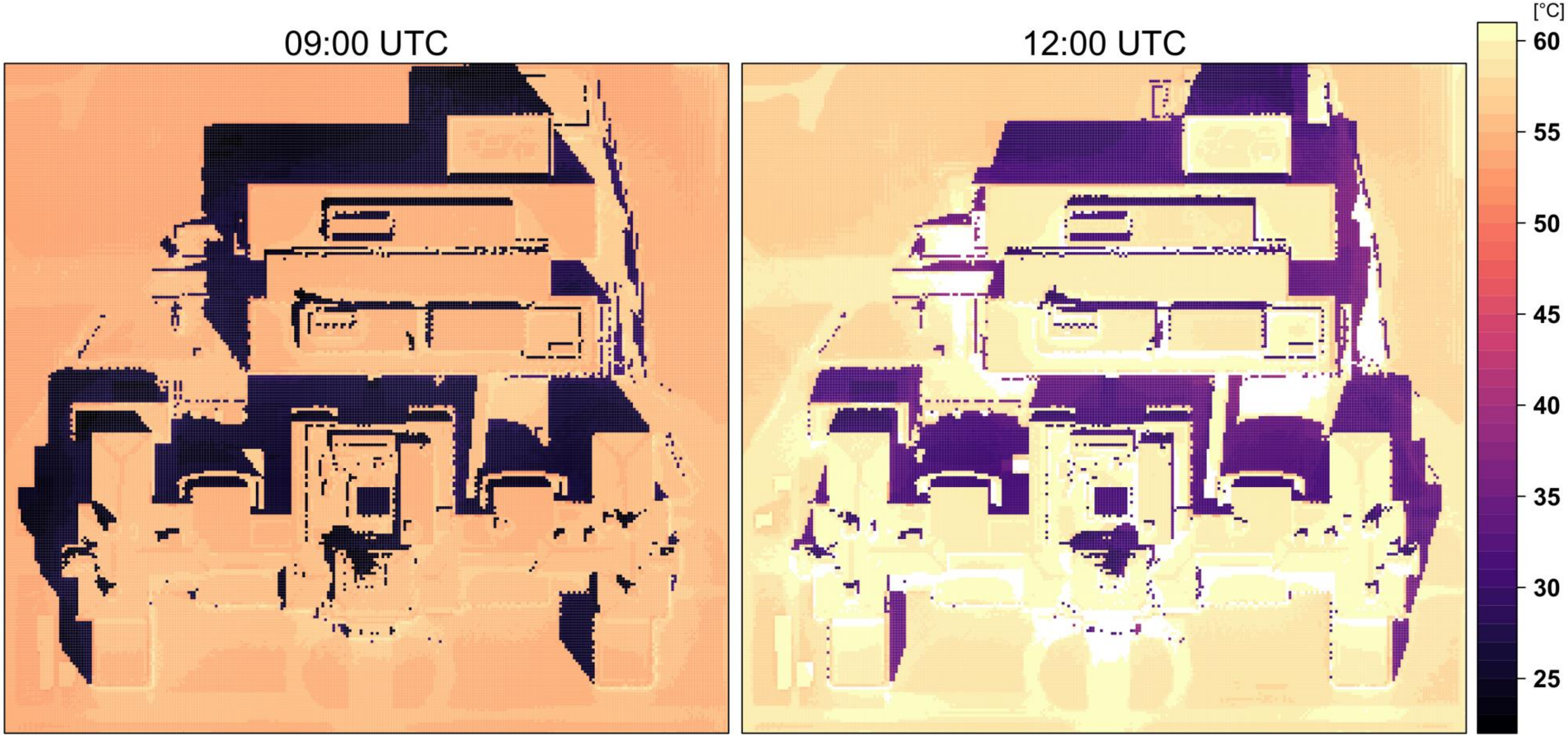

3.1. Überprüfung der von TEB berechneten Strahlungsflüssen in einem Strassencanyon

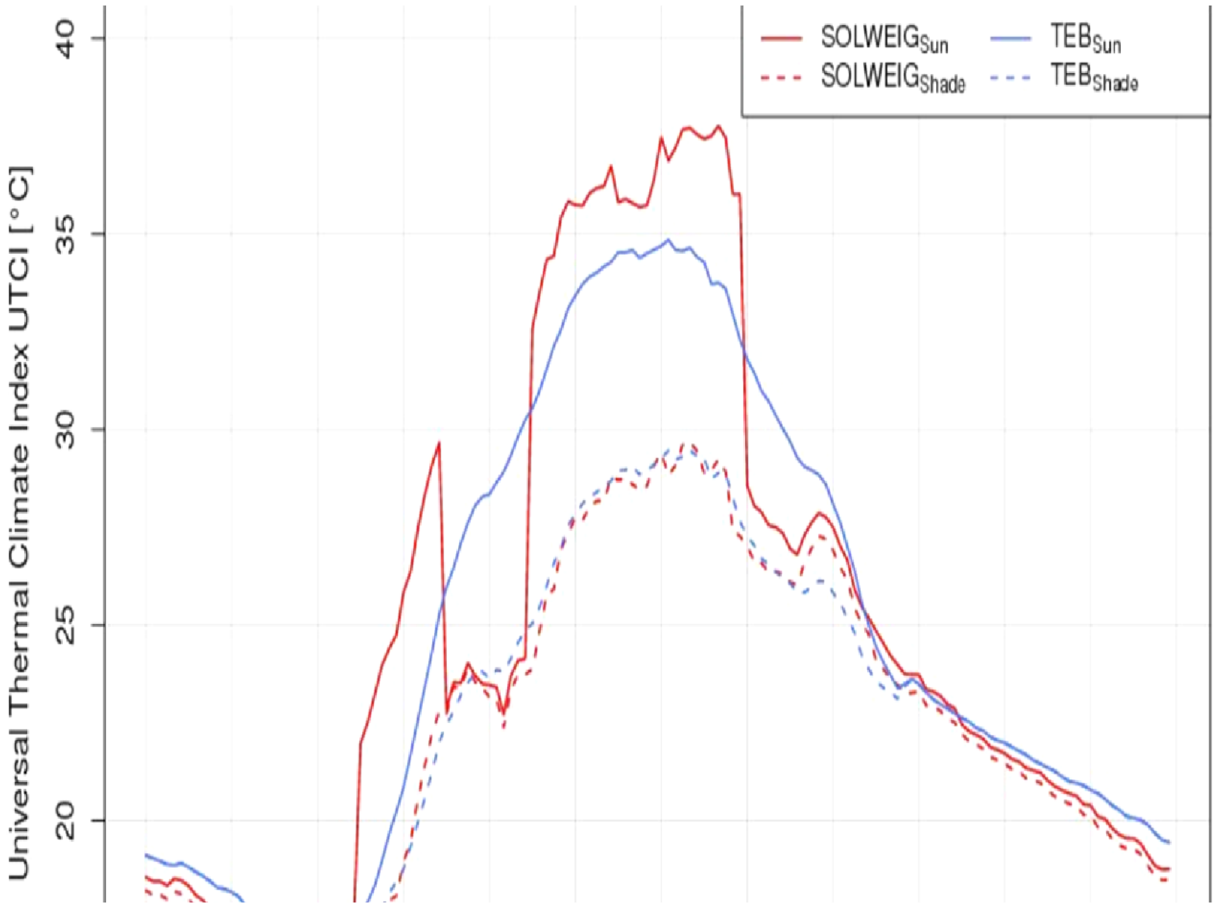

Weitere Schritte:

- Validierung SOLWEIG durch Vergleich mit Messungen

- Vergleich SOLWEIG TEB für klassischen Strassencanyon

3.1. Überprüfung der von WRF-TEB berechneten Lufttemperaturverteilungen

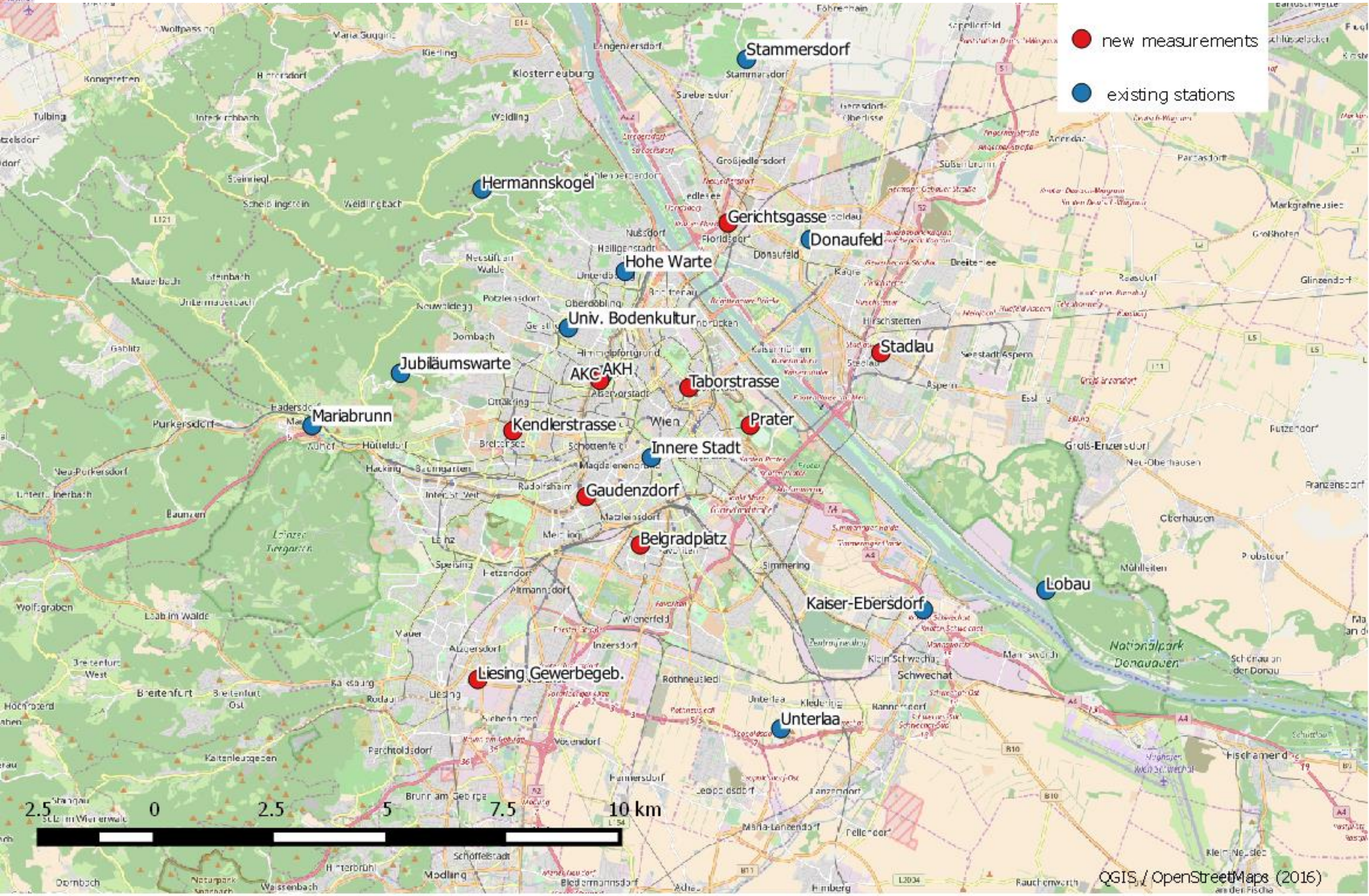

Erste Simulationen mit TEB

3.2. Erste Simulationen mit TEB

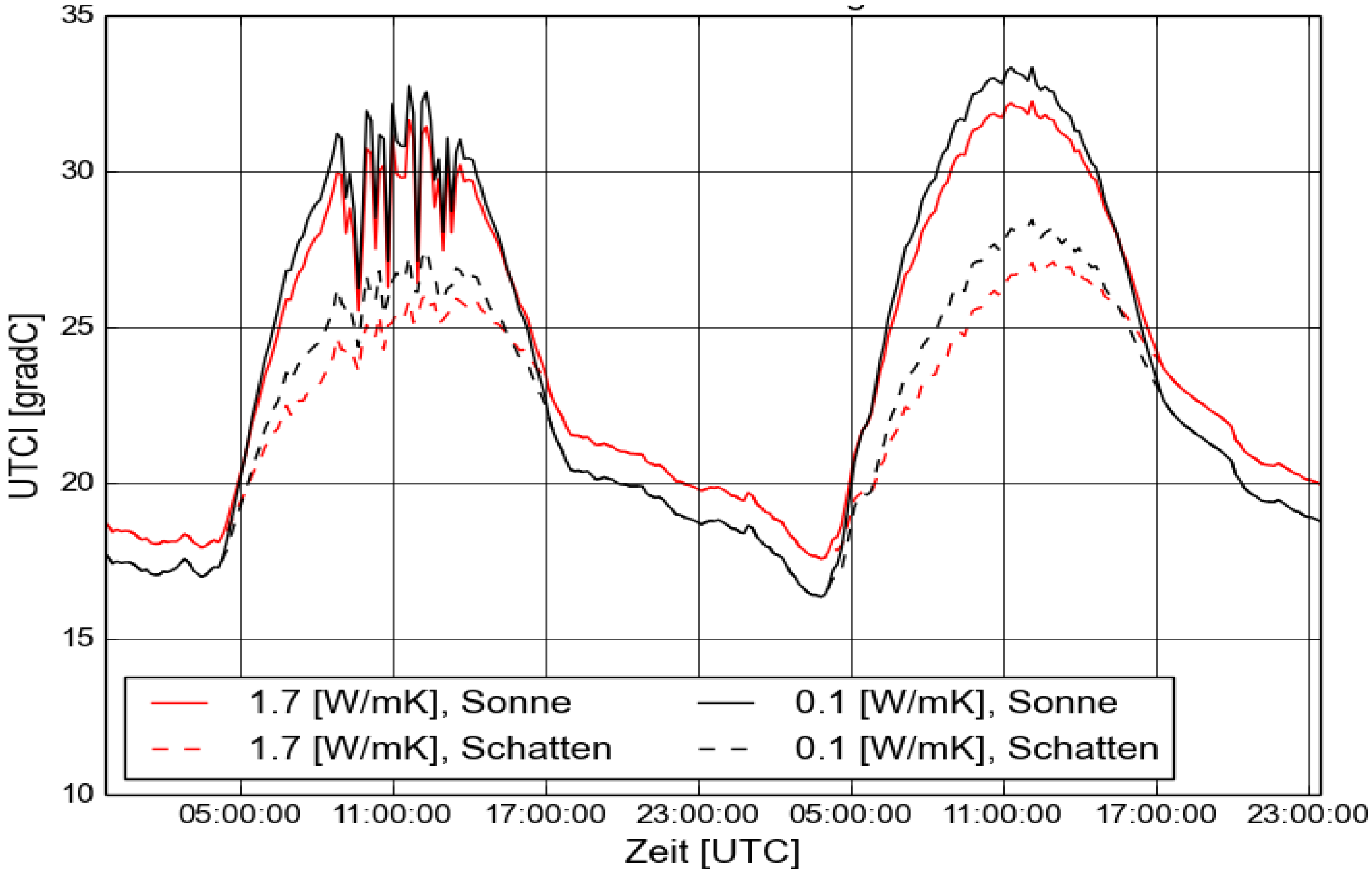

Abb. 16: Simulation des Tagesgangs des universellen thermalen Klimaindex (UTCI) mit dem open source Town Energy Balance Modell (TEB) (Masson, 2000)[1] *für zwei ausgewählte Tage.*
In einer Strassenschlucht mit gut wärmegedämmten Häuserreihen, kommt es zu einem höheren thermischen Stress als bei Häusern mit normaler Wärmedämmung

Erste Simulationen mit WRF

1. Ergebnisse – WRF Simulation

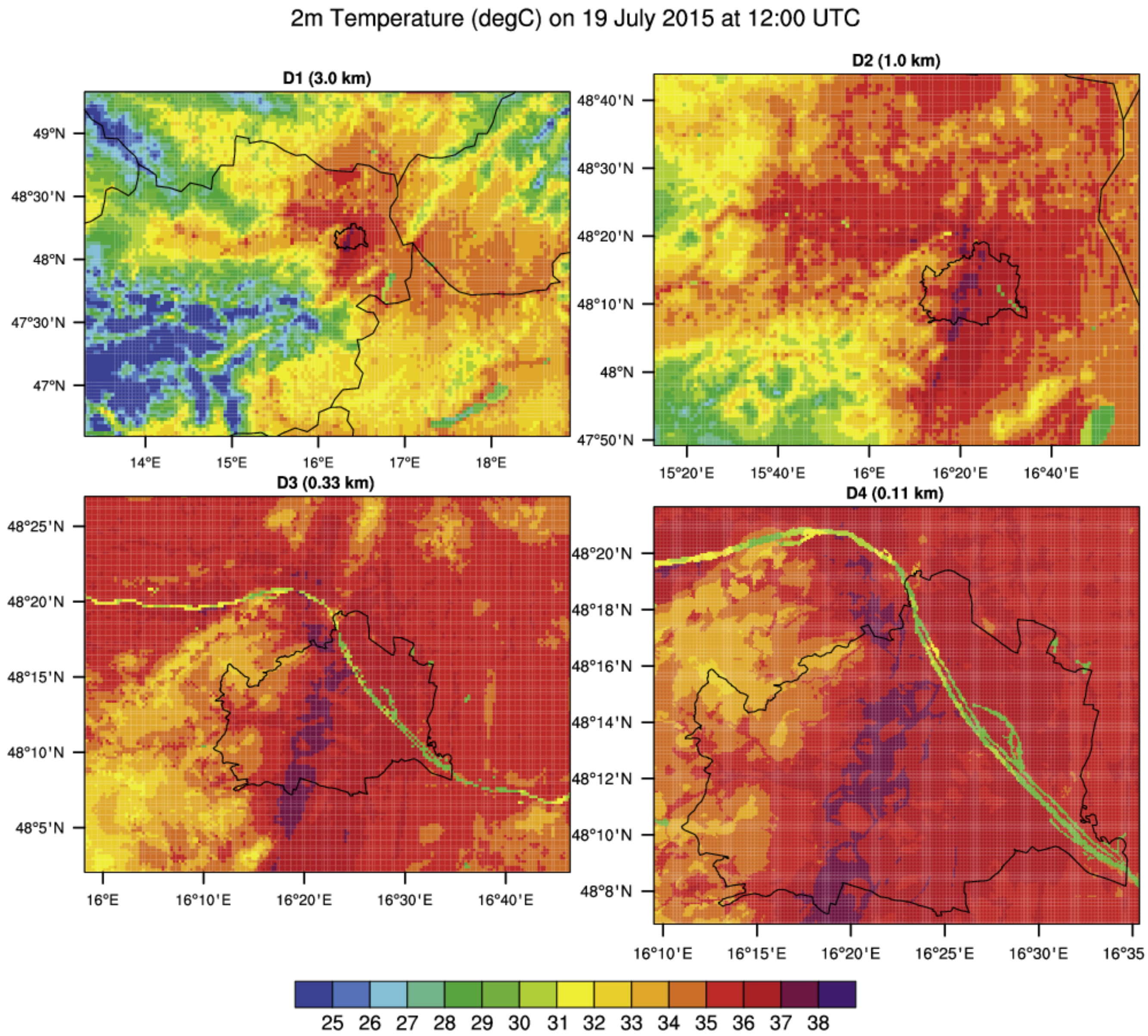

1. Ergebnisse – WRF Simulation

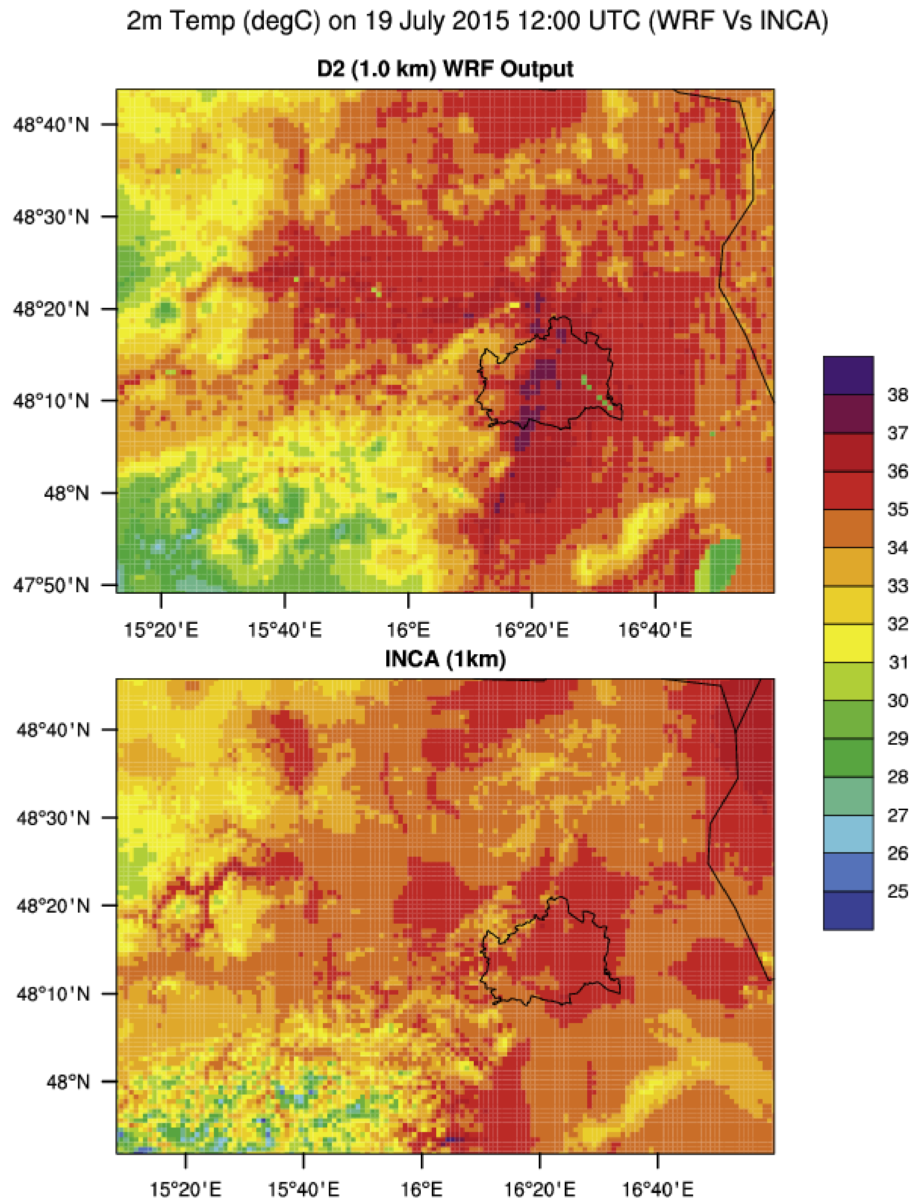

Arbeitspaket 4:

Berechnung der Szenarien und Analyse

Szenarien - Klimawandel

- Timeframe: 2030 + 2050
- Selection of typical heat waves
- Preparation of meteorological data

Szenarien - Stadtplanung

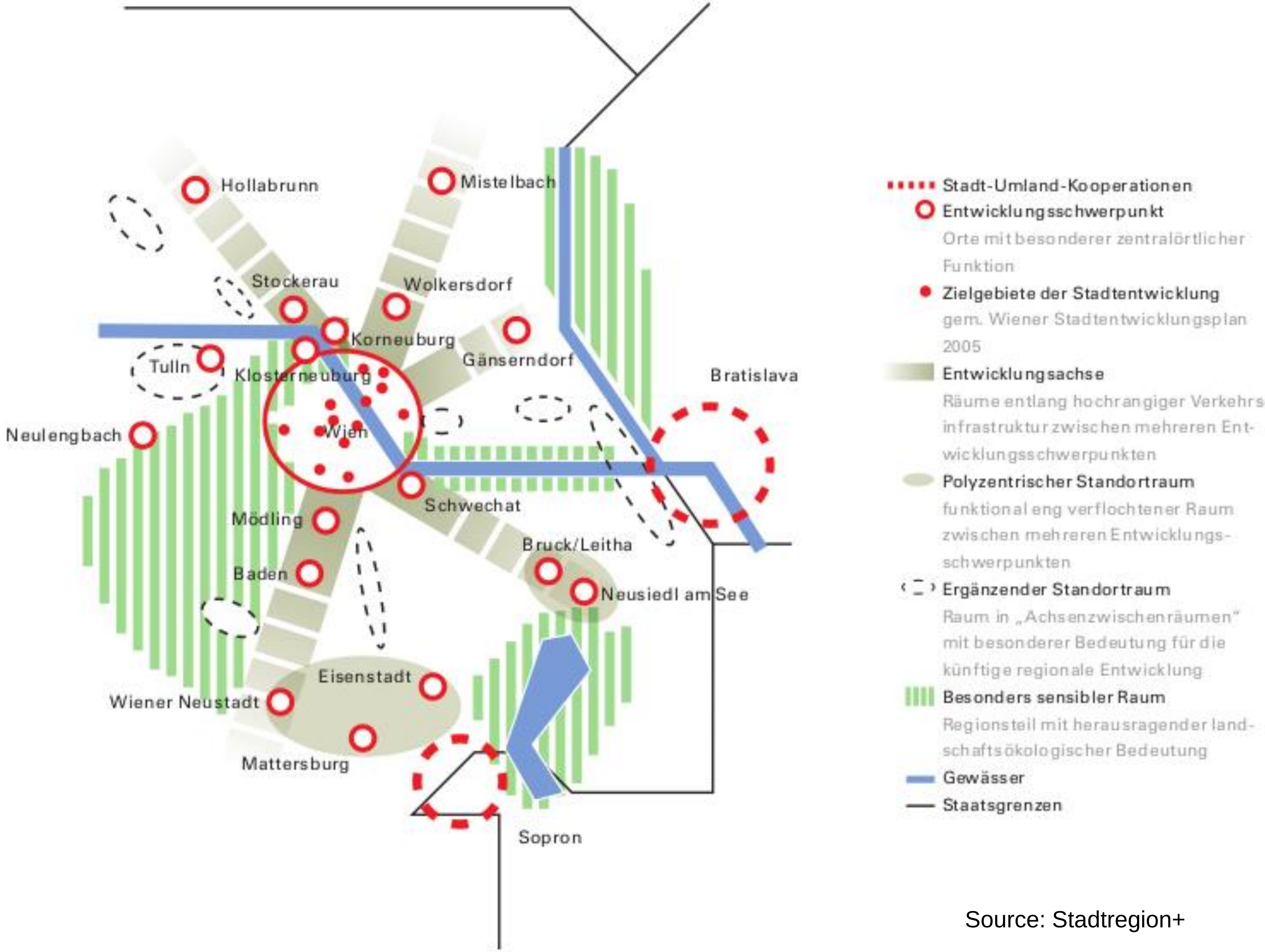

Source: Stadtregion+

Szenarien - Stadtplanung

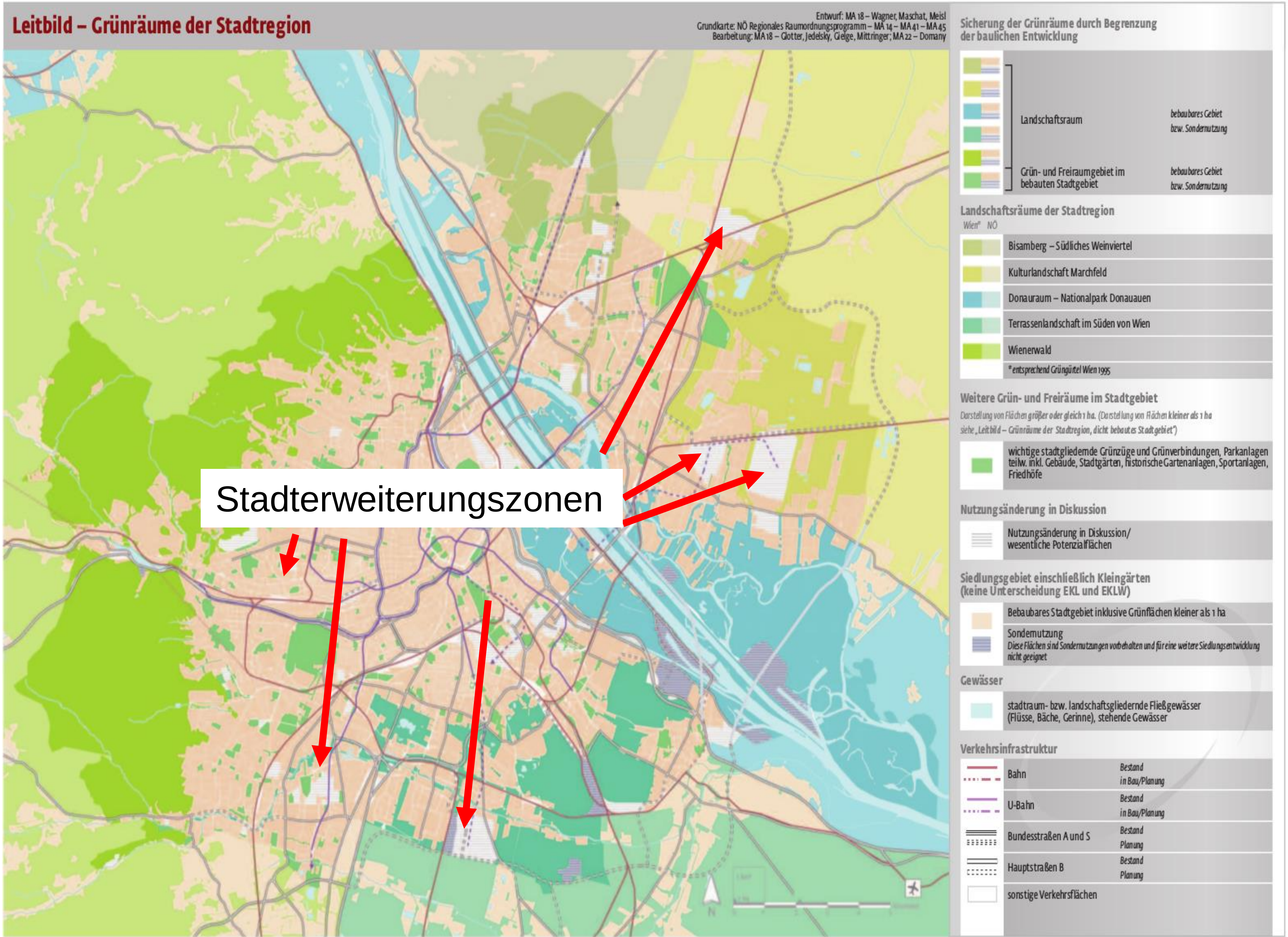

Nächste Schritte

- Validierung WRF-TEB für alle Messtationen in Wien (Lufttemperatur, Oberflächentemperatur, Luftfeuchte, Bodenfeuchte,…)
- weitere Vergleiche SOLWEIG-TEB
- Vergleich Simulationen WRF-UCM mit WRF-TEB
- Test der 1km Bodenfeuchtedaten SCATSAR-SWI

(Copernicus SCATSAR-SWI (Scatterometer – SAR – Soil Water Index) verarbeitet Bodenfeuchte-Zeitserien (Surface Soil Moisture, SSM) von Metop ASCAT und Sentinel-1 CSAR zu einem gemeinsamen SWI Produkt, das mit einer Auflösung von 1 km und einem täglichen Zeitstempel - derzeit in Entwicklung nur für Forschungszwecke, geplant als frei verfügbares Copernicus Produkt, Department für Geodäsie und

Geoinformation der Technischen Universität Wien)

- Diskussion Zukunftsszenarien Bebauung

Danke für Ihre Aufmerksamkeit

Beispiel Messstandort

Taborstrasse

Bilder © 2016 Google,Karte

“inner urban”
Land cover zone (LCZ) 2: compact mid-rise
Corine 111: continuous urban fabric
Urban Atlas: continuous urban fabric (S.L.>80%)
Urban Fabric Type (UFT) 2c: dichtes Stadtgebiet – erweiterter Stadtkern
Realnutzungskartierung: Wohn(misch)gebiet mittlerer Dichte

kontinuierliches Messetup:
Lufttemperatur/Luftfeuchte

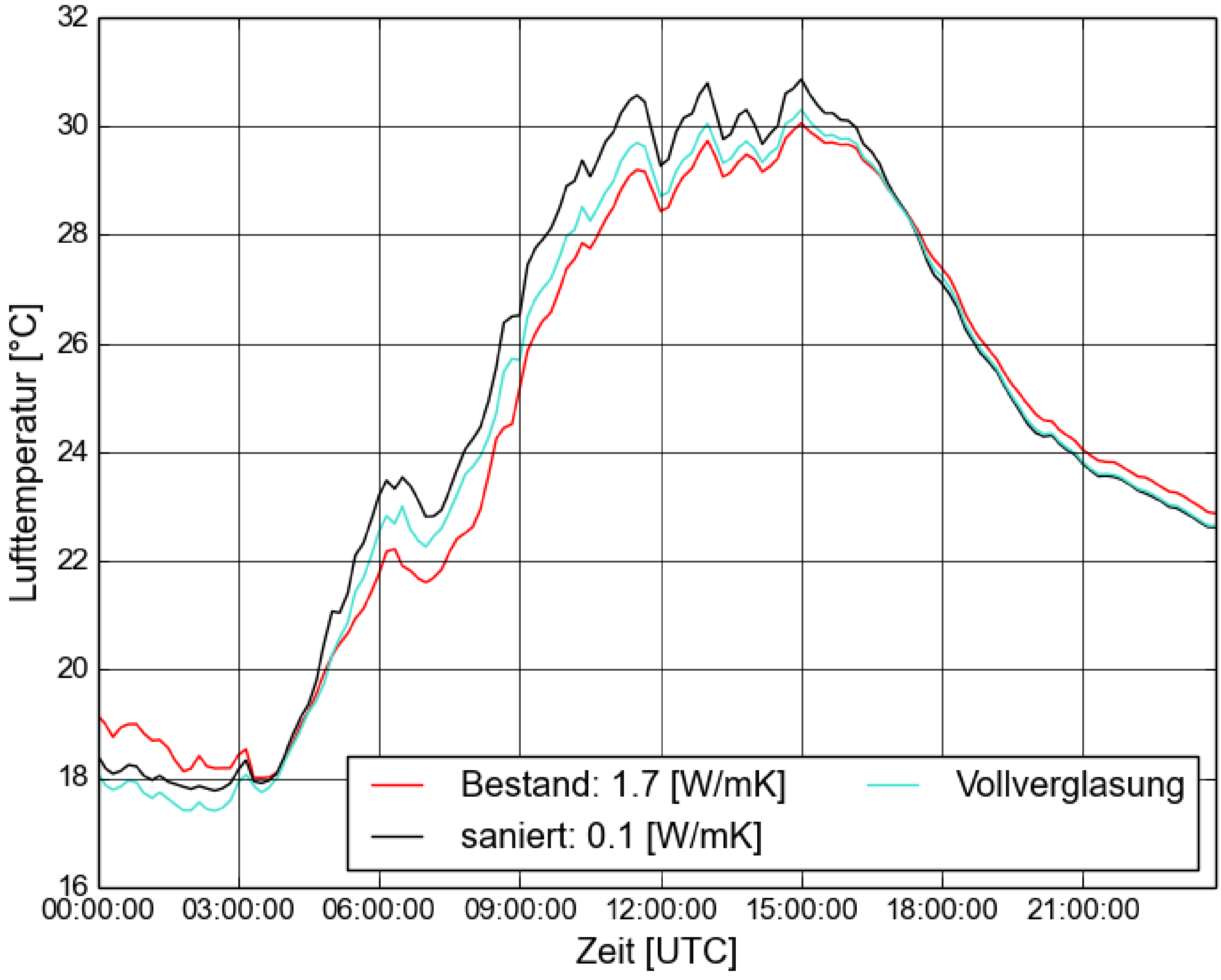

32
30
28
26
24
22
20
18
16
Lufttemperatur [°C]
00:00:00
03:00:00
06:00:00
09:00:00
12:00:00
15:00:00
18:00:00
21:00:00
Zeit [UTC]
Bestand: 1.7 [W/mK]
saniert: 0.1 [W/mK]
Vollverglasung

Zukunftsszenarien – Klimawandel/Stadtentwicklung

- Timeframe: 2030 + 2050
- Selection of typical heat waves, Preparation of meteorological data

Nachverdichtung / Sanierung im Bestand + Neue Stadtviertel

1) Starker Bevölkerungsanstieg (BV++)
   - 1a) Wachstum angepasst an Klimawandel (K+)
   - 1b) Profitorientiertes Wachstum (K-)
2) Schwacher Bevölkerungsanstieg(BV+)
   - 2a)Wachstum angepasst an Klimawandel (K+)
   - 2b) Profitorientiertes Wachstum (K-)

Erster Vergleich: Morphologische Szenarien

	2016 Wohn(misch)gebiet	**2016 Geschäfts-Kern u-Mischgebiet**	**BV+, K+ 20% dichter, grüner**	**BV++,K+ ~40% höher ~40% dichter**	**BV+,K- ~20% höher voll versiegelt**	**BV++, K- ~40% höher ~40% dichter voll versiegelt**
Gebäudehöhe[m]	14.6	20.6	14.6	20.6	18	20.6
bebaute Fläche [0-1]	0.55	0.74	0.64	0.74	0.55	0.74
versiegelte Fläche [0-1]	0.28	0.16	0.4	0.2	0	0
Wärmekapazität Wand [J/m³K]	1520000	1520000	1496000	1496000	1496000	1496000
Wärmekapazität Dach[J/m³K]	1554000	1554000	1496000	1496000	1496000	1496000
Thermische Leitfähigkeit Wand [W/mK]	1.7	1.7	0.1	0.1	0.1	0.1
Thermische Leitfähigkeit Dach [W/mK]	1.4	1.4	0.1	0.1	0.1	0.1

LEITBILD SIEDLUNGSENTWICKLUNG

Abb. 08
Quelle: MA 18, MA 21, MA 41,
Urban Atlas, WKW;
Inhalt und Darstellung: MA 18

SIEDLUNGSENTWICKLUNG

- **Bestandsentwicklung** gründerzeitlich geprägter Gebiete
- **Weiterentwicklung** Gebiete geprägt in den 1950er- bis 1970er-Jahren
- **Gebiete mit Entwicklungspotenzial** für Wohnen und Arbeiten

ENTWICKLUNG WIRTSCHAFT UND ZENTREN

- **City** Zone hochrangiger Büro- und Verwaltungsfunktionen, Universitäten, Handel, Kultur etc.
- **Zone für nicht mischfähige Betriebe** (gemäß Wiener Betriebszonen-analyse 2008)
- **City-Erweiterung** Vorrangzone für die künftige Ergänzung von City-Funktionen
- **Etabliertes Stadtteilzentrum**
- **Stadtteilzentrum mit Entwicklungsbedarf** (Funktionsergänzung, Aufwertung)
- **Geschäftsstraße mit übergeordneter Bedeutung**

SITUATION

- Bebautes Gebiet (2013)
- Donaugewässer
- Stadtgrenze

VERKEHRSINFRASTRUKTUR

- U-Bahn/S-Bahn (inkl. Strecken im Bau)
- Hochrangiges Straßennetz
- Autobahnen/ Schnellstraßen
- Autobahnen/ Schnellstraßen in Vorbereitung

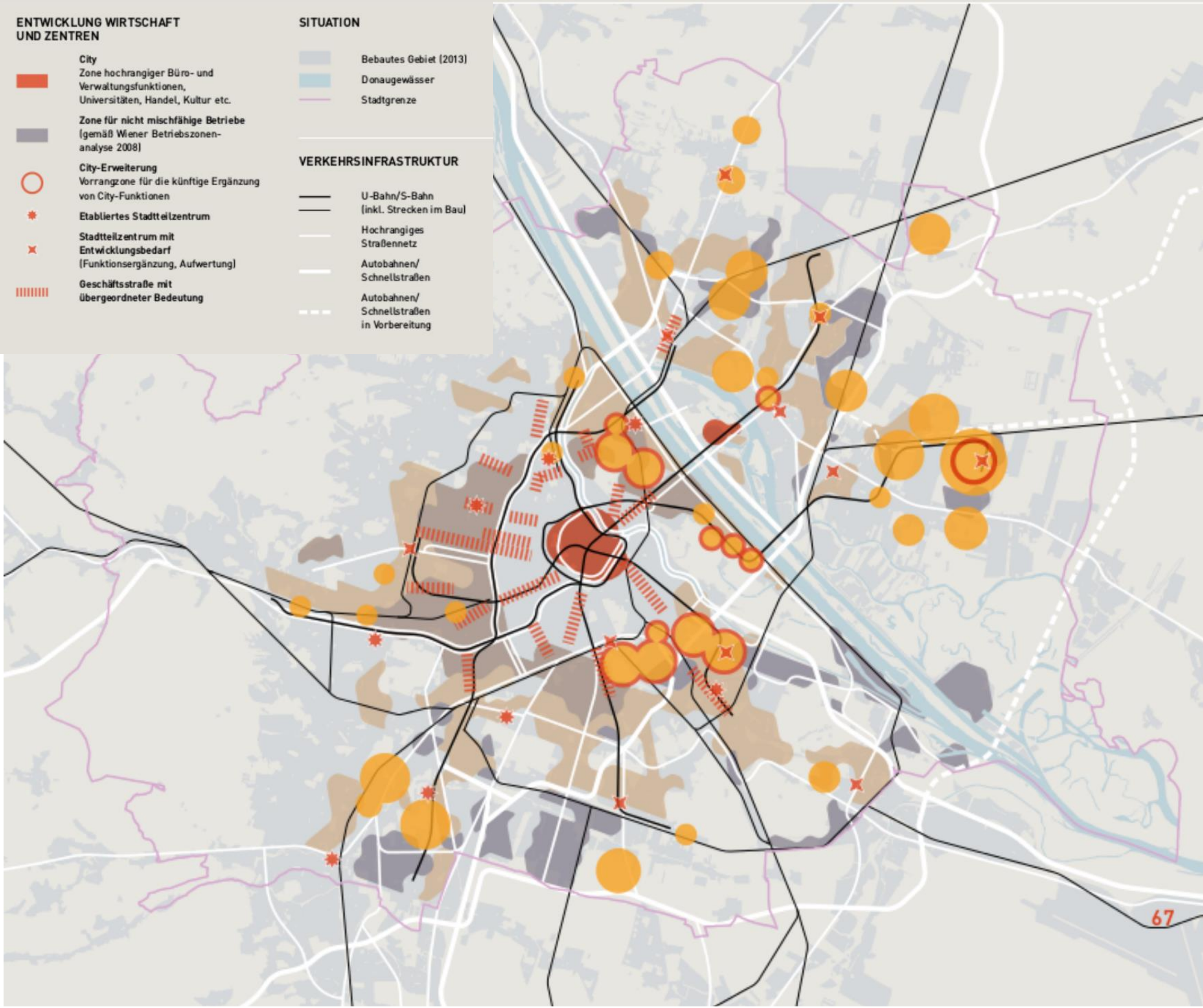

Erster Vergleich: Morphologische Szenarien

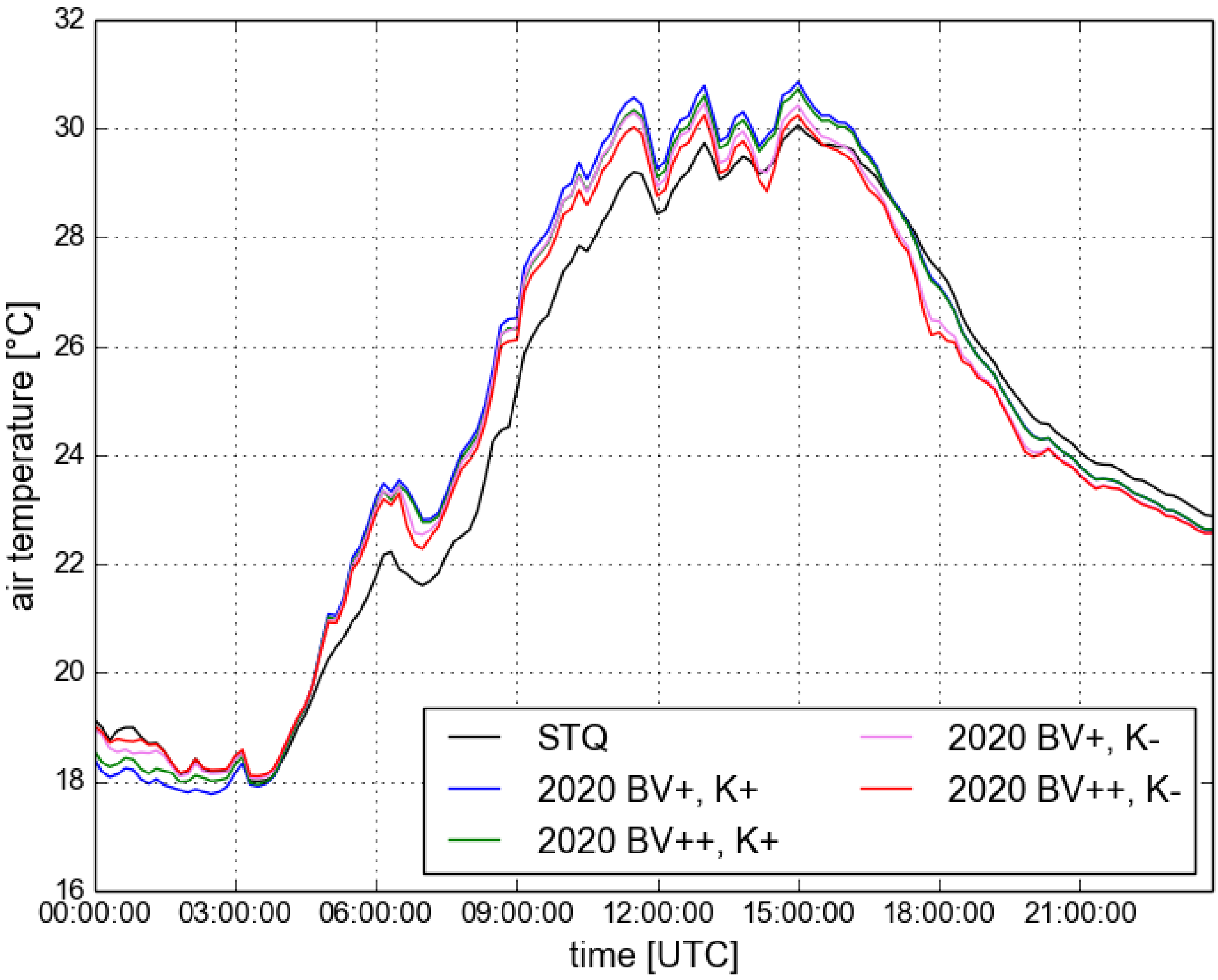

Nr.	Szenario	Annahmen künftiger Entwicklung
S1	Rück- und Umbau in privater Verantwortung	Geringe öffentliche Mittel, suburbane Expansion
S2	Florierender Wirtschaftsstandort und Anstieg des anthropogenen Flächenbedarfs	Hohe Priorität für Wirtschaftsförderung
S3	Kompakte Stadt als Zentrum für Innovationen im Bereich Umwelt	Starkes Wachstum, hohe Priorität für Umweltbelange

Tab. 2: Überblick über die im Rahmen von KLIMZUG-NORD entwickelten sozio-ökonomischen Entwicklungsszenarien und Anpassungsstrategien für das Modellgebiet Wandse

Einflussfaktor	Szenario 1 Rück- und Umbau	Szenario 2 Florierender Wirtschaftsstandort	Szenario 3 Kompakte Stadt
Bevölkerungsentwicklung	-	=	+
Flächenbedarf Innenstadt	-	+	+
Flächenbedarf Stadtrand und Umland	+	+	-
Öffentlicher Personennahverkehr (ÖPNV)	-	+	+
Motorisierter Individualverkehr (MIV)	+	-	-
Finanzielle Mittel der öffentlichen Hand	-	+	+
Investitionen in Umwelt und erneuerbare Energien	nur privat	privat und öffentlich	privat und öffentlich
Sensibilisierung für Klimaanpassung	niedrig	niedrig	niedrig
Umsetzung von Klimaschutz- und Anpassungsmaßnahmen	nur privat	privat und öffentlich	privat und öffentlich
Steuerung durch Anreize von Seiten der öffentlichen Hand	nur negative Anreize	nur negative Anreize	positive und negative Anreize
Anpassungsstrategie	„Abwarten“	„Schützen“	„Anpassen“

Legende: **-** Abnahme **+** Zunahme **=** in etwa gleich bleibende Verhältnisse

Tab. 3: Kurzgegenüberstellung der für die drei Szenarien verwendeten Treiber und der daraus resultierenden Strategien im Umgang mit dem Klimawandel

Source: KLIMZUG-NORD 2014

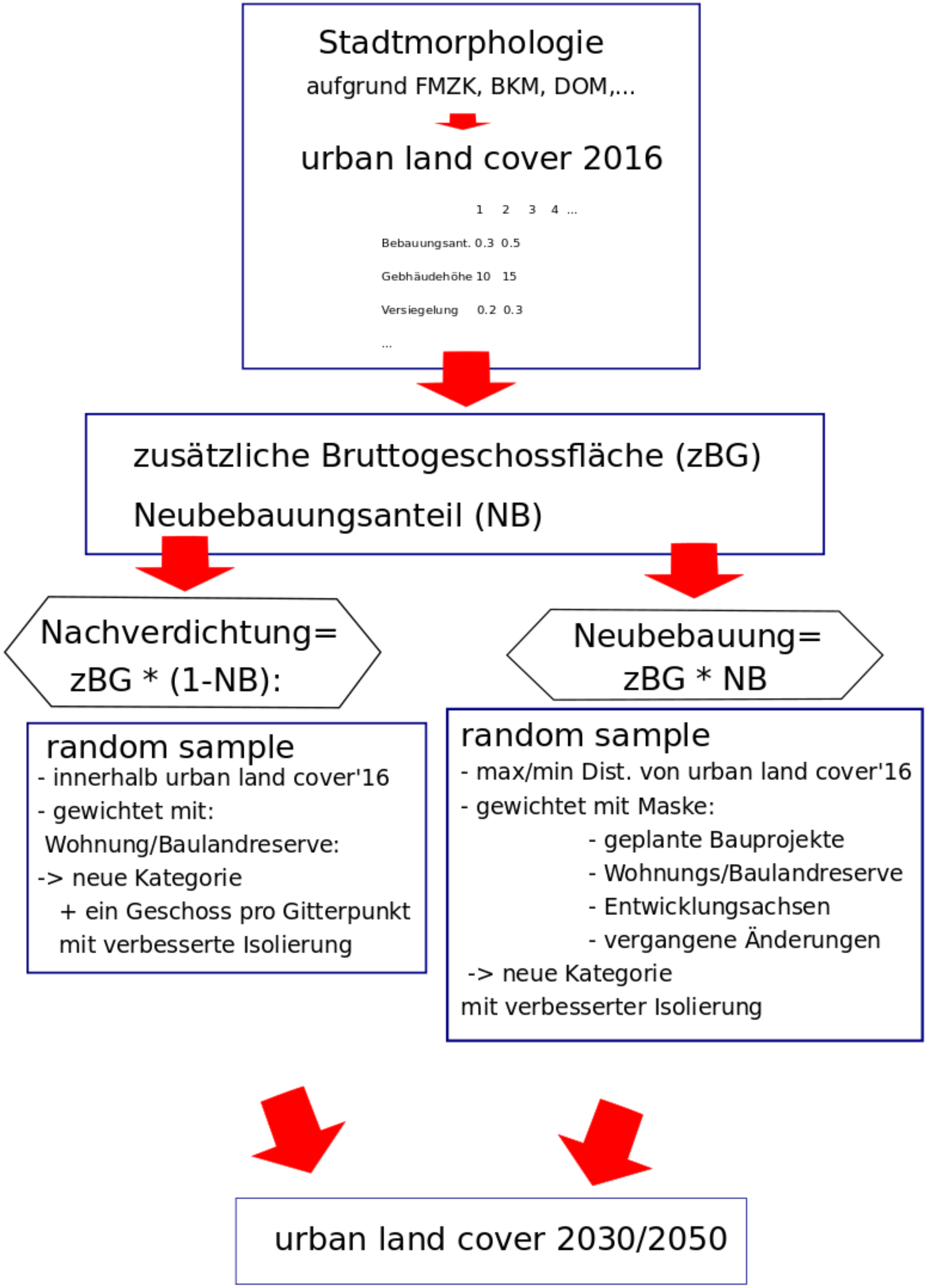
Stadtmorphologie
aufgrund FMZK, BKM, DOM,...
urban land cover 2016
1 2 3 4 ...
Bebauungsant. 0.3 0.5
Gebhäudehöhe 10 15
Versiegelung 0.2 0.3
...
zusätzliche Bruttogeschossfläche (zBG)
Neubebauungsanteil (NB)
Nachverdichtung= zBG * (1-NB):
Neubebauung= zBG * NB
random sample
- innerhalb urban land cover'16
- gewichtet mit:
Wohnung/Baulandreserve:
-> neue Kategorie
+ ein Geschoss pro Gitterpunkt
mit verbesserte Isolierung
random sample
- max/min Dist. von urban land cover'16
- gewichtet mit Maske:
- geplante Bauprojekte
- Wohnungs/Baulandreserve
- Entwicklungsachsen
- vergangene Änderungen
-> neue Kategorie
mit verbesserter Isolierung
urban land cover 2030/2050

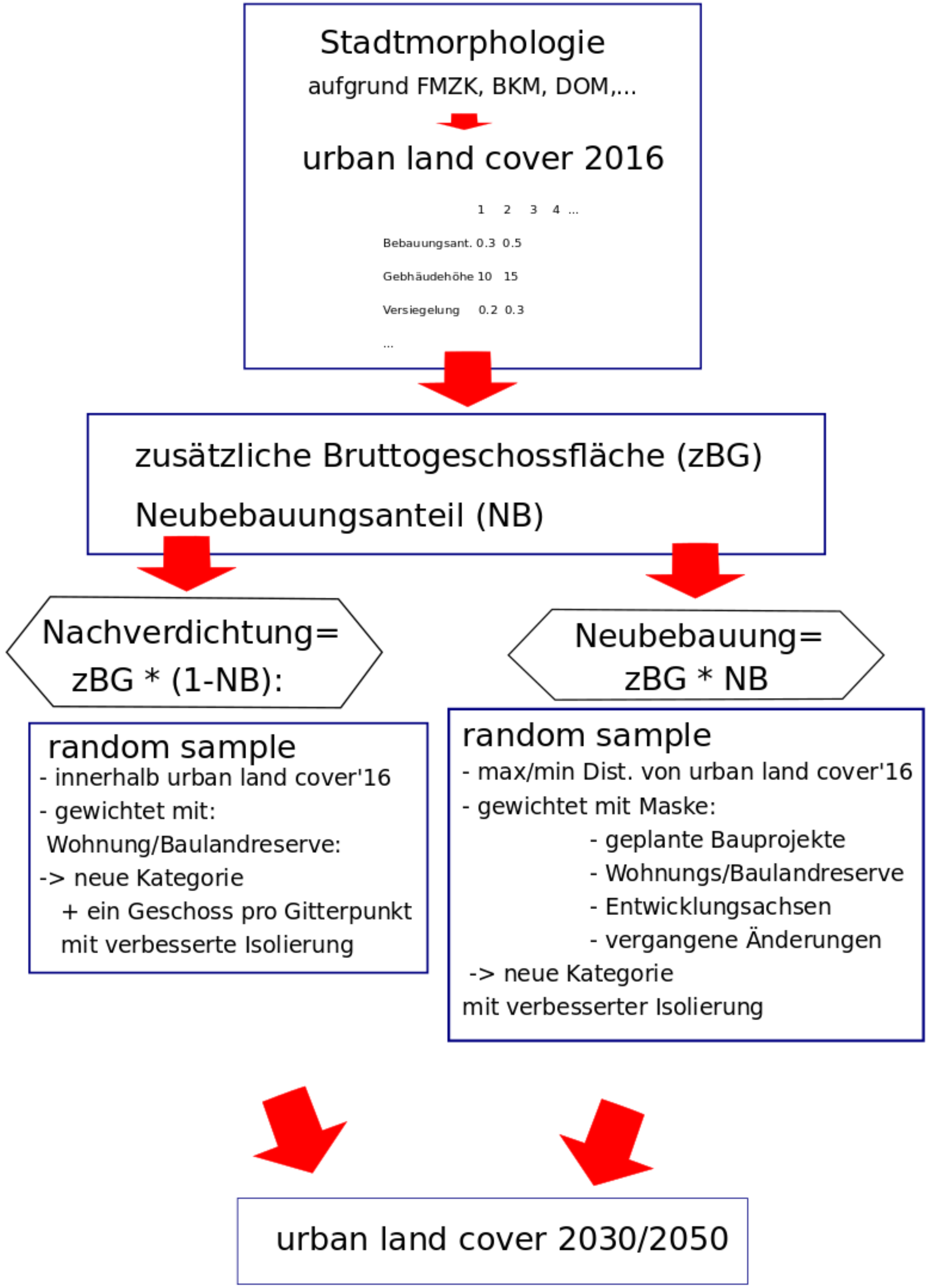

Stadtmorphologie
aufgrund FMZK, BKM, DOM,...
urban land cover 2016
1 2 3 4 ...
Bebauungsant. 0.3 0.5
Gebhäudehöhe 10 15
Versiegelung 0.2 0.3
...
zusätzliche Bruttogeschossfläche (zBG)
Neubebauungsanteil (NB)
Nachverdichtung= zBG * (1-NB):
Neubebauung= zBG * NB
random sample
- innerhalb urban land cover'16
- gewichtet mit:
Wohnung/Baulandreserve:
-> neue Kategorie
+ ein Geschoss pro Gitterpunkt
mit verbesserte Isolierung
random sample
- max/min Dist. von urban land cover'16
- gewichtet mit Maske:
- geplante Bauprojekte
- Wohnungs/Baulandreserve
- Entwicklungsachsen
- vergangene Änderungen
-> neue Kategorie
mit verbesserter Isolierung
urban land cover 2030/2050

Nächste Schritte

- Validierung TEB für alle Messtationen in Wien
- Vergleich Simulationen WRF-UCM mit WRF-TEB
- Test der 1km Bodefeuchtedaten SCATSAR-SWI
- Diskussion Zukunftsszenarien Bebauung

Table 6: Time schedule

	Months 1-4	Months 5-8	Months 9-12	Months 13-16	Months 17-20	Months 21-24
WP1						
WP2						
WP3						
WP4						
WP5						

Simulation – Methode

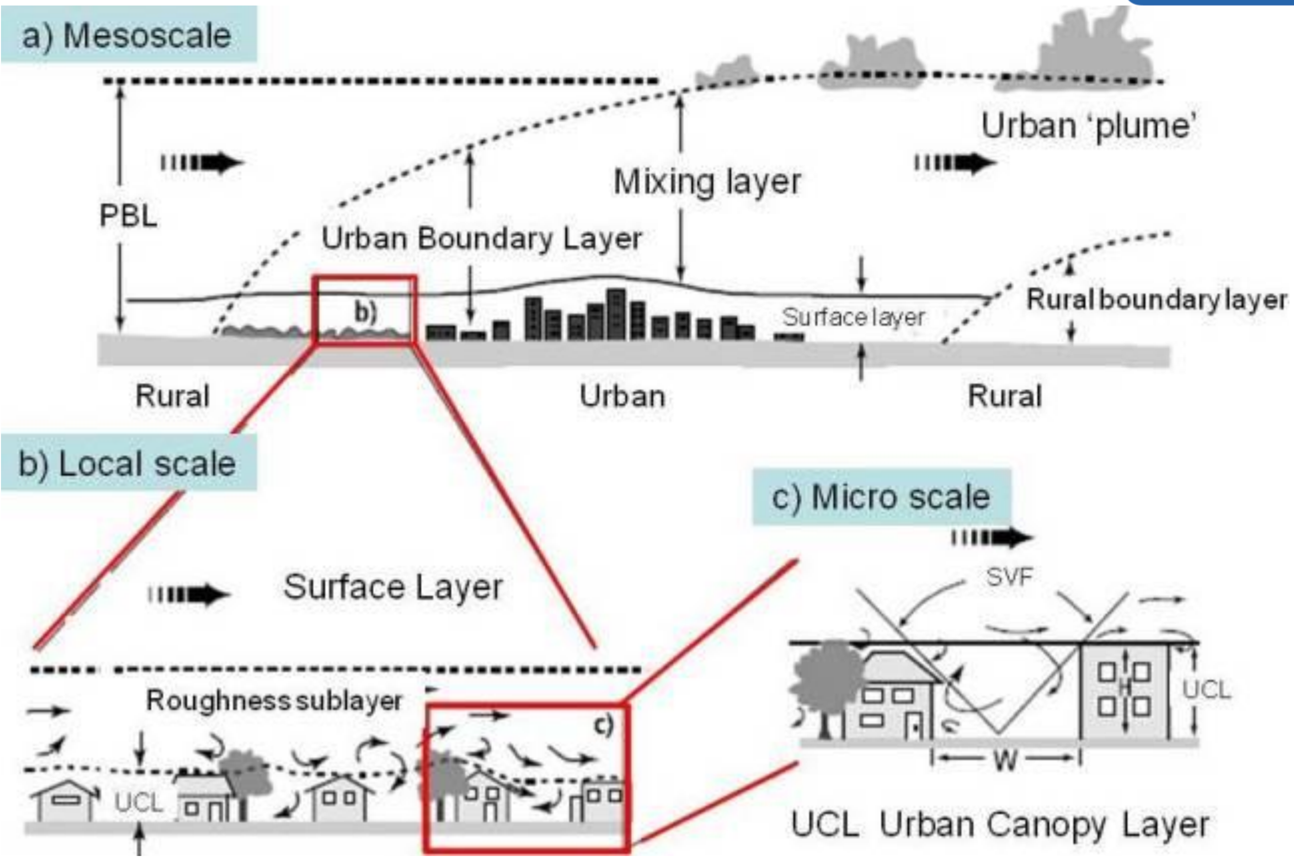

Source: T.R. Oke

Simulation – Methode

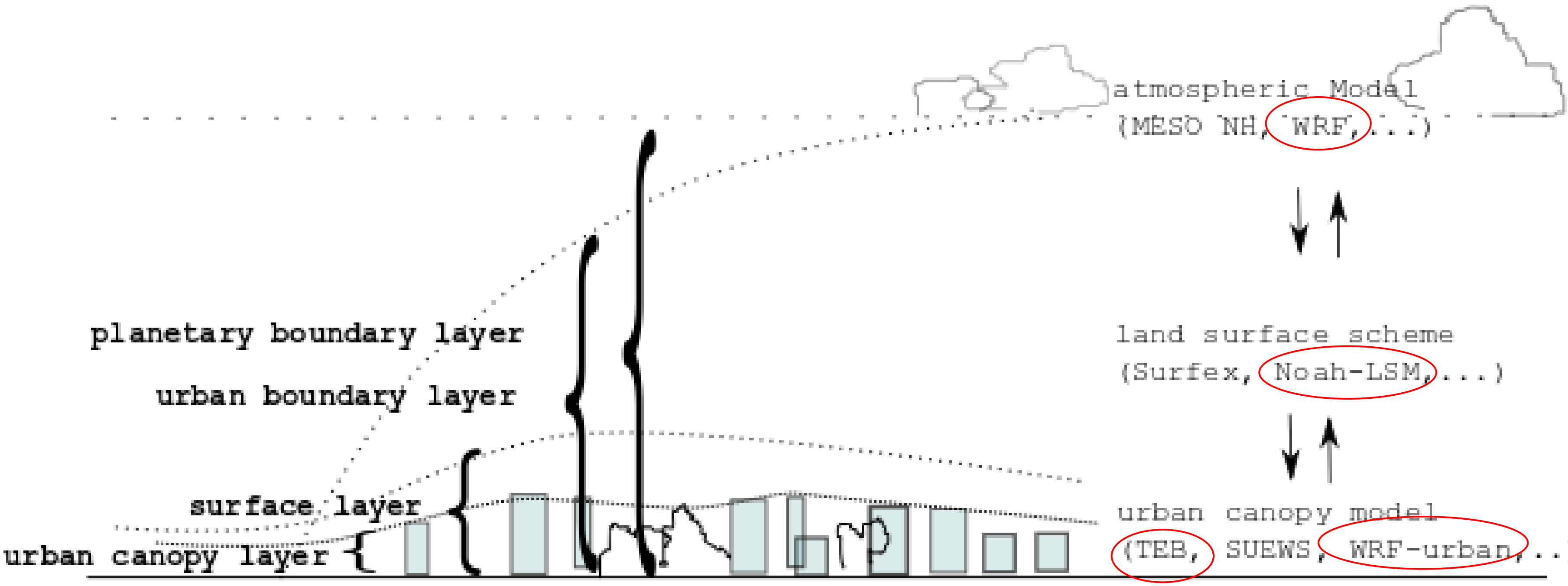

Hypothesis to be tested: The project will focus on the following research questions:

- Does growing of the city influence the local climate of the central districts?
- Does this influence depend on the architectural design and on the planning of suburban districts?
- Do we improve the urban microscale climate modelling by using multiscale approaches?
- Can urban planning contribute to mitigate climate change impacts on urban microclimate?
- Can planning of the suburban districts mitigate climate change impacts on the central districts of Vienna?
- Will climate change lead to higher rise in temperature in central districts of Vienna as compared to the surrounding rural areas?

The anticipated project results will include

- A validation and adaptation of a multi scale climate model for the city of Vienna will be performed
- The accuracy of multiscale modelling will be determined and appropriate methods to improve the accuracy will be identified
- The influence of climate change on the climate of the districts of the city of Vienna will be determined
- The influence of city growth and the development of outlying districts on climate of the districts of Vienna will be determined
- The best urban planning measures for the outlying districts of Vienna for the mitigation of climate change impact on the urban heat island of Vienna will be identified

  These measures include among others:

  - The appropriate inclusion of vegetation in the new districts
  - The choice of the appropriate dimensions concerning building heights and street width
  - The choice of the appropriate building materials concerning their heating storage characteristics and their reflection properties

Table 4

	Project management and dissemination	
	Preparation of input data, adaptation of the models	
	Validation of the town and building energy model	
	Creation of scenarios	

Arbeitspaket 2: Vorbereitung der Modellinputdaten Adaptierung der Modelle

Stadterweiterung 2025

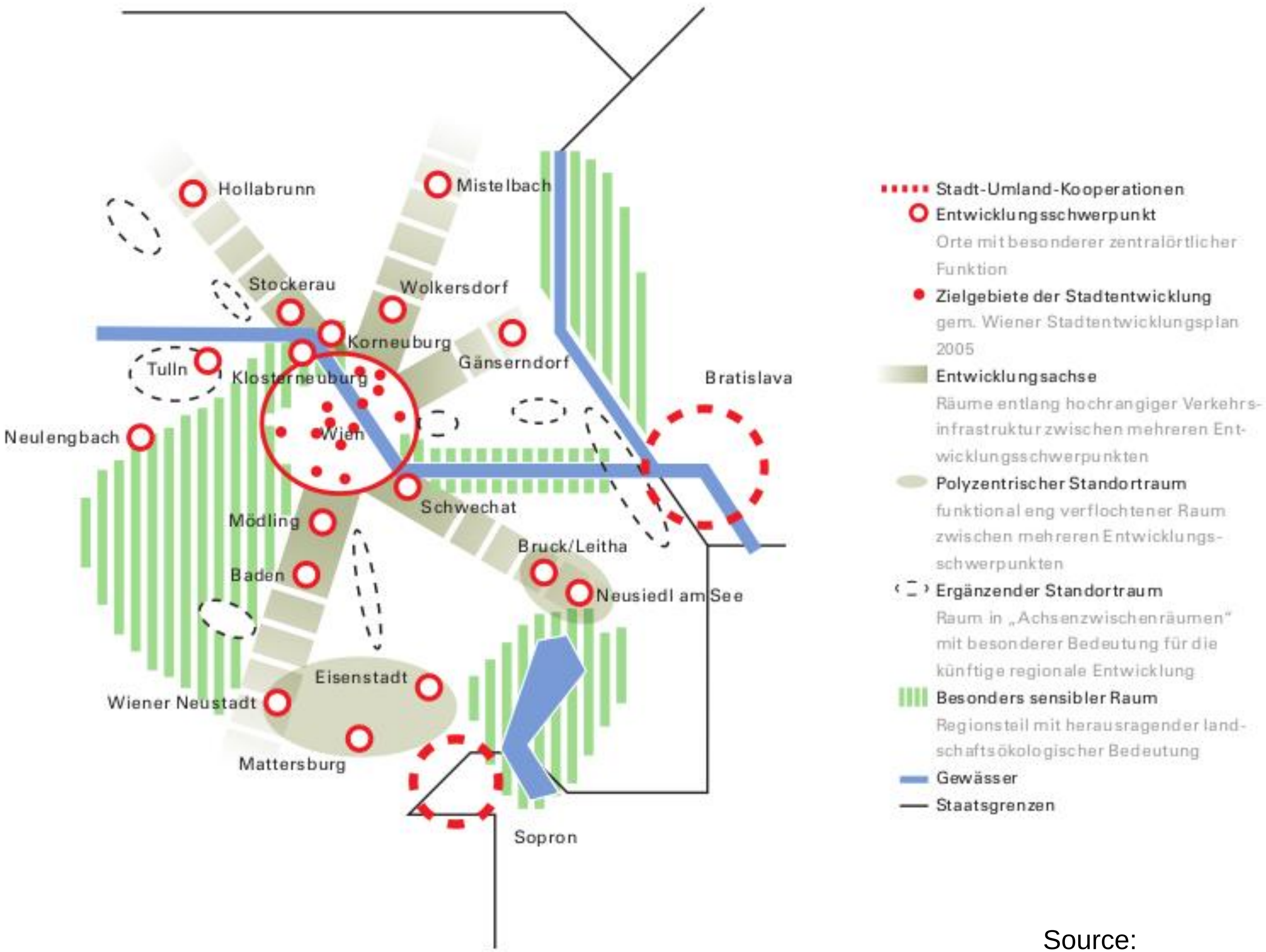

Source:
Stadtregion+

Koppelung des **Energiebilanz Modells TEB** mit dem **multiskaligen Wettermodell WRF**

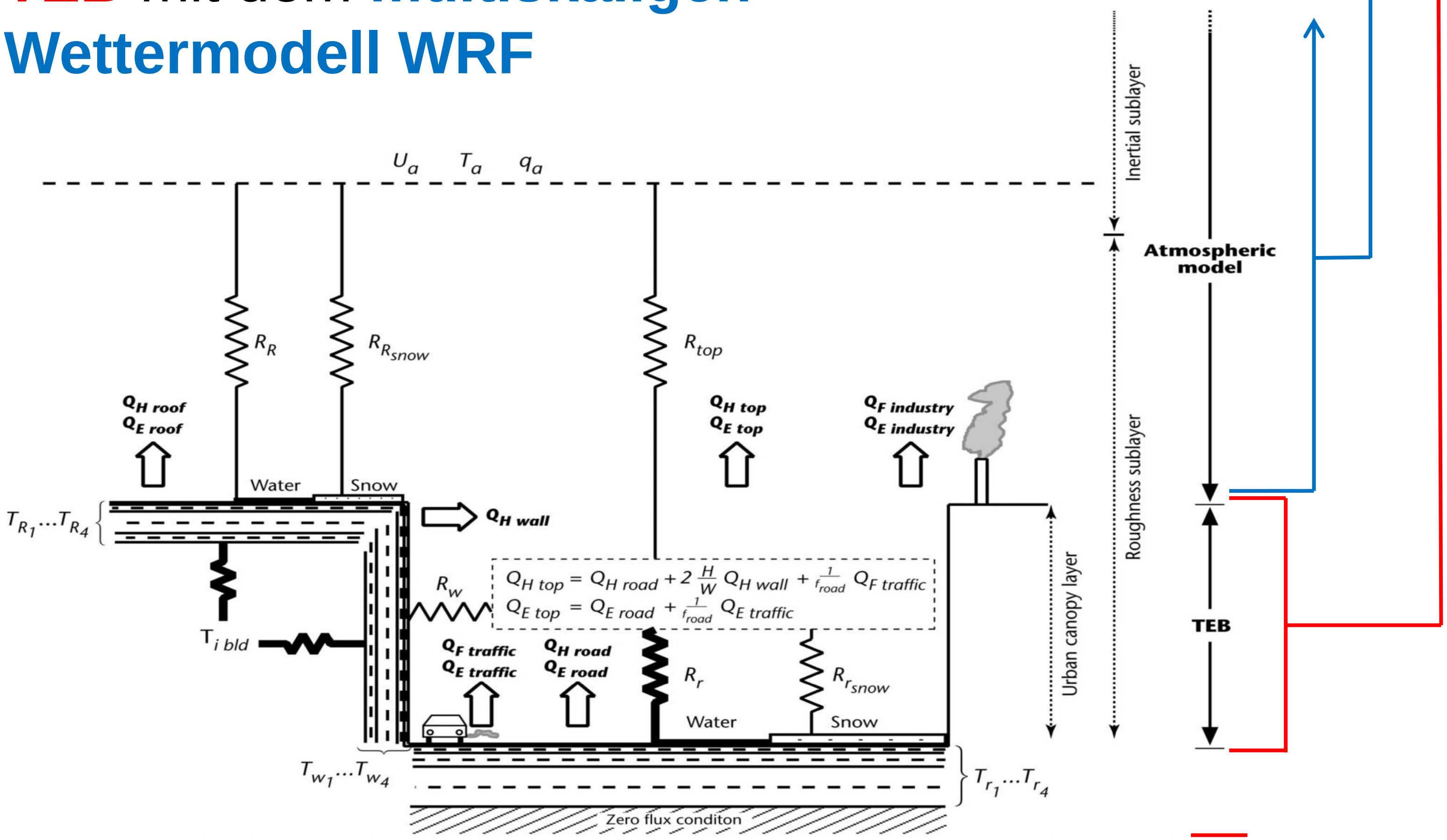

FIG. 2. Schematic representation of the surfaces (roof, wall, road indicated by subscript R, w, and r, respectively), prognostic temperatures (T), and aerodynamic resistances (R) used in TEB and the output fluxes. Resistances shown with thick lines have been altered from the original scheme (Masson 2000). Thus, $Q_{HTEB} = f_{roof}Q_{Hroof} + f_{road}Q_{Htop} + Q_{Findustry}$ and $Q_{ETEB} = f_{roof}Q_{Eroof} + f_{road}Q_{Etop} + Q_{Eindustry}$.

Source: Masson, 2000

1. Ergebnisse – Vergleich TEB mit

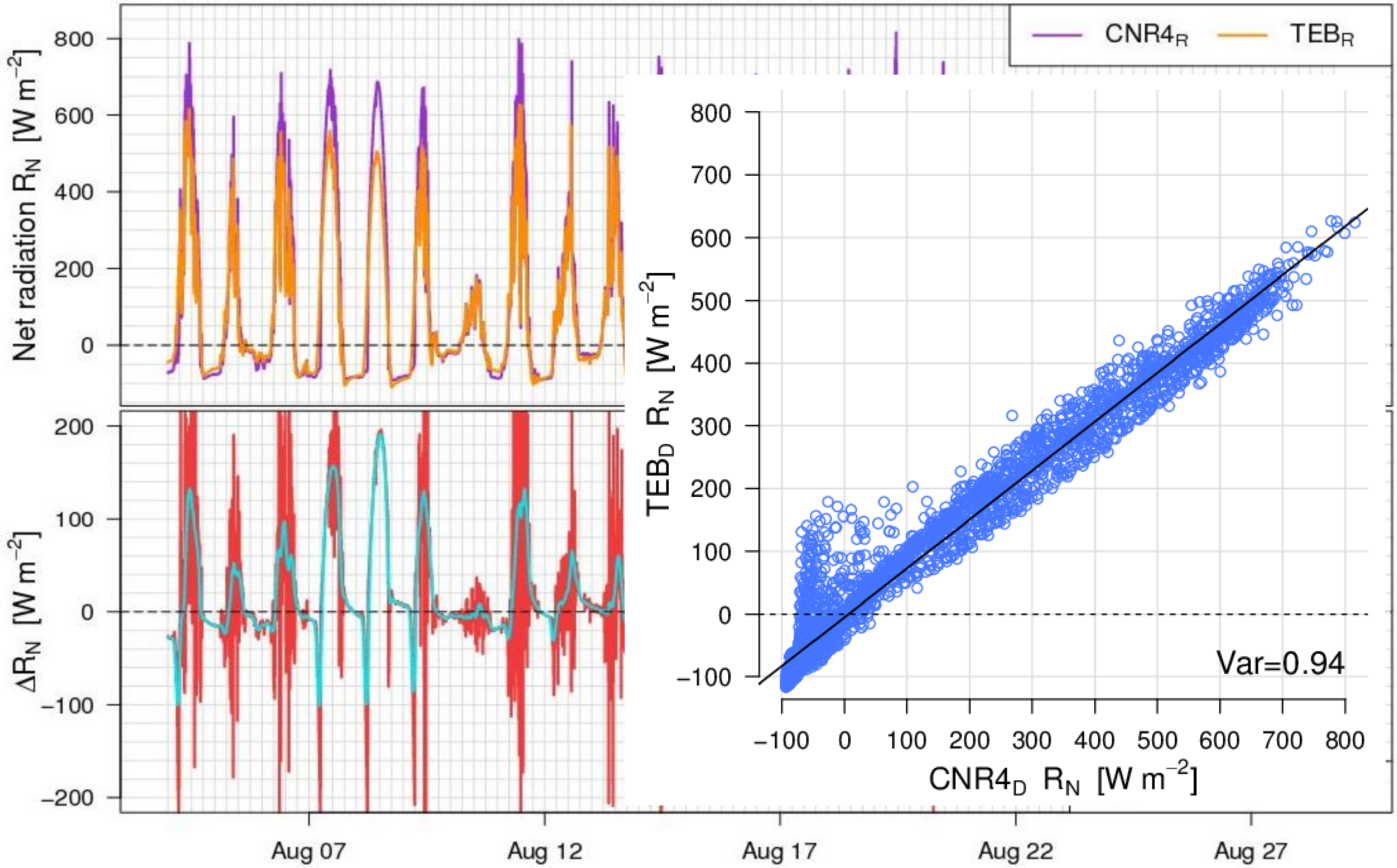

Übersicht Modelle

WRF (– UCM)	Weather Research and Forecast model (- urban canopy model)	Open source
Source: ...		
SOLWEIG (UMEP)	Solar and longwave environmental irradiance geometry model	Open source
Source: https://bitbucket.org/fredrik_ucg/umep/downloads		
TEB	Town Energy Balance	Open source
Source: http://www.cnrm-game-meteo.fr/spip.php?article199&lang=fr		

TEB Input for Test site

built surface: 0.59 (from FMZK)
 0.54 (from BKM)!
sealed surface: 0.22 / 0.27
gardens: 0.19
building height: 17.1m (from BKM)
roughness length: 1.71 (builheght/10)
facade lenght: 817m
wall ver_hor. ratio: 1.0

roof albedo: 0.26 (0.05 - 0.7)
road albedo: 0.13
wall albedo: 0.3
garden albedo: 0.2
roof emissivity: 0.79 (0.2-0.9)
road emissivity: 0.9
wall emissivity: 0.9
garden emissivity: 0.98
thickness of roof, road and wall layer: all 0.05, only road: 0.05, 0.25, 0.5, 0.75 (as WRFu)
thermal conductivity: 1.68 (as WRFu)
heat capacity: 2000000 (as WRFu)

Urban canopy model: Input

Fractions of buildings, roads, vegetation

Mean building height
Ratio of surface of walls to horizontal surface
Building roughness length z0 (Grimmond 1999)

Albedo and emissivity of roof, wall, road
Insulation (Thermal conductivity, heat conduction, thickness) of roof, wall, road

Anthropogenic heat flux (latent and sensible heat)
Irrigation

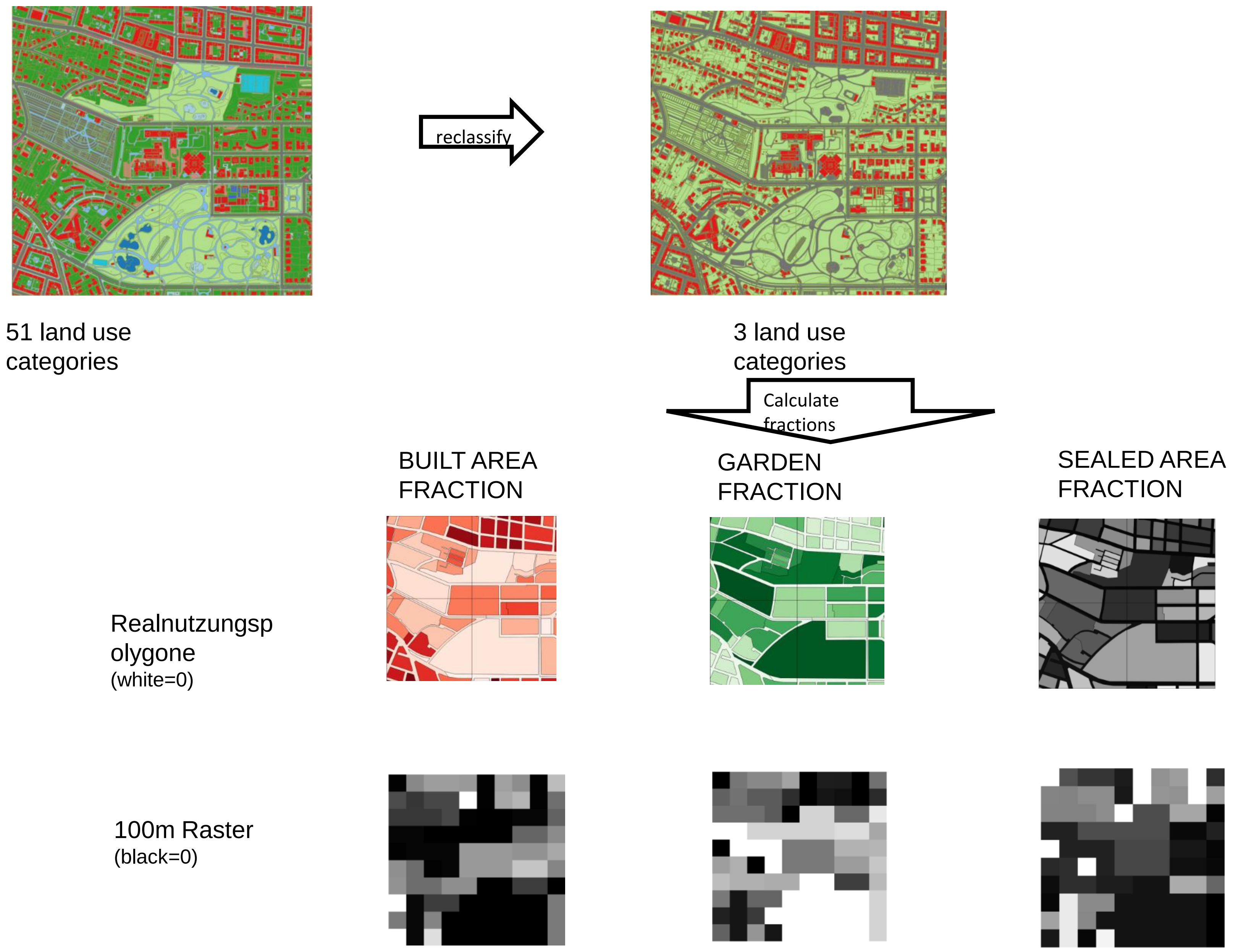
reclassify
51 land use categories
3 land use categories
Calculate fractions
BUILT AREA FRACTION
GARDEN FRACTION
SEALED AREA FRACTION
Realnutzungspolygone (white=0)
100m Raster (black=0)

Built types	Definition	Land cover types	Definition
1. Compact high-rise 	Dense mix of tall buildings to tens of stories. Few or no trees. Land cover mostly paved. Concrete, steel, stone, and glass construction materials.	A. Dense trees 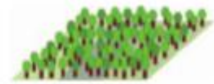	Heavily wooded landscape of deciduous and/or evergreen trees. Land cover mostly pervious (low plants). Zone function is natural forest, tree cultivation, or urban park.
2. Compact midrise 	Dense mix of midrise buildings (3–9 stories). Few or no trees. Land cover mostly paved. Stone, brick, tile, and concrete construction materials.	B. Scattered trees 	Lightly wooded landscape of deciduous and/or evergreen trees. Land cover mostly pervious (low plants). Zone function is natural forest, tree cultivation, or urban park.
3. Compact low-rise 	Dense mix of low-rise buildings (1–3 stories). Few or no trees. Land cover mostly paved. Stone, brick, tile, and concrete construction materials.	C. Bush, scrub 	Open arrangement of bushes, shrubs, and short, woody trees. Land cover mostly pervious (bare soil or sand). Zone function is natural scrubland or agriculture.
4. Open high-rise 	Open arrangement of tall buildings to tens of stories. Abundance of pervious land cover (low plants, scattered trees). Concrete, steel, stone, and glass construction materials.	D. Low plants 	Featureless landscape of grass or herbaceous plants/crops. Few or no trees. Zone function is natural grassland, agriculture, or urban park.
5. Open midrise 	Open arrangement of midrise buildings (3–9 stories). Abundance of pervious land cover (low plants, scattered trees). Concrete, steel, stone, and glass construction materials.	E. Bare rock or paved 	Featureless landscape of rock or paved cover. Few or no trees or plants. Zone function is natural desert (rock) or urban transportation.
6. Open low-rise 	Open arrangement of low-rise buildings (1–3 stories). Abundance of pervious land cover (low plants, scattered trees). Wood, brick, stone, tile, and concrete construction materials.	F. Bare soil or sand 	Featureless landscape of soil or sand cover. Few or no trees or plants. Zone function is natural desert or agriculture.
7. Lightweight low-rise 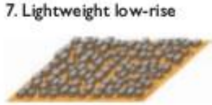	Dense mix of single-story buildings. Few or no trees. Land cover mostly hard-packed. Lightweight construction materials (e.g., wood, thatch, corrugated metal).	G. Water 	Large, open water bodies such as seas and lakes, or small bodies such as rivers, reservoirs, and lagoons.
8. Large low-rise 	Open arrangement of large low-rise buildings (1–3 stories). Few or no trees. Land cover mostly paved. Steel, concrete, metal, and stone construction materials.	**VARIABLE LAND COVER PROPERTIES** Variable or ephemeral land cover properties that change significantly with synoptic weather patterns, agricultural practices, and/or seasonal cycles.	
9. Sparsely built 	Sparse arrangement of small or medium-sized buildings in a natural setting. Abundance of pervious land cover (low plants, scattered trees).	*b. bare trees* *s. snow cover*	Leafless deciduous trees (e.g., winter). Increased sky view factor. Reduced albedo. Snow cover >10 cm in depth. Low admittance. High albedo.
10. Heavy industry 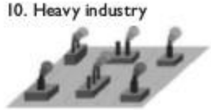	Low-rise and midrise industrial structures (towers, tanks, stacks). Few or no trees. Land cover mostly paved or hard-packed. Metal, steel, and concrete construction materials.	*d. dry ground* *w. wet ground*	Parched soil. Low admittance. Large Bowen ratio. Increased albedo. Waterlogged soil. High admittance. Small Bowen ratio. Reduced albedo.

Source: Steward and Oke (2012)

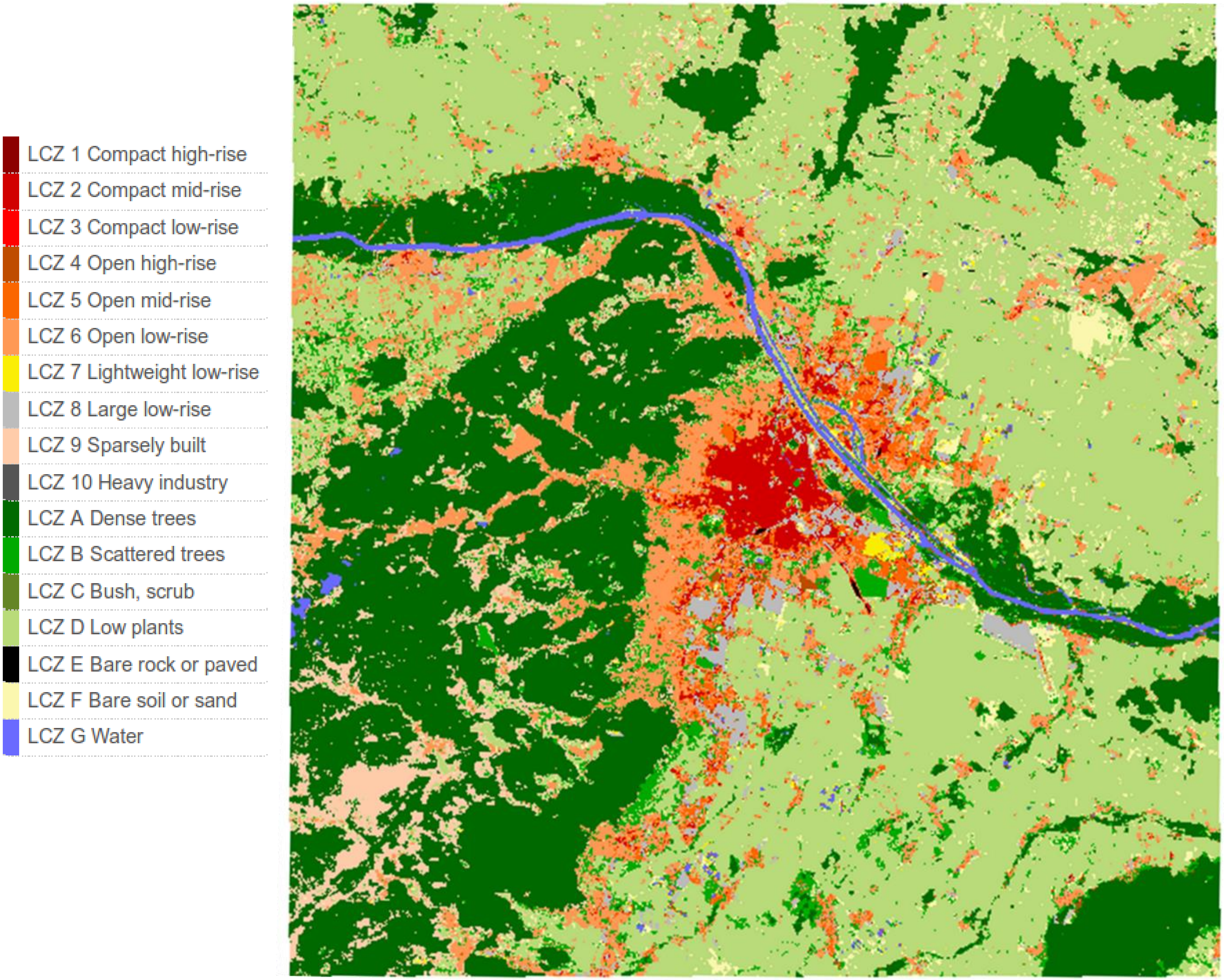
LCZ 1 Compact high-rise
LCZ 2 Compact mid-rise
LCZ 3 Compact low-rise
LCZ 4 Open high-rise
LCZ 5 Open mid-rise
LCZ 6 Open low-rise
LCZ 7 Lightweight low-rise
LCZ 8 Large low-rise
LCZ 9 Sparsely built
LCZ 10 Heavy industry
LCZ A Dense trees
LCZ B Scattered trees
LCZ C Bush, scrub
LCZ D Low plants
LCZ E Bare rock or paved
LCZ F Bare soil or sand
LCZ G Water

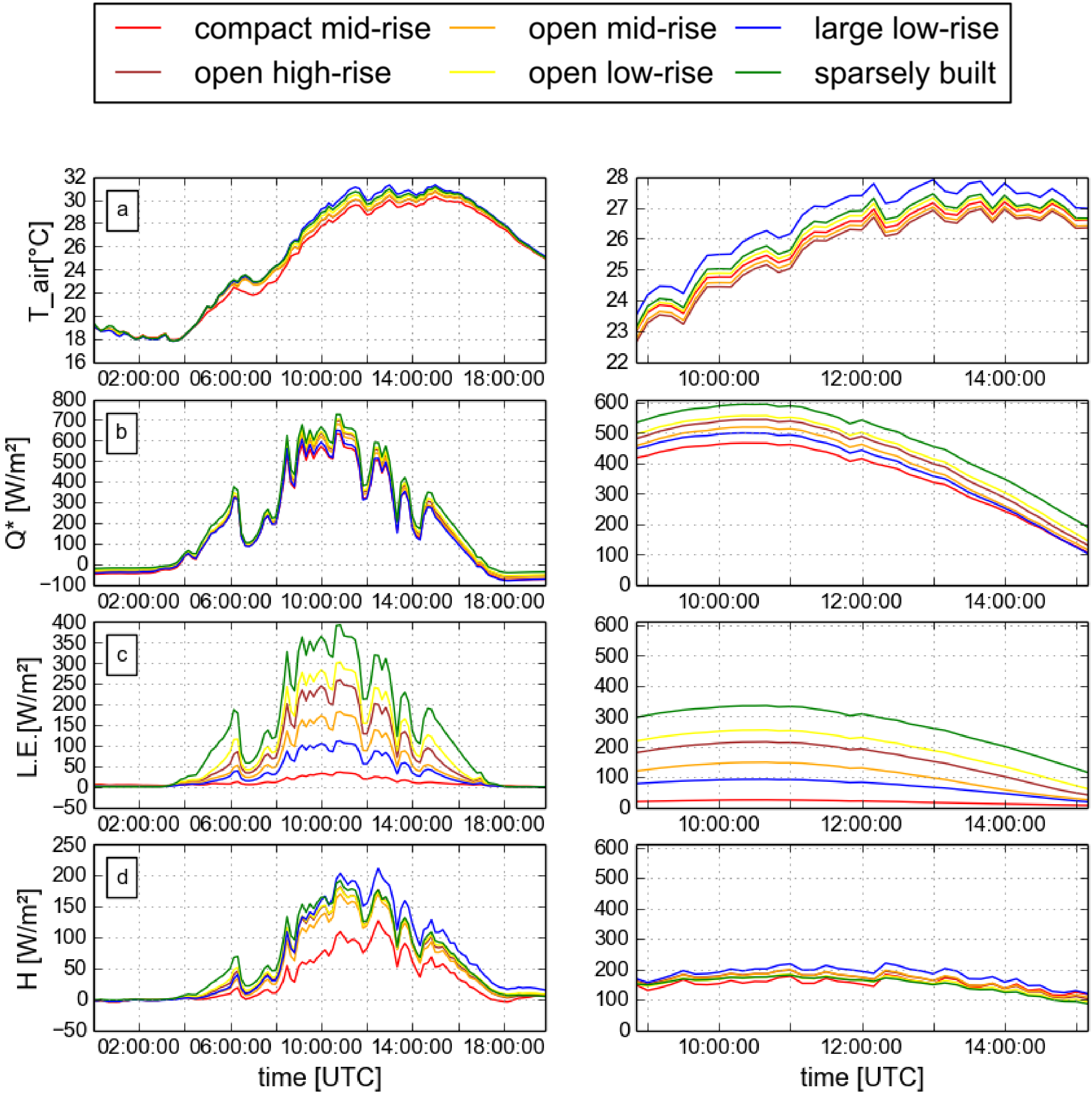

compact mid-rise
open mid-rise
large low-rise
open high-rise
open low-rise
sparsely built
a
b
c
d
T_air[°C]
Q* [W/m²]
L.E.[W/m²]
H [W/m²]
time [UTC]
time [UTC]

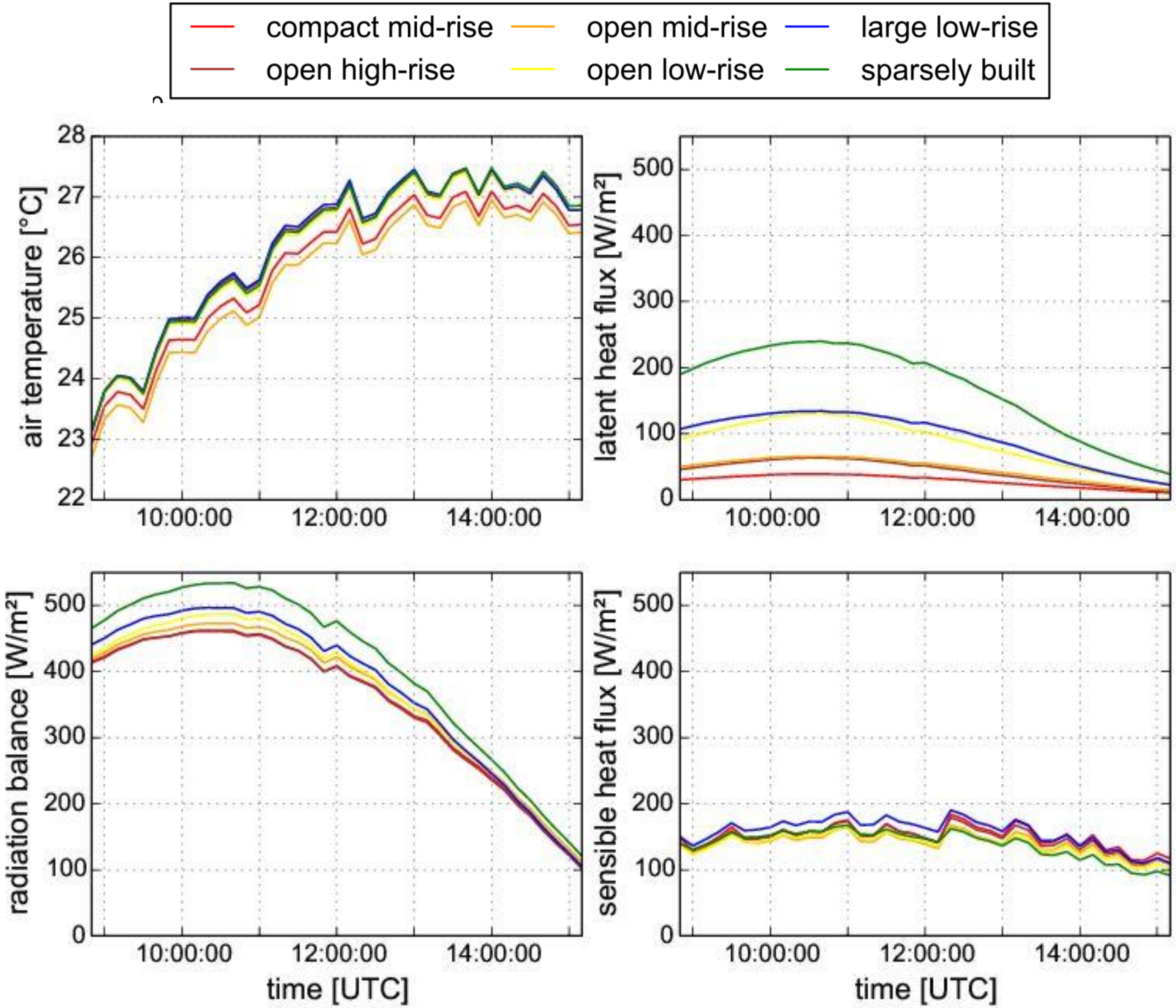
compact mid-rise
open mid-rise
large low-rise
open high-rise
open low-rise
sparsely built
air temperature [°C]
latent heat flux [W/m²]
radiation balance [W/m²]
sensible heat flux [W/m²]
time [UTC]
10:00:00
12:00:00
14:00:00

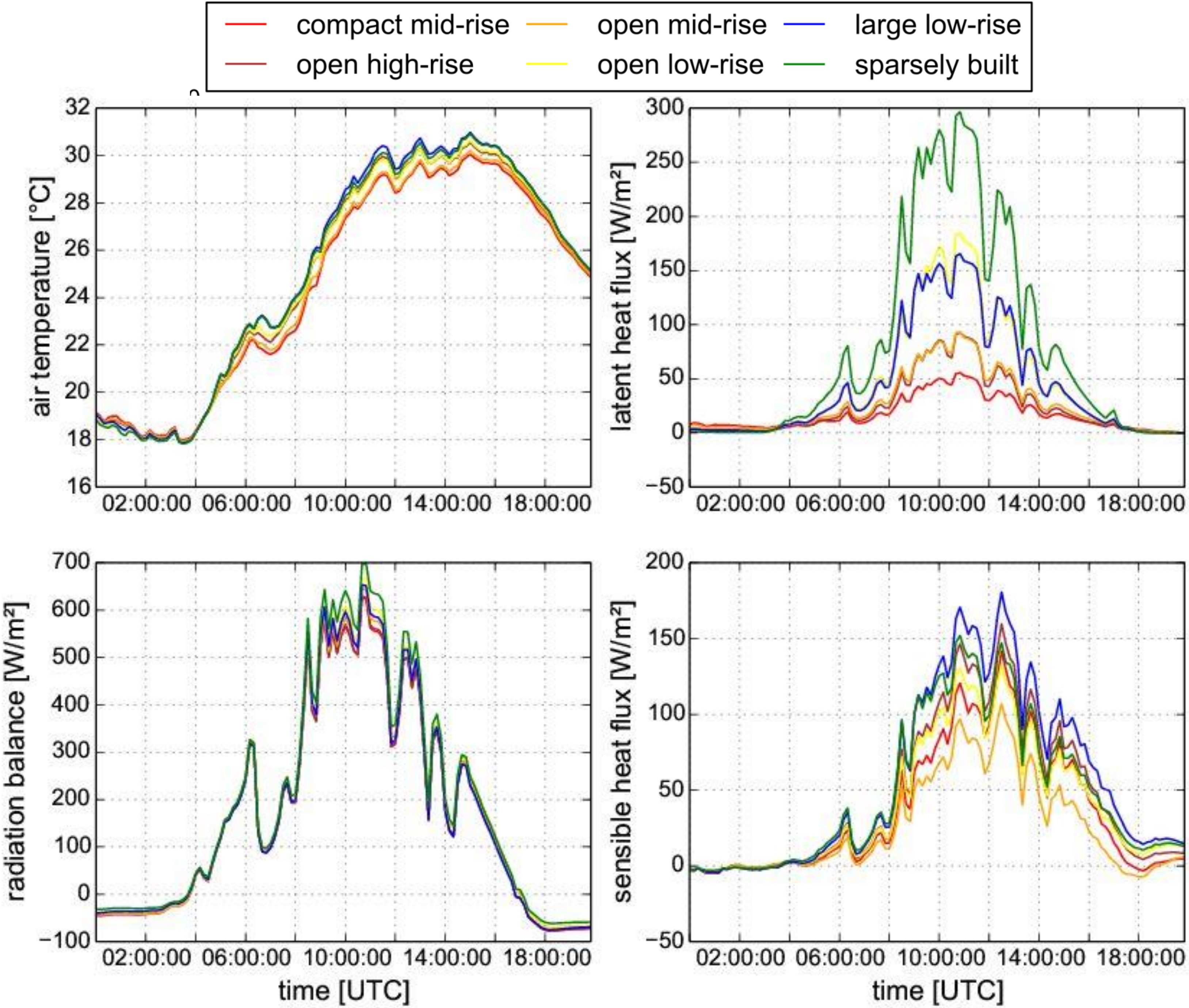
compact mid-rise
open mid-rise
large low-rise
open high-rise
open low-rise
sparsely built
air temperature [°C]
latent heat flux [W/m²]
radiation balance [W/m²]
sensible heat flux [W/m²]
time [UTC]
02:00:00
06:00:00
10:00:00
14:00:00
18:00:00

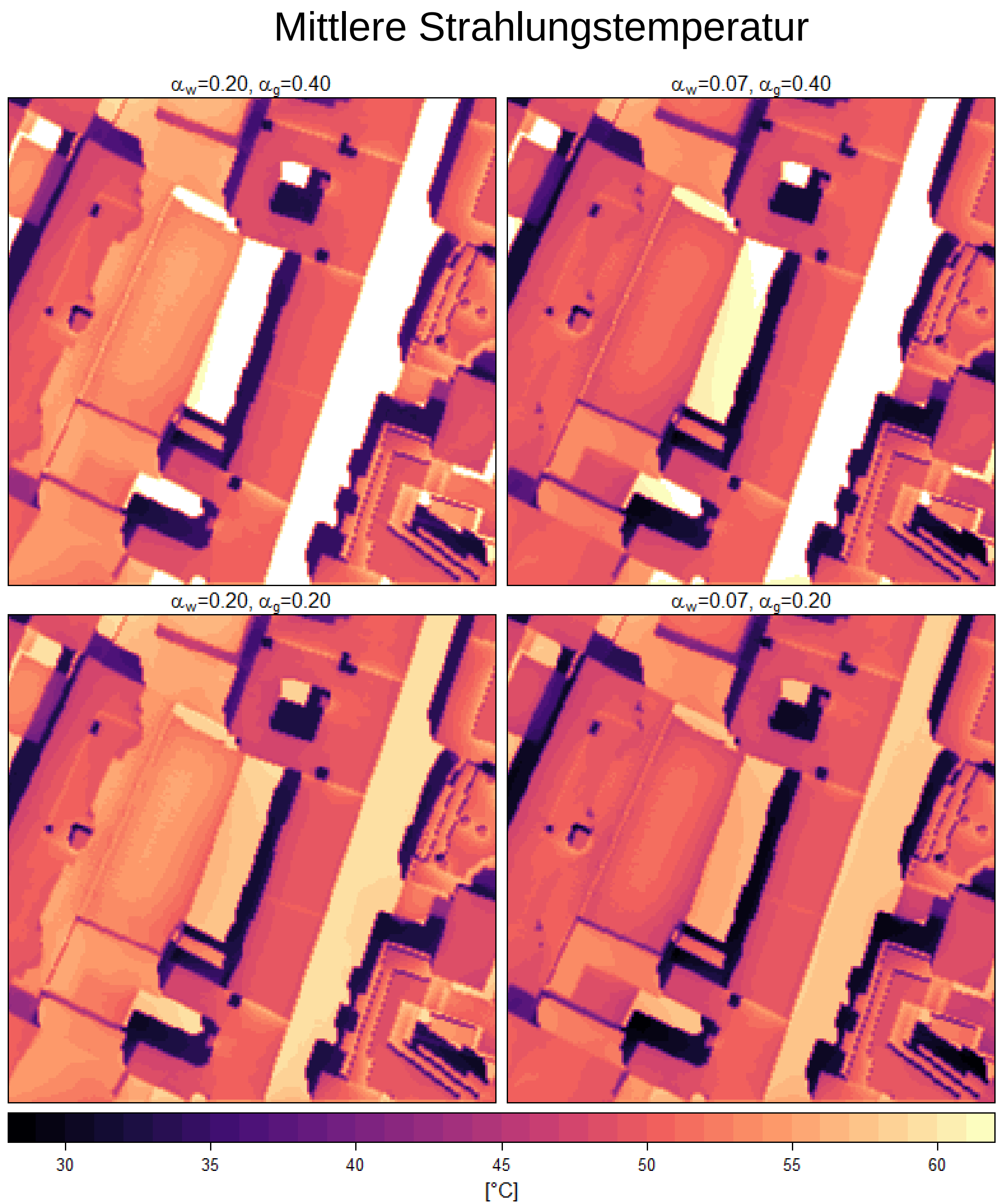

Mittlere Strahlungstemperatur
α_w=0.20, α_g=0.40
α_w=0.07, α_g=0.40
α_w=0.20, α_g=0.20
α_w=0.07, α_g=0.20
30
35
40
45
50
55
60
[°C]

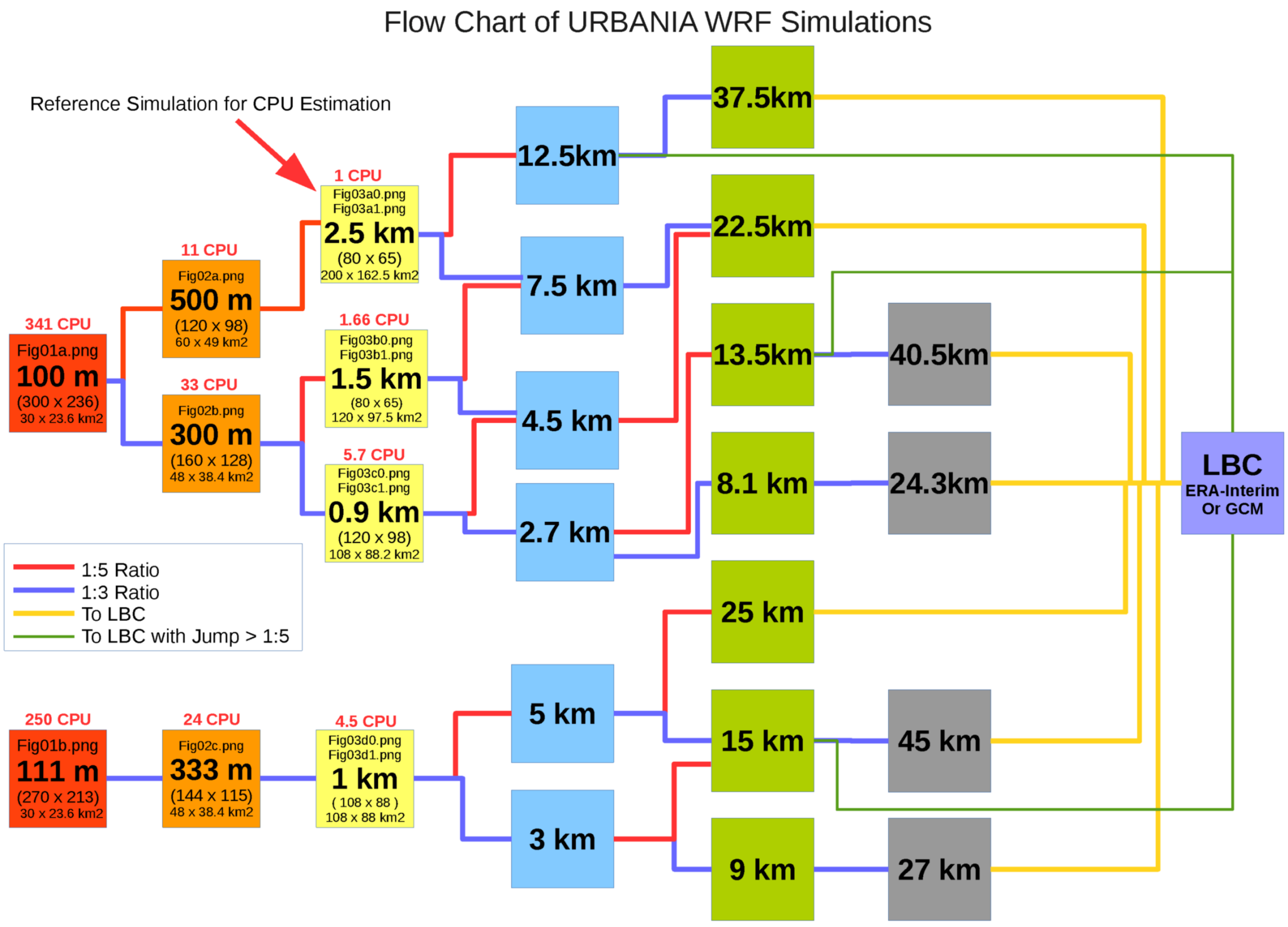
Flow Chart of URBANIA WRF Simulations
Reference Simulation for CPU Estimation
341 CPU
Fig01a.png
100 m
(300 x 236)
30 x 23.6 km2
11 CPU
Fig02a.png
500 m
(120 x 98)
60 x 49 km2
33 CPU
Fig02b.png
300 m
(160 x 128)
48 x 38.4 km2
1 CPU
Fig03a0.png
Fig03a1.png
2.5 km
(80 x 65)
200 x 162.5 km2
1.66 CPU
Fig03b0.png
Fig03b1.png
1.5 km
(80 x 65)
120 x 97.5 km2
5.7 CPU
Fig03c0.png
Fig03c1.png
0.9 km
(120 x 98)
108 x 88.2 km2
12.5km
7.5 km
4.5 km
2.7 km
37.5km
22.5km
13.5km
8.1 km
40.5km
24.3km
LBC
ERA-Interim
Or GCM
1:5 Ratio
1:3 Ratio
To LBC
To LBC with Jump > 1:5
250 CPU
Fig01b.png
111 m
(270 x 213)
30 x 23.6 km2
24 CPU
Fig02c.png
333 m
(144 x 115)
48 x 38.4 km2
4.5 CPU
Fig03d0.png
Fig03d1.png
1 km
(108 x 88)
108 x 88 km2
5 km
3 km
25 km
15 km
9 km
45 km
27 km

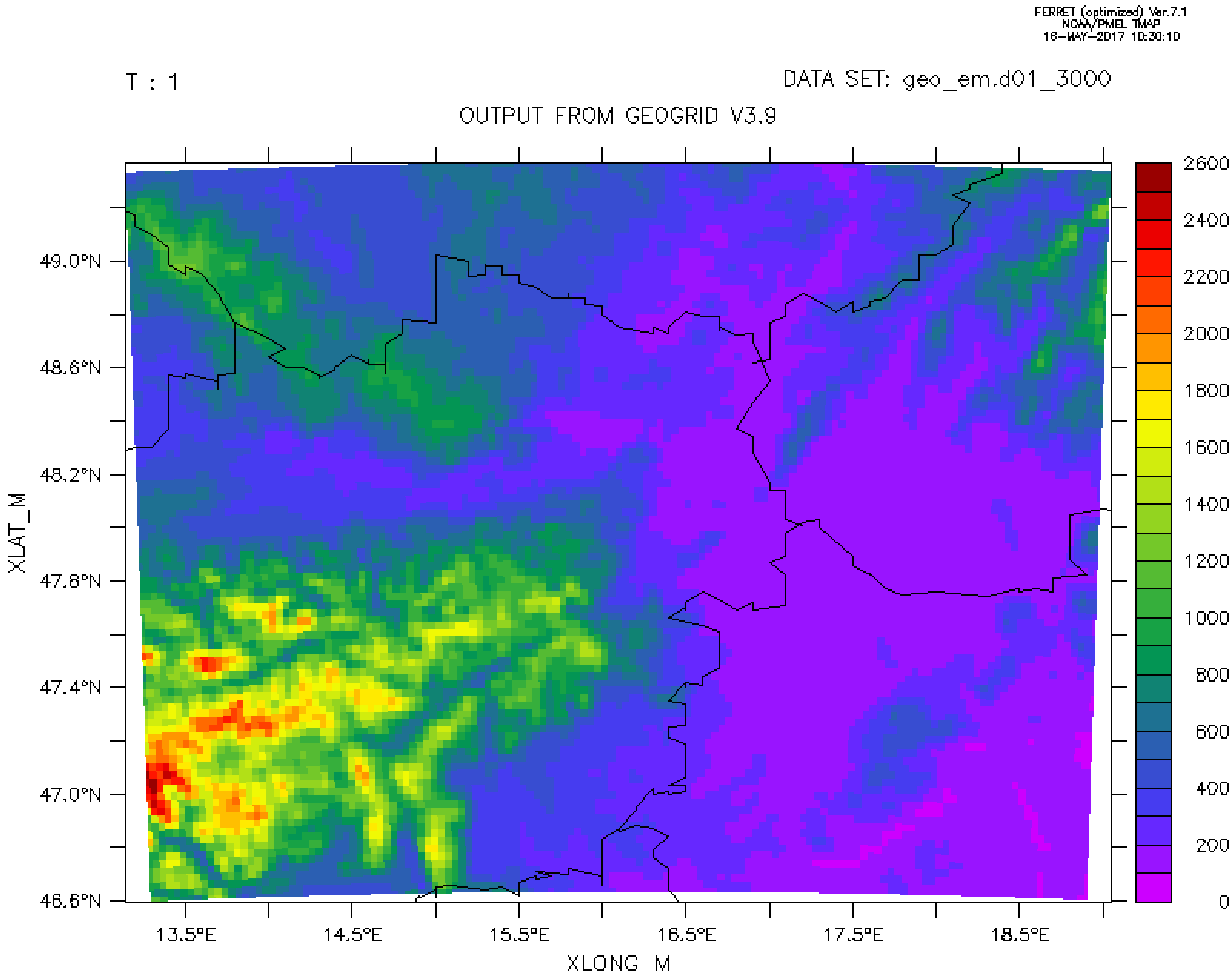

HGT_M (meters MSL)

Input Data from WRF [MKS unit]:

```
!
!    UTYPE  [-]     : Urban type. 1=Commercial/Industrial; 2=High-intensity residential;
!                   : 3=low-intensity residential
!    TA     [K]     : Potential temperature at 1st wrf level (absolute temp)
!    QA     [kg/kg] : Mixing ratio at 1st atmospheric level
!    UA     [m/s]   : Wind speed at 1st atmospheric level
!    SSG    [W/m/m] : Short wave downward radiation at a flat surface
!                     Note this is the total of direct and diffusive solar
!                     downward radiation. If without two components, the
!                     single solar downward can be used instead.
!                     SSG = SSGD + SSGQ
!    LSOLAR [-]     : Indicating the input type of solar downward radiation
!                     True: both direct and diffusive solar radiation
!                     are available
!                     False: only total downward ridiation is available.
!    SSGD   [W/m/m] : Direct solar radiation at a flat surface
!                     if SSGD is not available, one can assume a ratio SRATIO
!                     (e.g., 0.7), so that SSGD = SRATIO*SSG
!    SSGQ   [W/m/m] : Diffuse solar radiation at a flat surface
!                     If SSGQ is not available, SSGQ = SSG - SSGD
!    LLG    [W/m/m] : Long wave downward radiation at a flat surface
!    RAIN   [mm/h]  : Precipitation
!    RHOO   [kg/m/m/m] : Air density
!    ZA     [m]     : First atmospheric level
!                     as a lowest boundary condition
!    DECLIN [rad]   : solar declination
!    COSZ           : = sin(fai)*sin(del)+cos(fai)*cos(del)*cos(omg)
!    OMG    [rad]   : solar hour angle
!    XLAT   [deg]   : latitude
!    DELT   [sec]   : Time step
!    ZNT    [m]     : Roughnes length
!
m (not used)
```

! Output Data to WRF [MKS unit]:
!
! TS [K] : Surface potential temperature (absolute temp)
! QS [-] : Surface humidity
!
! SH [W/m/m/] : Sensible heat flux, = FLXTH*RHOO*CPP
! LH [W/m/m] : Latent heat flux, = FLXHUM*RHOO*ELL
! LH_INEMATIC [kg/m/m/sec]: Moisture Kinematic flux, =
FLXHUM*RHOO
! SW [W/m/m] : Upward shortwave radiation flux,
! = SSG-SNET*697.7*60.
(697.7*60.=100.*100.*4.186)
! ALB [-] : Time-varying albedo
! LW [W/m/m] : Upward longwave radiation flux,
! = LNET*697.7*60.-LLG
! G [W/m/m] : Heat Flux into the Ground
! RN [W/m/m] : Net radiation
!
! PSIM [-] : Diagnostic similarity stability function for
momentum
! PSIH [-] : Diagnostic similarity stability function for heat
!
! TC [K] : Diagnostic canopy air temperature
! QC [-] : Diagnostic canopy humidity
!
! TH2 [K] : Diagnostic potential temperature at 2 m
! Q2 [-] : Diagnostic humidity at 2 m
! U10 [m/s] : Diagnostic u wind component at 10 m
! V10 [m/s] : Diagnostic v wind component at 10 m
!
! CHS, CHS2 [m/s] : CH*U at ZA, CH*U at 2

Realnutzungskartierung

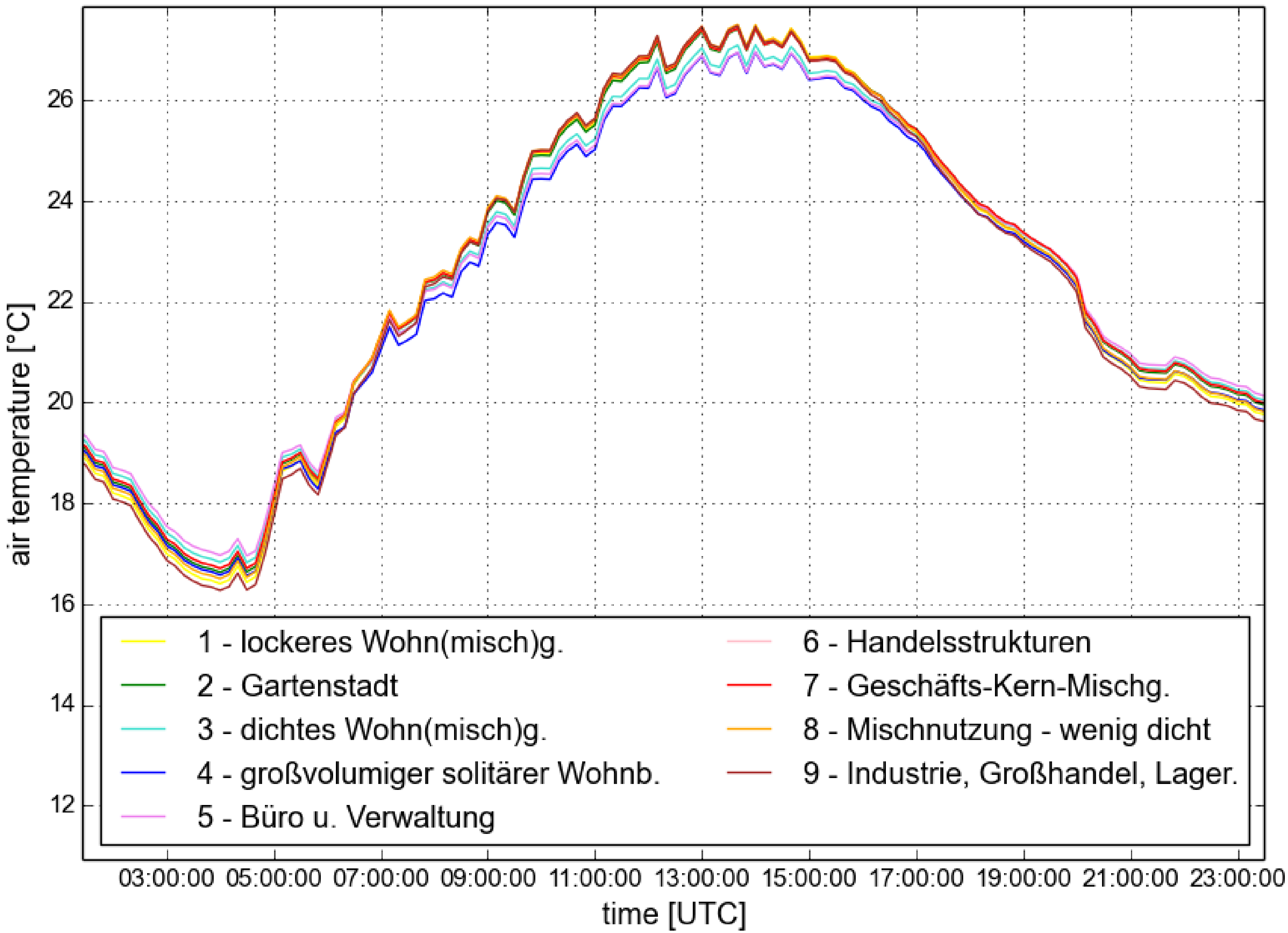

3.1. Überprüfung der von TEB berechneten Strahlungsflüssen in einem Strassencanyon

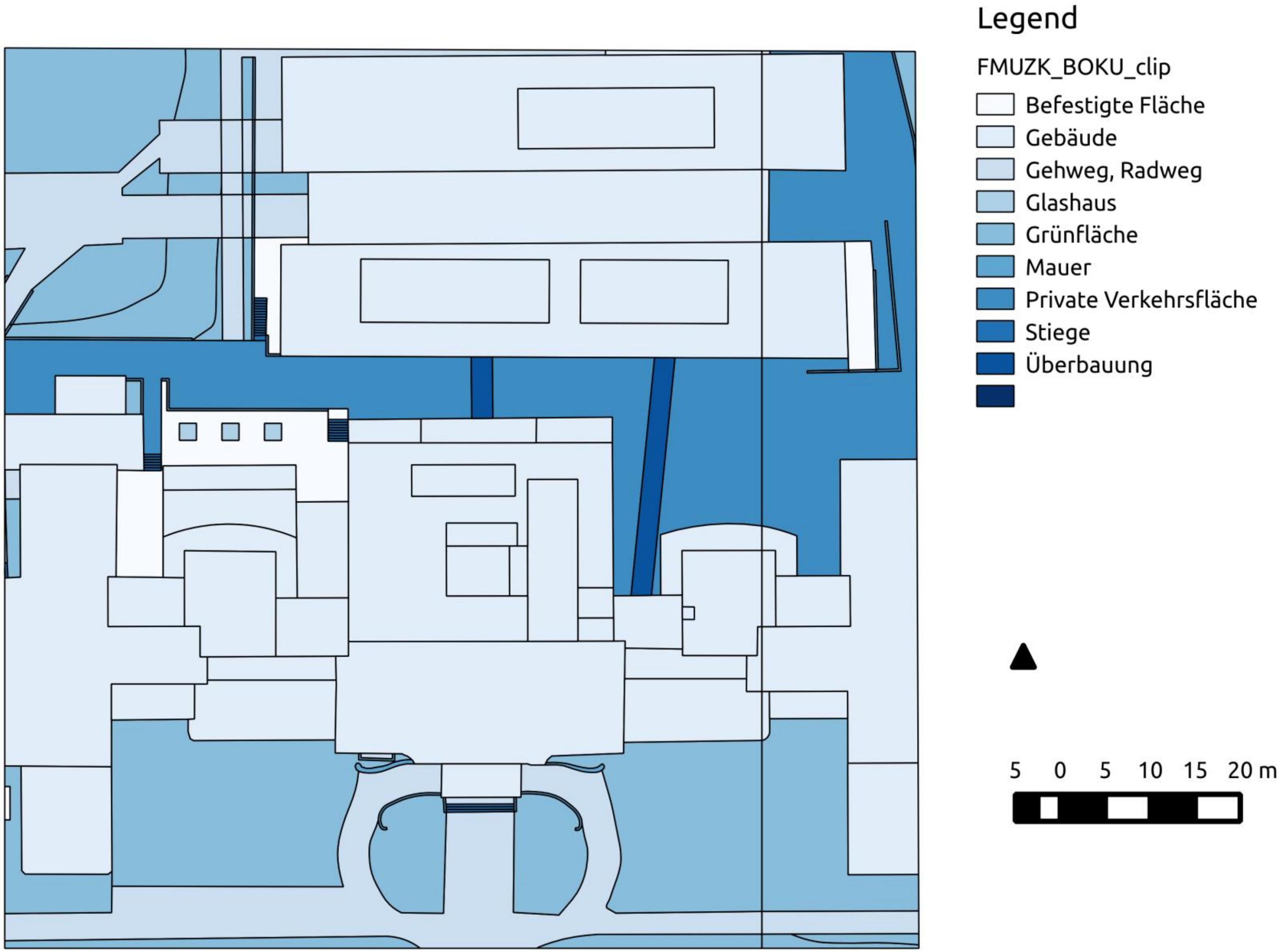
Legend
FMUZK_BOKU_clip
Befestigte Fläche
Gebäude
Gehweg, Radweg
Glashaus
Grünfläche
Mauer
Private Verkehrsfläche
Stiege
Überbauung
5 0 5 10 15 20 m

3.1. Überprüfung der von TEB berechneten Strahlungsflüssen in einem Strassencanyon

Validierung – Oberflächentemperatur

- thermal photography of wall, roof and roofs surfaces
- hourly around noon, on 9,16, 18 + 25 August 2016

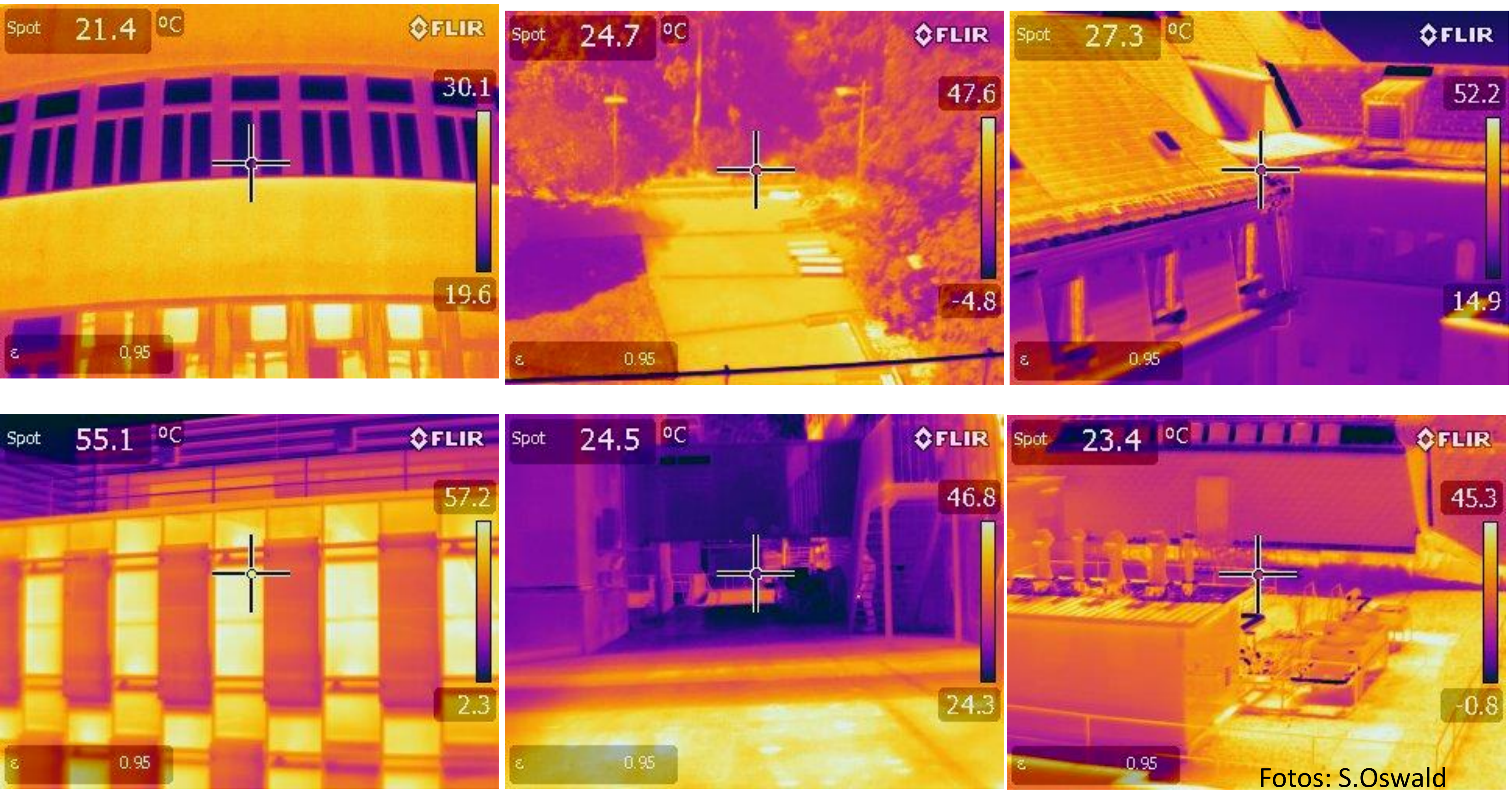

Fotos: S.Oswald

Bebauungshöhe

Verhältnis vertikale/horizontale Fläche

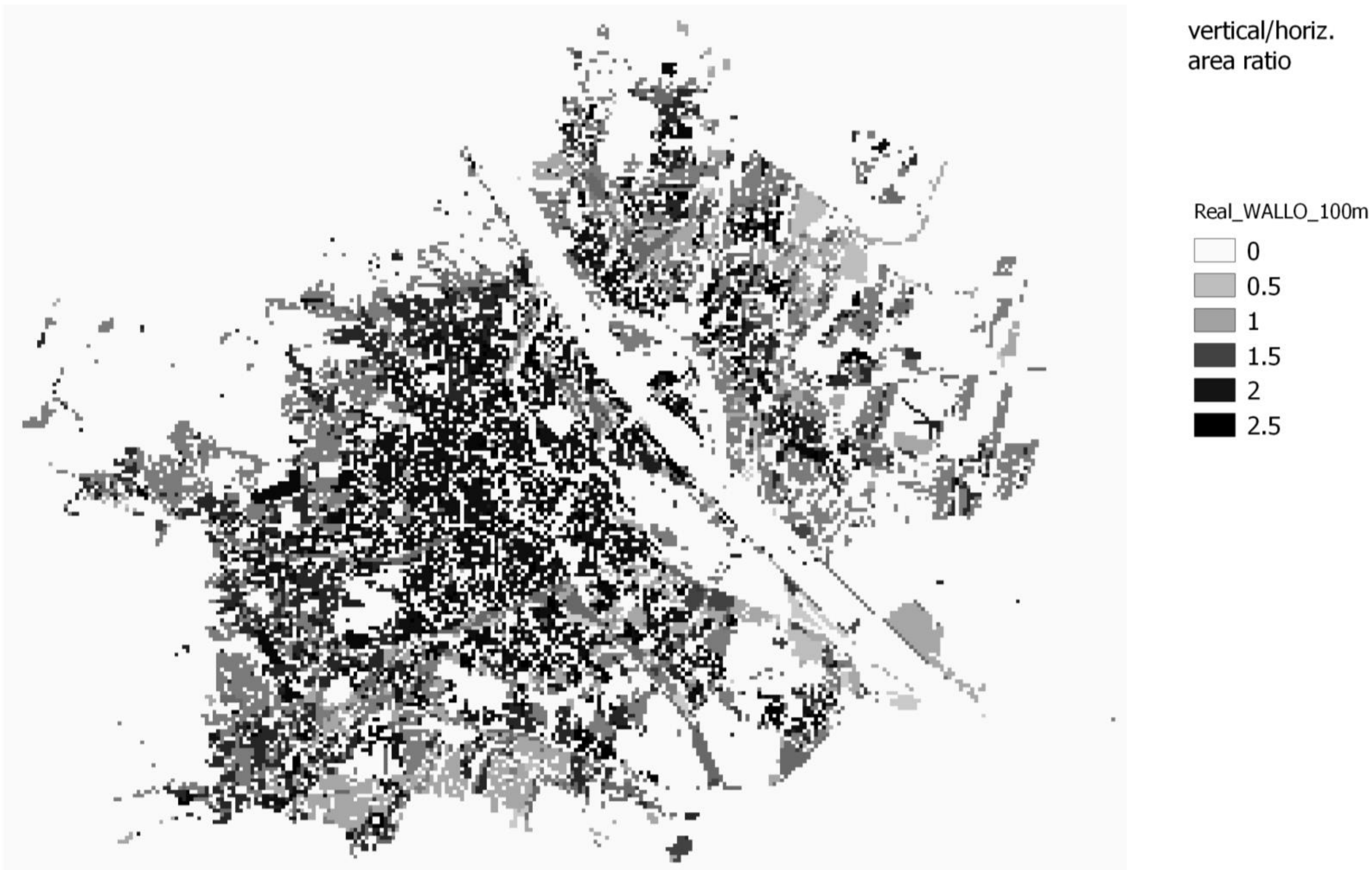

Wärmeleitfähigkeit Gebäudewände

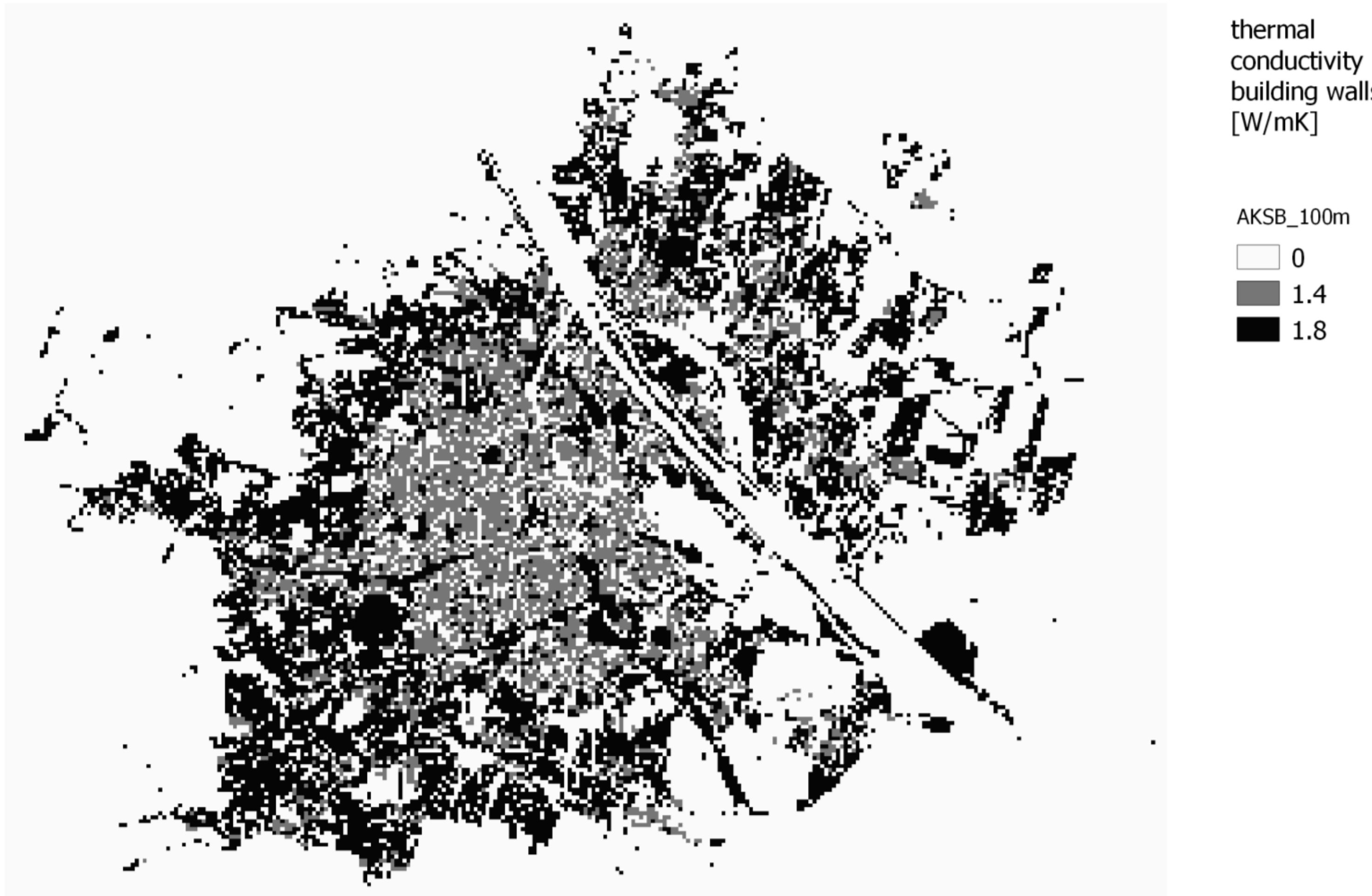

Wärmeleitfähigkeit Dächer

Surface types

- determination of area of all surface types
- measurement/definition of albedo of all relevant road/roof/wall surfaces
- definition of emissivity (literature)
- average for road/roof/wall

3.2. Erste Simulationen mit TEB

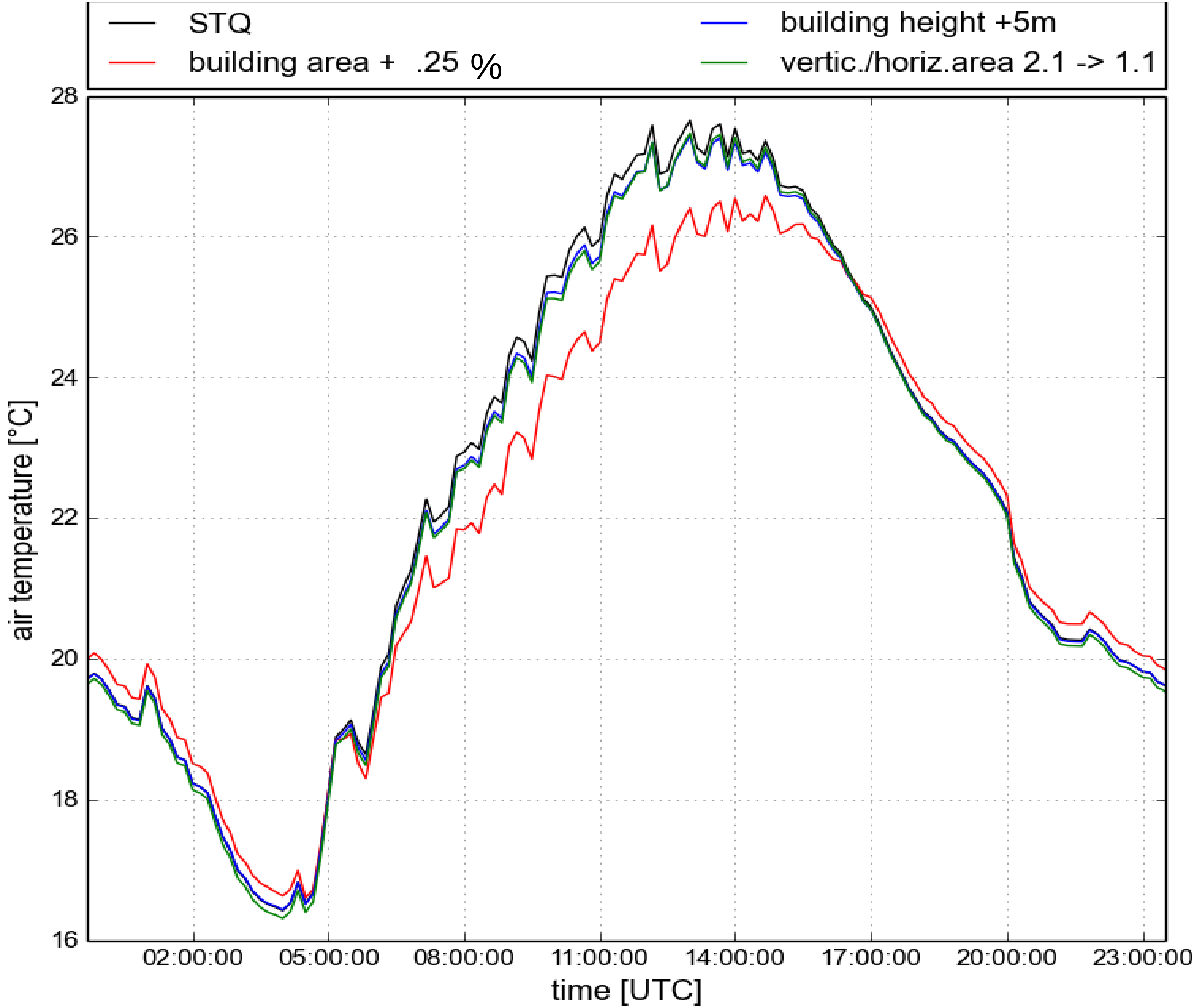

First characterization and comparison of TEB model simulations with in situ measurements regarding radiation balance in a single urban canyon at the BOKU site (Vienna)

Sandro M. Oswald[1], Heidelinde Trimmel[1], Michael Revesz[2], Valéry Masson[3], Philipp Weihs[1]
[1] Institute of Meteorology, University of Natural Resources and Applied Sciences (BOKU), Vienna, Austria
[2] Austrian Institute of Technology (AIT), Vienna, Austria

University of Natural Resources and Applied Life Sciences, Vienna
Department of Water, Atmosphere and Environment
Institute of Meteorology (BOKU-Met)

Introduction

According to the World Health Organization more than half of the world population lives in a city since 2010. Predictions foresee that by 2030 six out of ten people will live in an urban area. As a result, many cities are expanding in size. There are several effects in cities which strongly influence human health. Visible influences like the severe emissions of air pollutants by industry and traffic (e.g. Mayer H., 1999, Grimmond et al., 2010) are obvious to people but thermal stress in urban areas is only recently recognized for its strong devastating effect on human health. As a consequence, the urban environment virtually influences all weather parameters that have an impact on human comfort and thermal stress. Within this study, we investigate effects of city growth and the development of outlying districts on the local climate of Vienna. We focus particularly on the influence of urban heat island and consequent the risk for heat related illnesses or thermal stress for people. To quantify radiation balance and other important meteorological factors, we performed an extensive field campaign with three types of net radiometer in three different heights at BOKU site in August 2016.

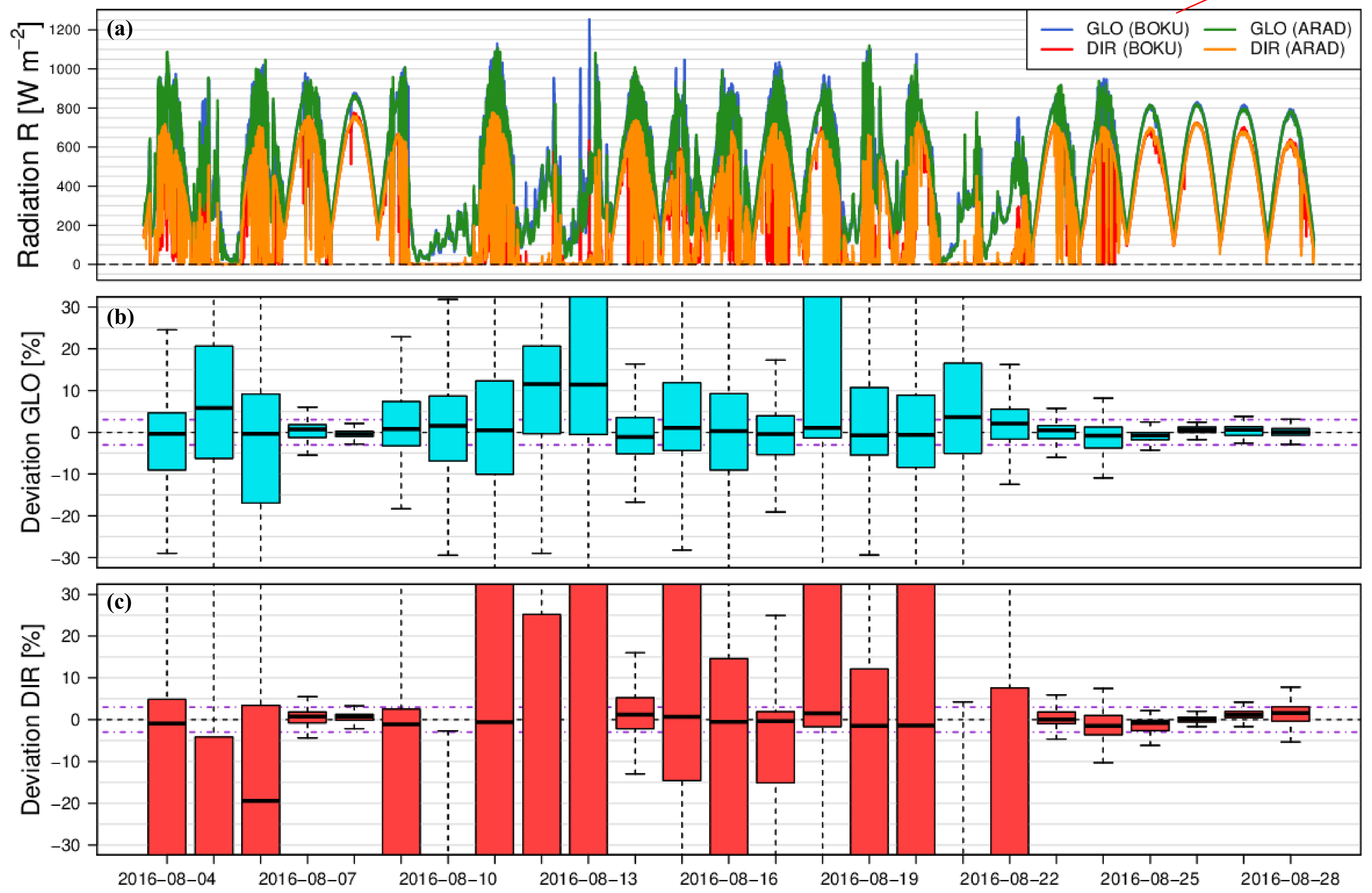

Fig. 1: Panel (a) shows time series of the radiation (R) with 1-min resolution measured at the Wien Hohe Warte ARAD site and the BOKU site. System acronyms represent measurements of global (GLO; EKO MS-802 and Kipp&Zonen CMP21) and direct (DIR; both Kipp&Zonen CHP1) solar radiation. Panel (b) shows the daily percentage deviation of global radiation measurements, panel (c) shows the daily percentage deviation of direct radiation measurements between BOKU site and Wien Hohe Warte ARAD site. The purple dot-dashed horizontal lines mark ± 3% of the deviation, respectively.

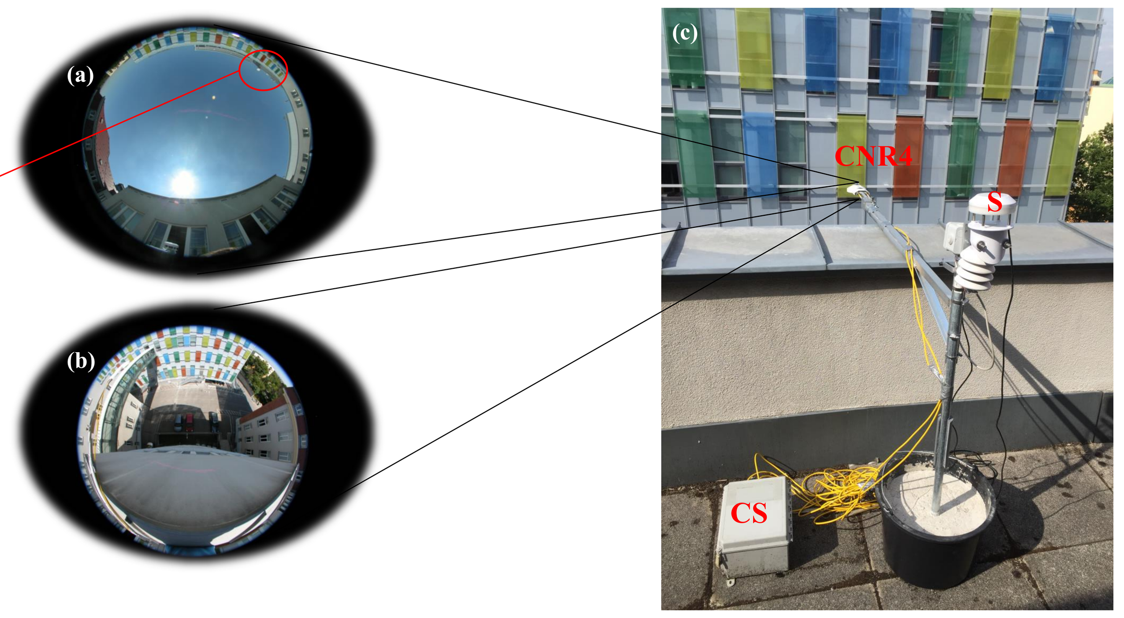

Fig. 2: Panel (a) shows the upper half space seen from the highest net radiometer (Kipp&Zonen CNR4), the red circle marks the measurement site BOKU of Fig. 1 at the rooftop on the opposite building. Panel (b) shows the lower half space of the BOKU site. Panel (c) shows a photo of the CNR4, an Sonic anemometer (S) and Campbell Scientific Logger CR1000 (CS) at one measurement point at the BOKU site.

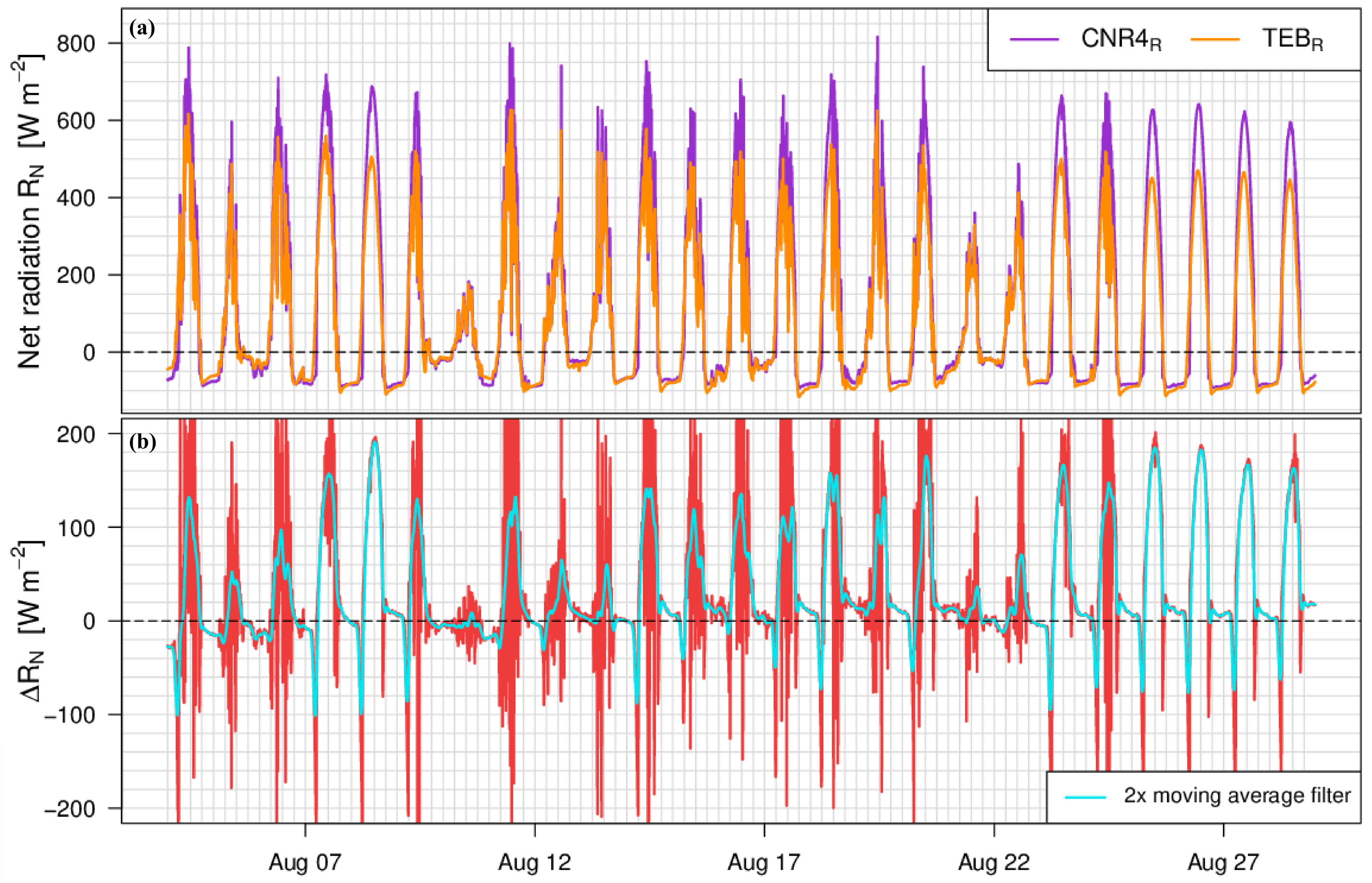

Fig. 3: Time series of (a) the net radiation (R_N) balance measured by the Kipp&Zonen CNR4 radiometer (1-min resolution averaged to 10-min resolution) and the simulation of TEB (10-min resolution) with inputs of the rooftop (Index R in the legend) measurement site. For convenience, panel (b) shows the difference (ΔR_N) between $CNR4_R$ and TEB_R and two times 60 minute symmetric, multi-step moving average filter.

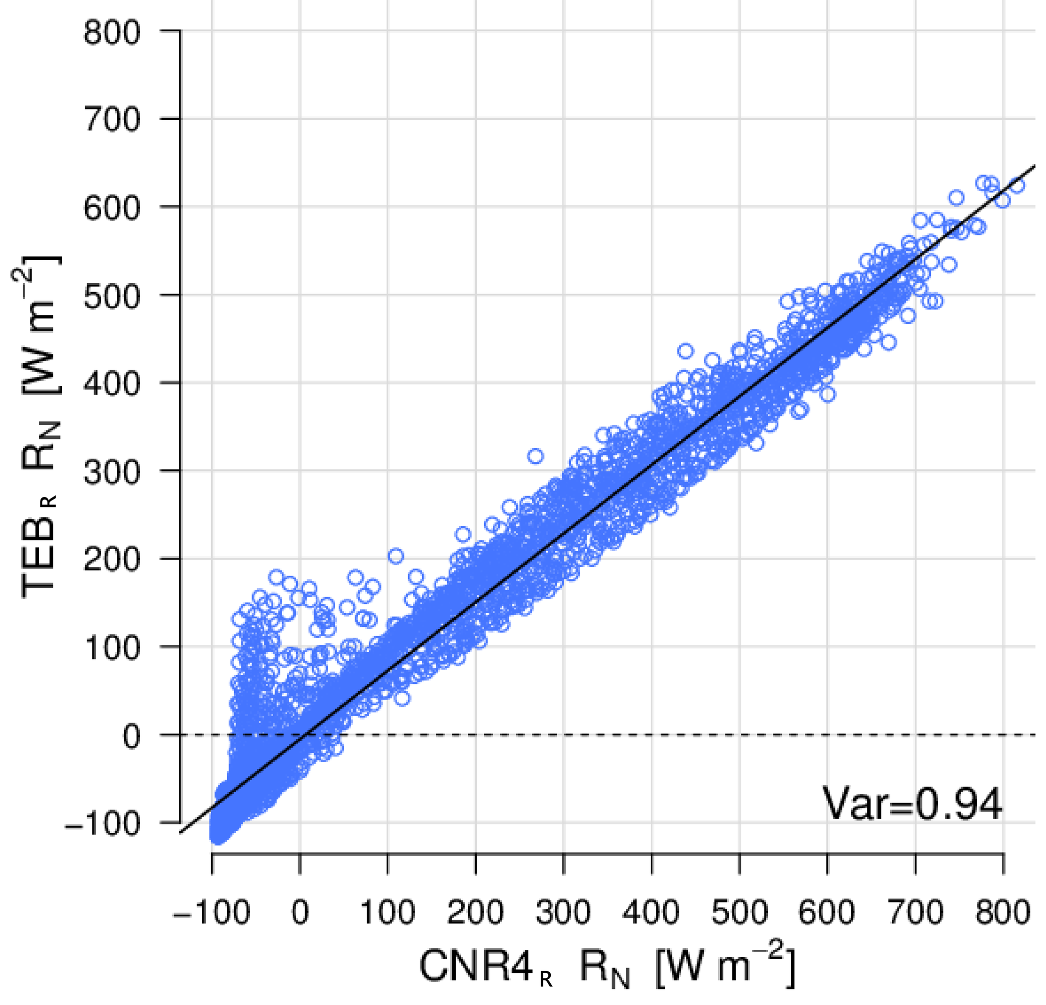

Fig. 4: Scatter plot of the measured and simulated values (R_N) between the net radiometer CNR4 and the TEB model regarding the time period of Fig. 3. The relationship between CNR4 and TEB is characterized by the squared Spearman's rank correlation coefficient (Var).

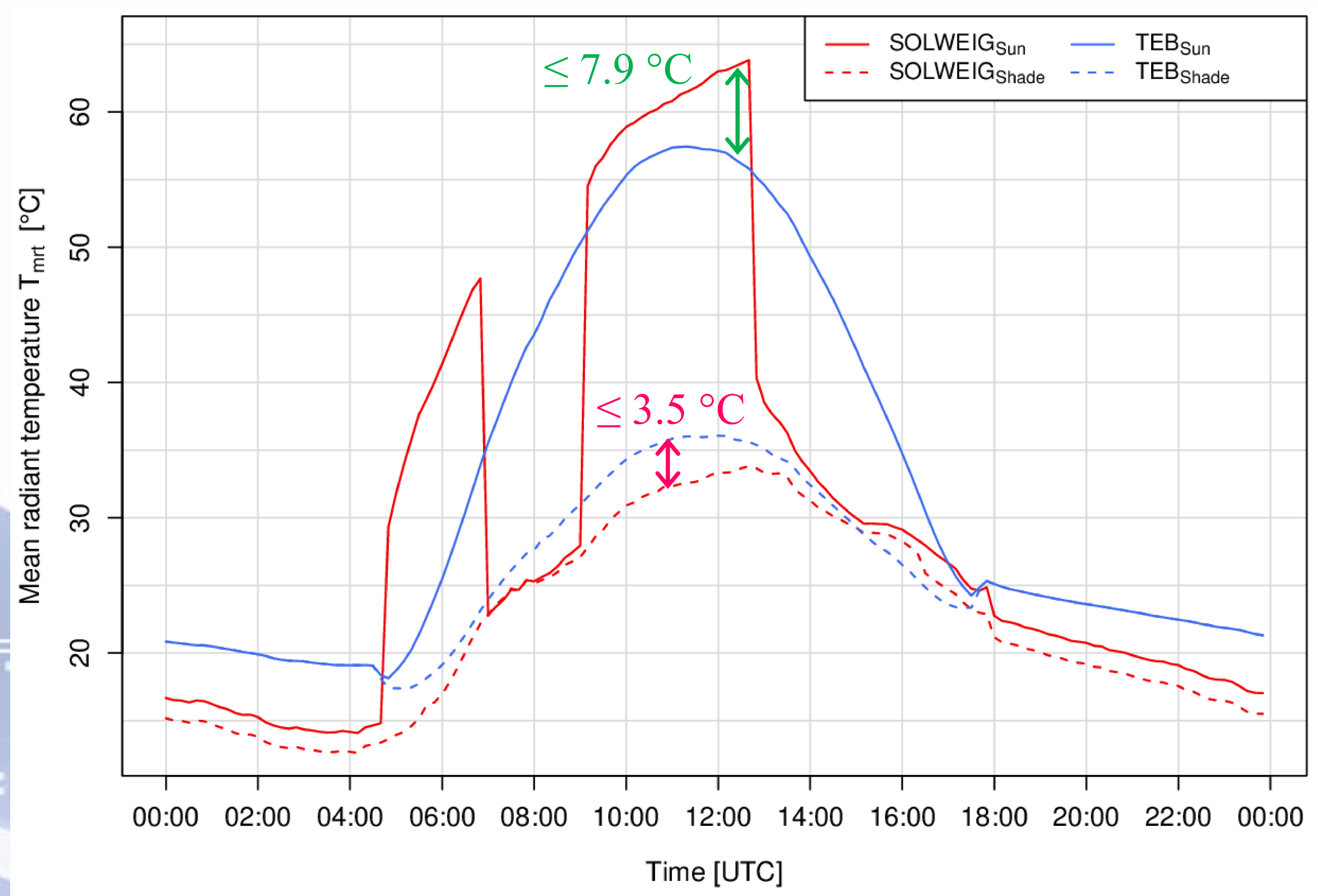

Fig. 5: Time series of the mean radiant temperature (T_{mrt}) simulated with an additional radiation balance model compared to TEB. The Solar Long-Wave Environmental Irradiance Geometry (SOLWEIG) model simulates spatial variations of mean radiant temperature and 3D fluxes of longwave and shortwave radiation. The model is available through a graphical user-friendly interface that can be downloaded for free.

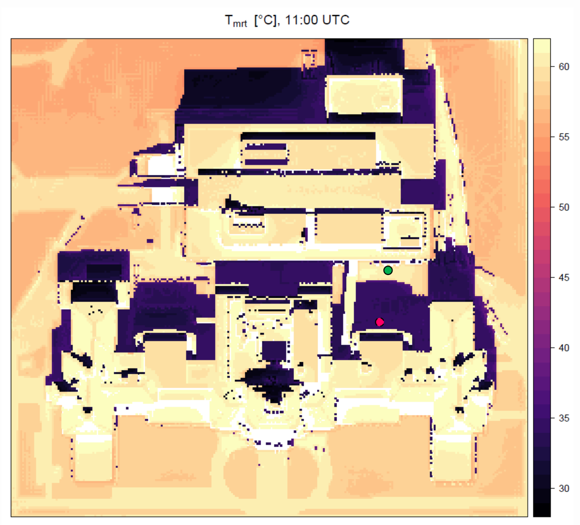

Fig. 6: Illustration of the possible outputs of SOLWEIG. With a digital surface model and different landcover types, SOLWEIG can calculate a 2.5D model of various radiation values like T_{mrt}.

Fig. 7: As Fig. 6 but for the Universal Thermal Climate Index (UTCI). The two points (Sun and shade) inside Fig. 6 and 7 mark the position of the calculated outputs from Fig. 5 and 8.

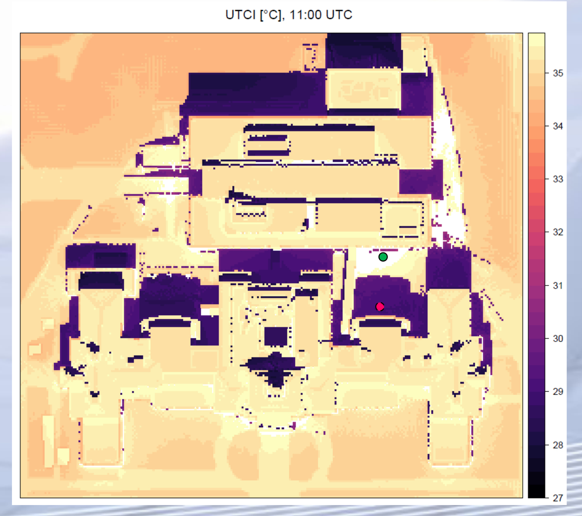

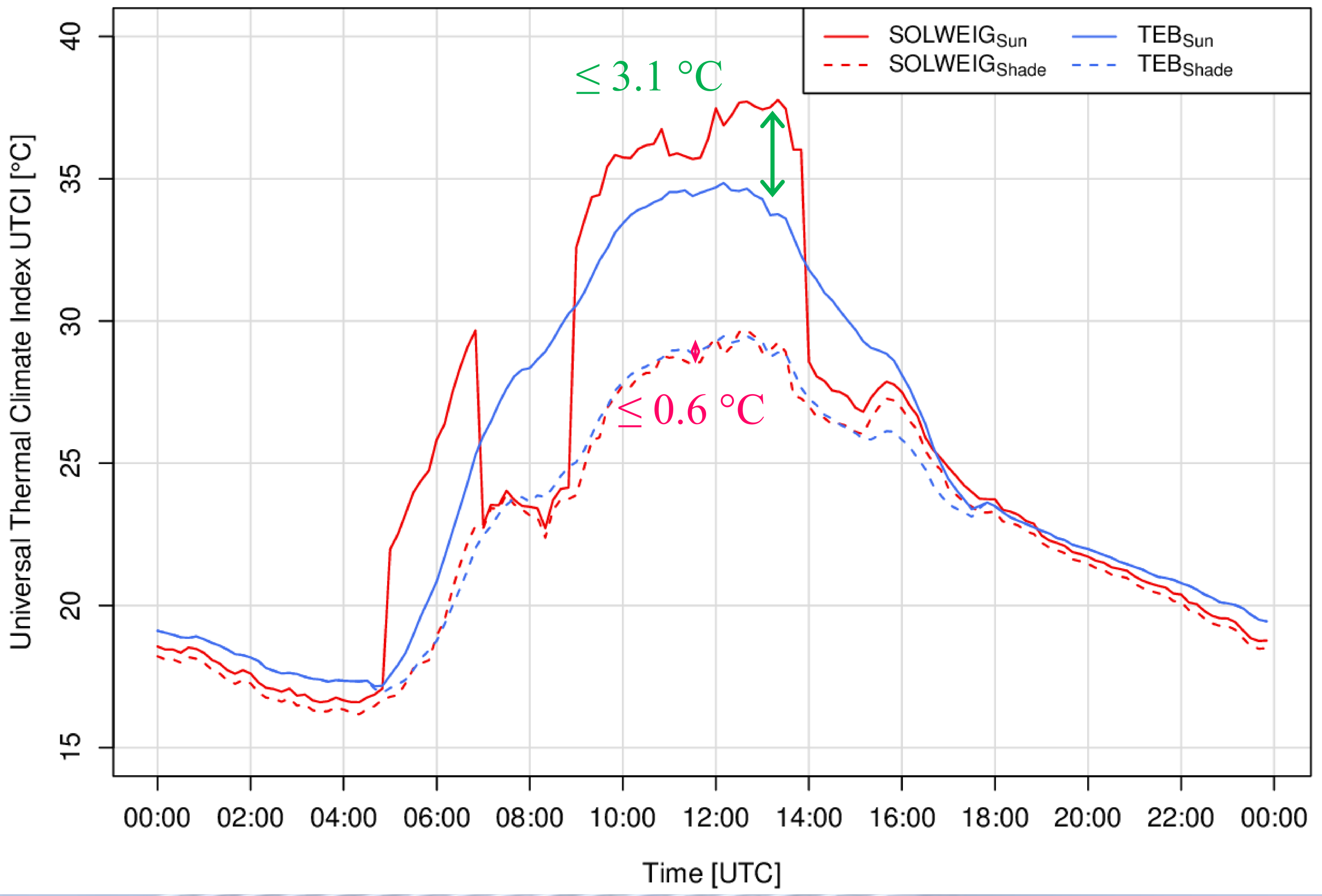

Fig. 8: As Fig. 5 but for the UTCI. Below the UTCI range is illustrated by ClimateCHIP.

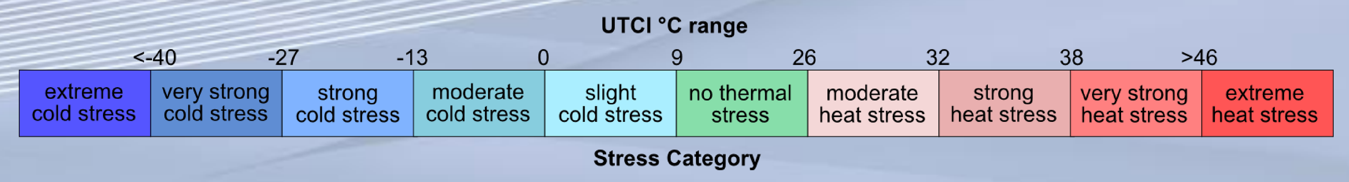

Conclusion

- TEB model input values of the BOKU measurement site at the rooftop show a deviation under 3% on approx. clear sky days regarding the inner-quartile range of solar global and direct radiation.
- Net radiation measurements in roof level show a strong correlation with TEB simulations.
- To quantify human comfort and thermal stress in future, the Universal Thermal Climate Index (UTCI) calculated by the TEB model show a very good behavior in shade, but is slightly underestimated in sun.

References

Grimmond C.S.B., et al.: *Climate and More Sustainable Cities: Climate Information for Improved Planning and Management of Cities (Producers/Capabilities Perspective).* Procedia Environmental Sciences 1, 247-274, 2010.
Mayer H.: *Air pollution in cities.* Atmospheric Environment, 33, 4029 - 4037, 1999.
Lindberg F., et al.: *The SOLWEIG-model.* University of Gothenburg, 2016
ClimateCHIP: *Universal Thermal Climate Index.* http://climatechip.org/DBSERVER/img/UTCI_scale.png (access on April 2017)

University of Natural Resources and Applied Life Sciences, Vienna, Department of Water, Atmosphere and Environment, Institute of Meteorology
Gregor-Mendel-Strasse 33, A-1180 Vienna, Austria, Tel.: +43 1 47654 81432, email: sandro.oswald@boku.ac.at

LAND USE AND URBAN MORPHOLOGY PARAMETERS FOR VIENNA REQUIRED FOR INITIALISATION OF THE URBAN CANOPY MODEL TEB DERIVED VIA THE CONCEPT OF “LOCAL CLIMATE ZONES ”

Heidelinde Trimmel [1], Philipp Weihs [1], Sandro M. Oswald [1], Valéry Masson [2], Robert Schoetter [2] , Kristopher Hammerberg[3]

[1] Institute of Meteorology, University of Natural Resources and Life Sciences, Gregor-Mendelstrasse 33, 1180 Vienna, Austria.

[2] Centre National de Recherches Météorologiques (CNRM), Météo France, 42 Avenue Gaspard Coriolis, 31100, Toulouse, France.

[3] Department of Building Physics and Building Ecology, Vienna University of Technology, Karlsplatz 13, 1010 Vienna, Austria.

heidelinde.trimmel@boku.ac.at

Motivation

Urban settlements are generally known for their high fractions of impermeable surfaces, large heat capacity and low humidity compared to rural areas, all of which contribute to the well known phenomena of urban heat islands. The urbanized areas are growing, which can further amplify the intensity and frequency of heat stress events that are already likely to increase with global climate change. Due to the highly diverse morphology of the urban environment the distribution of the urban heat island is not uniform. Building heights, building contiguity and the configuration of open spaces and trees vary, which cause changes in the aerodynamic resistance for heat transfers and drag coefficients for momentum and radiation trapping. Furthermore, cities are characterized by highly variable physical surface properties such as albedo, emissivity, heat capacity and thermal conductivity. The distribution of the urban heat island is influenced by these morphological and physical parameters as well as the distribution of unsealed soil and vegetation. These aspects influence the urban climate at the micro- and mesoscale. This drives the need for a classification that is: (1) climate sensitive, (2) easily updated, (3) reproducible.

Urban parameters for Vienna

For larger Vienna high resolution vector and raster geodatasets were processed to derive land use surface fractions and building morphology parameters on block scale following the methodology of Cordeau (2016). A dataset of building age and typology was cross checked and extended using satellite visual and thermal bands and linked to a database joining building age and typology with typical physical building parameters obtained from different studies (Berger et al. 2012, Amtmann M and Altmann-Mavaddat N (2014) and the OIB (Österreichisches Institut für Bautechnik). Using dominant parameters obtained using this high resolution mainly ground based data sets (building height, built area fraction, unsealed fraction, sky view factor) a local climate zone classification was produced using an algorithm. The threshold values were chosen according to Stewart and Oke (2012).

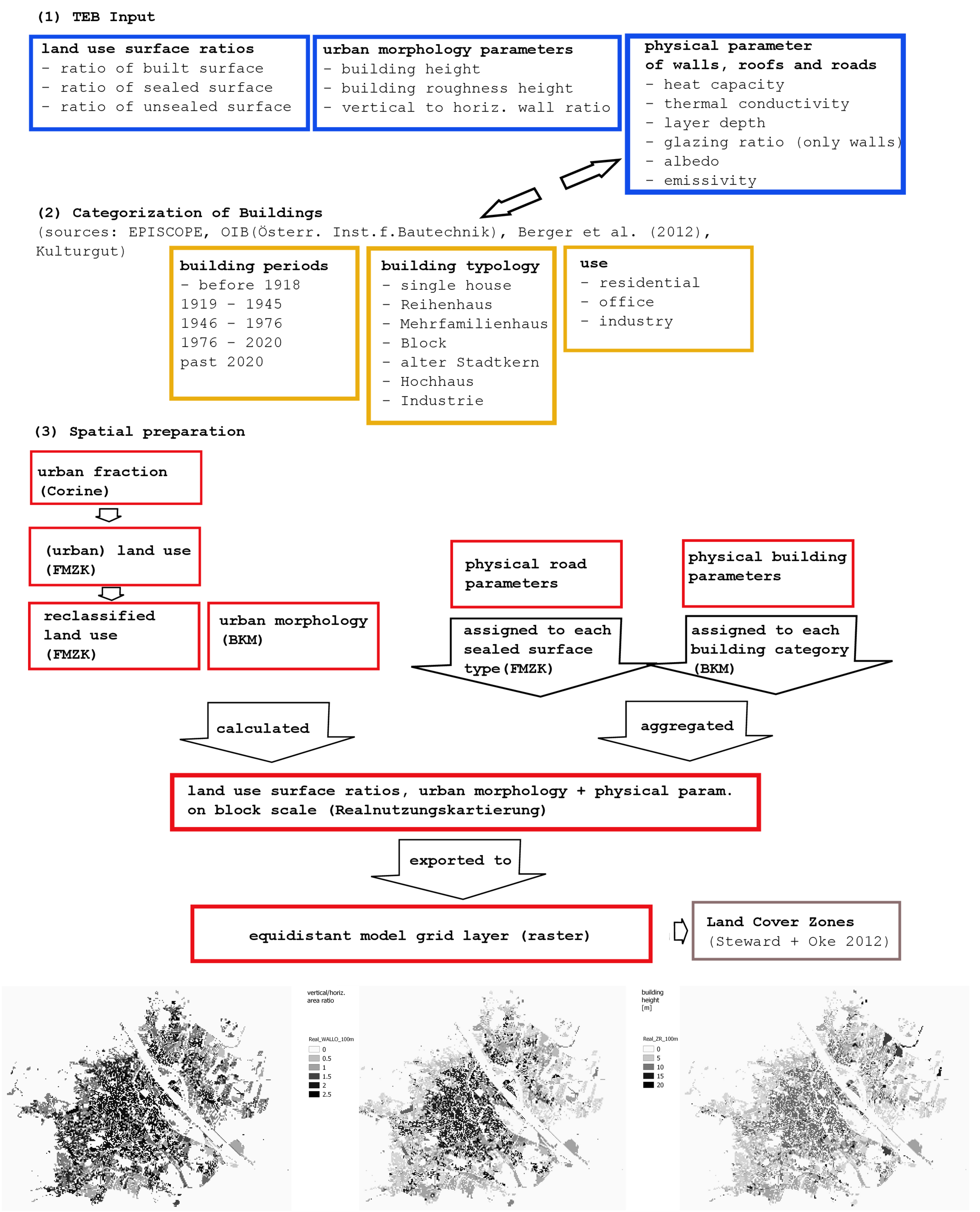

Fig. 1: Graphical overview of method and results for vertical to horizontal area fraction, building height, building fraction.

Amtmann M and Altmann-Mavaddat N (2014) Eine Typology österreichischer Wohngebäude, Österreichische Energieargentur – Austrian Energy Agency, TABULA/EPISCOPE

Bechtel B, Alexander P, Böhner J, et al (2015) Mapping Local Climate Zones for a Worldwide Database of the Form and Function of Cities. ISPRS Int J Geo-Inf 4:199–219. doi: 10.3390/ijgi4010199

T. Berger, H. Formayer, R. Smutny, C. Neururer, R. Passawa (2012) Auswirkungen des Klimawandelsauf den thermischen Komfort in Bürogebäuden, Berichte aus Energie- und Umweltforschung

Cordeau, Erwan / Les îlots morphologiques urbains (IMU) / IAU îdF / 2016

MA 18 (2014) Stadtentwicklungsplan STEP 2025, www.step.wien.at

Masson V (2000) A physically-based scheme for the urban energy budget in atmospheric models. Bound-Layer Meteorol 94:357–397. doi: 10.1023/A:1002463829265

PGO (Planungsgemeinschaft Ost) (2011) stadtregion +, Planungskooperation zur räumlichen Entwicklung der Stadtregion Wien Niederösterreich Burgenland.

Stewart ID, Oke TR (2012) Local climate zones for urban temperature studies. Bull Am Meteorol Soc 93:1879–1900.

WUDAPT – Land cover zones

Further a land cover classification was created using the methodology of Bechtel et al. (2015), which is based on machine learning algorithms depending on satellite imagery and expert knowledge. WUDAPT methodology is a supervised machine learning technique using random forest classifier which can be subject to over- or underfitting. 10 different training sets were tested until a robust result was reached.

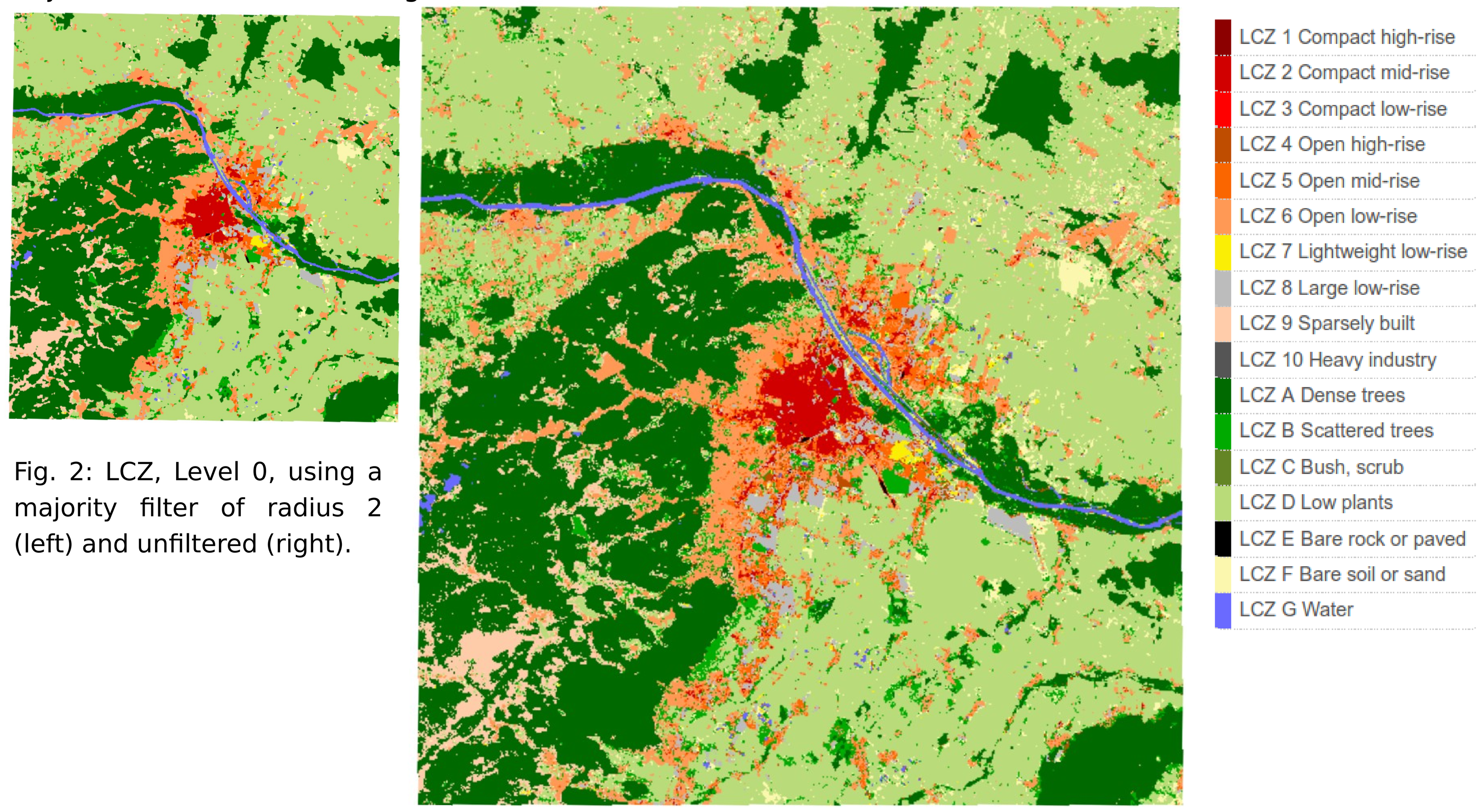

Fig. 2: LCZ, Level 0, using a majority filter of radius 2 (left) and unfiltered (right).

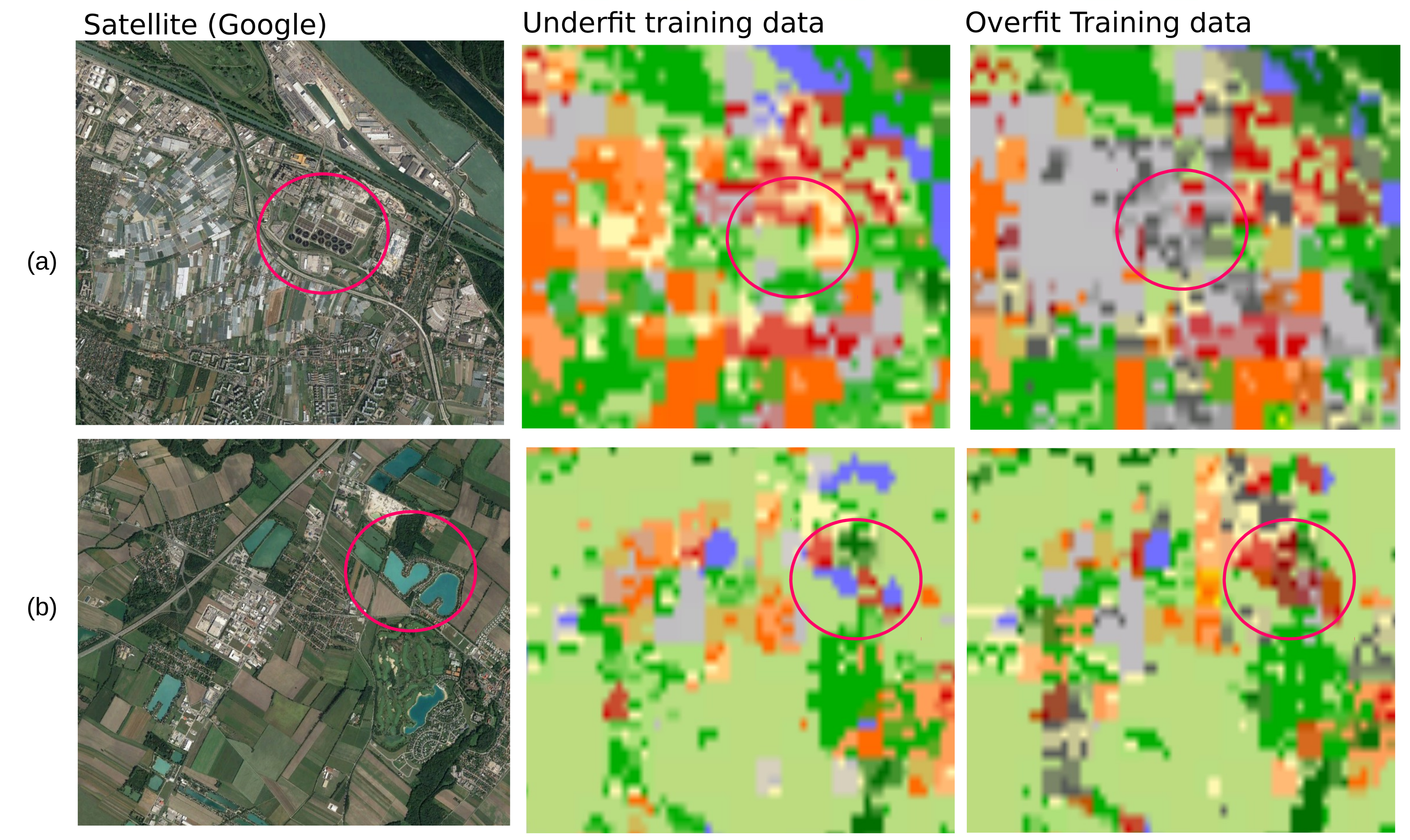

Fig. 3: Comparison of two classifications using underfit and overfit training data. (a) Heavy industry is not recognized by underfit data. (b) Overfit data gives settlements and industry where there is are lakes.

CONCLUSIONS

(1) The central and pre 1919 structure is more uniform than the later building structure of Vienna regarding morphological as well as physical building parameters. Therefore large uncertainties are possible at the urban rims where also the highest development is expected.

(2) As Vienna is constantly transforming, the date of all used data sets has to be considered (e.g. the satellite image date used for classification may not correspond to date of training zones).

(3) Generally the spatial distribution detected by the WUDAPT method goes in line with CORINE land cover (EEA). The method was least robust in the recognizing different smooth surfaces (lakes, glasshouses, large concrete areas, uniform vegetation). Underfit data lead to better more general results, but missing unique land use areas. This can be improved by including more classes.

(5) Using the Viennese data averaged over the LCZ produced by the WUDAPT method lead to clearer differentiated zones in regard of energy fluxes than using existing classifications for Vienna as the Realnutzungskartierung (MA18/21/41) or the Urban Atlas (EEA).

(6) Improved insulation without changes in changes and morphology may lead to local increases in air temperature peaks.

Simulations

The data on urban land use and morphology described in Fig. 1 and averaged over the LCZ (Fig. 2) are used for initialisation of the town energy balance scheme TEB (offline v1_1550) (Fig. 4). The sensitivity of canyon air and energy fluxes by the town energy balance scheme TEB (Masson, 2000) regarding the dominant parameters (building height, built area fraction, unsealed fraction, sky view factor) within the range determined for the present urban structure of Vienna and expected changes (MA 18 (2014), PGO (2011), Amtmann M and Altmann-Mavaddat N (2014)) was calculated. The identical meteorological forcing (BOKU-met, which is situated close to the suburban area in the west) was used for all simulation runs. Changes are only caused by the difference in land use fraction, morphology and physical parameters and not by the position within the urban heat island. For the inner LCZs the air temperature is therefore underestimated in this sensitivity analysis.

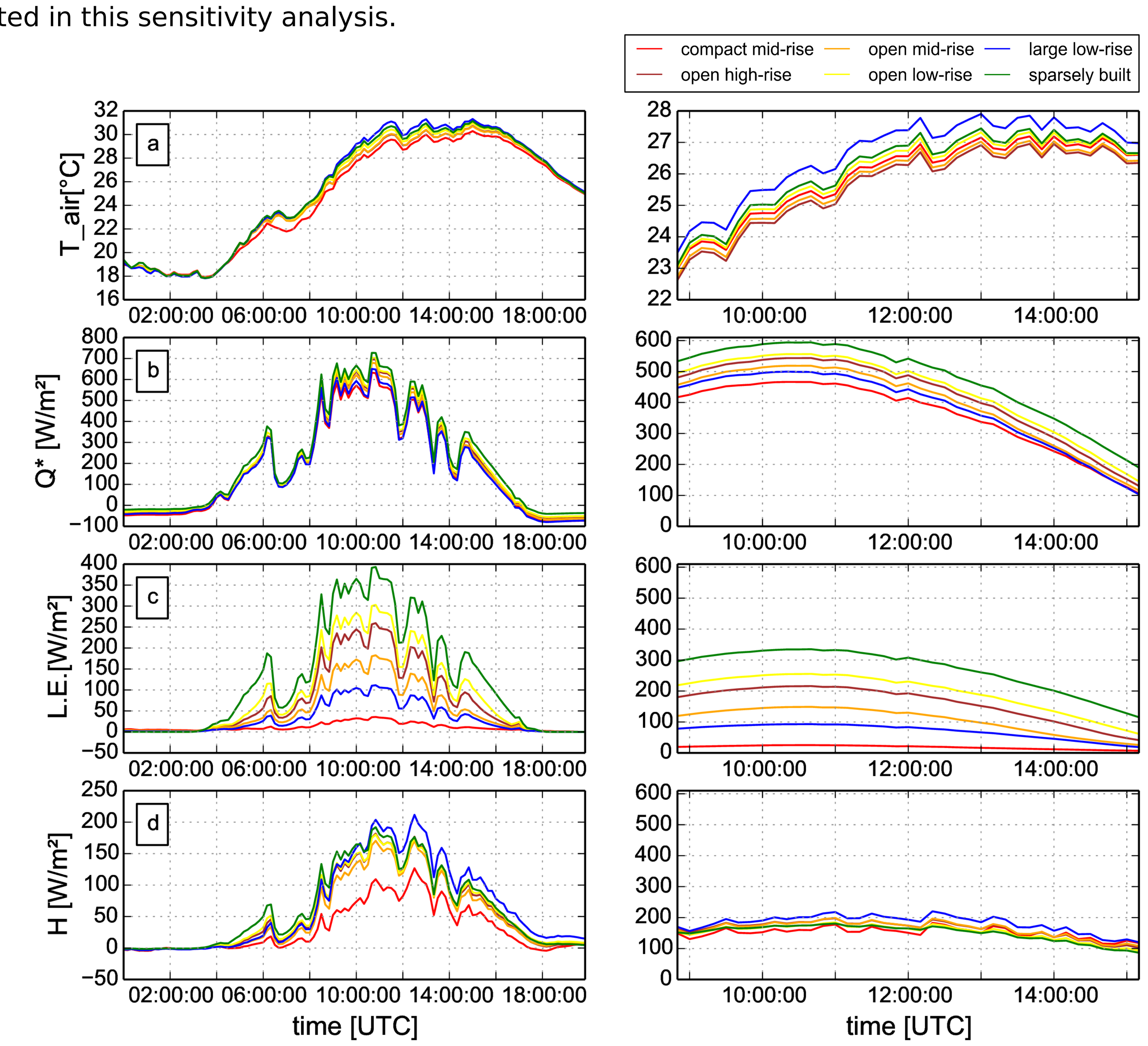

Fig. 4: TEB simulation of (a) canyon temperature, (b) radiation balance, (c) latent and (d) sensible heat flux for the 24 August 2016 (left) and the same day around midday (right) for the average values of the dominant LCZ of Vienna: Compact mid rise (LCZ2), open high- (LCZ4), mid- (LCZ5) and low rise (LCZ6), large low rise (LCZ8) and sparsely built (9).

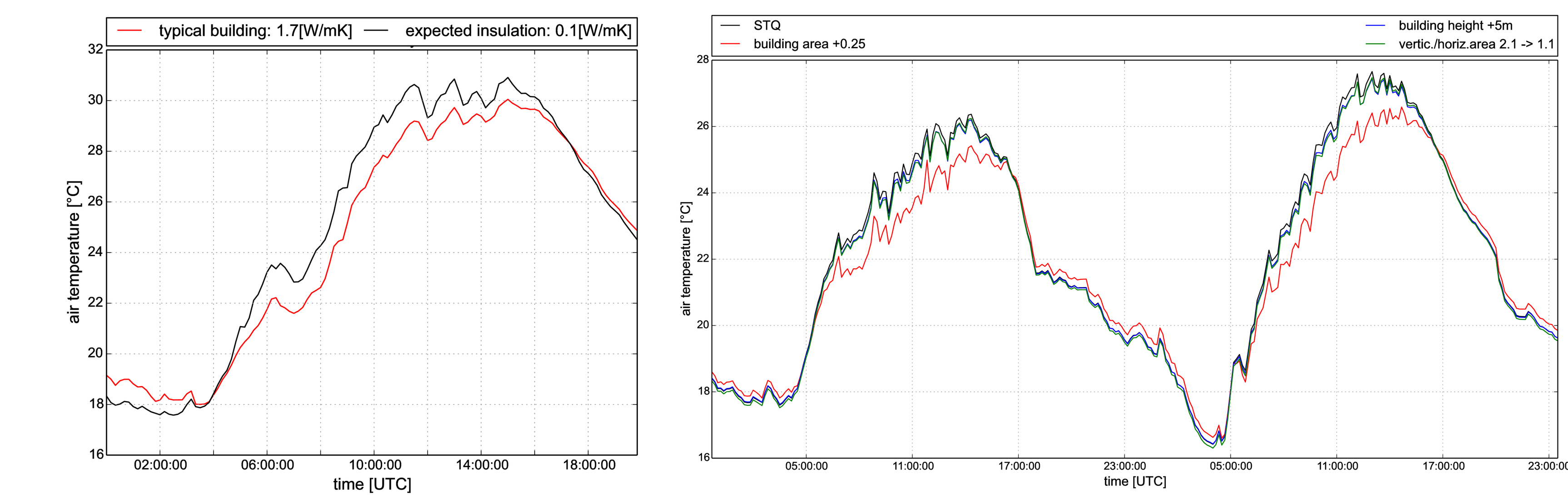

Fig 5: Changes in canyon air temperature caused by possible changes in morphology (building height, building density, vertical to horizontal area) and thermal conductivity due to better insulation for the average condition of LCZ3 „compact low rise“, 24/25 August 2016.

The research leading to these results has received funding from the ACRP Call No 8 under grant agreement number KR15AC8K12615 (URBANIA).
Thanks are given to Benjamin Bechtel, Arthur Lehner, Oscar Brousse and Jürgen Preiss for help and feedback.

Entwicklung der Urbanen Wärmeinsel Wiens bis 2030/2050 bei Berücksichtigung der Erweiterung der Stadt Wien

Heidelinde Trimmel[1], Herbert Formayer[1], Valéry Masson[2], Erich Mursch-Radlgruber[1], Imran Nadeem[1], Sandro M. Oswald[1], Robert Schoetter[2], Philipp Weihs[1]*

[1] *Institute of Meteorology, University of Natural Resources and Life Sciences, Gregor-Mendelstrasse 33, 1180 Vienna, Austria.*

[2] *Centre National de Recherches Météorologiques (CNRM), Météo France, 42 Avenue Gaspard Coriolis, 31100, Toulouse, France.*

*heidelinde.trimmel@boku.ac.at

Urbanes Wachstum

Das Wachstum des Ballungsraumes Wiens hat verschiedene Komponenten:

- Zusätzlicher Raumbedarf für Wohnung (bebautes Gebiet)
- Zusätzliche Flächen für Gewerbe, Industrie, Dienstleistung (bebautes Gebiet)
- Zusätzliche Verkehrsflächen für Mobiliät (versiegelte Flächen)

Dieser zusätzliche Raumbedarf wird zum einen durch eine wachsende Bevölkerung (Abb.1) jedoch auch über einen wachsenden Platzbedarf pro Person verursacht. Ein Anstieg von mindestens 10% Bevökerung bis 2030 betrifft den Großraum Wien in Umkreis von 50km von Stadtzentrum, der als stadtregion+ (PGO 2011) bereits untersucht wurde. Die Verdichtung der Bebauung aber auch Ausdehnung des bebauten Gebietes wird eine Herausforderung für den menschlichen Komfort darstellen - welcher bereits gegenwärtig während der Sommermonate beeinträchtigt wird.

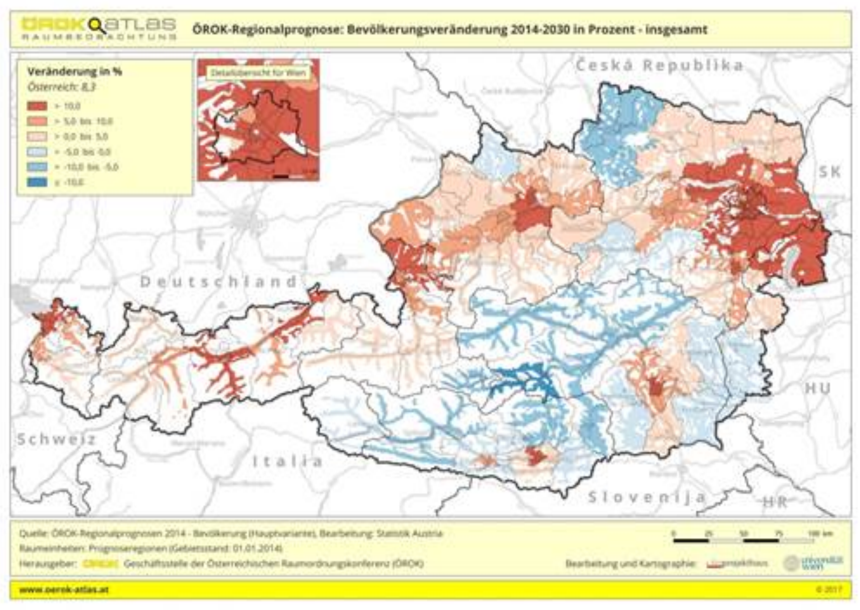

Maximales erwartetes Bevölkerungswachstum (ÖROK, MA23)	2030	2060
Innerhalb Stadtgrenze (pro Bezirk)	+ 15,15%	+ 29.30%
Stadtregion+ (pro Bezirk)	+ 27.2%	+ 55.2 %

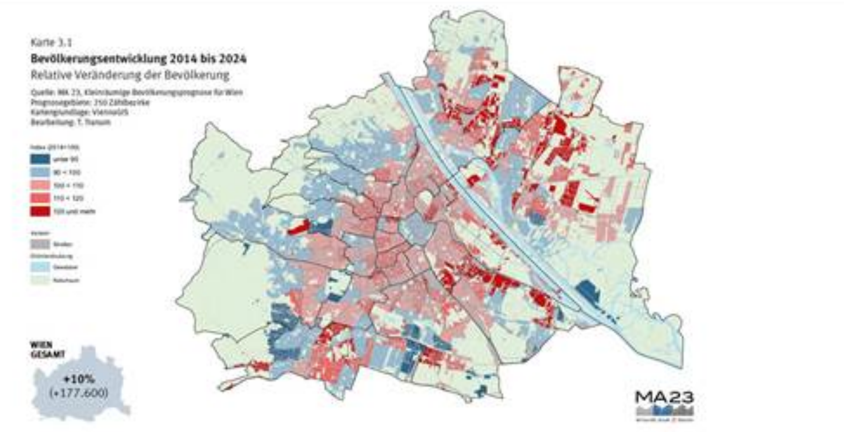

Abb. 1: Prognostiziertes Bevölkerungswachstum in Österreich (ÖROK 2017) und Wien (MA23 2018) .

Ziel des Projektes URBANIA

Ziel des Projektes URBANIA ist es, die Belastung des thermischen Komforts für Bewohner innerhalb der Bebauung abzuschätzen, die durch eine expandierende und sich verdichtende Agglomeration im Zeitraum 2030/2050 durch mögliche Stadtentwicklungs- und Klimawandelszenarien verursacht werden könnte.

Das zweite Ziel besteht darin, Optionen hervorzuheben, welche die Auswirkungen auf die Temperatur und den menschlichen Wärmekomfort innerhalb der gebauten Struktur abschwächen können. Die wichtigsten Methoden sind die Reduktion der Erwärmung durch eine Reduktion der kurzwelligen und langwelligen Strahlungsbilanz auf Straßenniveau, durch Erhöhung des latenten Wärmeflusses bzw. durch Verringerung der Wärmespeicherung in Gebäude und Verkehrsflächen.

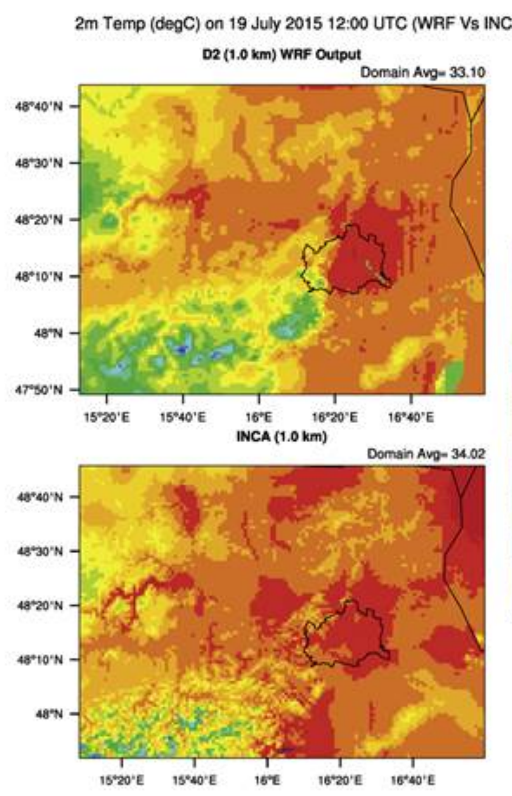

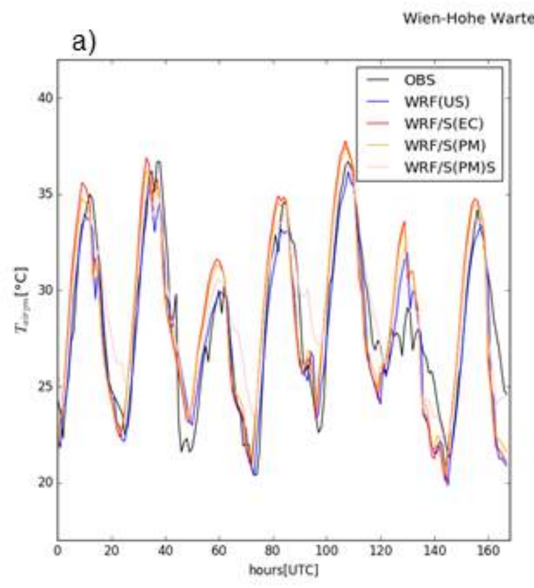

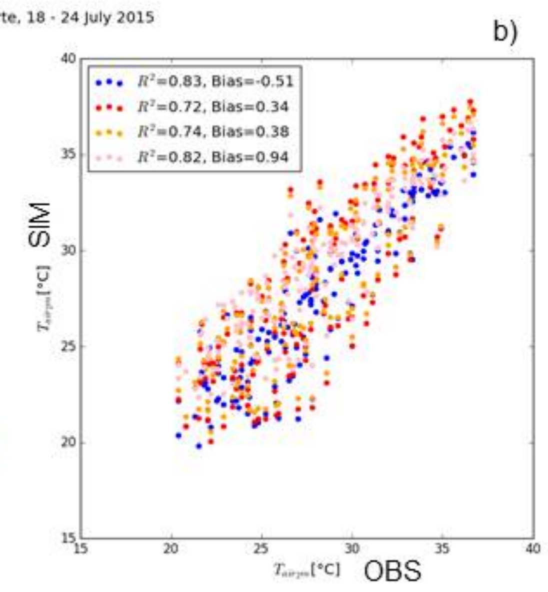

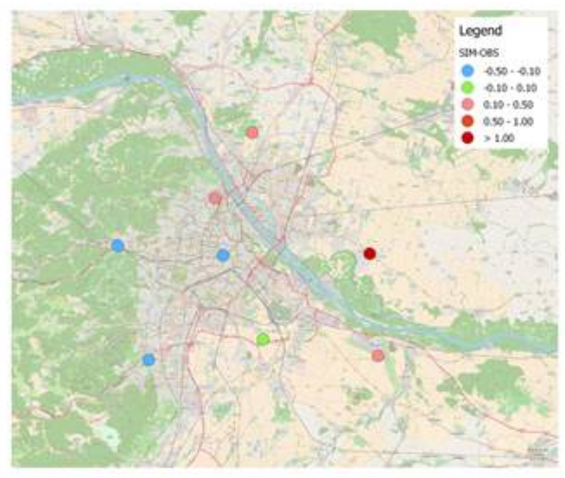

Abb. 2: (links) Vergleich zwischen WRF Simulation und INCA Datensatz (Haiden et al. 2011)
Abb. 3: (mittig) Beobachtungsdaten OBS und Modelläufe WRFv3.9.1 (Skamarock et al. 2008) using USGS classes (US) , SURFEXv8 (Boone et al. 2017, Masson 2000) offline runs forced by WRF: WRF/S using ECOCLIMAP (EC), WRF/S high resolution parameter maps (PM), WRF/S (PM)S forced by first sigma level (~40m) (a) Stundenwerte der Luffttemperatur 18. – 24. Juli 2015 (b) Punktwolke der Stundenwerte
Abb. 4: (rechts) Karte der mittleren Abweichungen des WRF-Laufes von 8 Bodenstationen der ZAMG für 18. – 24. Juli 2015

Simulation und Validierung

Simulationen werden mit dem Weather Research and Forcasting Model WRF v3.7.1 (Skamarock et al. 2008) durchgeführt. WRF und das Town Energy Balance Modell TEB (Masson 2000) werden gekoppelt und online für historische Hitzeepisoden betrieben. Die WRF-Läufe werden verwendet, um SURFEXv8 (Boone et al. 2017) offline-Simulationen anzutreiben, wobei Parameterkarten basierend auf verfügbaren Geodaten der Stadt Wien und dem Urban Atlas verwendet werden, um jeden Gitterpunkt zu definieren.

Der Vergleich von WRF-Simulationen und dem interpoliertem Messdatensatz INCA (Haiden et al. 2011) zeit eine gute Übereinstimmung der räumlichen Muster (Abb. 2). Einige räumliche Elemente, wie z.B. die Donau oder der Neusiedlersee sind in den WRF Simulationen erkennbar, während sie in den INCA daten nicht ersichtlich sind. Das Flächenmittel zeigt eine sehr geringe Abweichung (<1°C) zwischen den beiden Datensätzen, wobei WRF die Lufttemperatur mittags leicht unterschätzt, nachts überschätzt. Dies zeigt sich auch im Tagesverlauf (Abb 3). Der Vergleich mit ZAMG Bodenstationen zeigt, dass die mittlere Abweichung während der untersuchten einwöchigen Hitzewelle unter +/- 0.5 liegt (Abb 4). Nur für Großenzersdorf zeigen sich größere Abweichungen.

Stadtentwicklungsszenarien

Es wurden erste vier Szenarien für die Simulation aufgrund der Analyse der vergangenen Landnutzung (EEA/Copernicus 2018) sowie räumlicher Entwicklungsszenarien in der stadtregion+ (PGO2011) aufbereitet, welche den gesamte Ballungsraum berücksichtigen (Tabelle 1). Für die Verdichtungsszenarien (S1,S4) konnten die Parameterkarten adaptiert werden. Für die Erweiterungsszeanrien wurde als erste Annäherung ein einheitlicher Bebauungsanteil von 0.5 und eine Gebäudehöhe von 10m angenommen. Erste Modellergebnisse zeigen nur unter Berücksichtigung der Änderung der Energiebilanz für einen examplarischen Wüstentag (Tmax >35°C) folgende mögliche relative Änderungen der Lufttemperatur:

Kürzel	STQ	S1	S2	S3	S4
Name	„STATUS QUO“	„DENSER“	„SCATTERED SPREAD“	„STRUCTURED SPREAD“	„DENSER, ISOLATED“
Modelsetup	WRF/S(PM)	WRF/S(PM)	WRF/S(PM-XUNIF)	WRF/S(PM-XUNIF)	WRF/S(PM)
Urban fraction	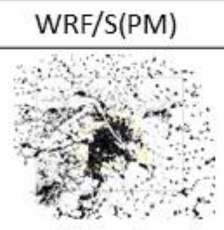	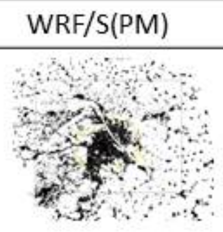	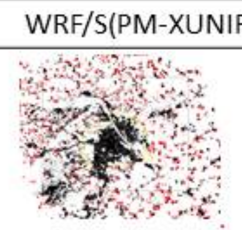	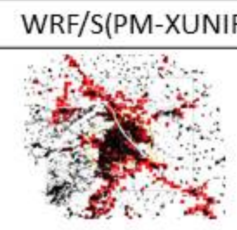	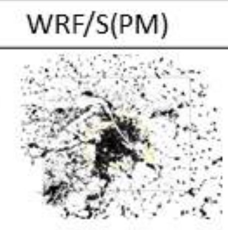
Gesamtfläche Prozentsatz	902km² (100%)	902km² (100%)	1 113 (123%)	1 449 (161%)	902km² (100%)
„Nature“ fraction [km²]	3 284 (100%)	3 284 (100%)	3 073 (94%)	2 736 (83%)	3 284 (100%)
Bebauungsanteil		+10%			+10%
Wärmekapazität Wand [J/m³K]	1.520 *10⁶	1.520 *10⁶	1.520 *10⁶	1.520 *10⁶	1.496 *10⁶
Wärmecapaziät Dach [J/m³K]	1.554 *10⁶	1.554 *10⁶	1.554 *10⁶	1. 554 *10⁶	1.496 *10⁶
Wärmeleitfähigkeit Wand [W/mK] (1,2)	1.7	1.7	1.7	1.7	0.1
Wärmeleitfähigkeit Dach [W/mK] (1,2)	1.4	1.4	1.4	1.4	0.1

Tabelle 1: Übersicht über die verwendeten Szenarien

(1,2) Amtmann and Altmann-Mavaddat (2014), Berger et al. (2012)

1) Verdichtung (Abb. 5) der bereits bebauten Fläche um 10%: nur leichter Anstieg <0.5°C

2) Stadterweiterung (Abb. 6-8)
> max. +1°C in den neuen Bebauungsgebieten (räumliches Mittel) (Abb. 8)
-> auch die aktuell bebaute Fläche it betroffen mit bis zu 0.3°C (Abb.7- 8)

STQ – „STATUS QUO“

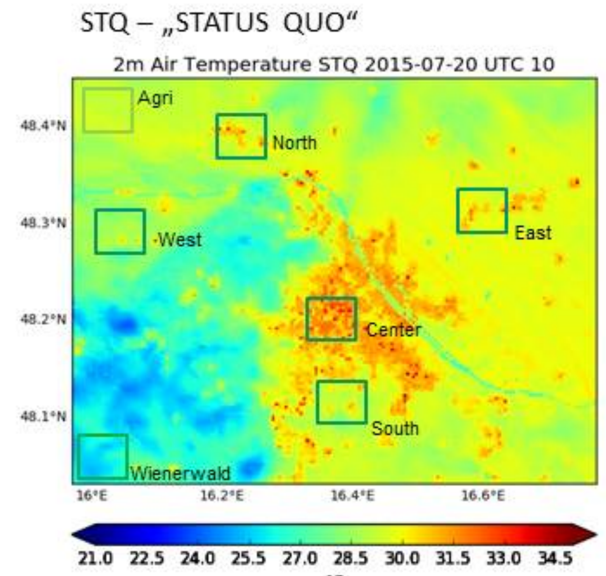

Abb 6: Auswahl von 5 Referenzflächen (je 11km²) im bebauten, bzw. bebaubaren Gebiet sowie je einer Wald- und Ackerfläche.

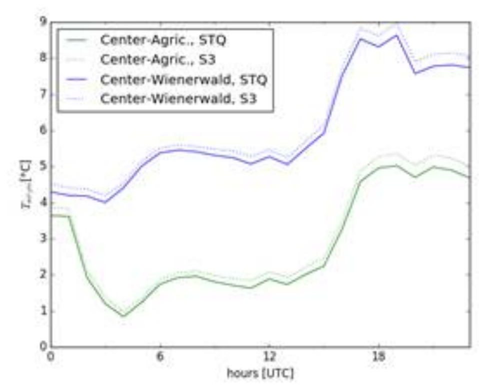

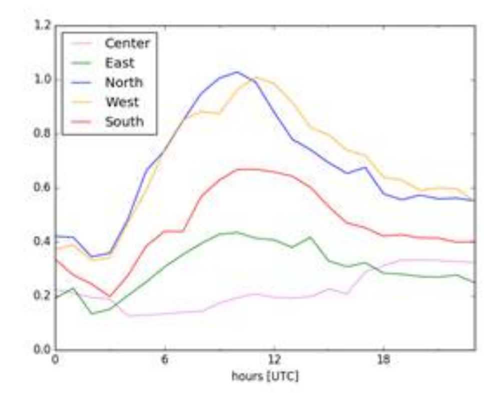

Abb 7: (links) ("Urban Heat Island Intensity": Tagesgang der Differenz Stadtzentrum-Ackerfläche bzw. Wienerwald und Anstieg im S3 Szenario (Flächenmittel)

Abb 8: (rechts) Anstieg der Lufttemperatur (Flächenmittel) im Tagesverlauf der 5 Referenzflächen für das STRUCTURED SPREAD (S3) Szenario im Vergleich zu STQ. Beachten Sie bitte die Uhrzeit in UTC angegeben ist (MESZ -2) .

S1- „DENSER“ S2-“SCATTERED SPREAD S3-“STRUCTURED SPREAD S4-“DENSER,ISOLATED“

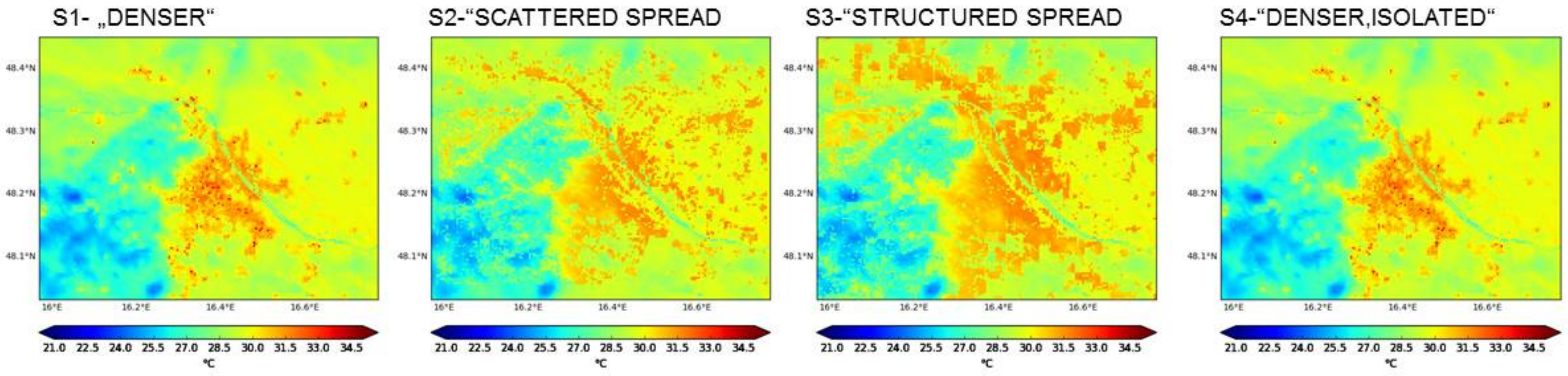

Abb. 5 Änderung der 2m Lufttemperatur am 20.Juli 2015 um 10UTC und für 4 Stadtentwicklungsszenarien (sh. Tabelle 1)

3) Gegenmaßnahmen wie ambitionierte Isolierung (Abb.9):
-> -0.5°C innerhalb aktueller Bebauung nachts
-> sogar bei Verdichtung der Bebauung
-> auch Mittags innerhalb der dichten inneren Bezirke konnte die Lufttemperatur gesenkt werden wenn die Stadt verdichtet wird

Abb. 9 Differenz zwischen STQ und DENSE, ISOLATED (S4) Szenario um 0 (links) und 12 UTC (rechts)

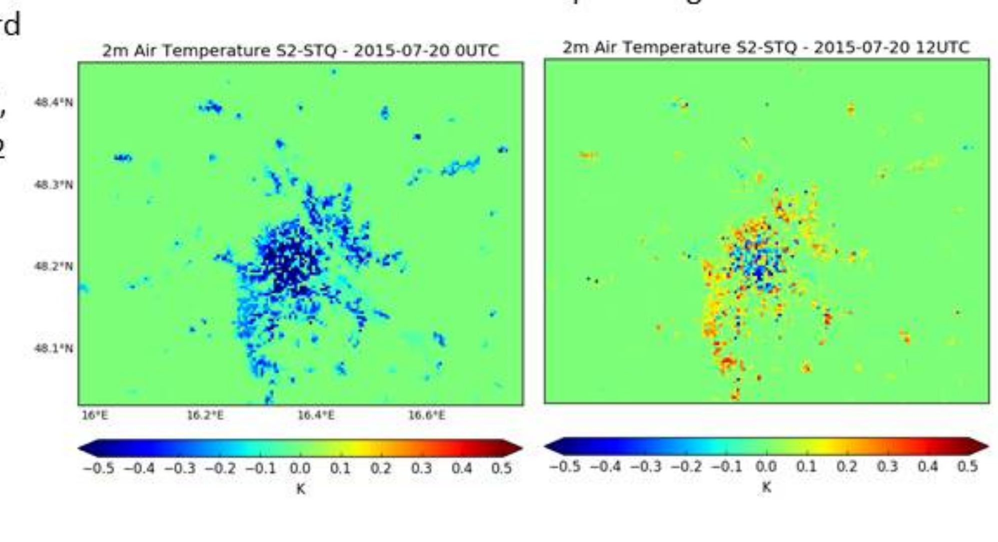

Nächste Schritte und Ausblick

- In Folge wird die Auswirkung der Verdichtung und Stadterweiterung auf die Temperatur unter Berücksichtigung des durch die geänderte Rauigkeit veränderte Windfeld sowie der Änderung der urbanen Grenzschicht durch untersucht. Die Ergebnisse zwischen WRF und WRF-TEB online werden verglichen.
- Analyse der Auswirkungen auf den thermischen Komfort innerhalb des urbanen Canyons
- Konkretisierung der Schlüsselfaktoren für effektive urbane Szenarien (zusammen mit Stadt Wien): Änderung der Bebauungsverteilung, der Bebauungsformen- und Baumaterialien (Albedo, neue Materialien, latente Wärme, ...)
- Simulation der Stadtentwicklungsszenarien für durch Klimawandel bis 2030/2050 veränderte Hitzewellen auf der Grundlage lokaler Klimaszenarien, die mit RCP4.5 und RCP8.5 erzwungen werden.
- Website Start geplant Juli 2018: http://urbania.boku.ac.at

Amtmann M and Altmann-Mavaddat N (2014) Eine Typology österreichischer Wohngebäude, Österreichische Energieargentur – Austrian Energy Agency, TABULA/EPISCOPE

Berger T, , H. Formayer, R. Smutny, C. Neururer, R. Passawa (2012) Auswirkungen des Klimawandelsauf den thermischen Komfort in Bürogebäuden, Berichte aus Energie- und Umweltforschung

Boone, A. et al. 2017: The interactions between soil–biosphere–atmosphere land surface model with a multi-energy balance (ISBA-MEB) option in SURFEXv8 – Part 1: Model description, Geosci. Model Dev., 10, 843-872.

EEA/Copernicus: CORINE Land Cover data set, https://land.copernicus.eu/pan-european/corine-land-cover, last access: 17.4.2018

Haiden, T., A. Kann, C. Wittmann, G. Pistotnik, B. Bica, and C. Gruber, 2011: The Integrated Nowcasting through Comprehensive Analysis (INCA) system and its validation over the eastern Alpine region. Wea. Forecasting, 26, 166–183.

MA 18 (2014) Stadtentwicklungsplan STEP 2025, www.step.wien.at

MA23 *(2018) https://www.wien.gv.at/statistik/bevoelkerung/prognose/#abbildungen, last access: 17.4.2018*

Masson V (2000) A physically-based scheme for the urban energy budget in atmospheric models. Bound-Layer Meteorol 94:357–397. doi: 10.1023/A:1002463829265

PGO (Planungsgemeinschaft Ost) (2011) stadtregion +, Planungskooperation zur räumlichen Entwicklung der Stadtregion Wien Niederösterreich Burgenland.

Masson V. 2000: A physically-based scheme for the urban energy budget in atmospheric models. Boundary-Layer Meteorol. 94:357-397.

ÖROK 2017: www.oerok-atlas.at

Skamarock, W.C. et al. 2008: A Description of the Advanced Research WRF Version 3. NCAR. Tech.Note NCAR/TN-475+STR,113pp

Das Projekt URBANIA wird vom ACRP Call No 8 (KR15AC8K12615) gefördert. Wir bedanken uns bei Jürgen Preiss, der MA18 und Stéphanie Faroux für Feedback und Hilfe.

EGU 2018-7927
CL.18
11/4/2018

1 Viennese Growth

2 Models

3 Urban Szenarios

4 Conclusion and outlook

Evolution of the Viennese Urban Heat Island caused by expected Reduction of Vegetation Fraction in favour of Built-up Land until 2030/2050

Project: URBANIA - Influence of the development of outlying districts and urban growth on the urban heat island of the city of Vienna in the context of climate change
ACRP 8th call: KR14AC7K11944

Project team:

Institute of Meteorology, University of Natural Resources and Life Sciences (BOKU):
BOKU-Rad: Philipp Weihs, Heidelinde Trimmel, Sandro Oswald
BOKU-Klim: Herbert Formayer, Imran Nadeem
BOKU-Biomet: Erich Mursch-Radlgruber, Christian Gützer

Environmental Agency of Vienna (MA22): Jürgen Preiss, Christian Härtel

CNRS-Météo-France: Valéry Masson, Robert Schoetter, Aude Lemonsu, Stéphanie Faroux

EGU 2018-7927
CL.18
11/4/2018

1 Viennese Growth

2 Models

3 Urban Szenarios

4 Conclusion and outlook

Motivation

Vienna‘s population is growing ...
- > will reach 1900 level again 2028
-> but 1971:22.9m²/person, 2014:44.7m²/person (trend stabalizing)
-> amount of population growth uncertain (parameters: fertility, life expectancy, migration (national and international))

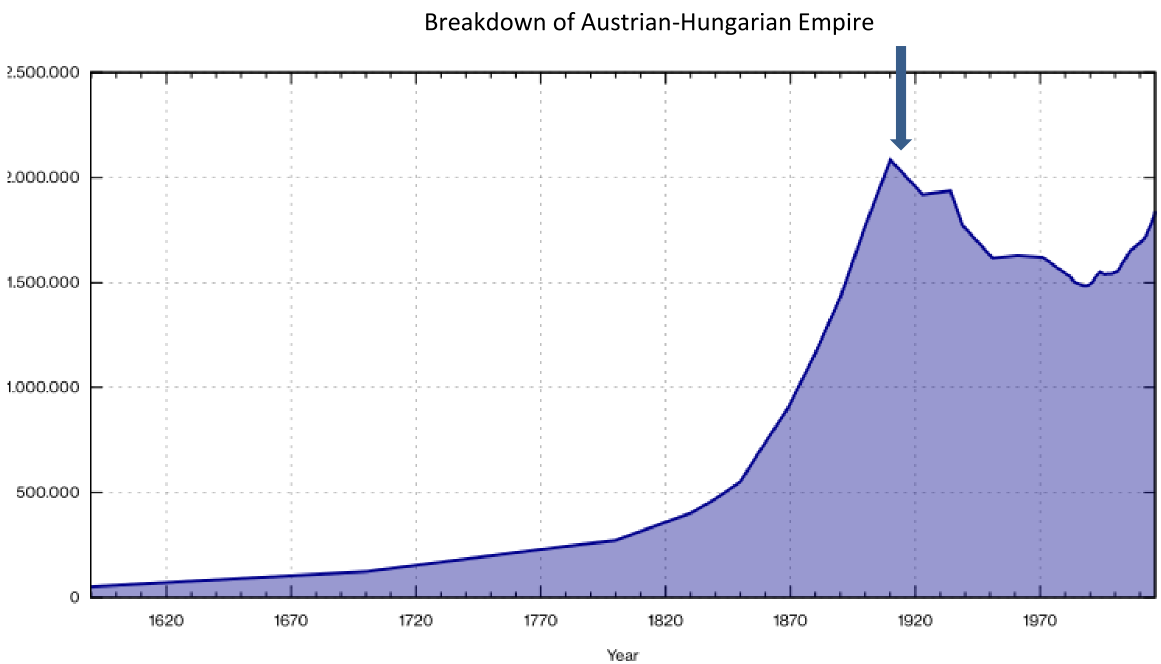

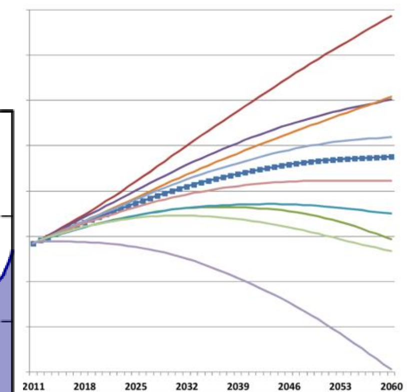

Von Lodp - Eigenes Werk, Statistischen Mitteilungen der Stadt Wien (Heft 4/2000)Statistik Austria. Statistisches Jahrbuch 2009.
http://www.statistik.at/web_de/static/bevoelkerung_zu_jahresbeginn_seit_1981_nach_bundeslaendern_031770.xlsx
http://www.statistik.at/web_de/static/bevoelkerung_zu_quartalsbeginn_seit_2002_nach_bundesland_023582.xlsx
http://www.statistik.at/web_de/statistiken/menschen_und_gesellschaft/bevoelkerung/bevoelkerungsstand_und_veraenderung/bevoelkerung_zu_jahres-_quartalsanfang/023582.html , CC BY-SA 3.0,
https://commons.wikimedia.org/w/index.php?curid=29606863

Motivation

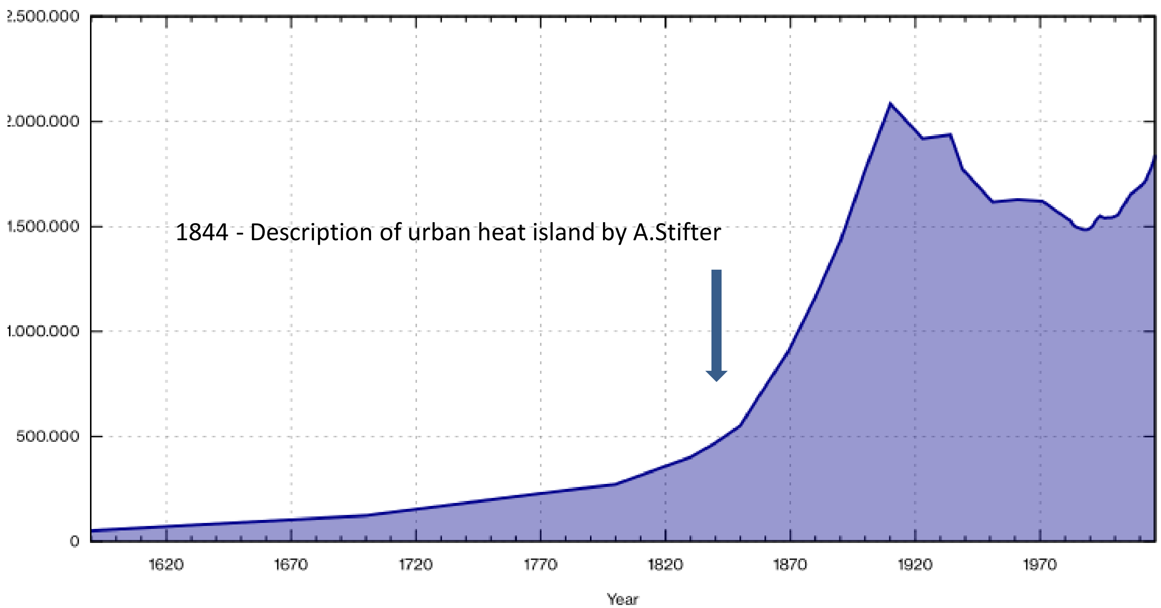

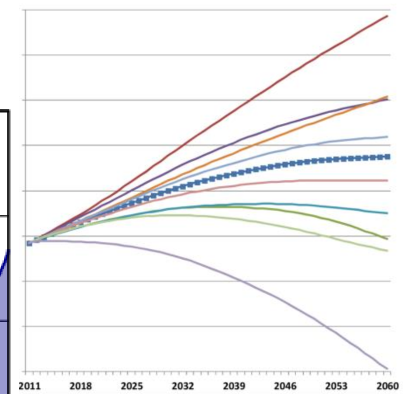

-> increased demand and supply of residential and other urban areas

-> increased urban heat island

Problem? Lets have EGU in summer to discuss...

EGU 2018-7927
CL.18
11/4/2018

1 Viennese Growth

2 Models

3 Urban Szenarios

4 Conclusion and outlook

How much + where?

Population is growing in widespread around city borders

Greater Vienna: 2030: max +15.15% per district

2060: max +29.30% per district

-> main growth in „stadtregion+“ (see: PGO 2010)

within city borders: 2030: max +27.2 % per district

2060: max +55.2 % per district

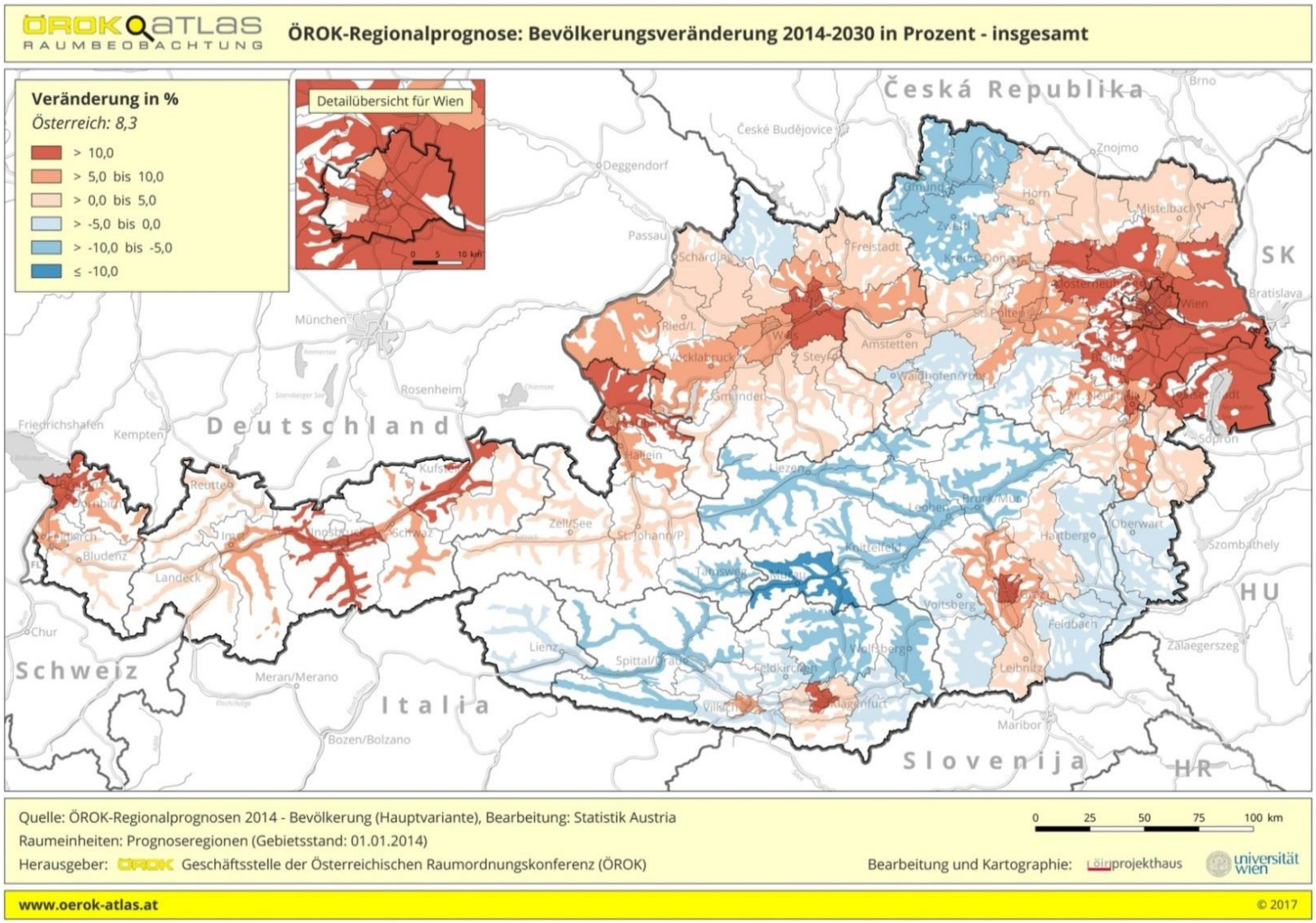

METEO FRANCE

Selection of reference period

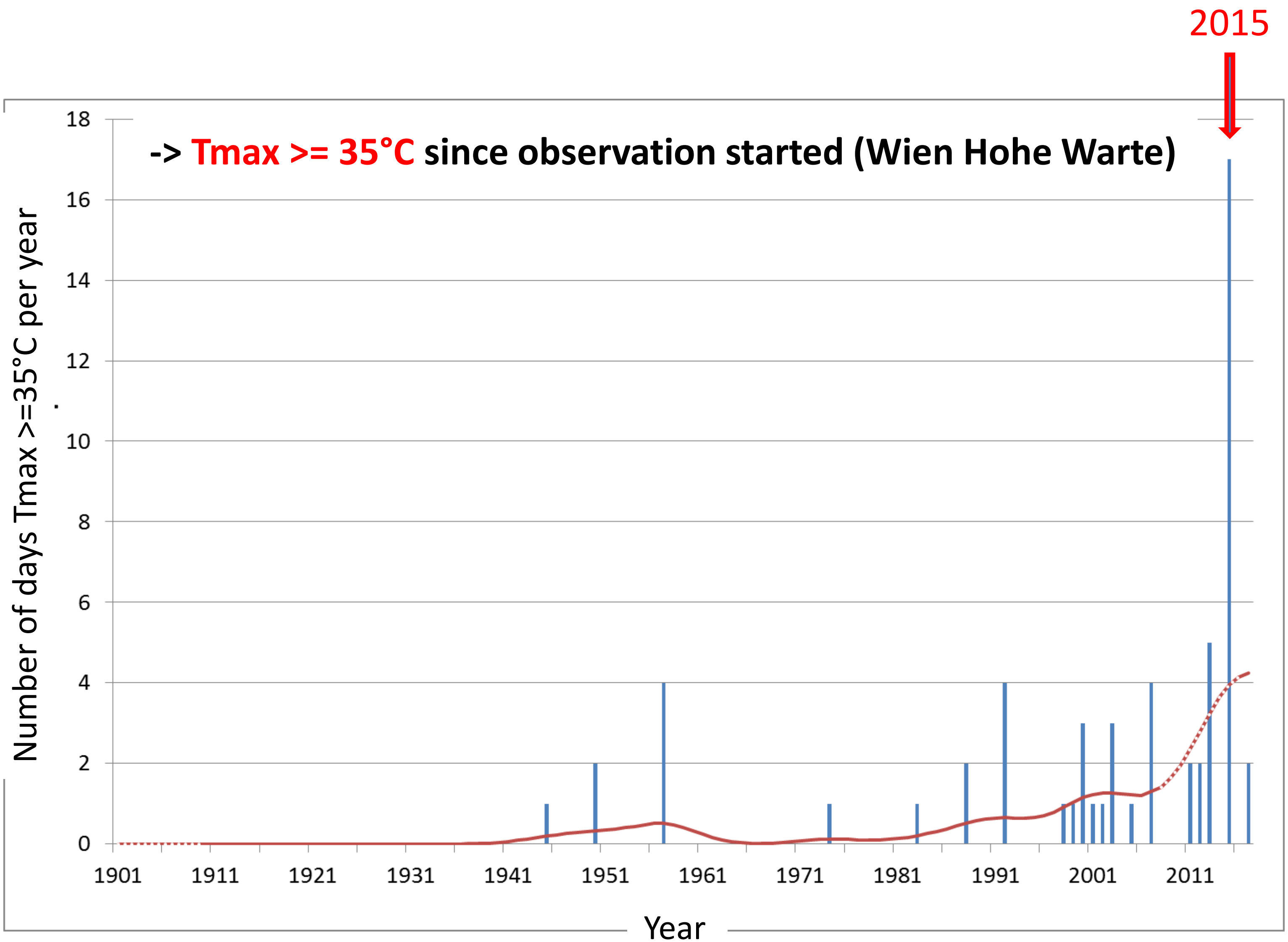

METEO FRANCE

EGU 2018-7927
CL.18
11/4/2018

1 Viennese Growth

2 Models

3 Urban Szenarios

4 Conclusion and outlook

Lateral boundary conditions:
9km ECMWF analysis data (6h)
Static: Topography-SRTM1Arc:30m)
Landcover-USGS Classes (1 urban class)

WRF v3.9.1

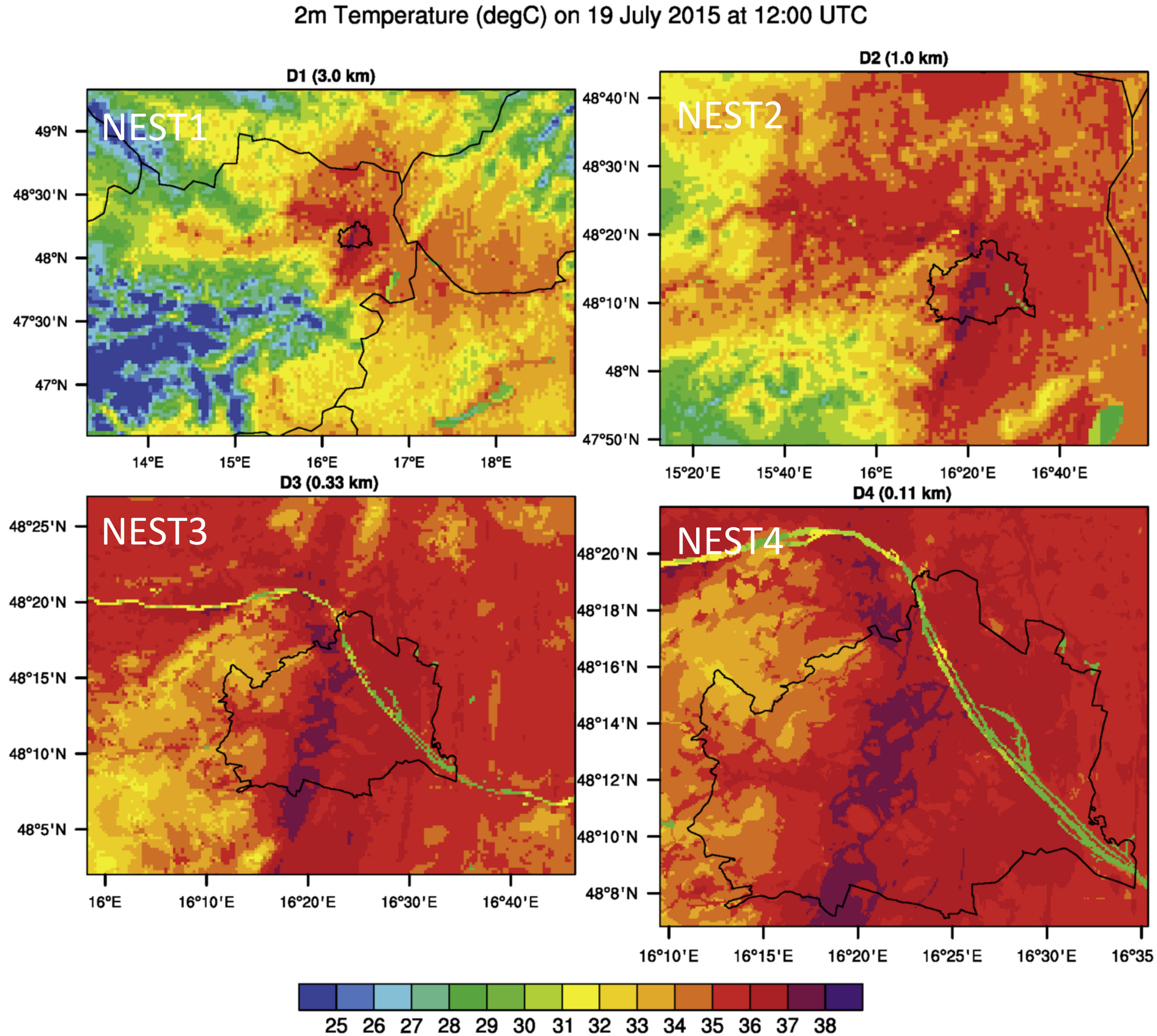

EGU 2018-7927
CL.18
11/4/2018

1 Viennese Growth

2 Models

3 Urban Szenarios

4 Conclusion and outlook

Comparison with observation data

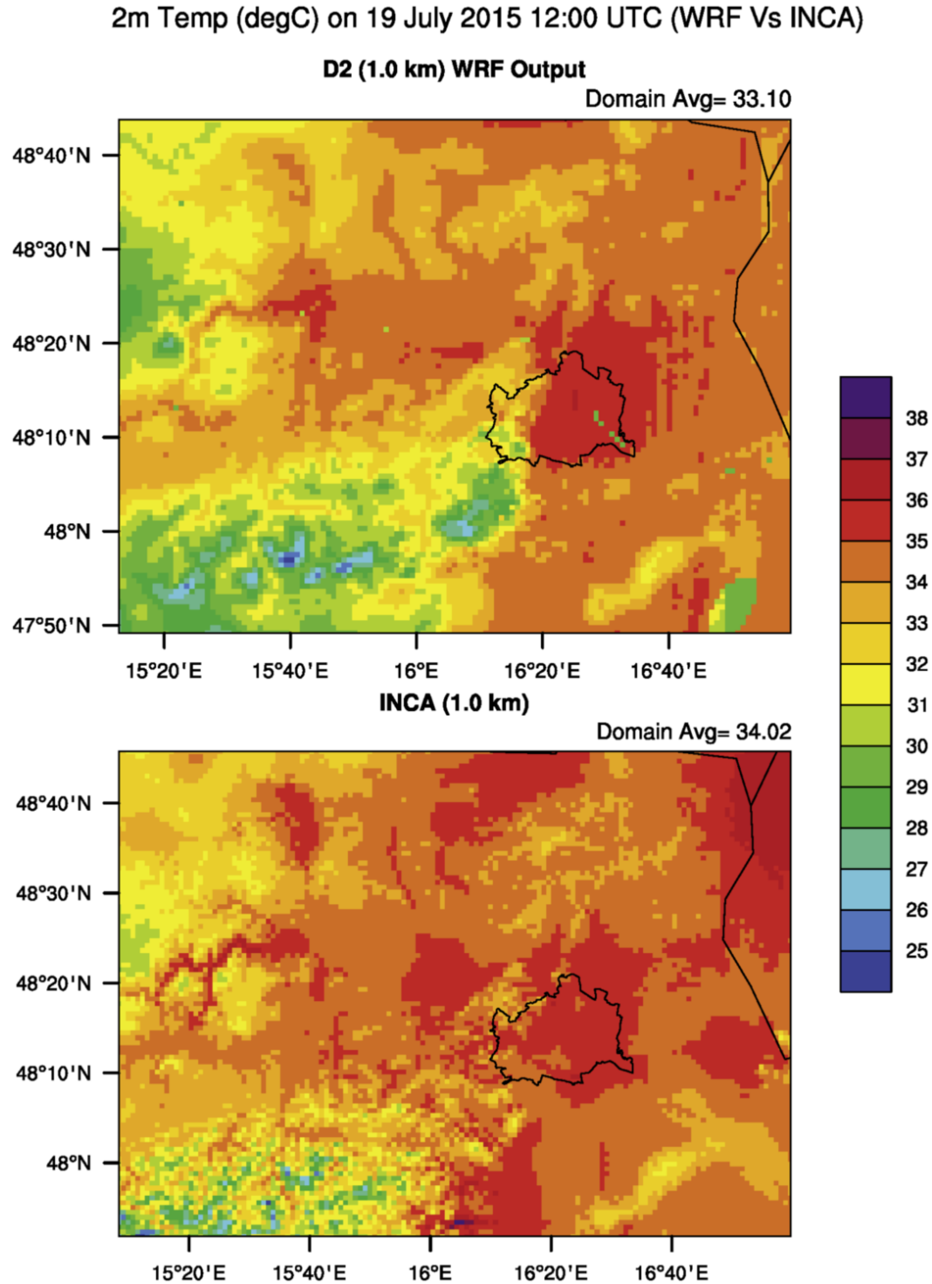

-Spatial distribution fits good to gridded interpolated observations data set (INCA[1])

- Spatial patterns are represented even better (rivers and lakes, urban area)

-Absolute values fit good <1°C on average

- WRF slightly underestimates air temperature

[1] Haiden et al. 2011

EGU 2018-7927
CL.18
11/4/2018

1 Viennese Growth

2 Models

3 Urban Szenarios

4 Conclusion and outlook

Comparison WRF, WRF/SURFEX offline and ground stations

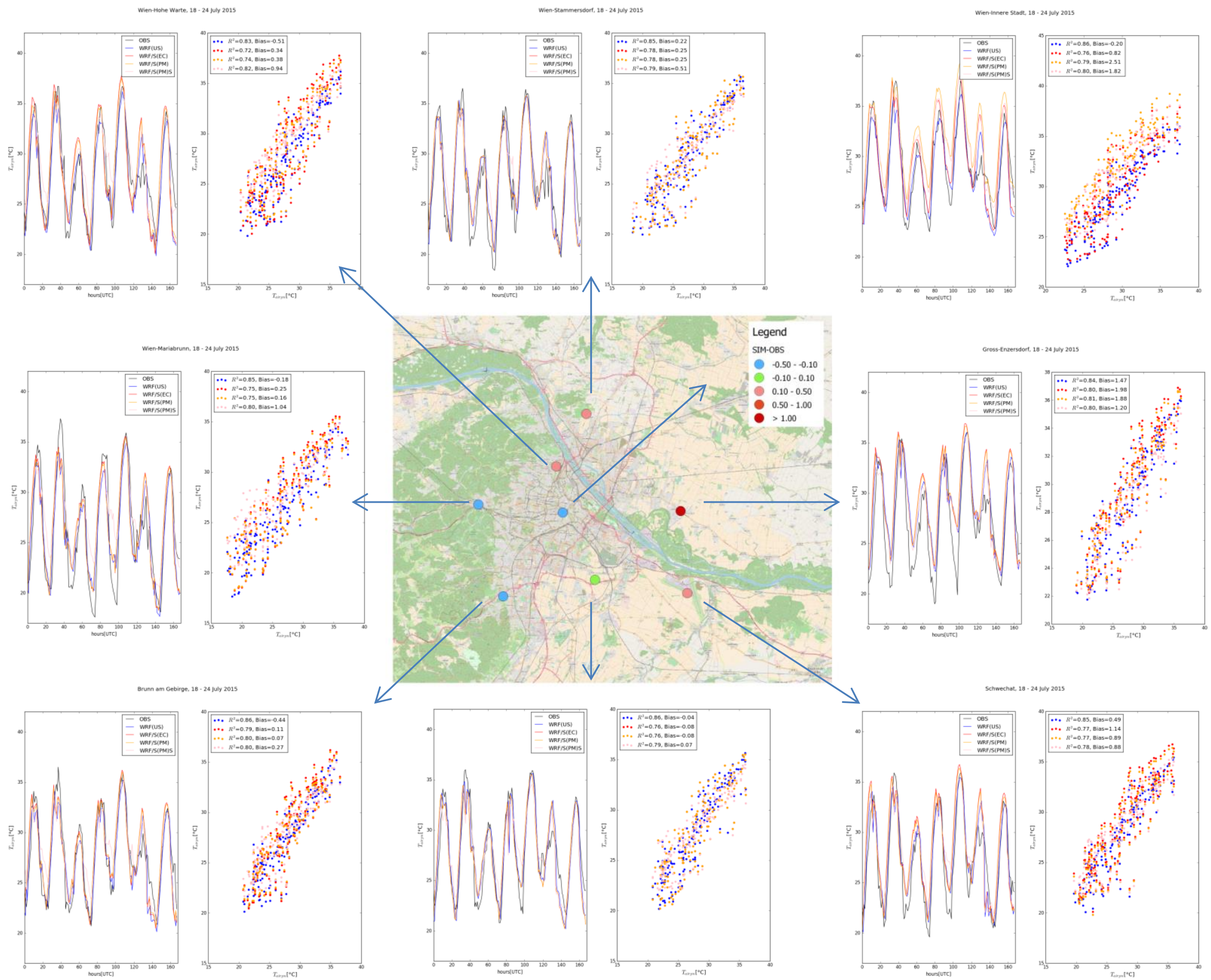

Mit unserer Umwelt MA22

METEO FRANCE

EGU 2018-7927
CL.18
11/4/2018

1 Viennese Growth

2 Models

3 Urban Szenarios

4 Conclusion and outlook

Comparison WRF, WRF/SURFEX offline and ground stations

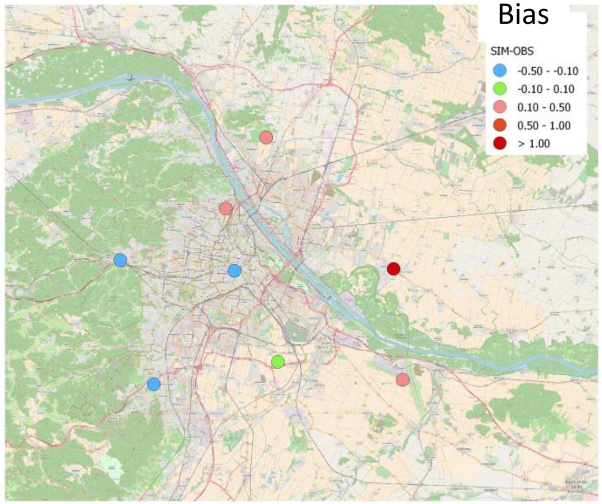

Model runs:

- WRFv3.9.1 using USGS classes (US)

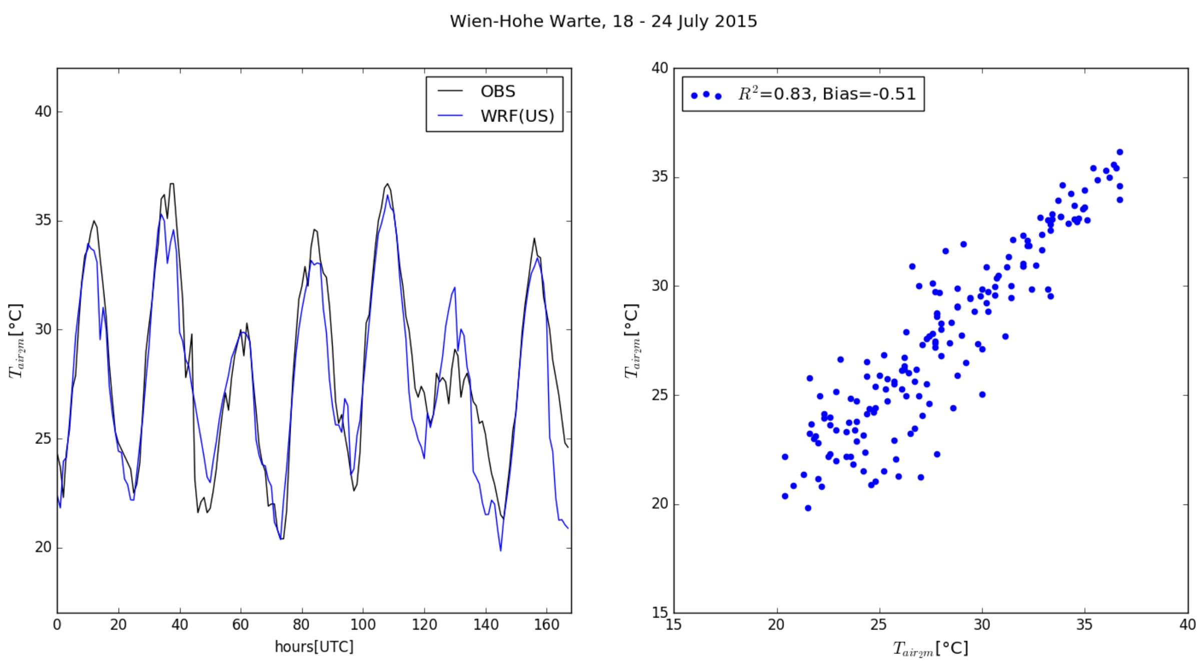

Comparison WRF, WRF/SURFEX offline and ground stations

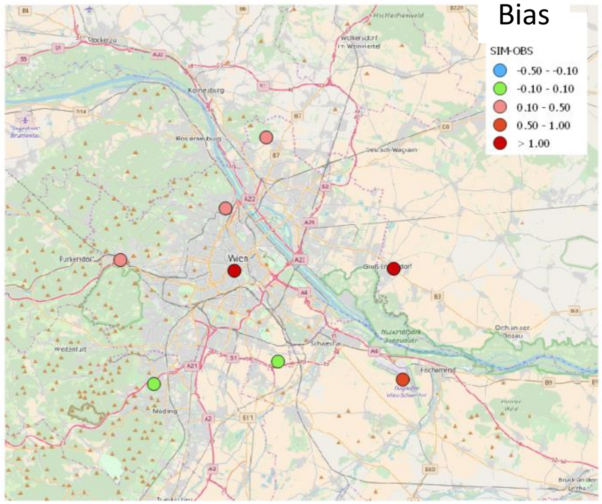

Model runs:

- WRFv3.9.1 using USGS classes (US)

SURFEXv8 offline runs forced by WRF:

- WRF/S using ECOCLIMAP (EC)

Wien-Hohe Warte, 18 - 24 July 2015

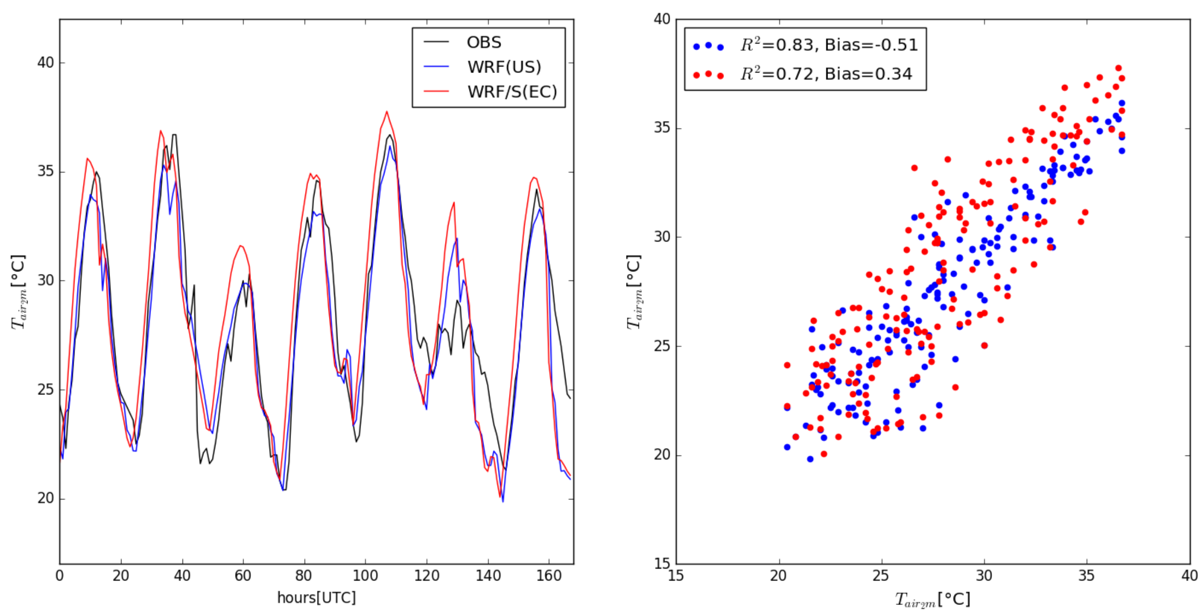

EGU 2018-7927
CL.18
11/4/2018

1 Viennese Growth

2 Models

3 Urban Szenarios

4 Conclusion and outlook

Comparison WRF, WRF/SURFEX offline and ground stations

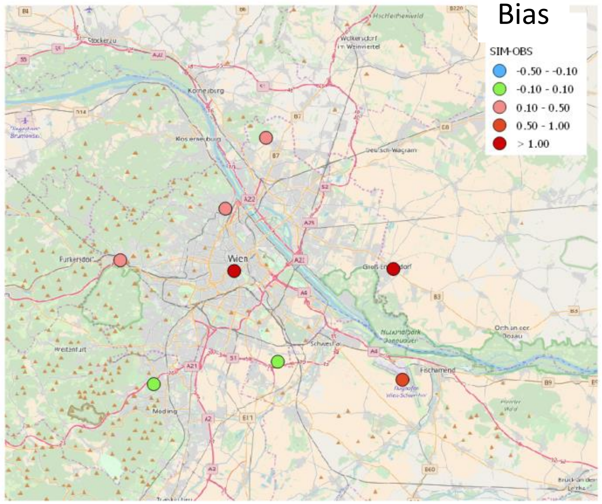

Model runs:

- WRFv3.9.1 using USGS classes (US)

SURFEXv8 offline runs forced by WRF:

- WRF/S using ECOCLIMAP (EC)
- WRF/S high resolution maps (PM)

using: highres. building height, surface fractions, UrbanAtlas,CORINE,...

Wien-Hohe Warte, 18 - 24 July 2015

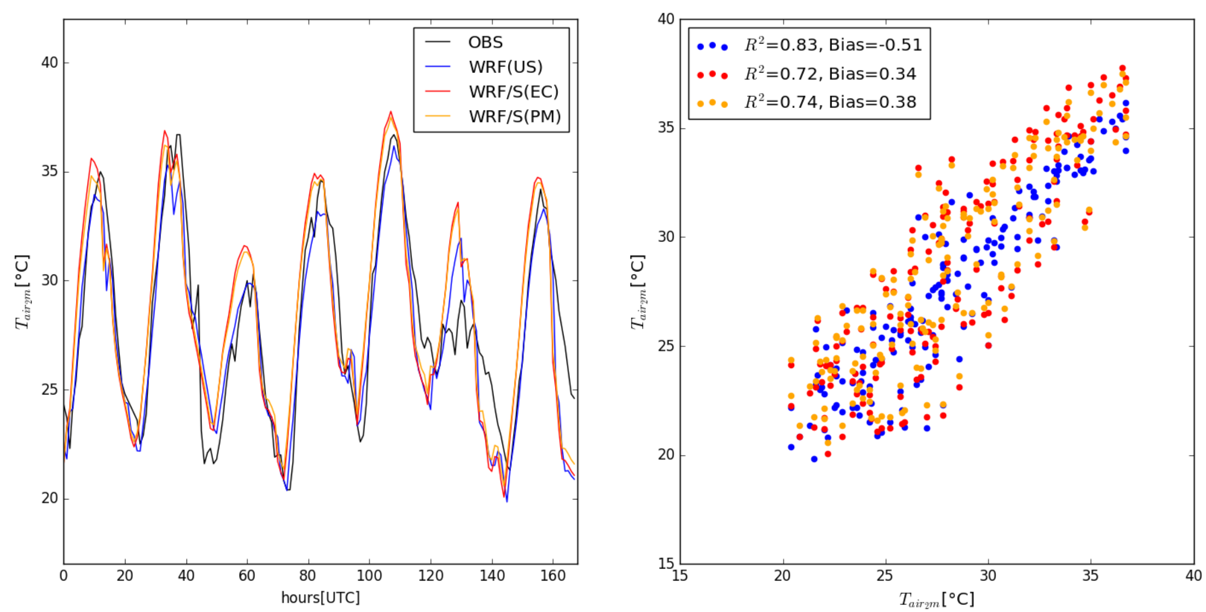

EGU 2018-7927
CL.18
11/4/2018

1 Viennese Growth

2 Models

3 Urban Szenarios

4 Conclusion and outlook

Comparison WRF, WRF/SURFEX offline and ground stations

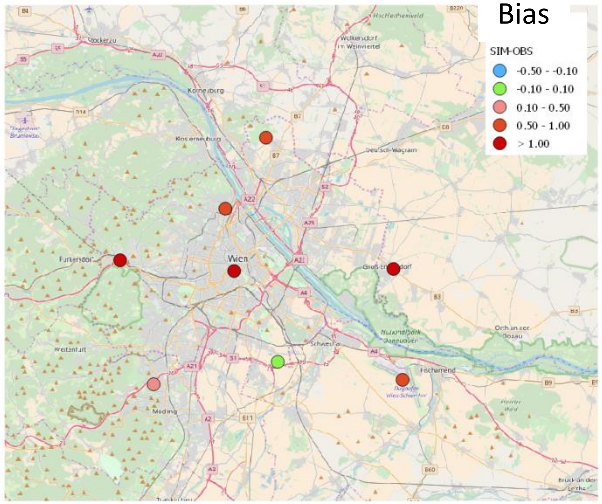

Model runs:

- WRFv3.9.1 using USGS classes (US)

SURFEXv8 offline runs forced by WRF:

- WRF/S using ECOCLIMAP (EC)
- WRF/S high resolution maps (PM)
- WRF/S (PM)S forced by first sigma level (~40m)

Wien-Hohe Warte, 18 - 24 July 2015

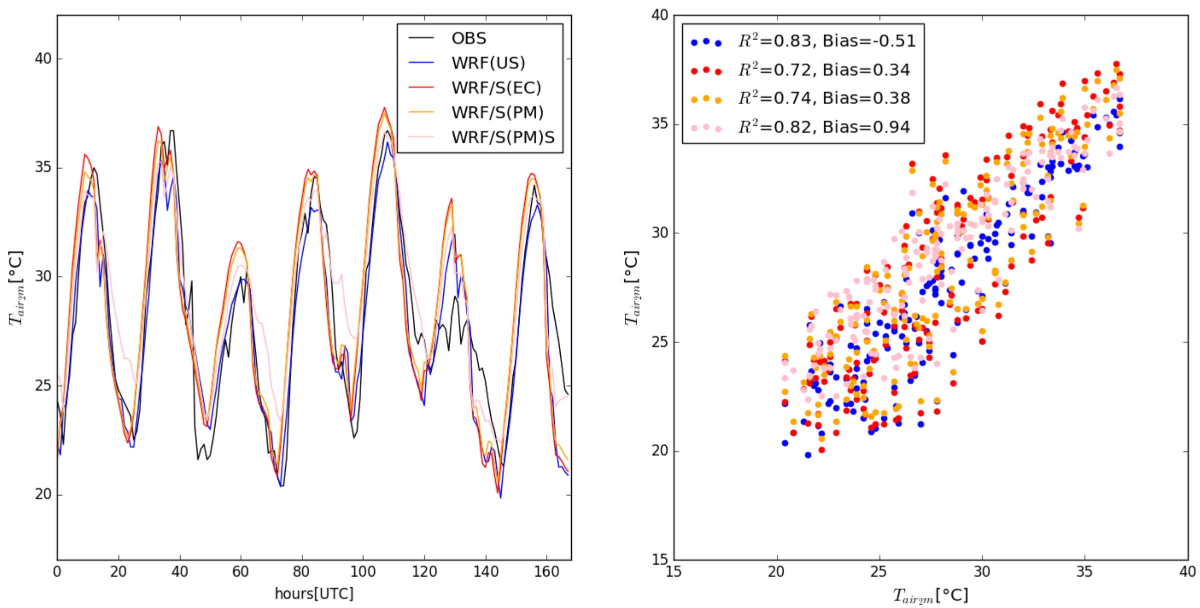

EGU 2018-7927
CL.18
11/4/2018

1 Viennese Growth

2 Models

3 Urban Szenarios

4 Conclusion and outlook

Comparison WRF, WRF/SURFEX offline and ground stations

-> WRF tends to underestimate maxima
-> WRF/SURFEX tends to overestimate maxima
-> both overestimate minima
-> clouds are not predicted well

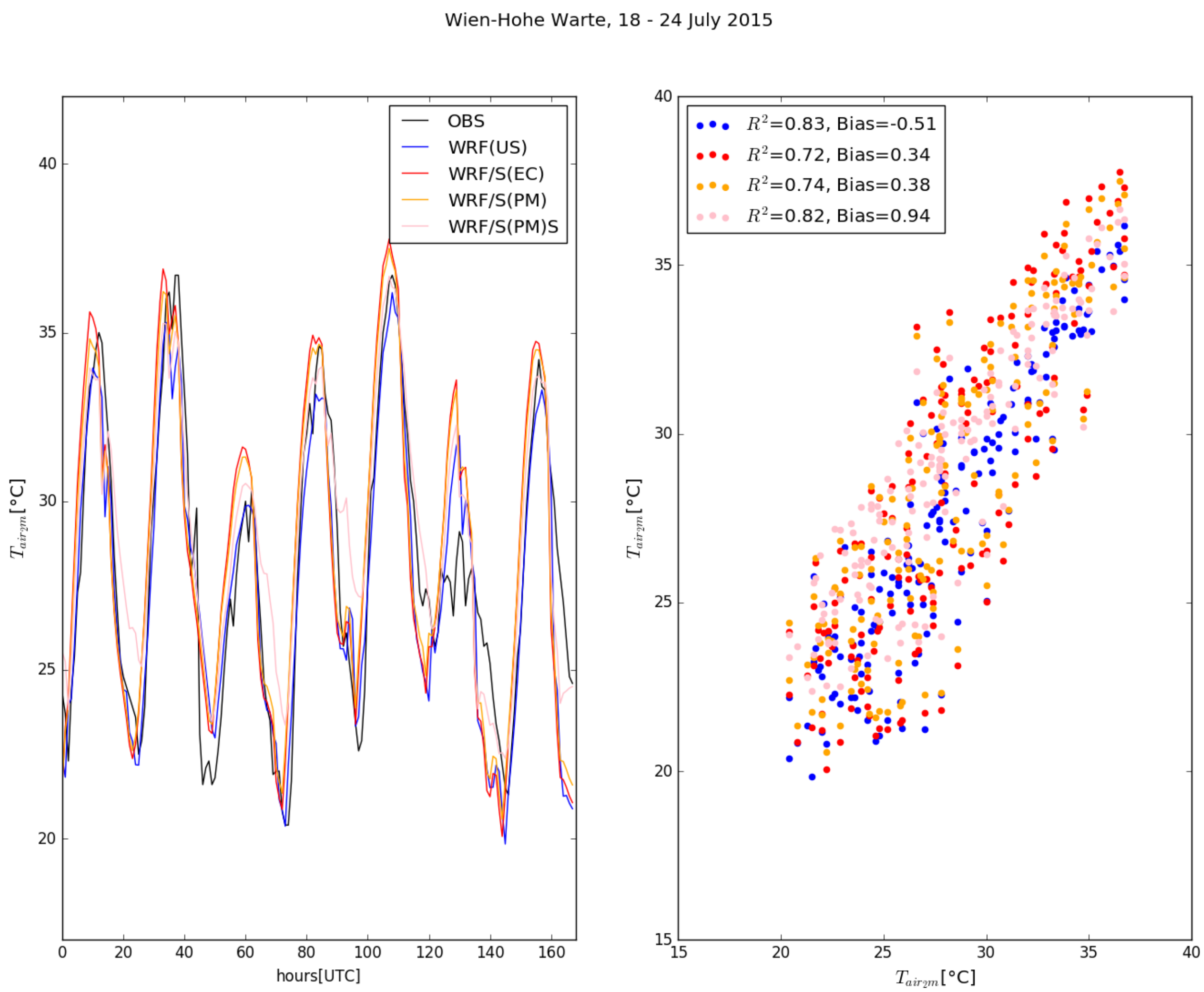

EGU 2018-7927
CL.18
11/4/2018

1 Viennese Growth

2 Models

3 Urban Szenarios

4 Conclusion and outlook

observed land use change

people within Vienna city borders:
2001: 1.550.123

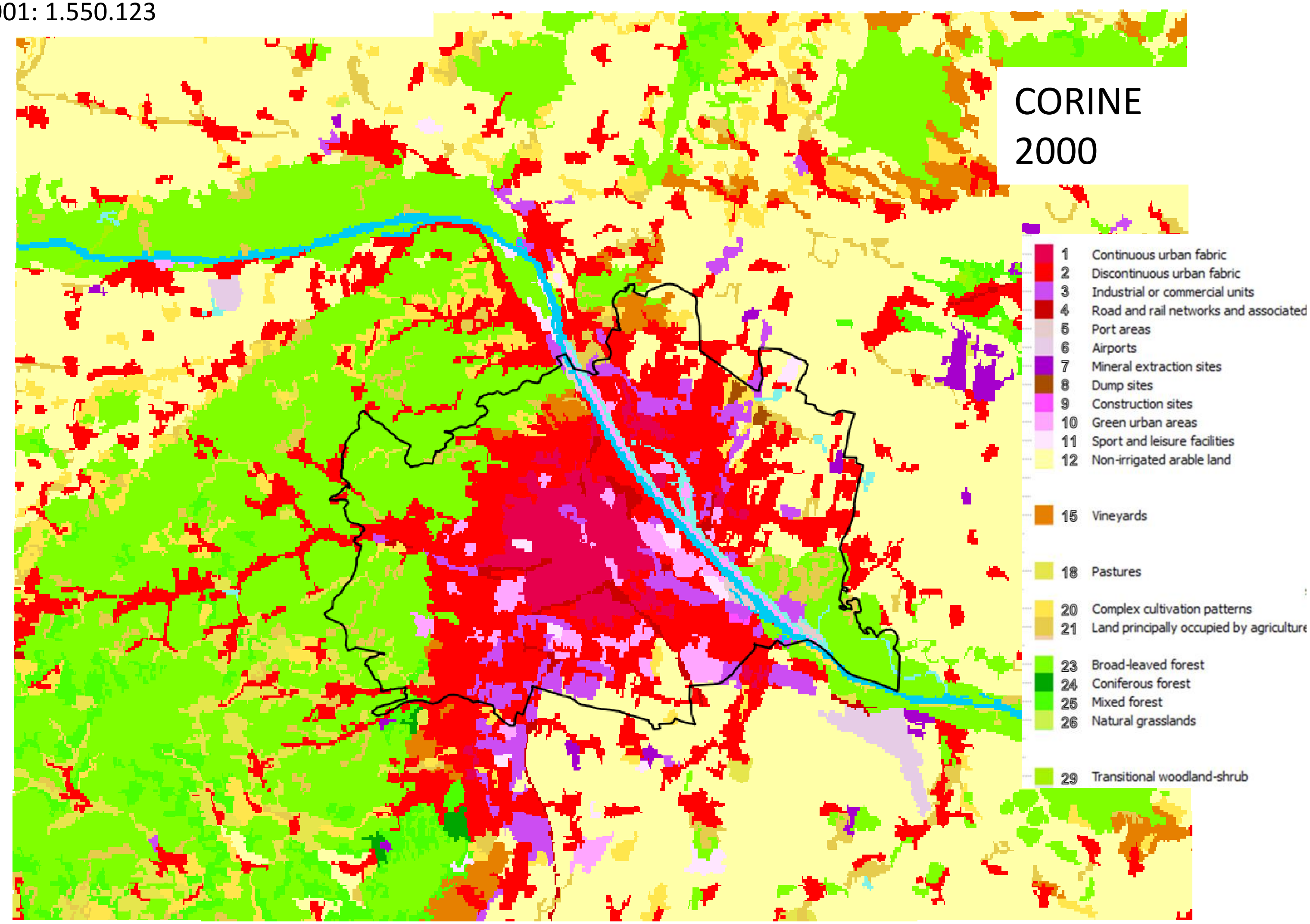

observed land use change

people within Vienna city borders:
2014: 1.766.746 (13J: +216.623) +14% ref. to 2001
2030: 2.077.300 (16J: +310.554) +18% ref to 2014
2050: 2.286.094 (36J: +519.348) +30% ref to 2014
Change of „Mobilitätsreserve?“

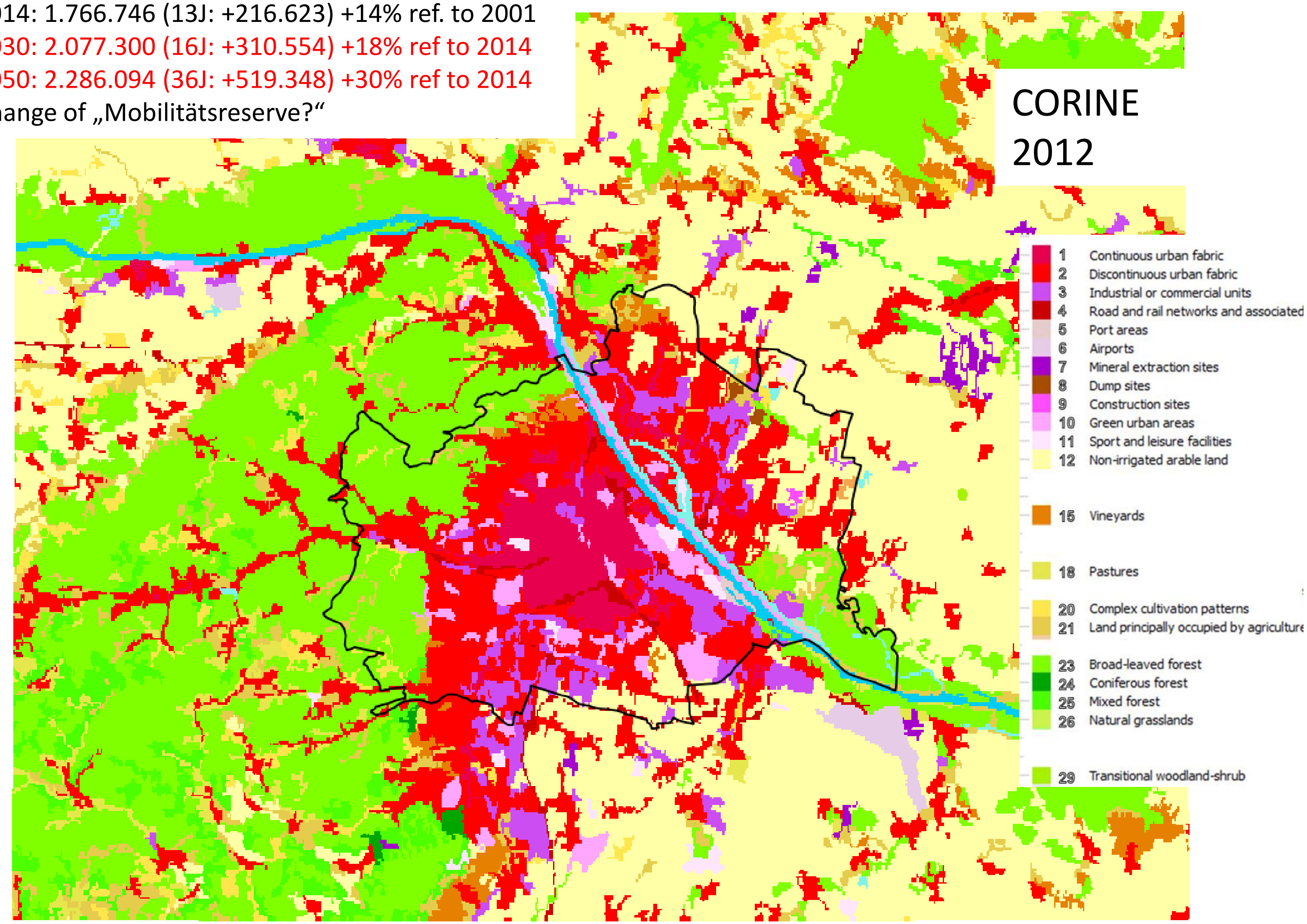

EGU 2018-7927
CL.18
11/4/2018

1 Viennese Growth

2 Models

3 Urban Szenarios

4 Conclusion and outlook

Diurnal circle of air temperature on day Tmax>35°C („Wüstentag“)

„DENSER“

2030
Scenario 1)
increased built area >85% +10%

WRF/S (PM)

@ 2UTC+ @ 13UTC:
$T_{max\_urban} - T_{min\_rural} = 8°C$

STQ

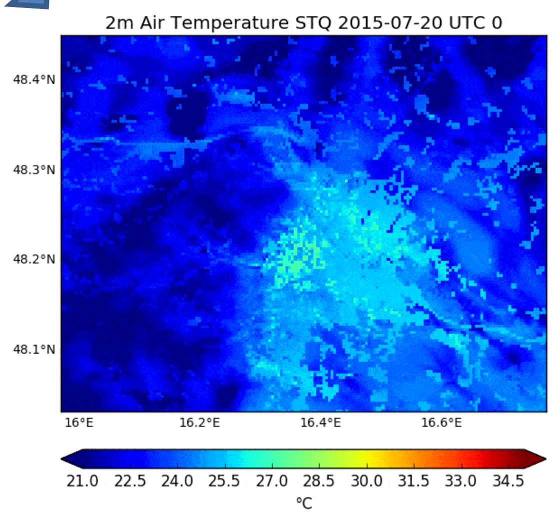

S1

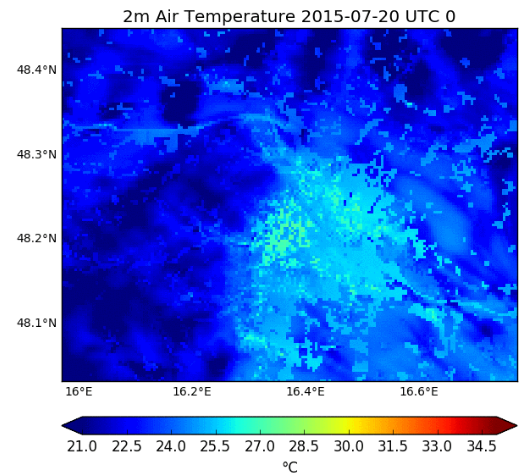

S1-STQ

Max: +0.3 °C

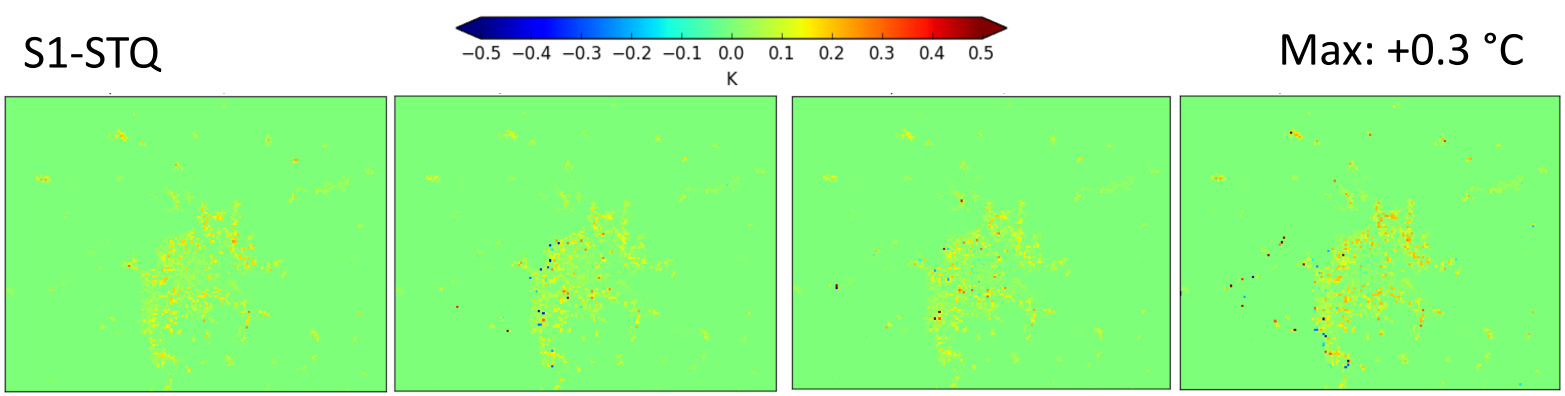

0UTC 6UTC 12UTC 18UTC

MA22 Mit unserer Umwelt

METEO FRANCE

EGU 2018-7927
CL.18
11/4/2018

1 Viennese Growth

2 Models

3 Urban Szenarios

4 Conclusion and outlook

„LARGER“

New urban areas: Lower buildings -> more space demand

		2012 „STQ“	2030 Scenario 2 „scattered“ extrapolated current growth	2050 Scenario 3 „structured“ development following traffic axes
Simulation input Nest3	„Built-up land“ fraction [km²]	9 02 (100%)	1 113 (123%)	1 449 (161%)
	„Nature“ fraction [km²]	3 284 (100%)	3 073 (94%)	2 736 (83%)
Real Stadtregion+	actual urban area [km²]	1 080 (100%)		

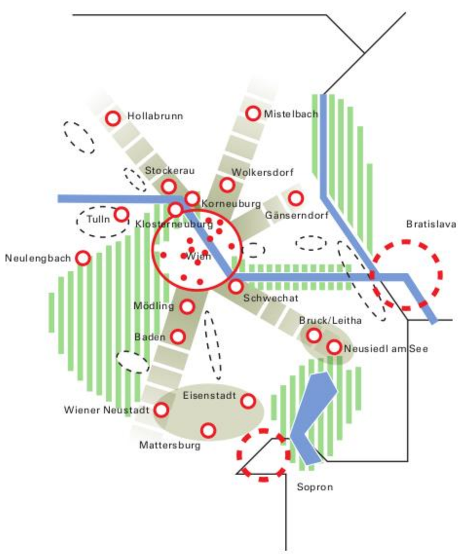

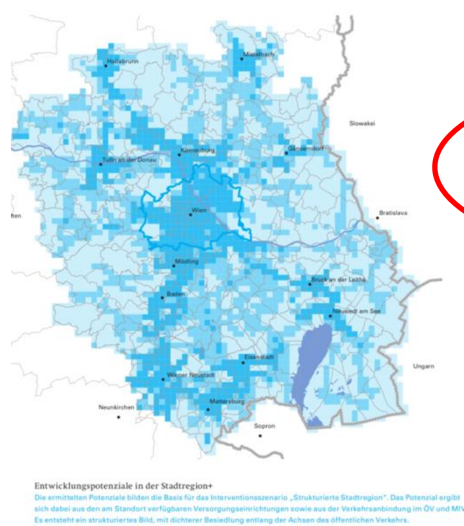

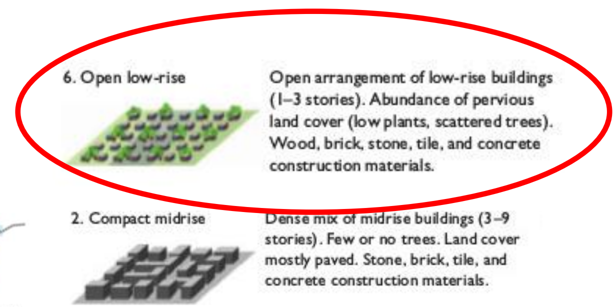

EGU 2018-7927
CL.18
11/4/2018

1 Viennese Growth

2 Models

3 Urban Szenarios

4 Conclusion and outlook

Diurnal circle of air temperature on day Tmax>35°C („Wüstentag“)

STQ

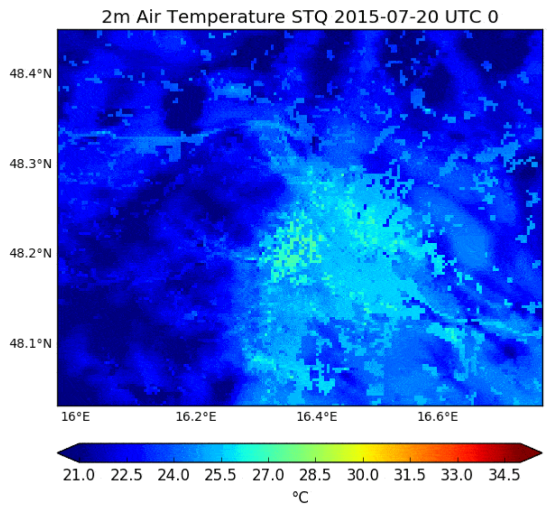

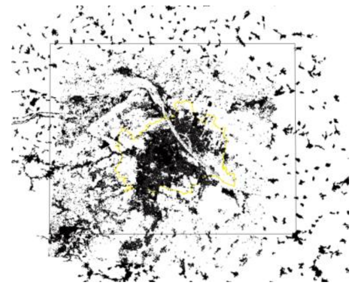

WRF/S (PM-XUNIF)

new urban area set uniform as first test:

BLT=0.5
GARDEN=0-2
BH=10
WALL_O=0.5

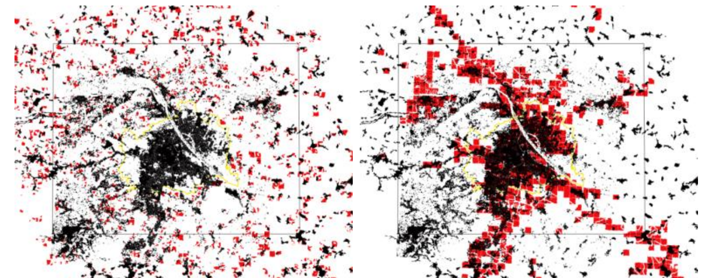

S2

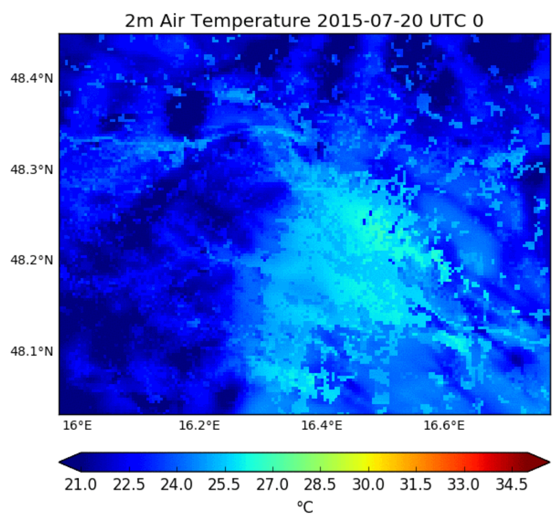

S3

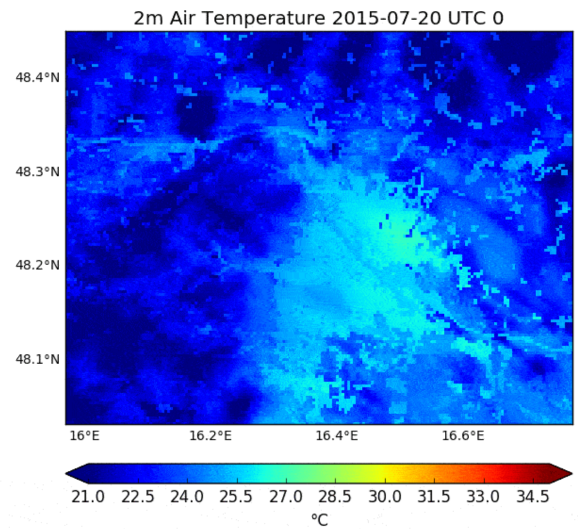

1 Viennese Growth

2 Models

3 Urban Szenarios

4 Conclusion and outlook

STQ

Regions:10x10points-> 11km²

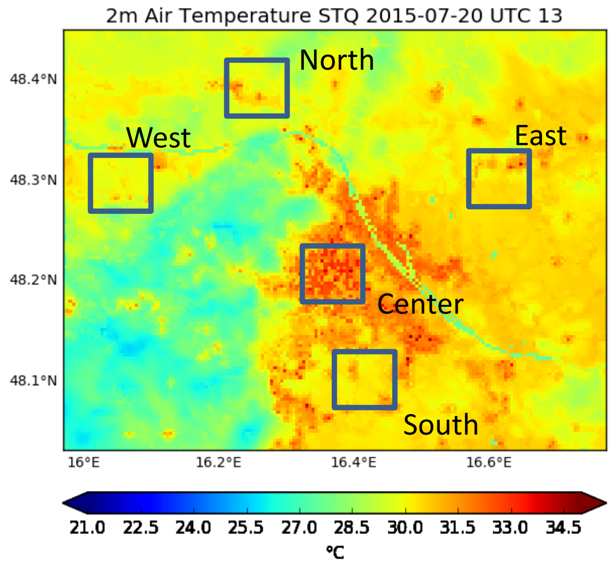

13UTC Tair	C	W	N	E	S
STQ	29.0	24.6	23.8	25.1	26.6
S4	29.3	25.2	24.3	25.4	27.0
Diff	+0.3	+0.6	+0.6	+0.3	+0.4

S3

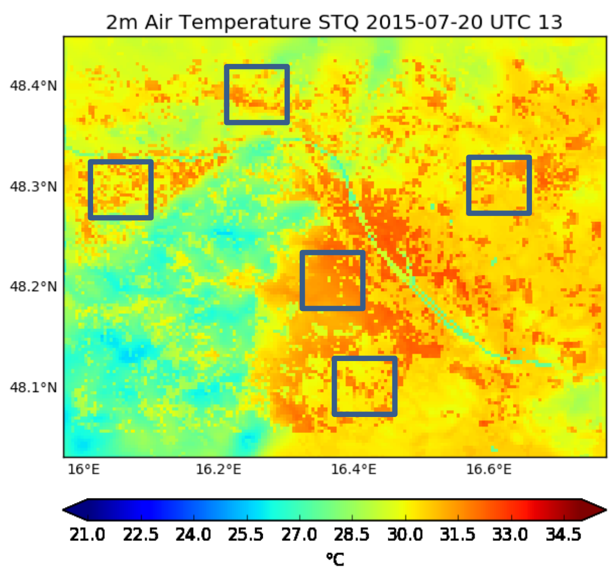

S4

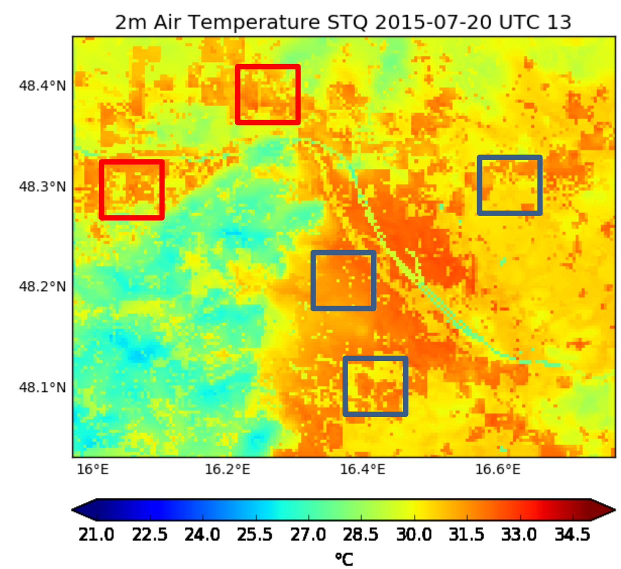

BOKU

klima+ energie fonds

MA22 Mit unserer Umwelt

METEO FRANCE

EGU 2018-7927
CL.18
11/4/2018

1 Viennese Growth

2 Models

3 Urban Szenarios

4 Conclusion and outlook

„TOWARDS SOLUTIONS“

	2012	2050 Scenario 4)
Heat capacity wall [J/m³K] Commercial High and low density residential	 0.975 $*10^6$ 1.520 $*10^6$	 0.975 $*10^6$ 1.496 $*10^6$
Heat capacity roof [J/m³K] (all categories)	1 554 000	1.496 $*10^6$
Thermal conductivity wall [W/mK] (all categories)	1.7	0.1
Thermal conductivity roof [W/mK](all categories)	1.4	0.1

Values of this table calculated using spatial data sets of Vienna and absolute values from: Amtmann M and Altmann-Mavaddat N (2014) Eine Typologie österreichischer Wohngebäude, Austrian Energy Agency, TABULA/EPISCOPE; Berger T et al. (2012) Auswirkungen des Klimawandels auf den thermischen Komfort in Bürogebäuden, Berichte aus der Energie- und Umweltforschung

WRF/S (PM)

S4-STQ:
increased built area + **insolation**

Min: -0.5 °C
Max:+0.3 °C

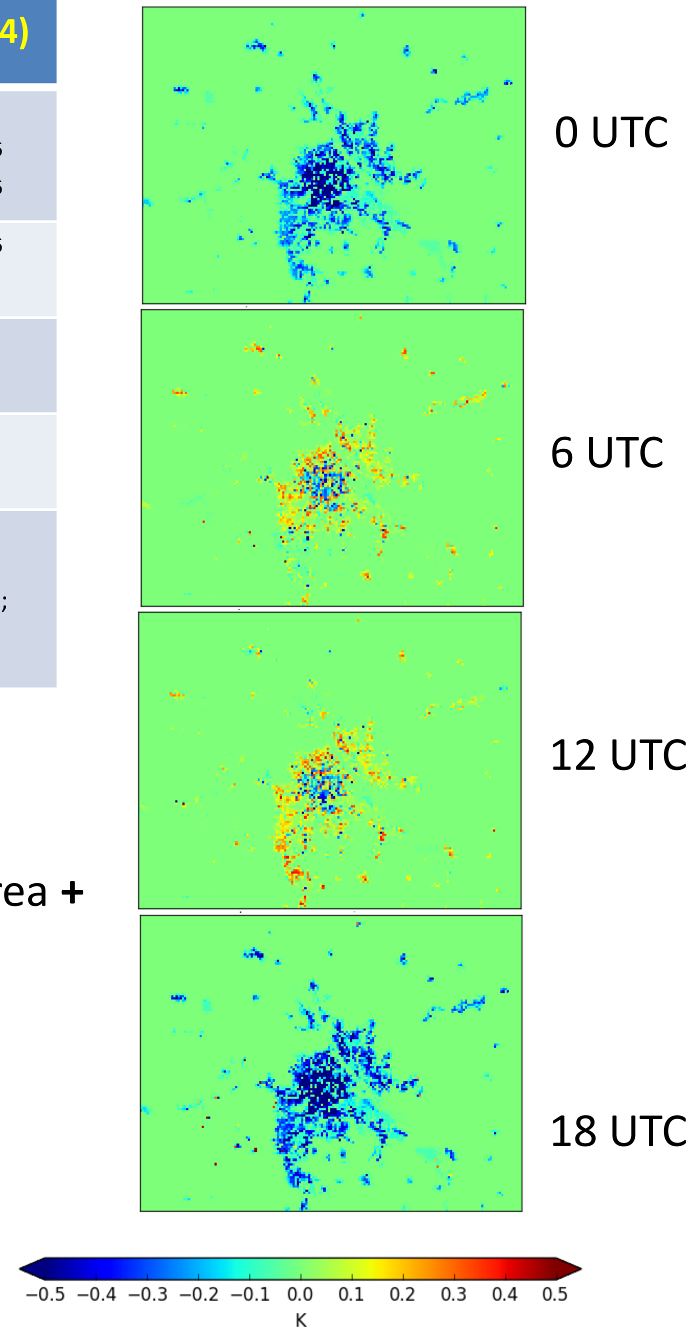

First conclusions - possible relativ changes of air temperature (derived only from surface energy balance changes):

- **Densification** of built up area
  -> maximum +0.3 °C within actual urban areas.
  -> Largest increases in the evenings.

- **Urban sprawl** -> maximum +2°C in the new urban area
  -> spatial average: 0.6°C.
  -> also the actual urban structure will be affected.

- **Countermeasures** as ambitioned insolation
  -> -0.5°C within the actual urban area during night
  -> even under increased building density
  -> also at noon in the inner districts air temperature could be reduced even when the built area is increased

klima energie fonds
BOKU
MA22 Mit unserer Umwelt
METEO FRANCE

Next steps:

Effects of urban densification and expansion on temperature including roughness modified wind field, change of urban boundary layer using WRF:

- **WRF-TEB coupling ongoing!**

Szenarios will be run with:

- 3 land use categories (simplified from LCZ categorization according to WUDAPT Methodology – Steward and Oke 2012, presented EGU2017)
- PBL-Scheme: Yonsei University Scheme

Lots more to do:

- **In depth spatio-temporal analysis of observed heat waves**

- **Analyze effect on thermal comfort within urban canopy**
  -> see poster: EGU2018-9582 Oswald et al. 2018
  today, 11 Apr, 17:30–19:00

- **Search for key factors and more effective urban szenarios (together with city authorities):**
- Change of spatial distibution of new building areas
- Change of building morphology
- Building properties (roof albedo, new materials, latent heat, ...)

- **Climate change 2030/2050 for RCP4.5 and RCP8.5**
- **Role of anthropogenic heat (spatio-temporal patterns)**

- website launch July 2018: **http://urbania.boku.ac.at**

Thank you for your attention!

Evolution of the Viennese Urban Heat Island and Mitigation Strategies in the Context of Urban Growth, Compacting and Climate Change by optimizing the Urban Surface Energy Balance

Project: URBANIA - Influence of the development of outlying districts and urban growth on the urban heat island of the city of Vienna in the context of climate change
ACRP 8th call: KR14AC7K11944

Trimmel H.[1], Weihs P. [1], Oswald S. [1], Revesz M. [1], Formayer H. [1], Nadeem I. [1], Leidinger D. [1], Laimighofer J. [1], Mursch-Radlgruber E. [1], Valéry Masson[2], Robert Schoetter[2], Aude Lemonsu[2], Stéphanie Faroux[2]

[1]Institute of Meteorology, University of Natural Resources and Life Sciences Vienna – Austria
[2]CNRS - Météo France

METEO FRANCE

MA22 Mit unserer Umwelt

klima+ energie fonds

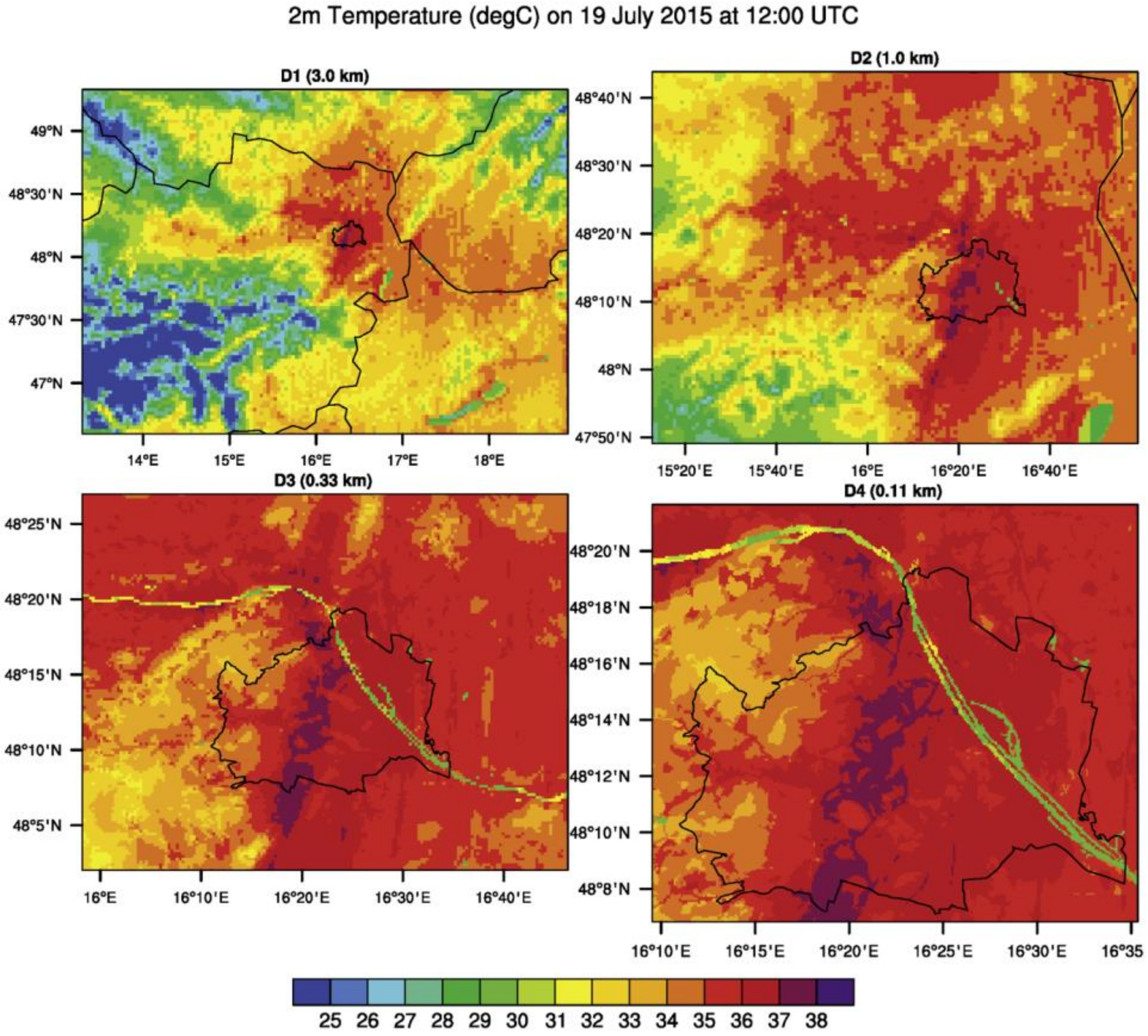

(1) Densification of Obervations in compact building area (+8 stations)

OBSERVATIONS

(2) WRFv3.9.1

- Run in 3-4 nests (3km-1km-0.33km-0.11km)
- 40 vertical layers
- Lateral boundary conditions: 9km ECMWF analysis data (6h)
- Static: Topography- SRTM1Arc:30m
- NOAH LSM, Landcover-USGS Classes (1 urban class, total 30 classes)
- Land use based on Corine reclassified to USGS

(3) WRFv3.9.1 – SURFEXv8 offline

WRF/SURFEX (including TEB)

- Domain 3 (0.33km is used)
- Parameter Maps are used

(4) WRFv3.9.1 - TEB_v1_1550 coupled

WRF-TEB

- Including BEM
- Parallelized
- 1.5 increase in computation time
- -> 7 days for all nests run in <24h
- 3 urban categories
- PBL-Scheme: Yonsei University Scheme

Comparison WRF, WRF-TEB and ground stations 2017.7.27-8.5

104°F

68°F

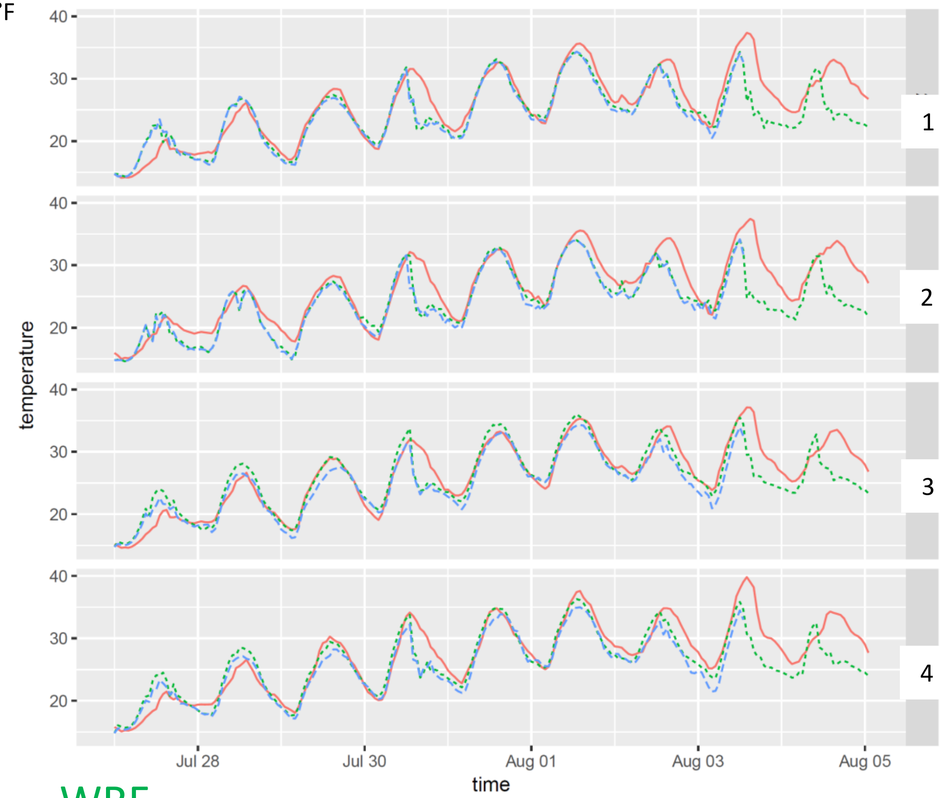

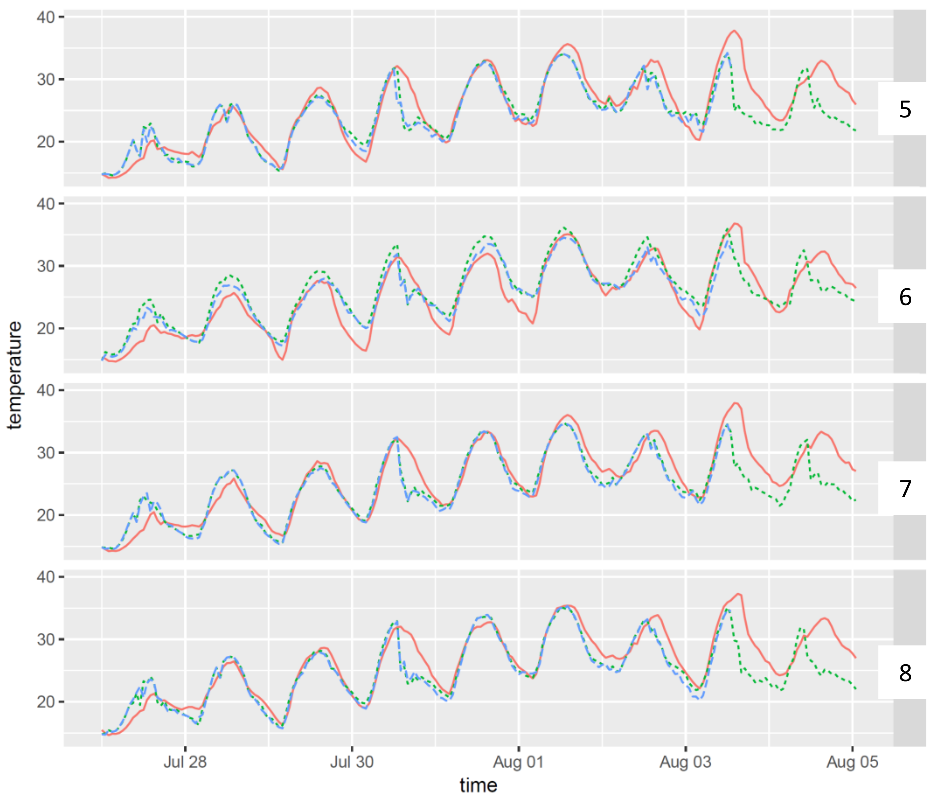

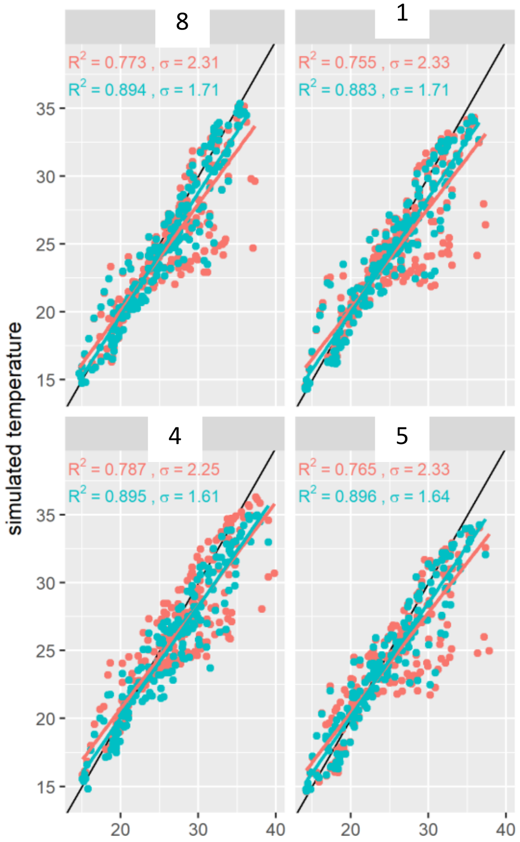

WRF

WRF-TEB

OBSERVATION

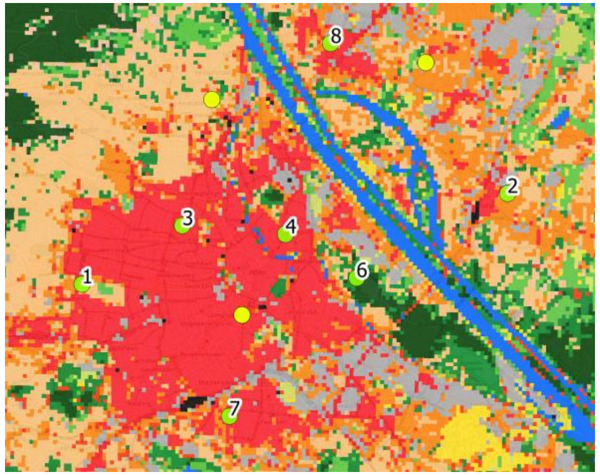

WRF

WRF-TEB

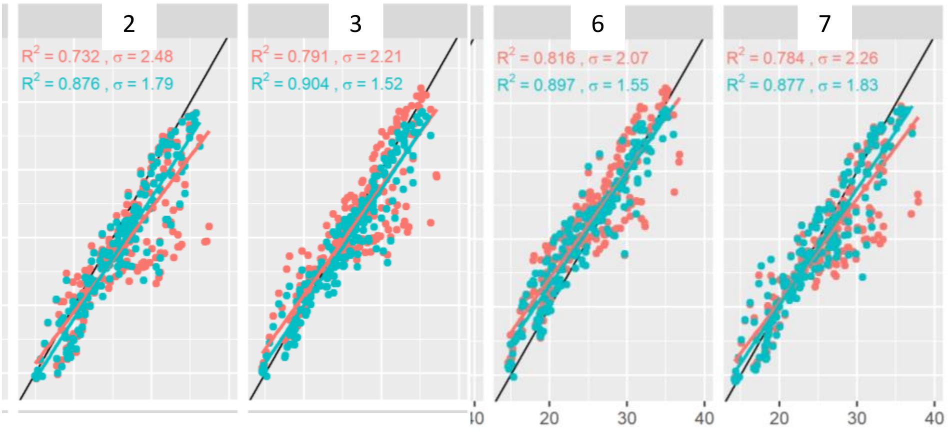

METEO FRANCE

BOKU

MA22 Mit unserer Umwelt

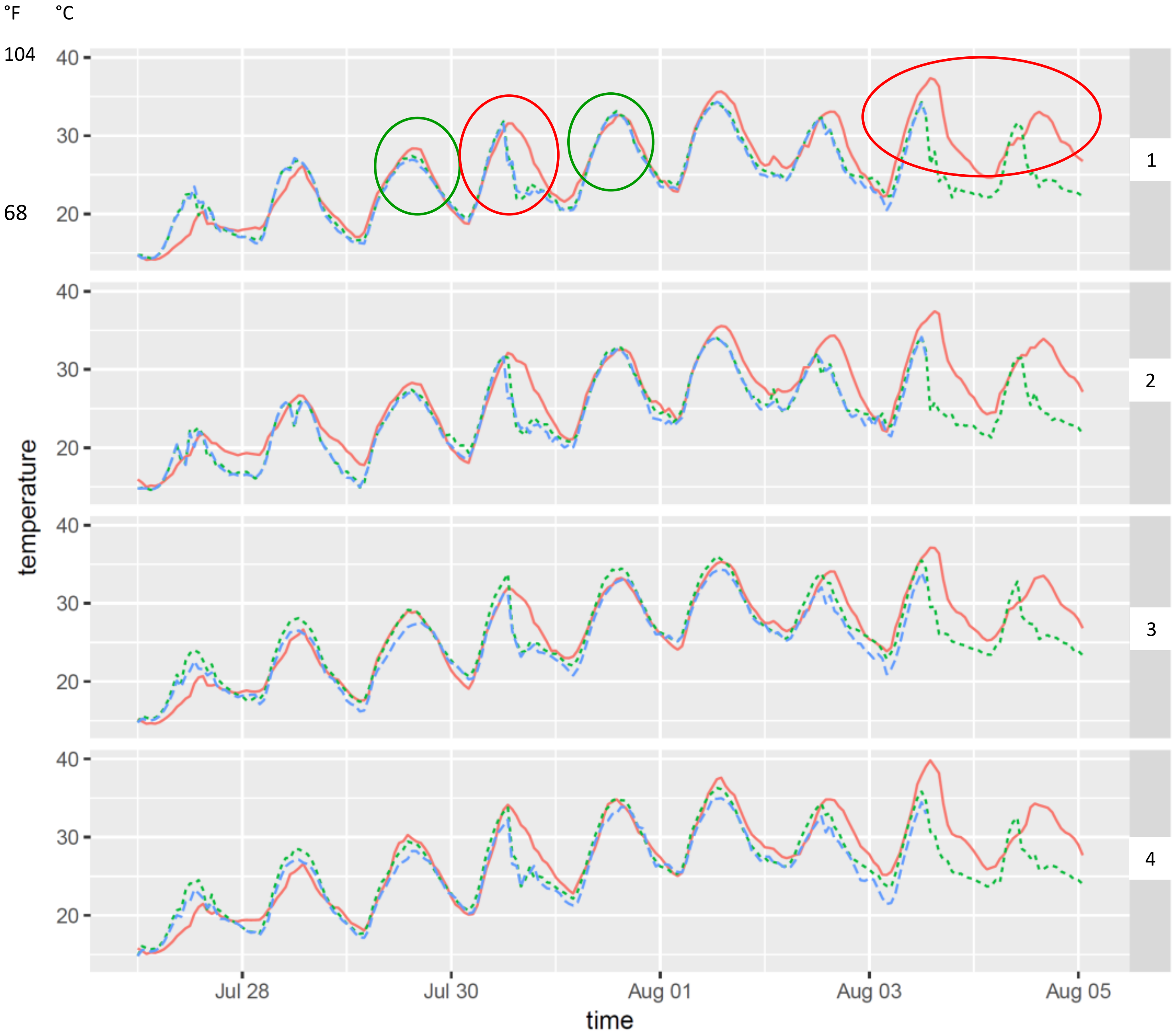
°F
°C
104
68
40
30
20
temperature
1
2
3
4
Jul 28
Jul 30
Aug 01
Aug 03
Aug 05
time
WRF
WRF-TEB
OBSERVATION

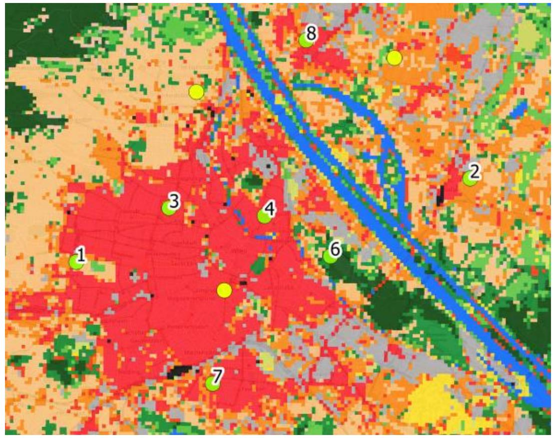
1
2
3
4
6
7
8

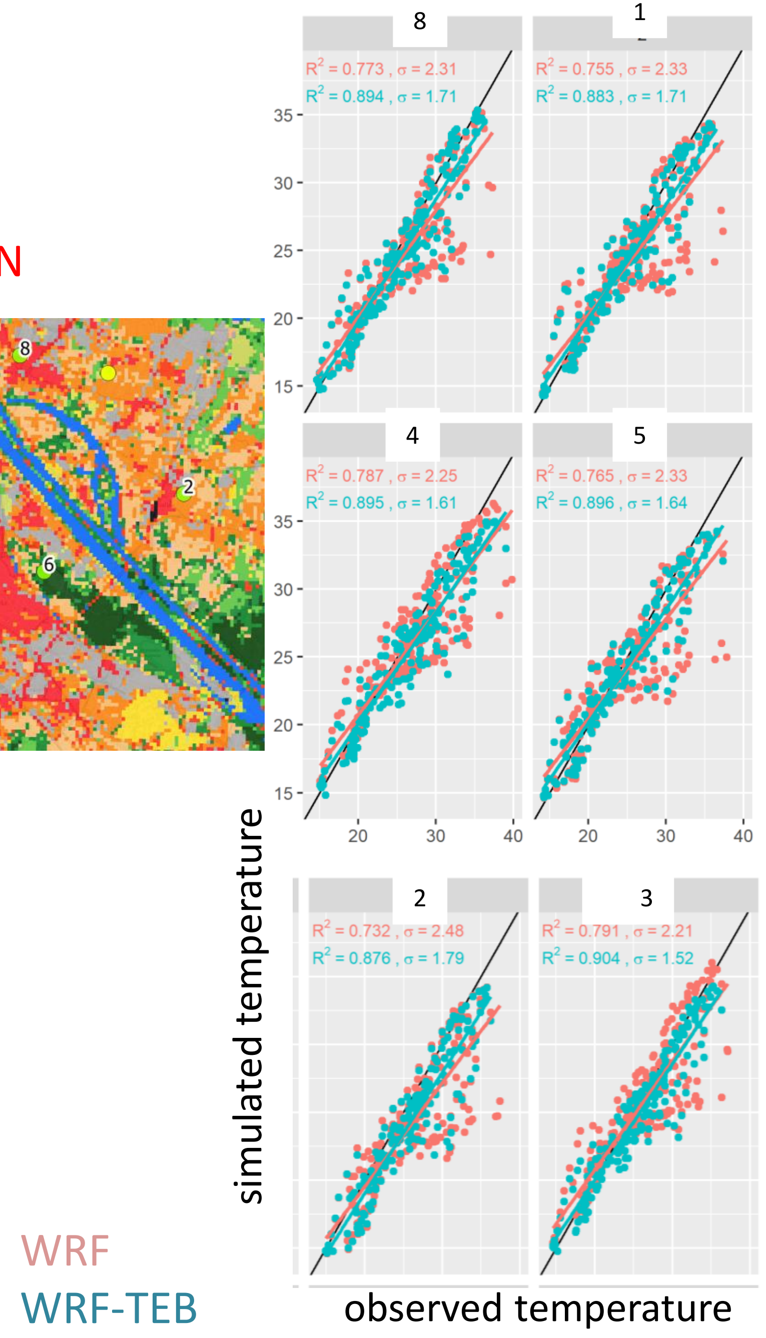
8
R^2 = 0.773 , σ = 2.31
R^2 = 0.894 , σ = 1.71
1
R^2 = 0.755 , σ = 2.33
R^2 = 0.883 , σ = 1.71
4
R^2 = 0.787 , σ = 2.25
R^2 = 0.895 , σ = 1.61
5
R^2 = 0.765 , σ = 2.33
R^2 = 0.896 , σ = 1.64
2
R^2 = 0.732 , σ = 2.48
R^2 = 0.876 , σ = 1.79
3
R^2 = 0.791 , σ = 2.21
R^2 = 0.904 , σ = 1.52
simulated temperature
observed temperature
WRF
WRF-TEB

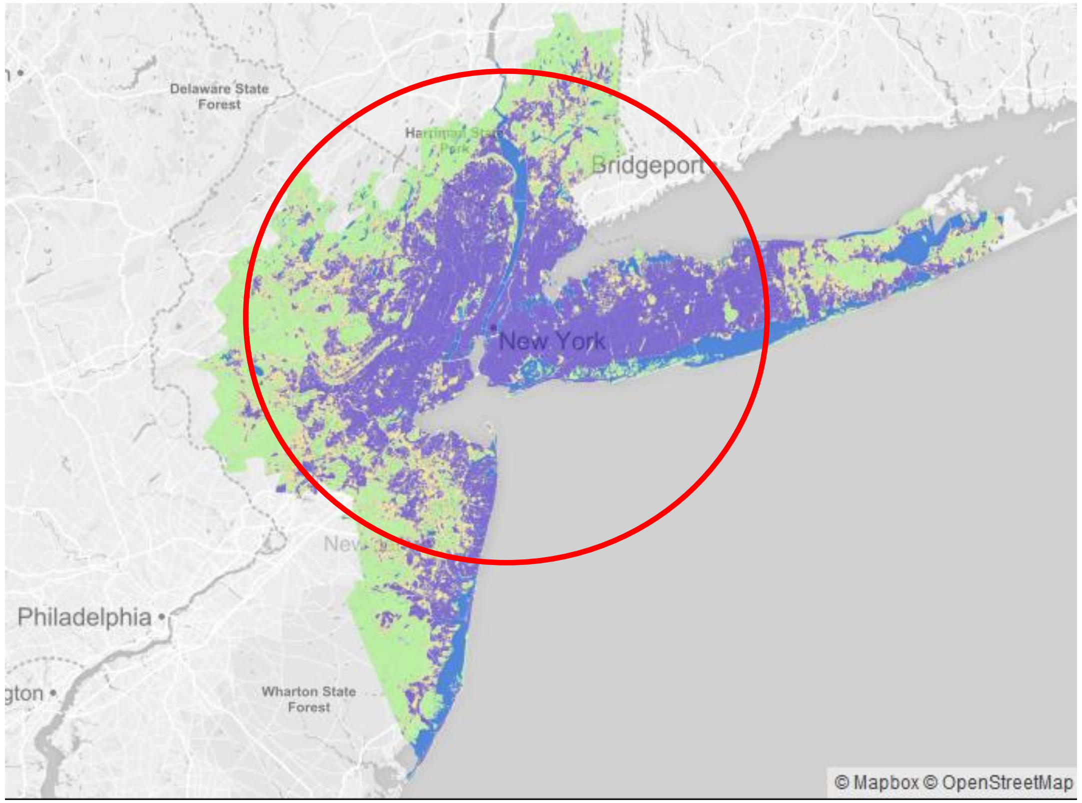

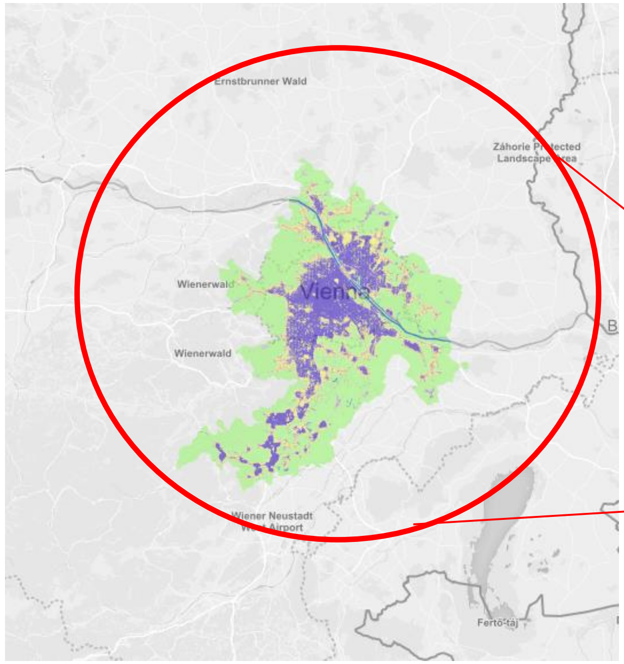

Radius of 50km/31miles

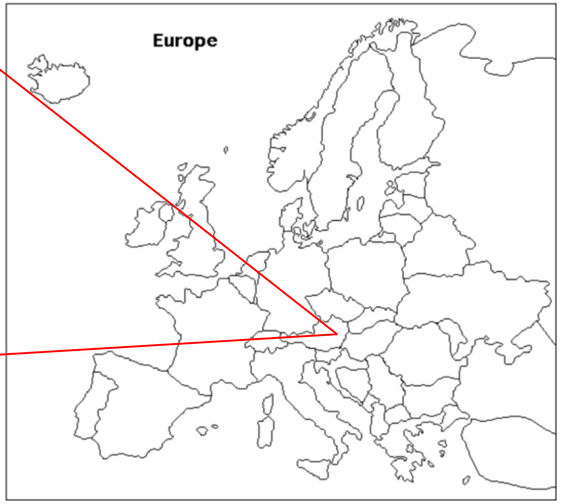

http://www.atlasofurbanexpansion.org/

18 Mio inhabitants

2 Mio inhabitants

Planetary Boundary Layer height + Vertical motion

WRF-TEB Simulation

29 Jul 2017
Tmax = 28°C, no clouds
Mean Windspeed = 2m/s, NW later SE
sunrise 3:26UTC
solar noon: 11 UTC
sunset 18:34 UTC

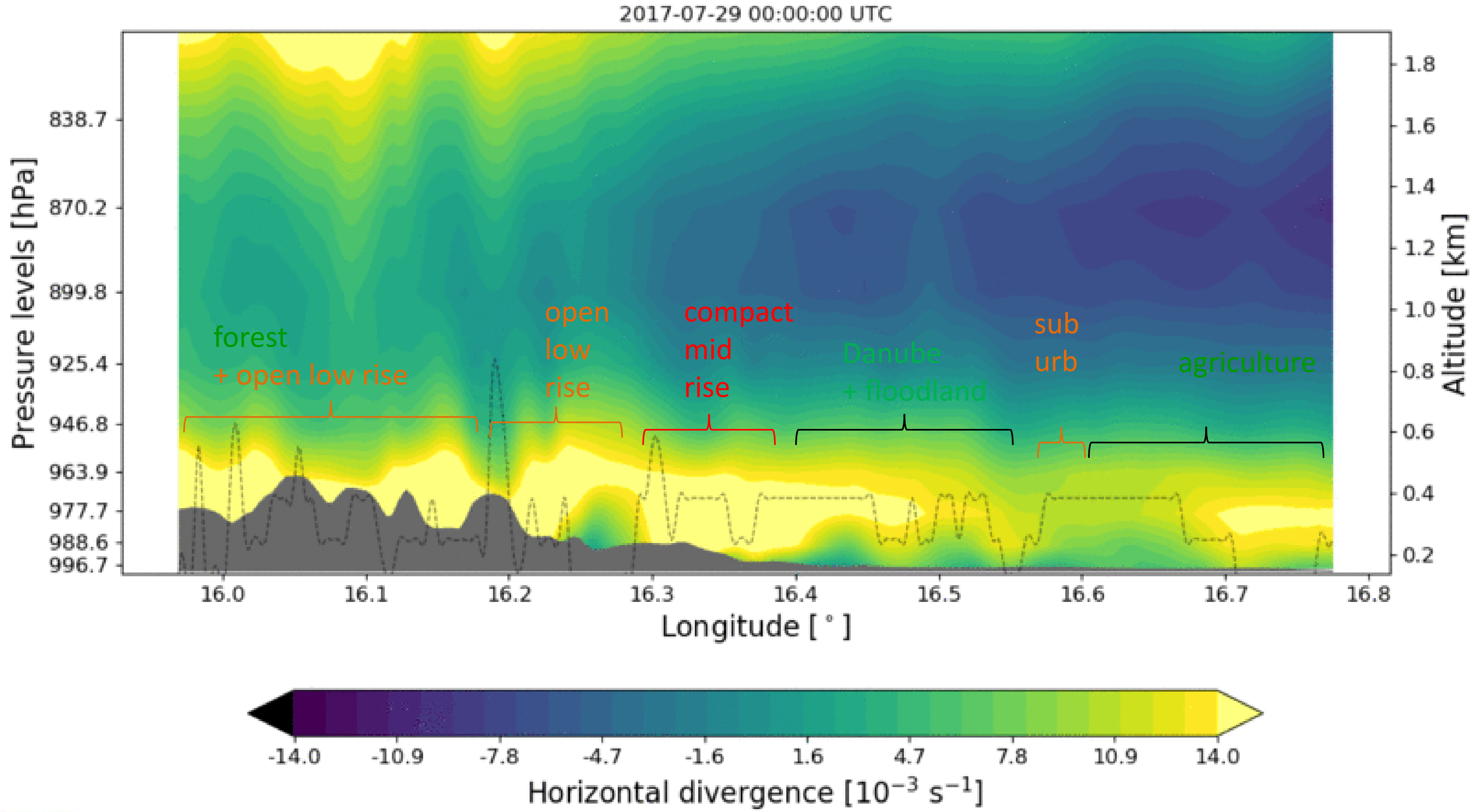

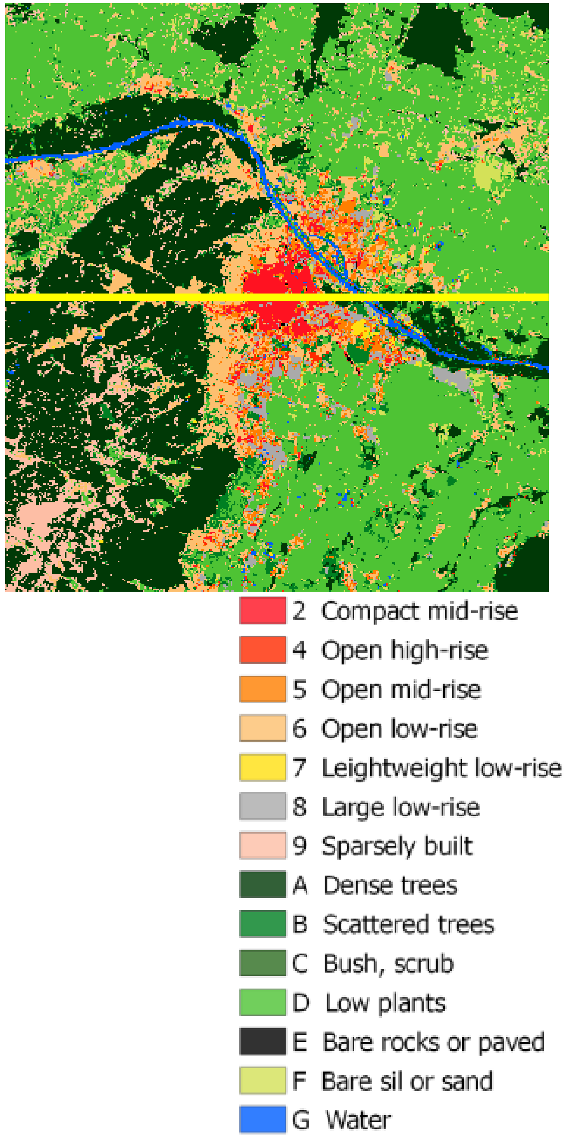

Planetary boundary layer height [km]

METEO FRANCE
BOKU
MA22 Mit unserer Umwelt

Vertical temperature distribution during heat wave

WRF-TEB Simulation

1 Aug 2017
Tmax = 34°C
No clouds
Mean Windspeed =
day: 6m/s, night 2m/s SE
sunrise 3:30 UTC
solar noon: 11 UTC
sunset 18:30 UTC

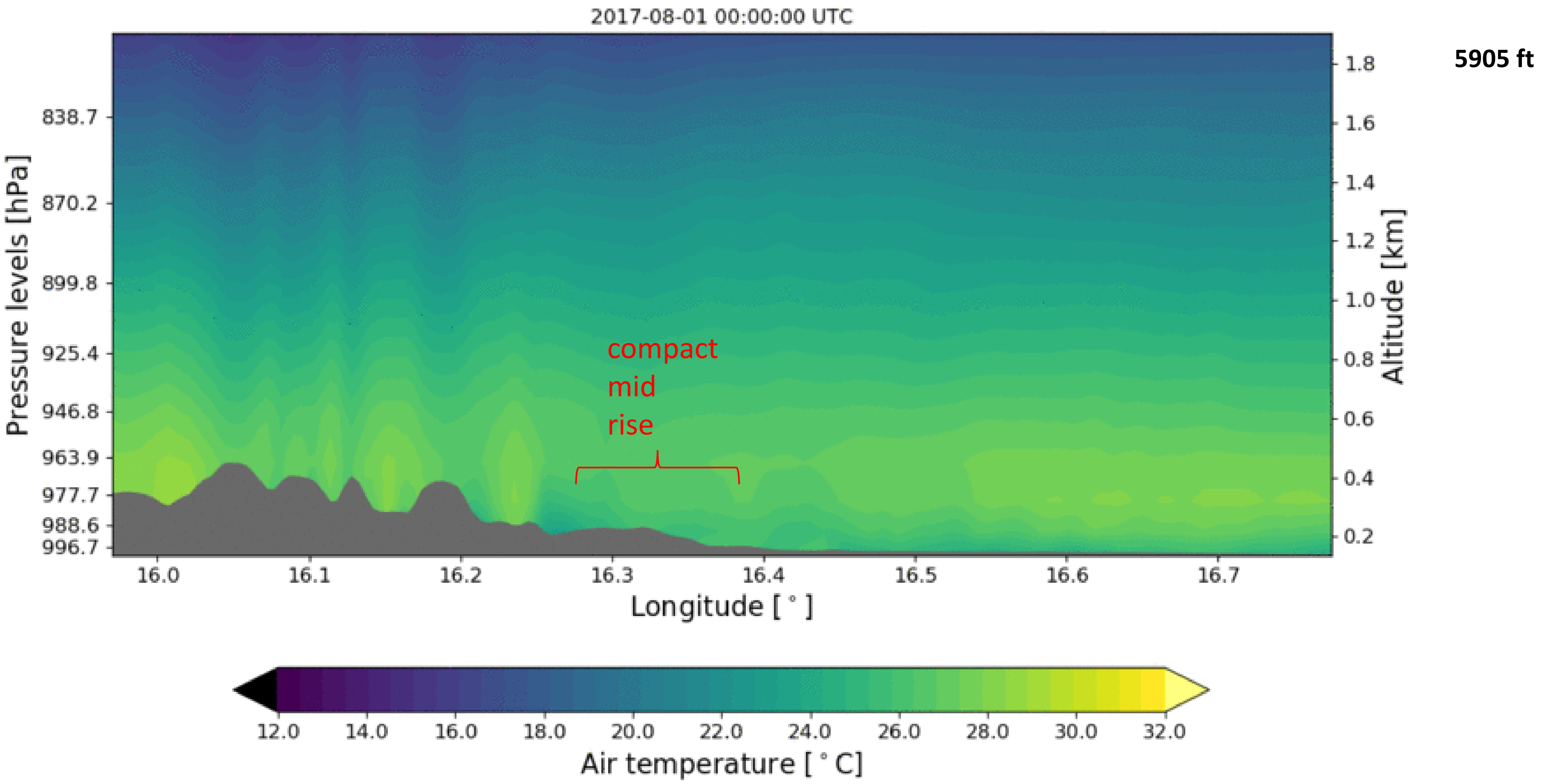

METEO FRANCE
MA22 Mit unserer Umwelt

Estimation of additional future brutto floor area + urban fraction

Stadtregion+ 2.7 Mio People

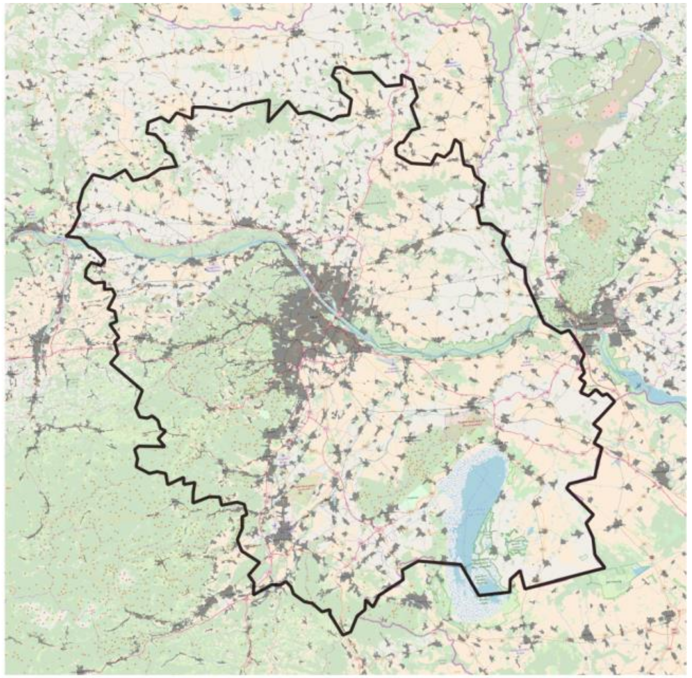

50km/31miles

UA ... Actual built area within Stadtregion+	929 km² (Corine 2012)
P_a ... Additional Popluation until 2050	800 000 (PGO 2011)
BGF_W ... Gross area for living per person	40 m² (MA18)
BGF_WS, BGF_PWS ... Gross area for working place	40 -100 m² (MA18)
WpP ... Workplace per person	0.76 (Loibl et al. 2002)
FBA ... Fraction of built up area	0.17 – 0.4 (MA41)

$$BGF\_a = P\_a*BGF\_W + WpP*P\_a*(0.5*BGF\_PWS+0.5*BGF\_WS)$$

->**Additional gross floor area needed for 2050: ~75 km²**

	Additional urban fraction
OPTION A) Densification of open mid- and low-rise, use of idle floor area, attics, industrial -> multistoried residential,...	**~ 0 km²**
OPTION B) Sprawl: Additional Urban Area (including low density areas)	**185.8km²**

METEO FRANCE

BOKU

MA22 Mit unserer Umwelt

How could future urban area look like

Areas with development potential

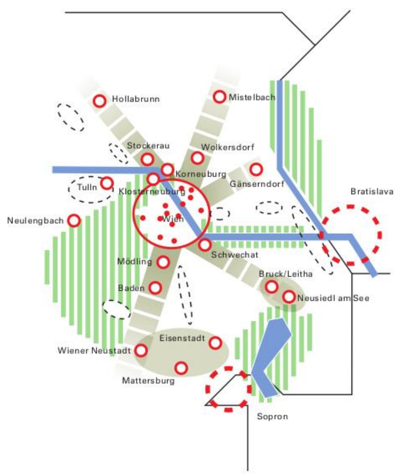

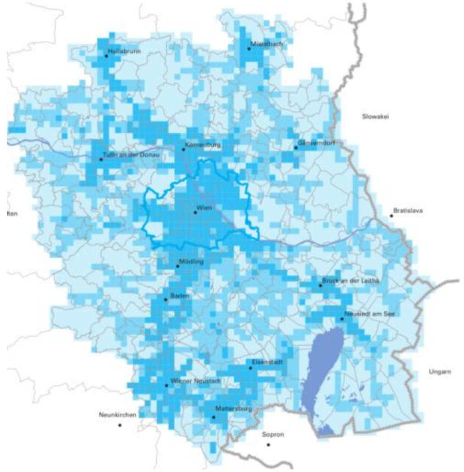

- Protected areas

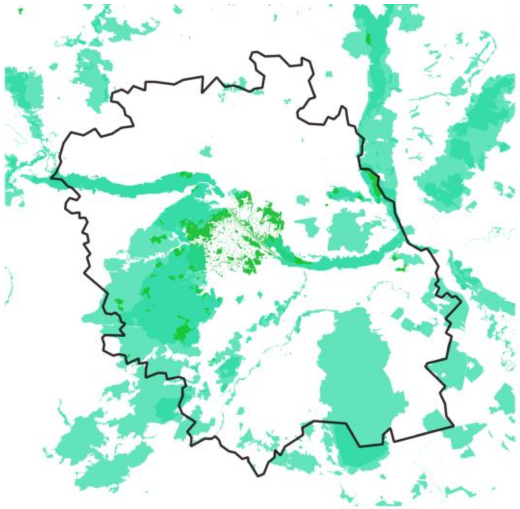

+ known development areas
+ 200-300m buffer to distribute additional space demands

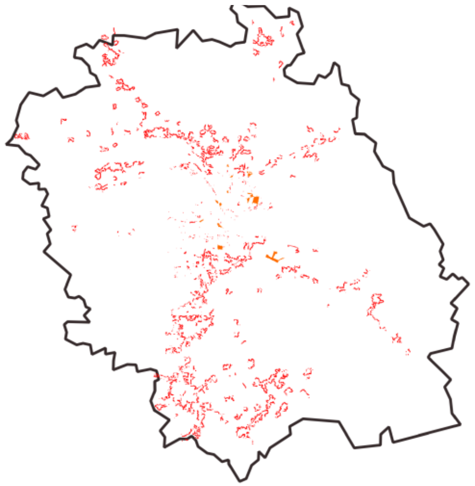

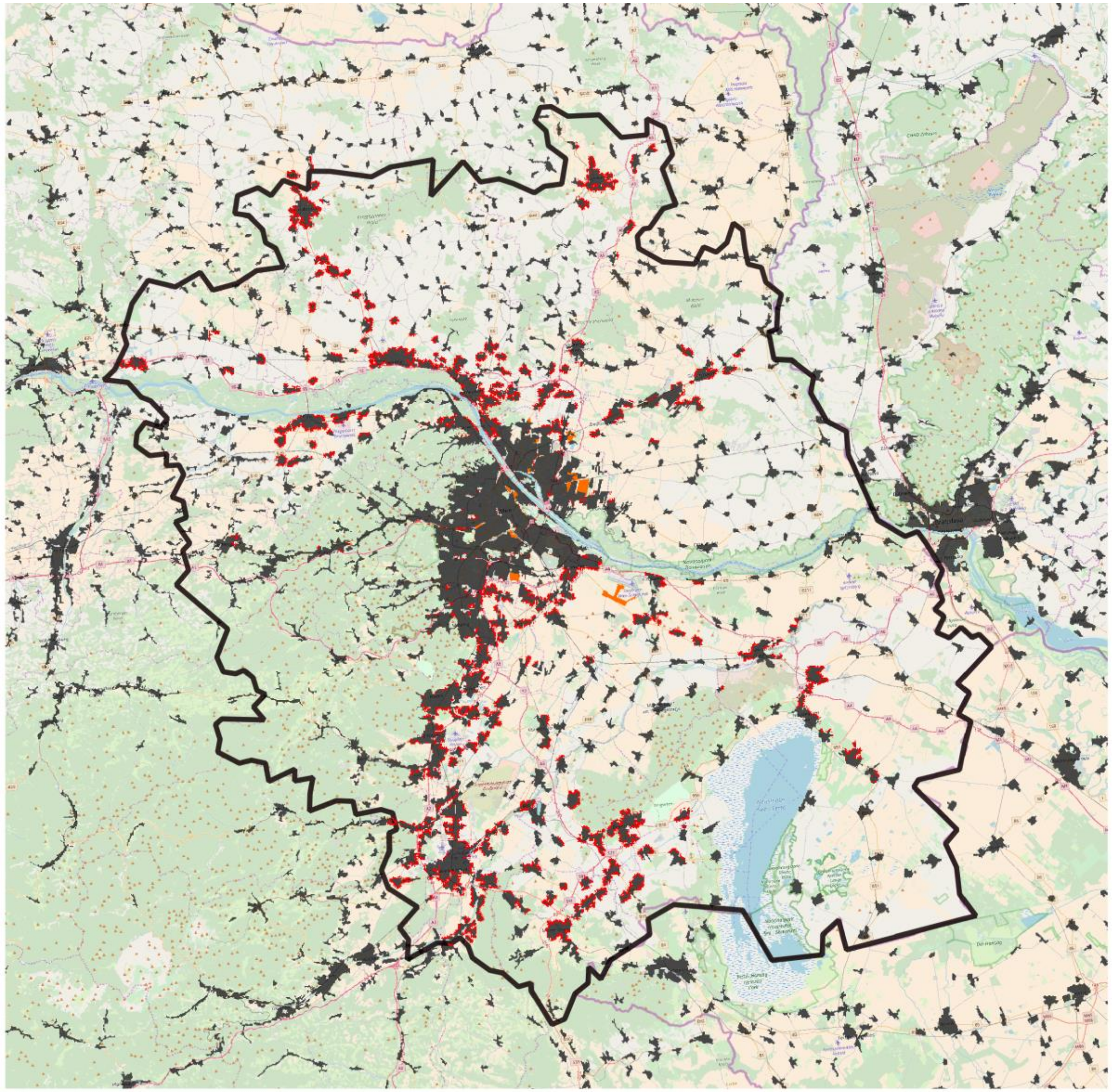

WRF/SURFEX Simulation

OPTION A: Densification

- BUILT for all pixels *1.1

Radiation Balance | Sensible Heat Flux | Latent Heat Flux

12UTC

18UTC

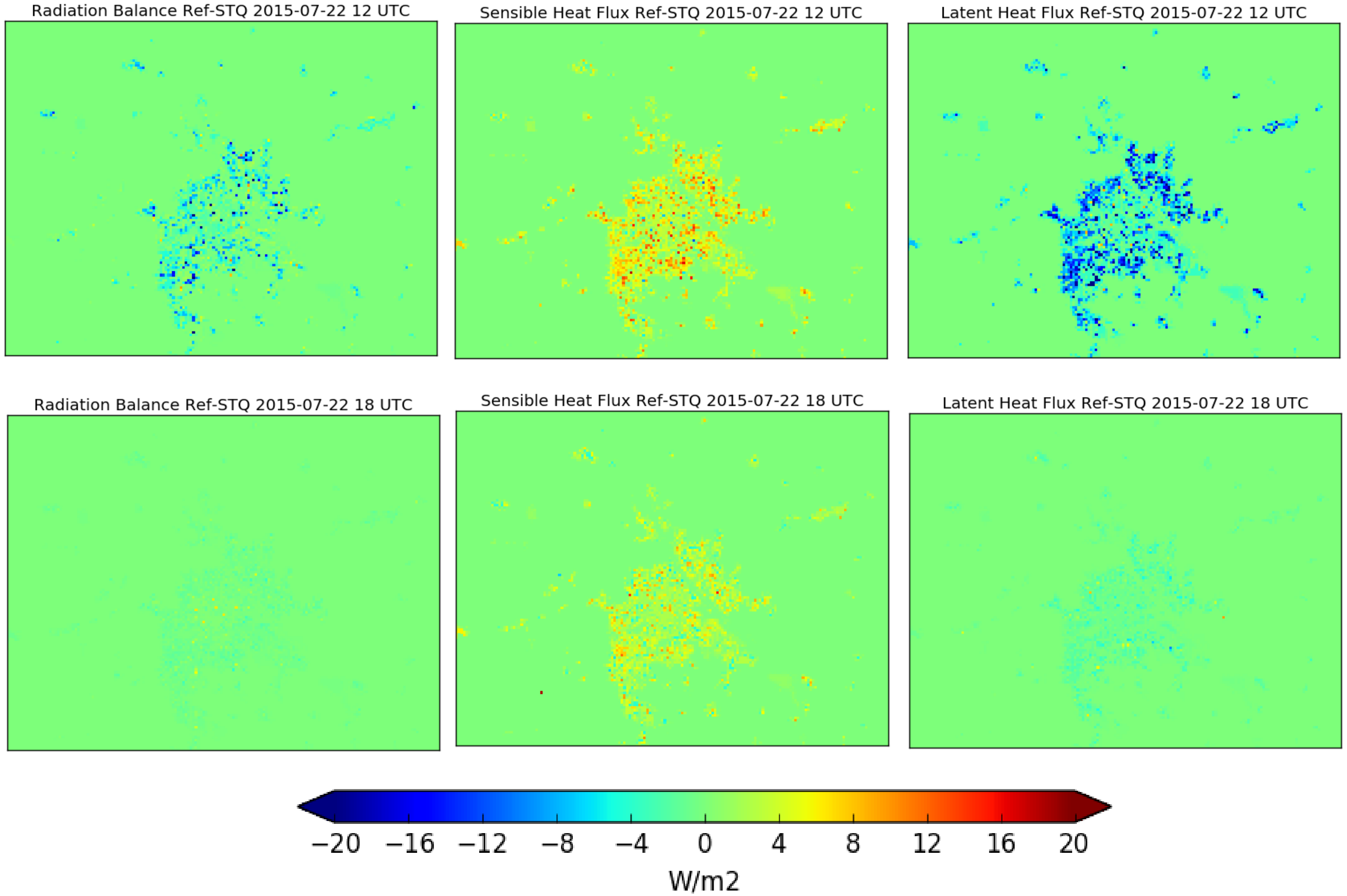

METEO FRANCE

MA22 Mit unserer Umwelt

OPTION B: Sprawl

WRF/SURFEX Simulation

- Additional urban area bordering existing urban area

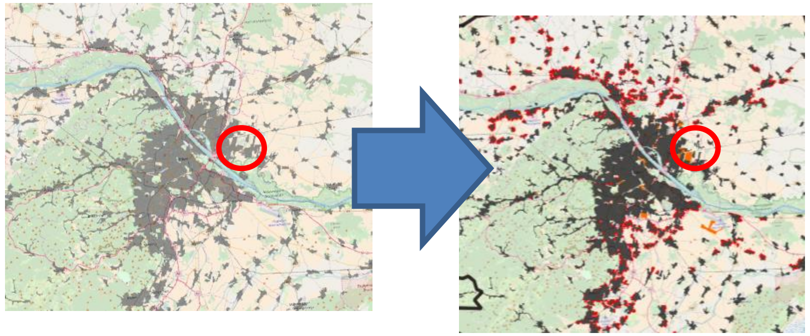

- Local changes in Energy Fluxes:
- Increase in Ground Heat Flux
- Decrease in Latent Heat Flux

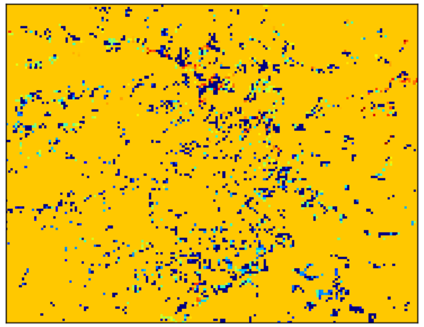

- Increase in Sensible Heat Flux

Sensible Heat Flux Sprawl-STQ 2015-07-22 12 UTC

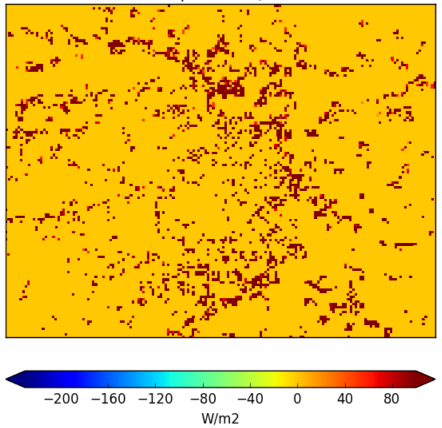

Energy flux difference in newly built area

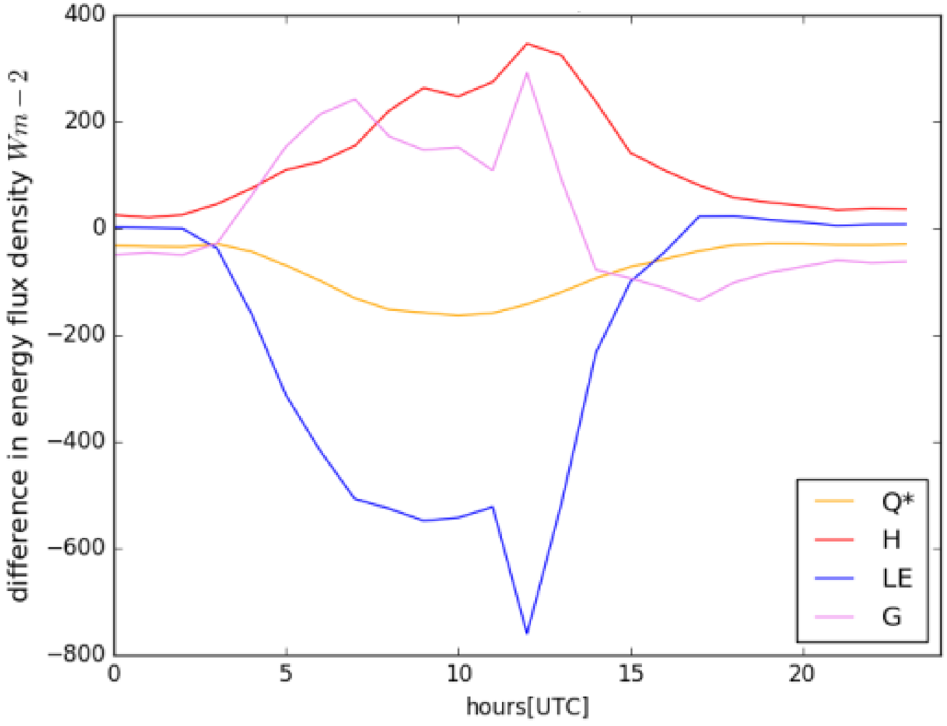

METEO FRANCE
BOKU
MA22 Mit unserer Umwelt

OPTION B: Sprawl

WRF-TEB
Simulation

- Mainly local air temperature changes

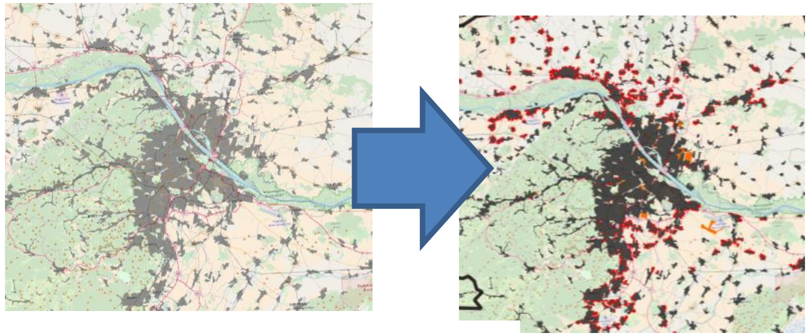

•Cooling during 6-15 UTC

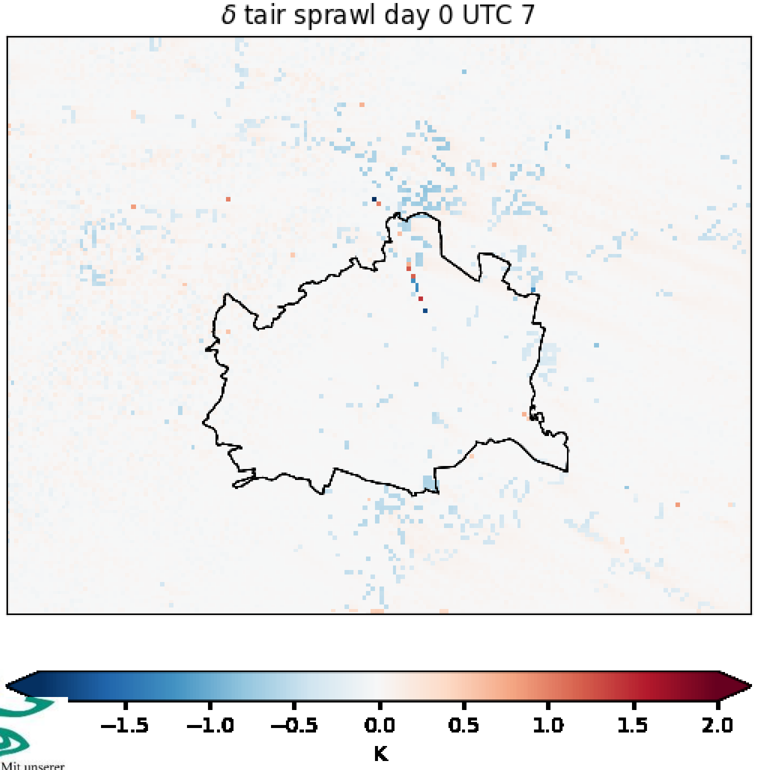

•Warming during 18-4 UTC

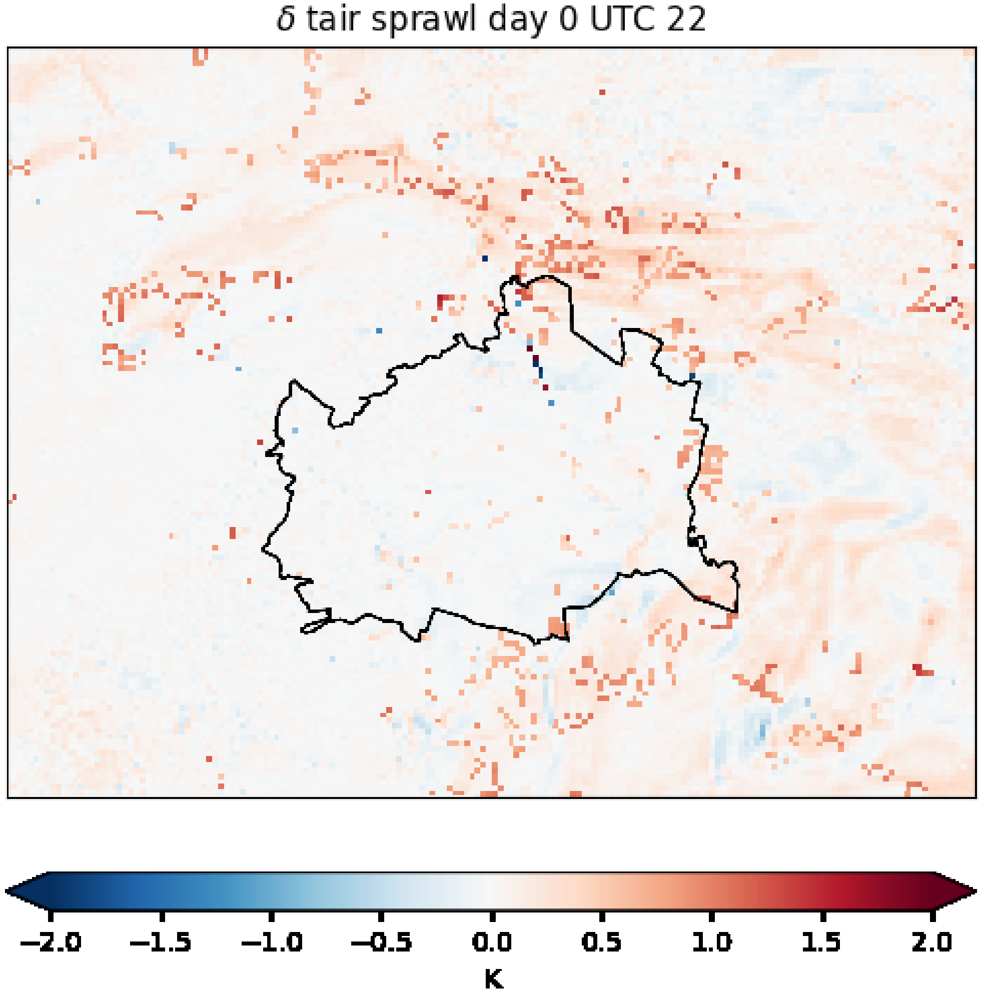

METEO FRANCE
BOKU
MA22 Mit unserer Umwelt

Albedo increases

Radiation Heat Flux | Ground Heat Flux | Sensible Heat Flux

WRF-TEB Simulation (29.7.17)

- Albedo Roof 0.15 -> 0.3
- Albedo Ground 0.138 -> 0.3
- Albedo Wall 0.2 -> 0.3

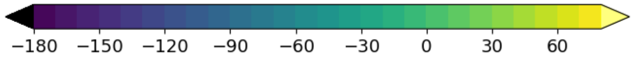

W/m²

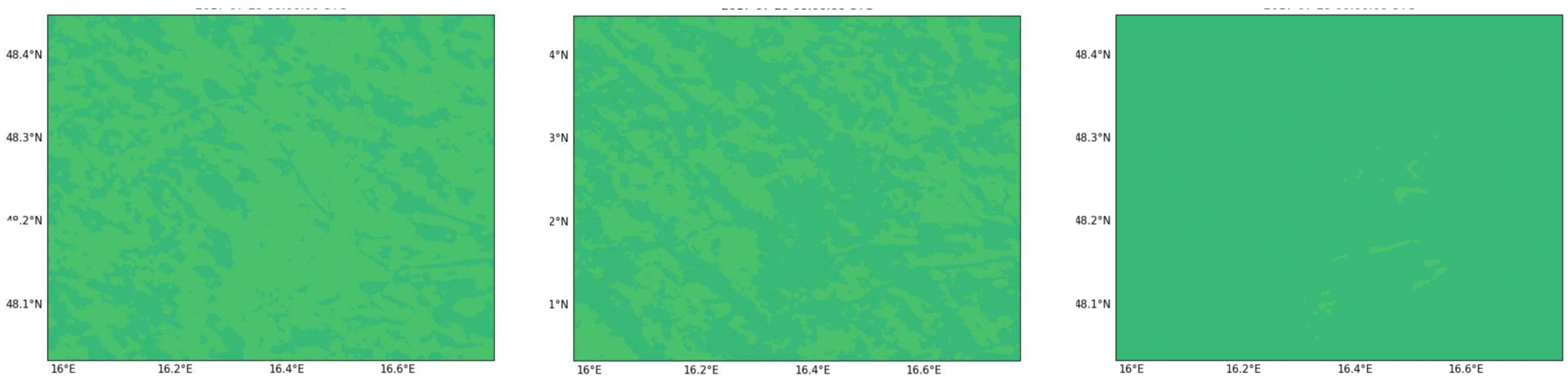

WRF/SURFEX Simulation (22.7.15)

- Albedo Roof 0.15 -> 0.68
- Albedo Ground 0.138 -> 0.3
- Albedo Wall 0.2 -> 0.3
- Tair reduction: 0.3 – 1.25 K

12 UTC

18 UTC

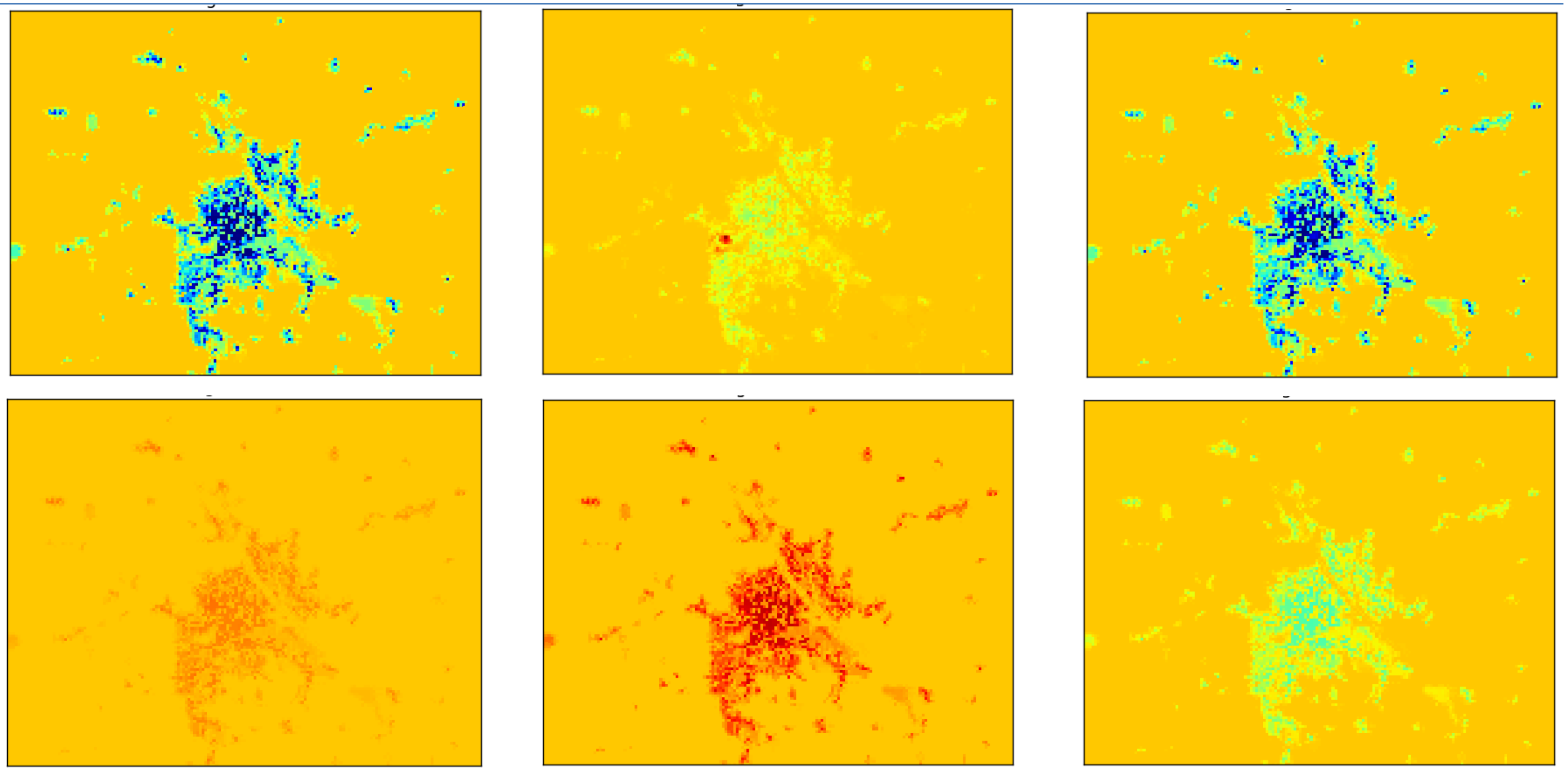

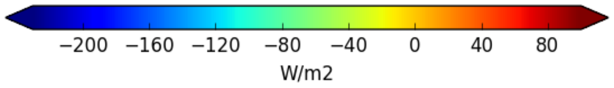

WRF/SURFEX Simulation

Albedo increases

- Albedo Roof 0.15 -> 0.68
- Albedo Ground 0.138 -> 0.3
- Albedo Wall 0.2 -> 0.3

Isolation

- Thermal Conductivity: 1.7/1.4 ->0.1 W/mK

Unsealing

- Unsealed Fraction *1.2

Roof-PV

- Efficiency 0.2
- Albedo: 0.1
- Emissivity: 0.9

Inner City

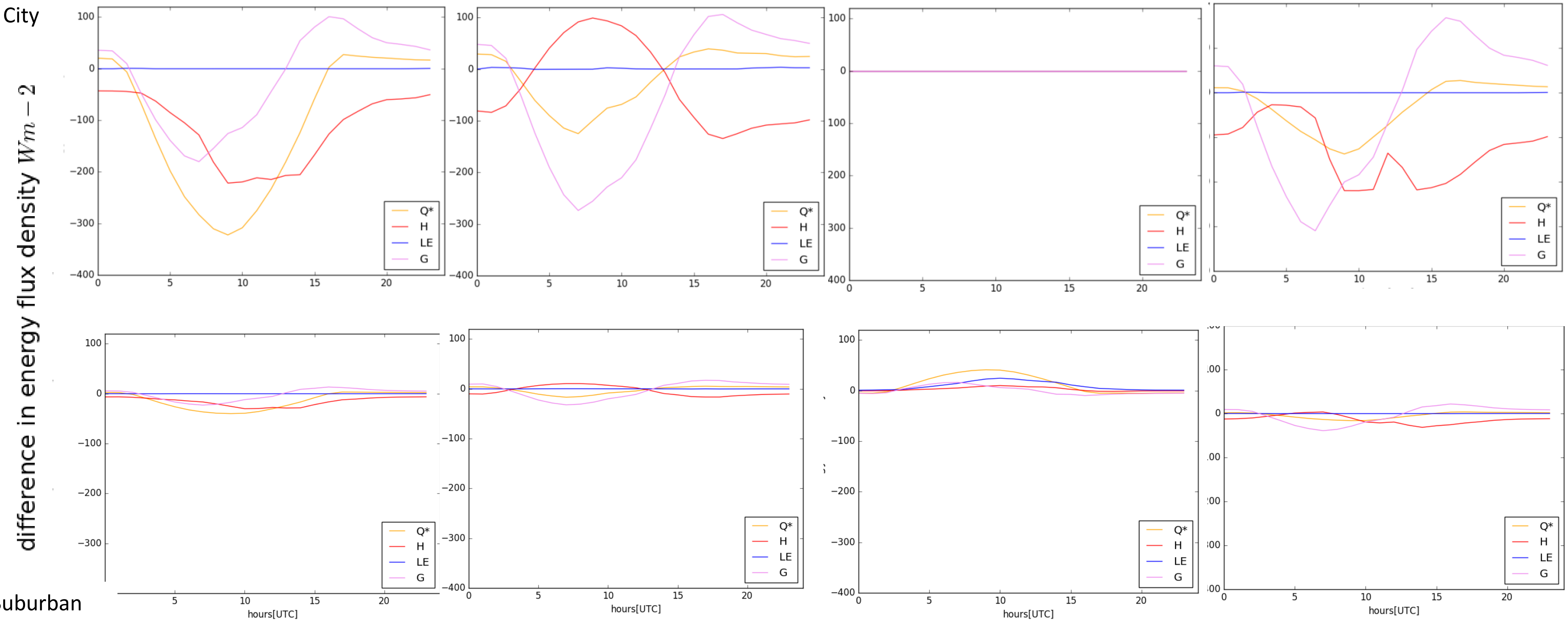

Suburban Area

Q* Radiation Balance H Sensible Heat Flux LE Latent Heat Flux G Ground Heat Flux

WRF/SURFEX Simulation

Reduction of Sensible Heat Flux

High Albedo | Insulation | Roof PV

12UTC

18UTC

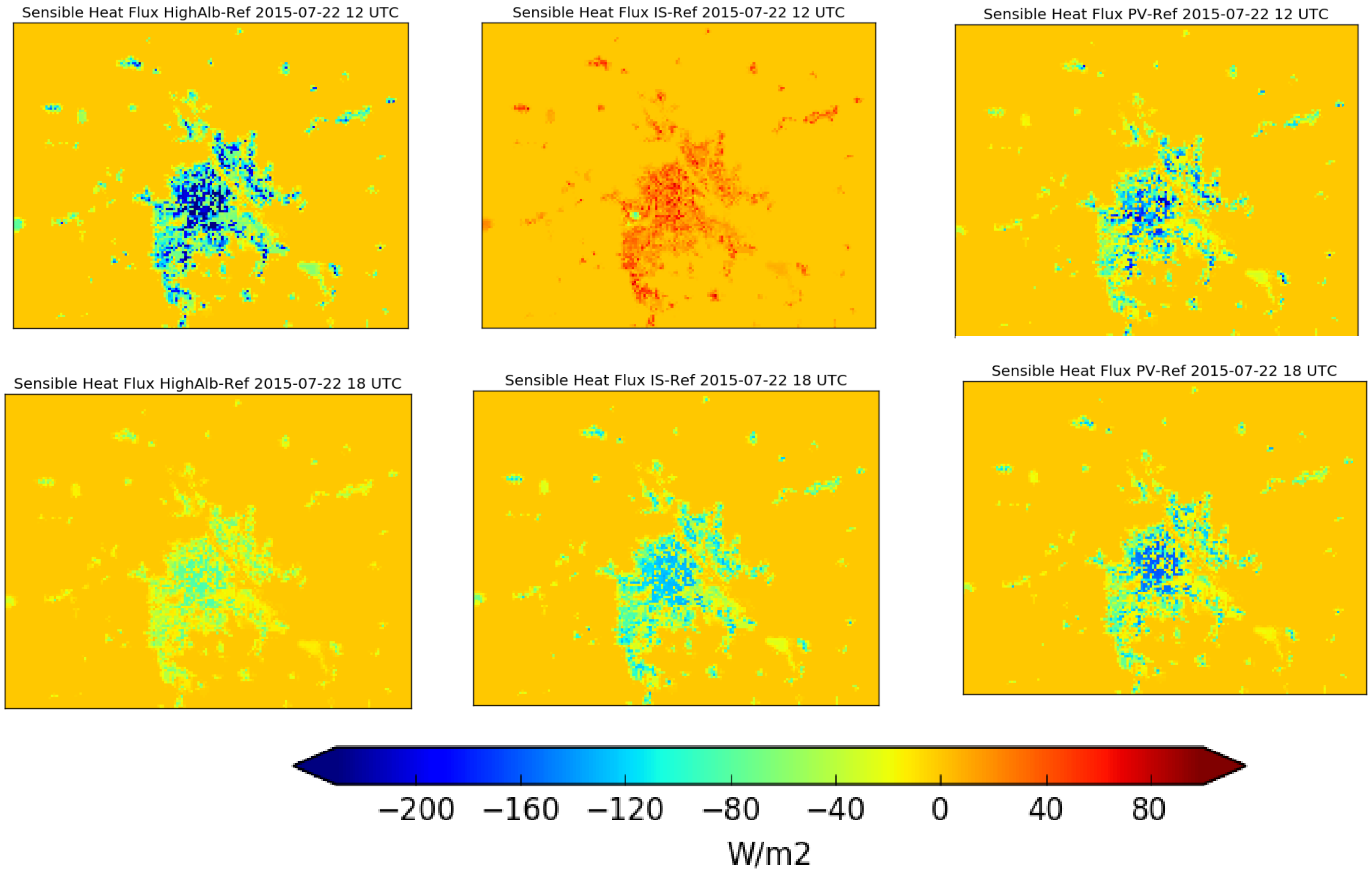

METEO FRANCE

MA22 Mit unserer Umwelt

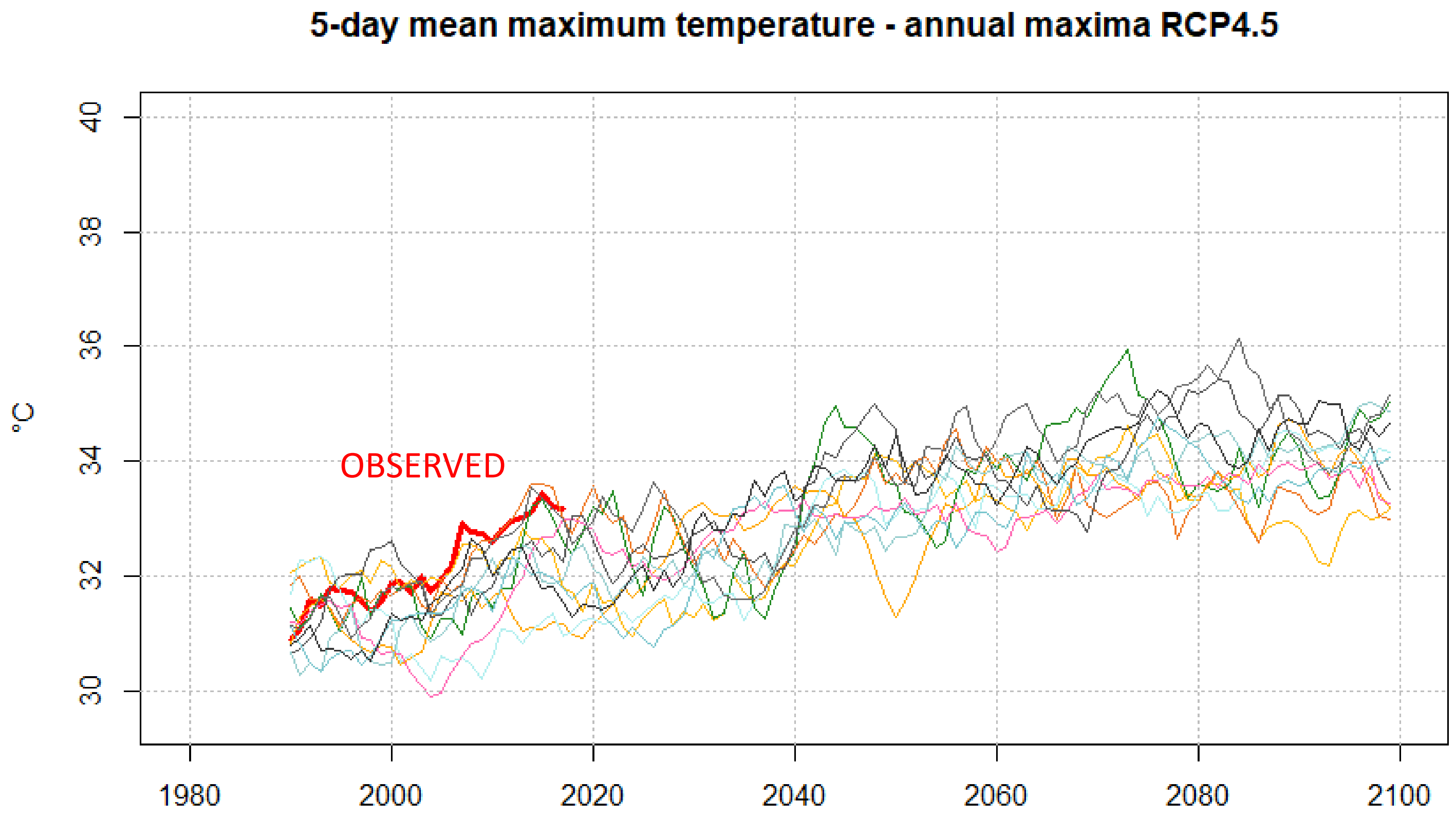

11 Models of OEKS15 (Uni Graz, Wegener Center, Leuprecht et al. 2016), Observed data - Sparatacus (ZAMG, Hiebl et al. 2015);

moving average of 10 years

METEO FRANCE

MA22 Mit unserer Umwelt

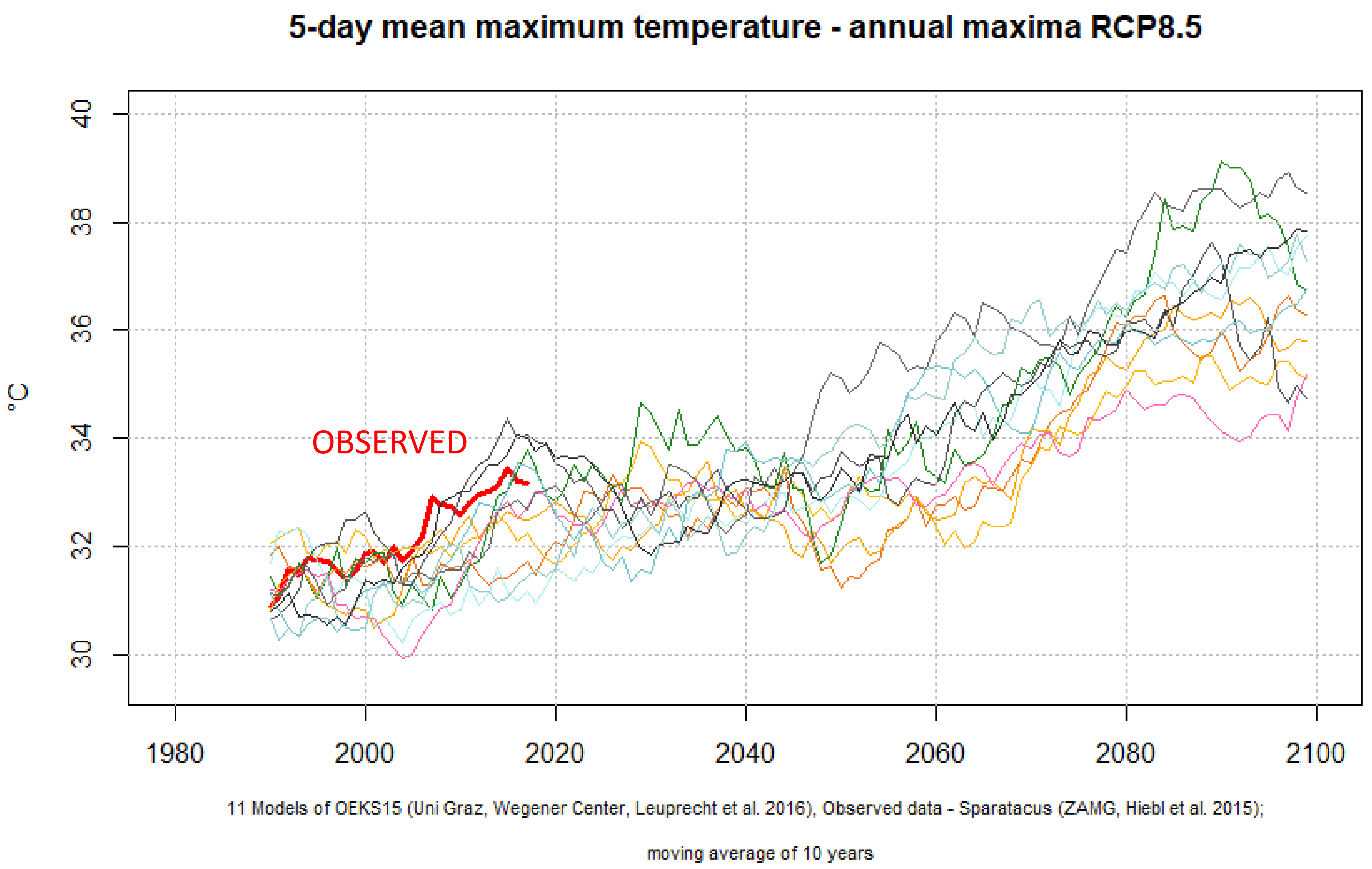

METEO FRANCE

Annual maxima of 5day maxima

- general extreme value distribution for 30 year period fitted for each model
- sampled with bootstrapping

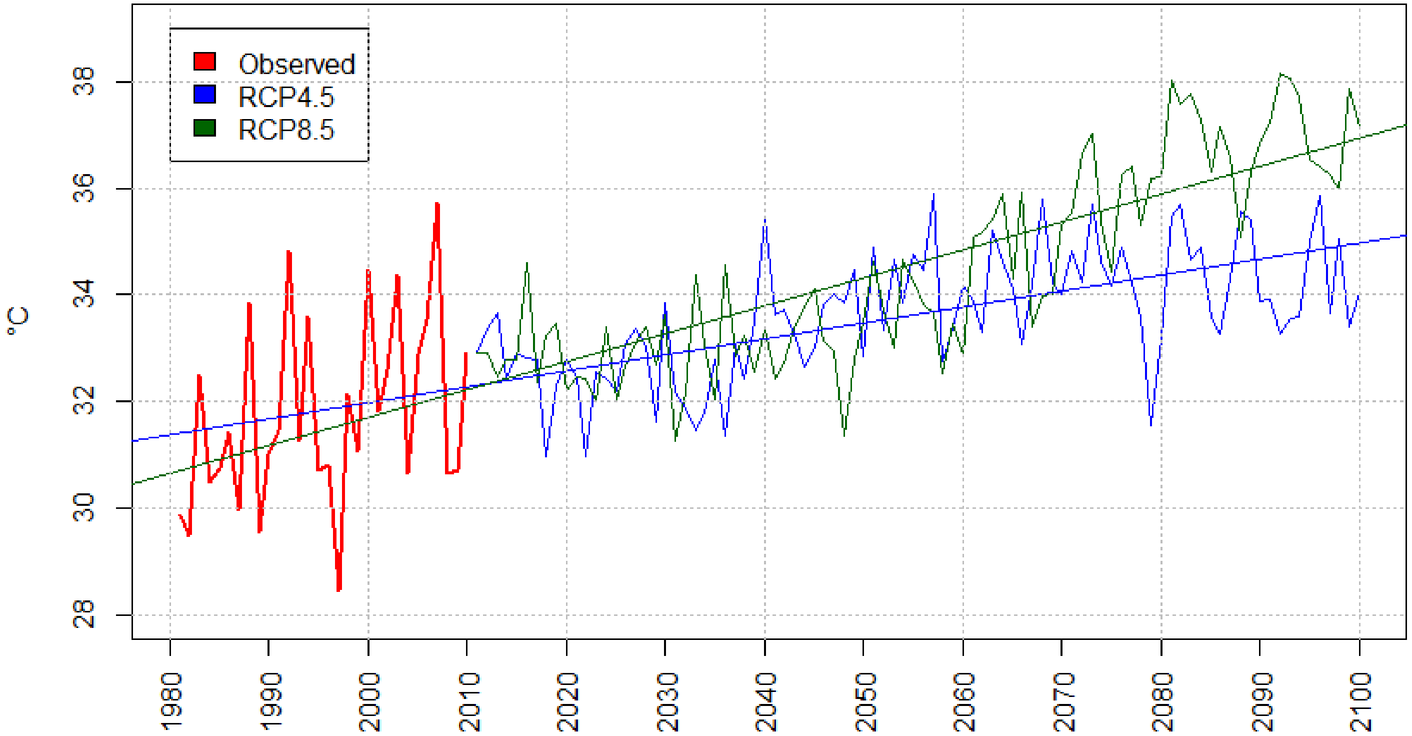

Median of 11 Models of OEKS15 (Uni Graz, Wegener Center, Leuprecht et al. 2016), Observed data - Sparatacus (ZAMG, Hiebl et al. 2015)

	2y event (0.5 percentile)	15y event (0.93 percentile)
Actual	31.6 °C	36.3 °C
2036-2065 („2050“) RCP8.5 median	33.7°C (+2.1 K)	38.7 °C (+2.4 K)
2036-2065 („2050“) RCP8.5 maximum	35.3°C (+3.7 K)	41.1 °C (+4.8 K)

METEO FRANCE

Summary

1) Methods: **- WRF and TEB LSM were coupled and represent city during heat waves very good**
- $R^2 > 0.78$, sigma < 1.83 K (for 8 stations, 9 days, better on cloud free days)
- WRF/SURFEX similar to WRF but higher maxima, while WRF tends to underestimate

2) Vienna UHI:
- urban-rural difference during heat waves greatest in evening (5 K)
- variations caused by surface diff.(up to 4 K) and convection at beginning of heat wave (+/- 1.5 K)

3) Vienna Growth:
- densification: - little effect on urban energy fluxes (H:+10 W/m²).
  - but small scale changes can affect thermal comfort
- urban sprawl: large effects (H: up to + 400 W/m²), but mainly local

4) Mitigation Strategies:
- insolation (nighttime cooling) (H: – 100 W/m²)
- albedo increases (daytime cooling) (H: up to – 200 W/m²)
- increasing in L.E. could be effective locally if implemented

5) Climate Change:
- temperature increase at upper limit of climate models
- extreme events (+2.4 K/+4.8 K) > mean events (+2.1 K/+3.7 K)

-> Main problem of Tair increases is the actual UHI and climate change.

-> Urban Growth will mainly affect small scale thermal comfort but also affect air temperatures downwind.

Next Steps

- **WRF/TEB Simulation for all selected future heat episodes (+/- isolation and albedo increase,…)**
- Analysis of thermal comfort

Thank you for your attention!

Interested in our final results? Please visit our website next year!

http://urbania.boku.ac.at